

REPUBLIC OF CAMEROON  
UNIVERSITY OF YAOUNDE I  
FACULTY OF SCIENCE



REPUBLIQUE DU CAMEROUN  
UNIVERSITE DE YAOUNDE I  
FACULTE DES SCIENCES

POSTGRADUATE SCHOOL OF SCIENCE, TECHNOLOGY AND GEOSCIENCES  
*CENTRE DE RECHERCHE ET DE FORMATION DOCTORALE EN SCIENCES, TECHNOLOGIE  
ET GEOSCIENCES*

RESEARCH AND DOCTORAL TRAINING UNIT IN CHEMISTRY AND APPLICATIONS  
*UNITE DE RECHERCHE ET DE FORMATION DOCTORALE EN CHIMIE ET APPLICATIONS*

DEPARTMENT OF INORGANIC CHEMISTRY  
*DEPARTEMENT DE CHIMIE INORGANIQUE*

LABORATORY OF APPLIED INORGANIC CHEMISTRY  
*LABORATOIRE DE CHIMIE INORGANIQUE APPLIQUEE*

**Enhancement of cementitious properties of alkali activated low reactive volcanic ashes: effects of curing regime and cassava peel ash replacement.**

A thesis submitted and defended in fulfillment of the requirements for the degree of  
Doctor of Philosophy in Chemistry

Specialty: Inorganic Chemistry  
Option: Physico-chemistry of Mineral Materials

By

**BAENLA Jean**

Registration n°: 13T2202  
M.Sc. in Chemistry (UY1)

Under the supervision of

**ELIMBI Antoine**

*Professor*

Year: 2021



UNIVERSITE DE YAOUNDE I  
UNIVERSITY OF YAOUNDE I



FACULTE DES SCIENCES  
FACULTY OF SCIENCE

DEPARTEMENT DE CHIMIE INORGANIQUE  
DEPARTMENT OF INORGANIC CHEMISTRY


**ATTESTATION OF THESIS CORRECTION**

We the undersigned, the members of the jury, attest that this Ph.D thesis defended on Tuesday the 21<sup>st</sup> December 2021 at 1 p.m. in the pedagogic block , hall S01 / 02 of the Faculty of Science, University of Yaoundé I, by Mr BAENLA Jean on the theme «*Enhancement of cementitious properties of alkali activated low reactive volcanic ashes : effects of curing regime and cassava peel ash replacement*», for the award of a Ph.D in Inorganic Chemistry, has been corrected in conformity with the recommendations of the defence jury.


In this testimony whereof, this attestation is issued.

Yaoundé..... 22 FEV. 2022 .....

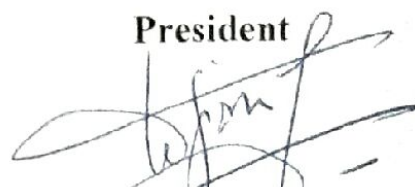
**Examiner**

  
ACAYANWA

**Supervisor**

  
Antoine Clément  
Professeur

**President**

  
Njopouo Daniel  
Professeur

## **Dedication**

To my late mom  
BAENLA Suzanne.

## Acknowledgements

This thesis has been carried out in the laboratory of Applied Inorganic Chemistry of the University of Yaoundé 1. Its realization has involved the participation of many persons and organizations that I would like to thank here below.

Firstly, I address my thanks to the Almighty who has made possible all the opportunities and conditions necessary for the realization of this research work.

Secondly, I will like to thank in most special way:

- My supervisor, Professor Antoine ELIMBI, for offering me the opportunity to undertake a PhD program under his supervision. I am very grateful for the constant and tremendous support, rigorous attitude, encouragement and guidance he offered me throughout these years in order to come out with this work;
- The “Bureau Afrique Centrale et des Grands Lacs de l’Agence Universitaire de la Francophonie” (BACGL-AUF) under the grant NS0020//10406 and “The World Academy of Sciences” (TWAS) under the grant N 13-018 RG/CHE/AF/AC G—UNESCO FR: 3240277723 for offering financial facilities related to the collection of raw materials and purchasing of laboratory equipment necessary for the good ongoing of this work;
- All the members of the jury for accepting and making themselves available to assess this research work;
- The head of the department of Inorganic Chemistry, Professor Moise ONDOH AGWARA, for all the administrative facilities;
- Professors Joseph KETCHA MBADCAM, Justin NENWA and Samuel LAMINSI for their multitude academic and paternal advices and encouragements;
- Professor Joseph DIKA MANGA for his confidence and encouragements;
- Doctors Beauregard Thomas MAKON, Jean Aimé MBEY, Hervé KOUAMO TCHAKOUTE , and Linda Dyorisse NYAMEN for their multitude advices and encouragements all through this research work;
- Doctors Amadou POUTOUENCHI, Igor Benjamin DJON LI NDJOCK, Jean Noel DJOBO, and Patrick LEMOUGNA for facilitating the characterization of raw materials and cement products used in this work;

- All my lab mates for the good mood and numerous support they brought throughout this work;
- My aunts Françoise BAENLA and Sariette BAENLA, my uncles François BAENLA and Serge MINOUE and my brothers and sisters for their invaluable support, love and encouragements:
- My late uncles Boniface YANGA and Marc Eric ETAME BAENLA for their invaluable support both financially and morally throughout my studies. They have always believed I could make it;
- My beautiful fiancée, Rosalie Estelle BIKIE ENGUENE for her love and invaluable support necessary for the good progress of this work;
- My friends Dr Samuel BISSIM, Serge TAGOUYIM, Dickson MISSOTA PRISO, Xavier MBOCK MBOCK, Pierre MBOCK and Godlove Michel NKEN PIPA for their multitude advices and encouragements.

Finally, I express my gratitude to all those who I might have forgotten to mention here but who have contributed in one way or the other towards the achievement of this work.

## Table of contents

<b>Dedication</b> .....	i
<b>Acknowledgements</b> .....	ii
<b>Table of contents</b> .....	iv
<b>List of Abbreviations</b> .....	vii
<b>List of Tables</b> .....	ix
<b>List of Figures</b> .....	x
<b>List of Symbols</b> .....	xiii
<b>Abstract</b> .....	xv
<b>Introduction</b> .....	1
<b>Chapter I: Literature review</b> .....	5
<b>I.1. Alkaline cements</b> .....	5
<b>I.1.1. Definition and historical aspect</b> .....	5
<b>I.1.2. Types of alkaline cement</b> .....	6
<b>I.1.3. Chemistry of alkaline cement</b> .....	7
<b>I.1.4. Raw materials and their reactivity in alkaline medium</b> .....	10
<b>I.2. Techniques for increasing reactivity of aluminosilicate raw materials</b> .....	20
<b>I.2.1. Mechanical activation</b> .....	20
<b>I.2.2. Physical separation</b> .....	22
<b>I.2.3. Thermal activation</b> .....	22
<b>I.2.4. Chemical activation</b> .....	23
<b>I.2.5. Curing regimes</b> .....	27
<b>I.3. Agricultural wastes as a resource in the cement technology</b> .....	29
<b>I.4. Summary and motivations of the thesis</b> .....	31
<b>Chapter II: Materials and experimental methods</b> .....	33
<b>II.1. Materials</b> .....	33

<b>II.1.1. Solid materials</b> .....	33
<b>II.1.2. Alkaline solution</b> .....	36
<b>II.2. Mix design and experimental procedures</b> .....	37
<b>II.2.1. Curing regime on mechanical strength and durability properties of inorganic polymers from alkali activated low reactive volcanic ash.</b> .....	37
<b>II.2.2. Alkali activation of cassava peel ash</b> .....	38
<b>II.2.3. Partial replacement of low reactive volcanic ash by cassava peel ash during alkali activation of volcanic ash</b> .....	39
<b>II.3. Analytical measurements</b> .....	41
<b>II.3.1. Leaching test</b> .....	41
<b>II.3.2. Particle size distribution</b> .....	41
<b>II.3.3. Chemical composition</b> .....	42
<b>II.3.5. Fourier transform infrared spectroscopy</b> .....	43
<b>II.3.6. Thermal analysis</b> .....	44
<b>II.3.7. Scanning electron microscopy and energy dispersive spectroscopy</b> .....	44
<b>II.3.8. Quantification of water loss</b> .....	45
<b>II.3.9. Compressive strength</b> .....	46
<b>II.3.10. Setting time</b> .....	47
<b>II.3.11. Durability</b> .....	47
<b>Chapter III: Results and discussion</b> .....	50
<b>III.1. Characterization of raw materials</b> .....	50
<b>III.1.1. Particle size distribution</b> .....	50
<b>III.1.2. Chemical composition</b> .....	52
<b>III.1.3. Thermal analysis of cassava peels</b> .....	54
<b>III.1.4. Fourier Transform Infrared spectroscopy analysis</b> .....	55
<b>III.1.5. X-ray diffraction analysis</b> .....	57

<b>III.1.6. Reactive phase content.....</b>	<b>59</b>
<b>III.2. Effects of curing regime on mechanical strength and durability of low reactive volcanic ash based alkaline cement.....</b>	<b>61</b>
<b>III.2.1. Water loss and microstructure .....</b>	<b>61</b>
<b>III.2.2. Compressive strength .....</b>	<b>72</b>
<b>III.2.3. Durability .....</b>	<b>73</b>
<b>III.2.4. Conclusion.....</b>	<b>81</b>
<b>III.3. Reactivity of cassava peel ash (C<sub>A</sub>) in alkaline medium.....</b>	<b>82</b>
<b>III.3.1. Dissolution capacity of C<sub>A</sub> in different concentrated alkaline solutions. ....</b>	<b>82</b>
<b>III.3.2. Characterization of cassava peel ash based alkaline activated materials .....</b>	<b>84</b>
<b>III.3.3. Conclusion.....</b>	<b>97</b>
<b>III.4. Effect of cassava peel ash in alkaline activation of low reactive volcanic ash.....</b>	<b>98</b>
<b>III.4.1. Initial setting time .....</b>	<b>98</b>
<b>III.4.2. Microstructure .....</b>	<b>99</b>
<b>III.4.3. Compressive strength .....</b>	<b>109</b>
<b>III.4.4. Efflorescence and durability.....</b>	<b>110</b>
<b>III.4.5. Conclusion.....</b>	<b>113</b>
<b>GENERAL CONCLUSION AND OUTLOOKS.....</b>	<b>114</b>
<b>REFERENCES.....</b>	<b>117</b>
<b>LIST OF PUBLICATION .....</b>	<b>136</b>
<b>PUBLISHED ARTICLE.....</b>	<b>137</b>



## List of Abbreviations

RHBA: Rice Husk Bark Ash

SBA: Sugarcane Bagasse Ash

PFOA: Palm Oil Fuel Ash

C<sub>A</sub>: Cassava Peel Ash

CP: Cassava Peel

RC<sub>A</sub>: Residue of Cassava Peel Ash

R<sub>C</sub>: Reactive Phase Content

Eq: Equation

D<sub>C</sub>: Dissolution Capacity

V<sub>n</sub>: Volcanic ash collected in the locality of Vina

Ma: Volcanic ash collected in the locality of Manjo

AAC<sub>2.3, 1.8, 1.5</sub>: Alkali Activated Cassava peel ash synthesized with activation solutions of SiO<sub>2</sub>/Na<sub>2</sub>O molar ratios equal to 2.3, 1.8 and 1.5

GMC<sub>0, 10, 20, 30</sub>: Volcanic ash based geopolymer containing 0, 10, 20 and 30 % by mass of cassava peel ash

SSP25: Sealing Specimens in Polyethylene bags at ambient temperature of laboratory

SOA25: Specimens cured in Open Atmospheric air of laboratory

ODS60: Oven Drying Specimens at 60 °C

L.O.I: Loss On Ignition

L<sub>x</sub>: Layer (x = 1, 2 and 3)

L / S: Liquid to Solid mass ratio

H<sub>2</sub>O / S: Water to Solid mass ratio

SiO<sub>2</sub> / Al<sub>2</sub>O<sub>3</sub>: silicon oxide to aluminium oxide molar ratio

CS: Compressive Strength

TGA: Thermogravimetry analysis

DSC: Differential Scanning Calorimetry

XRD: X-Ray Diffraction

FTIR: Fourier Transform Infra-Red spectroscopy

SEM: Scanning Electron Microscopy

EDX: Energy Dispersive X-ray spectroscopy

ASTM: American Society for Testing and Materials

EN: European Norm

## List of Tables

Table I: Mix design and curing conditions of synthesis procedure. ....	38
Table II: Summary of the mix design of alkali activated products.....	39
Table III: Mix proportions of volcanic ash (Ma), cassava peel ash (C <sub>A</sub> ) and alkaline solution. ...	40
Table IV: Particle sizes and specific surface area.....	52
Table V: Chemical composition (% by mass) of volcanic ashes (Ma and Vn) and cassava peel ash (CA).....	53
Table VI: Reactive phase content (R <sub>C</sub> ) in each raw material. ....	59
Table VII: Water loss (% by mass) versus the curing regime of alkaline cement.....	62
Table VIII: dissolution index of some mineral phases based on XRD patterns of alkali activated volcanic ashes suggested to various curing regimes. ....	66
Table IX: Residual strength of specimens after 30 days of immersion in water.....	81
Table X: Dissolution capacity (D <sub>C</sub> ) of C <sub>A</sub> versus the concentration of NaOH solution. ....	82
Table XI: Initial setting time and 28 day compressive strength. ....	97
Table XII: Elemental composition of chosen areas on geopolymer pastes aged 28 days.....	107
Table XIII: Mass loss (%) and residual strength of geopolymers, aged 28 days, immersed in 5 % by mass of sulphuric acid. ....	112

## List of Figures

Figure 1: Schematic representation of cross linked and non-cross linked tobermorite structures which represent the generalised structure of the C-(N)-A-S-H type. ....	10
Figure 2: 3D geopolymer network.....	10
Figure 3: Chart summarising the rational utilisation of volcanic ashes . ....	14
Figure 4: Volcanic ash powders used.....	33
Figure 5: (a) Whole cassava root and peeled pieces; (b) Washing and drying of cassava peels; (c) Cracked cassava peels and (d) Cassava peel ash used. ....	35
Figure 6: Electrical furnace (Nabertherm, model LH 60/14) used. ....	36
Figure 7: Calcination program of cassava peels used. ....	36
Figure 8: Thermal analysis device (LINSEIS STAPT-1000) used.....	44
Figure 9: Electro-hydraulic press used.....	46
Figure 10: VICAT apparatus used. ....	47
Figure 11: Summary of the experimental work carried out. ....	49
Figure 12: Particle size distribution of volcanic ashes and cassava peel ash. ....	51
Figure 13: Thermal analysis of cassava peel. ....	54
Figure 14: FTIR spectra of raw materials (CP: cassava peel, C <sub>A</sub> : cassava peel ash, Ma and Vn: volcanic ashes).....	56
Figure 15: XRD patterns of raw materials (Vn and Ma: volcanic ashes, C <sub>A</sub> : cassava peel ash)...58	
Figure 16: XRD pattern of cassava peel ash residue (R <sub>CA</sub> ) and Cassava peel ash (C <sub>A</sub> ).....60	
Figure 17: Thermographs of Ma based alkaline cement aged 28 days ( <b>a</b> : TGA and <b>b</b> : DSC). ....63	
Figure 18: Thermographs of Vn based alkaline cement aged 28 days ( <b>a</b> : TGA and <b>b</b> : DSC).....64	
Figure 19: XRD patterns of Ma based alkaline cements aged 28 days preserved under various curing regimes.....67	
Figure 20: XRD patterns of Vn based alkaline cements aged 28 days preserved under various curing regimes.....68	
Figure 21: Merged XRD pattern (from 0 to 40 ° 2θ) of volcanic ash based alkaline cements aged 28 days subjected to various curing regimes. ....69	
Figure 22: SEM images of volcanic ash based alkaline cement specimens aged 28 days.....71	
Figure 23: 28 days compressive strength of volcanic ash based alkaline cements.....73	

Figure 24: Mass loss (%) of volcanic ash based alkaline cement aged 28 days, immersed in 5 % by mass of sulphuric acid for 30 days. ....	74
Figure 25: Residual of strength of Ma based alkaline cement after immersion in 5 % by mass of sulphuric acid. ....	76
Figure 26: Residual strength of Vn based alkaline cement after immersion in 5 % by mass of sulphuric acid. ....	76
Figure 27: SEM images of volcanic ash based alkaline cement specimens cured on open atmospheric air (SOA25) for 28 days before and after subjection to sulphuric acid attack. ....	78
Figure 28: Residual compressive strength of alkali activated volcanic ashes immersed in water for 30 days. ....	79
Figure 29: Visual aspect of Ma based alkaline cement specimens immersed in water for 30 days. ....	80
Figure 30: XRD patterns of residues of leached cassava peel ash in different NaOH solutions. ....	83
Figure 31: FTIR spectra of cassava peel ash based alkali activated pastes. ....	85
Figure 32: XRD patterns of cassava peel ash based activated pastes. ....	88
Figure 33: TGA (a) and DSC (b) curves of alkali activated cassava peel ash. ....	91
Figure 34: SEM images of alkali activated cassava peel ash aged 28 days. ....	93
Figure 35: Elemental mapping of cassava peel ash based alkali activated pastes (AAC <sub>2.3</sub> ) aged 28 days. ....	94
Figure 36: Elemental mapping of cassava peel ash based alkali activated pastes (AAC <sub>1.5</sub> ) aged 28 days. ....	95
Figure 37: Initial setting of geopolymer pastes. ....	99
Figure 38: FTIR spectra for geopolymer pastes aged 28 days. ....	100
Figure 39: XRD patterns of geopolymers aged 28 days. ....	102
Figure 40: Thermograms (TGA and DSC) of GMC <sub>0</sub> and GMC <sub>30</sub> . ....	104
Figure 41. SEM images of volcanic ash based geopolymers aged 28 days containing various percentage of cassava peel ash (a: GMC <sub>0</sub> ; b: GMC <sub>10</sub> ; c: GMC <sub>20</sub> and d: GMC <sub>30</sub> ). ....	106
Figure 42: Elemental mapping of geopolymer aged 28 days (a: GMC <sub>0</sub> ; b: GMC <sub>10</sub> ; c: GMC <sub>20</sub> and d: GMC <sub>30</sub> ). ....	108
Figure 43: Compressive strength of geopolymer pastes aged 28 days. ....	110

Figure 44: Efflorescence test for geopolymer pastes aged 28 days exposed at ambient temperature of the laboratory for 90 days.....111

Figure 45: Visual aspect of inorganic polymer specimens before and after 30 days of immersion in acidic medium.....112

## List of Symbols

<b>Symbol</b>	<b>Definition</b>
MPa:	Mega Pascal
min:	Minute
m <sup>2</sup> / g:	Metre square per gram
F:	Force
A:	Surface area
KN:	Kilo newton
mm <sup>2</sup> :	Millimetre square
%:	Percentage
cm <sup>-1</sup> :	Per centimetre
µm:	Micrometre
pH:	Potential hydrogen
M:	Molar
Ca:	Calcium
Si:	Silicon
Al:	Aluminium
Na:	Sodium
Fe:	Iron
Al <sub>2</sub> O <sub>3</sub> :	Aluminium oxide
SiO <sub>2</sub> :	Silicon dioxide
CaO:	Calcium oxide
Fe <sub>2</sub> O <sub>3</sub> :	Iron oxide
BaO:	Barium oxide
K <sub>2</sub> O:	Potassium oxide
Na <sub>2</sub> O:	Sodium oxide
MgO:	Magnesium oxide

TiO <sub>2</sub> :	Titanium oxide
Cr <sub>2</sub> O <sub>3</sub> :	Chromium oxide
H <sub>2</sub> O:	Hydrogen oxide (water)
MnO:	Manganese oxide
P <sub>2</sub> O <sub>5</sub> :	Phosphorus oxide
SO <sub>3</sub> :	Sulphur trioxide
SrO:	Strontium oxide
F:	Fluorine



## Abstract

The present study aims at improving the cementitious properties of alkali activated low reactive volcanic ashes. It has two Major parts. It assesses the influence of three curing regimes of fresh pastes and powder of cassava peel ash on cementitious properties of two low reactive volcanic ashes. After the characterisation of starting raw materials, some characteristics on elaborated alkaline cement pastes were determined. Volcanic ashes denoted Vn and Ma and cassava peel ash ( $C_A$ ) have respectively 26, 18 and 72 % by mass of reactive phase. In the first part of this study, the cement pastes obtained from alkaline activation of Vn and Ma powders were cured for a fixed period in three regimes: sealing in a polyethylene bag at ambient temperature (SSP25), oven drying at 60 °C (ODS60) and maintaining in open atmospheric air of laboratory (SOA25). Results obtained revealed that SSP25 regime enables good dissolution of reactive phase but cement products express low durability and mechanic strength. The ODS60 and SOA25 regimes lead to cementitious products with fairly high durability and mechanical strength. According to thermal analysis results (TGA / DSC), the differences observed on these three curing regimes for cement paste are related to hygrometric water of the reaction medium. In the second part of this study, the low reactive phase content in Ma (18 % by mass) led to search for an improvement of its reactivity in alkaline medium. This consisted of substituting Ma powder with 0 to 30 % by mass of  $C_A$  powder. Thus, the substitution of Ma with  $C_A$  made it possible to optimise the activation of this precursor in alkaline medium. In synergy with Ma, the substitution of 30 % by mass of  $C_A$  enabled the lowering of initial setting time of paste and the enhancement of compressive strength of the cementitious product to about 60 and 733 % respectively. Moreover, the substitution of Ma with  $C_A$  diminishes the magnitude of efflorescence. In fact, the presence of arcanite ( $K_2SO_4$ ) in  $C_A$  assures a chemical reaction with excess  $Na^+$  ions (responsible of efflorescence) of synthesised product for the formation of aphthitalite ( $K_3Na(SO_4)_2$ ). Hence, during alkaline activation of volcanic ashes, ODS60 and SOA25 regimes are best suited for paste curing and  $C_A$  powder behaves as an additional precursor.

**Keywords:** volcanic ash; cassava peel; curing regime, alkaline cement; mechanical strength; efflorescence; durability.

## Résumé

Cette étude vise à rehausser les propriétés cimentaires des ciments alcalins à base de scories volcaniques peu réactives. Elle comporte deux parties. Elle évalue l'influence de trois régimes de conditionnement de la pâte fraîche et de la poudre des cendres de cortex de tubercules de manioc ( $C_A$ ) sur les propriétés cimentaires de deux scories volcaniques peu réactives. Après la caractérisation des matières premières, certaines caractéristiques sur les pâtes des ciments alcalins élaborés ont été déterminées. Les scories volcaniques dénommées Vn et Ma et les cendres de cortex de manioc ( $C_A$ ) ont respectivement 26, 18 et 72 % en masse de phase réactive. Dans la première partie de cette étude, les pâtes cimentaires obtenues de l'activation des poudres de Vn et Ma en milieu basique ont été conditionnées à des durées déterminées selon trois régimes : scellage dans un sac en polyéthylène à la température ambiante (SSP25), étuvage à 60 °C (ODS60), maintien dans l'air atmosphérique du laboratoire (SOA25). Les résultats obtenus ont montré que le régime SSP25 permet une bonne dissolution de la phase réactive mais les produits cimentaires ont une faible durabilité et les résistances mécaniques sont peu élevées. Les régimes ODS60 et SOA25 conduisent à des produits cimentaires ayant une durabilité et des résistances assez élevées. D'après les résultats d'analyse thermique (ATG / DTG), les différences observées sur ces trois régimes de conditionnement de la pâte de ciment sont en relation avec l'eau hygrométrique du milieu réactionnel. Dans la seconde partie de cette étude, la faible teneur en phase réactive dans Ma (18 % en masse) a conduit à rechercher une amélioration de sa réactivité en milieu basique. Ceci a consisté à substituer les poudres de Ma avec 0 à 30 % en masse de  $C_A$ . Ainsi, la substitution de Ma avec  $C_A$  a permis d'optimiser l'activation de ce précurseur en milieu basique. De synergie avec Ma, la substitution de 30 % en masse de  $C_A$  a permis d'amoinrir le temps de début de prise de la pâte et d'augmenter la résistance à la compression du produit cimentaire, respectivement de 60 et 733 %. Par ailleurs, la substitution de Ma avec  $C_A$  diminue l'efflorescence. En effet, la présence de l'arcanite ( $K_2SO_4$ ) dans  $C_A$  assure une réaction chimique avec l'excès d'ions  $Na^+$  (responsable de l'efflorescence) du produit de synthèse pour former l'aphthitalite ( $K_3Na(SO_4)_2$ ). Ainsi, au cours de l'activation en milieu basique de scories volcaniques, les régimes ODS60 et SOA25 sont les mieux indiqués au conditionnement des pâtes et les poudres de  $C_A$  se comportent comme un précurseur additionnel.

**Mots-clés** : Scories volcaniques ; cortex de manioc ; régime de conditionnement ; ciment alcalin ; résistance mécanique ; efflorescence ; durabilité

## Introduction

The increase in population with years throughout the earth globe leads to the expansion of urbanisation. This induces a high demand for housing and viable infrastructures around the world. In developing countries, this demand is tremendous due to poverty and lack of construction facilities such as insufficient skills and technology, low development support and low level of industrialisation [1]. Accordingly, the cost of building materials such as cement is not easily afforded by an ordinary citizen. So, a considerable percentage of the population in developing countries live in precarious conditions. Thus, there is a real need to bring in new solutions which can enable to overcome housing and infrastructure shortages.

In general, Portland cement remains the most used binder for civil engineering purposes. Though, for many decades, it has been satisfactory at certain levels to human's infrastructures, nowadays it seems harmful since its production is highly involved in environmental pollution and energy consumption. The production of 1 tonne of Portland cement yields about 0.8 to 1 tonne of CO<sub>2</sub> in the atmosphere, which contributes to greenhouse gas emission [2]. Thus, seeking for alternative construction binders with respect to our environment seems to be a concern. So, more and more interests are given to new forms of binders which are less expensive and friendly to the environment. Among a large variety of eco-friendly cement; alkaline cements, according to scientists, seem to be the most prominent.

Alkaline cements are new classes of binders resulting from alkaline activation of raw materials rich with reactive SiO<sub>2</sub> and Al<sub>2</sub>O<sub>3</sub> as well as CaO and Fe<sub>2</sub>O<sub>3</sub>. Their synthesis can be done either at room or slightly elevated temperature. One of the advantages of these binders is their diverse sources of raw materials (metakaolin, blast furnace slag, fly ash, volcanic ash, etc.) which can be either natural or synthetic necessary for their synthesis. Volcanic ash seems to be a prominent solid precursor due to its natural aspect compared to others which, prior to use, require specific pre-treatment.

Volcanic ashes are natural raw materials originating from volcanic eruption. These materials are highly abundant in areas where volcanic activities have been revealed. Like in Cameroon, they are hugely present along the "Cameroon Line". However, their utilizations are limited to either as additive for the production of Portland cement or as aggregates for the improvement of the quality

of untarred roads. Recently, the implication of volcanic ash as a primary raw material in the synthesis of an eco-friendly cement renders it more attractive. Regarding the environmental concern, in localities rich in volcanic ash, it will be judicious to lay more emphasis to the valorisation of this natural wealth in the synthesis of eco-friendly cements.

Many studies have revealed the potentiality of volcanic ash in alkaline cement synthesis [3–7]. Though results obtained seem worthy, volcanic ash is shown to express low reactivity in alkaline medium compared to other aluminosilicates (metakaolin, blast furnace slag and fly ash), which is characterized by long setting time, low mechanical strength and durability. This reactivity fluctuates negatively from one geological source to another. In order to enhance it, several interesting attempts have been done such as mechanical activation, alkali fusion, mineral admixing with metakaolin [4]. Nevertheless, all the latter investigations were limited on volcanic ashes with reactive phase content greater or equal to 30 % by mass [4]. Also, most of the above mentioned attempts are energy-consuming. So, other approaches that can reduce or eliminate the energy dependence will be of great interest, mostly in countries where energy production is limited. Thus, Djon li Ndjock et al. (2018) tried to suggest the selectivity of volcanic ashes for alkaline cement synthesis, and noticed that parameters such as reactive phase content,  $\text{SiO}_2 / \text{Al}_2\text{O}_3$  molar ratio of the reactive phase and the composition of the alkaline solution influence the reactivity of volcanic ash in alkaline medium. According to the authors, volcanic ash with reactive phase content lesser than 20 % by mass are not good for alkaline cement synthesis but rather as good fillers. Going across their study, it is well observed that no matter the reactive phase content (i.e. from 42.5 to 11.4 % by mass), all the volcanic ash samples activated with silicate solution expressed almost similar compressive strength (i.e. with volcanic ashes containing 11.4, 12.5 and 42.5 % by mass of reactive phase, 1, 1 and 1.1 MPa were respectively achieved after 14 days of curing) [8]. However, with 42.5 % of reactive phase content, the strength is expected to be more. With about 46 % of reactive phase content in volcanic ash, Djobo et al. (2016) obtained 8 MPa after 7 days of curing at ambient [9]. Elsewhere, Tchakoute et al. (2013) obtained 19 and 50 MPa with 34.8 and 64.8 % of reactive phase respectively in volcanic ashes after 28 days of curing [3]. This thus suggests that other parameters must have influenced the polycondensation process. It is important to highlight that all these above results were achieved on cement specimens that were sealed in polyethylene bag for a given period of time. Quite a few studies revealed that water management in the synthesis medium of some alkali activated aluminosilicate affects the polycondensation

reaction, thereby making the curing regime to vary from one aluminosilicate raw material to another [10–12]. In alkaline cement chemistry, there exists no standardized curing regime, but conventionally, the hardening process of cementing materials is water consuming. Thus, sealing curing is widely-spread since it minimizes water loss and prevents efflorescence formation during the hardening process. Nevertheless, the latter curing seems beneficial to alkaline activation of certain raw materials and harmful to others. Using fly ash as raw material in alkaline cement synthesis, Lee et al. (2016) obtained good results with sealing curing [12] while for Xie and Kayali (2013), unsealing curing was the best [10]. Concerning volcanic ash, no assessment has been done in that way. Hence, it will be judicious to investigate on that so as to bring more light on an appropriate curing method, if necessary at room temperature, to enable an efficient polycondensation in low reactive volcanic ash based alkaline cement. It will also be interesting to propose a novel, low cost and local approach which may help to overcome the deficiency in reactive phase content present in some volcanic ashes. Ashes of agro-wastes such as rice husk ash, sugarcane bagasse and palm oil kernel ash have several time been used in diverse raw aluminosilicates material but require heat curing for efficient reactivity. Other raw materials that can palliate the use of heat curing will be of great interest. Cassava peel ash possesses primary oxides which have been relevant to Portland cement substitution in pastes and mortars [13]. Not yet used in alkaline cement synthesis, its implication might have positive impact.

This work is inscribed as a continuation to the limits observed in former assessments related to the valorisation of volcanic ash in the synthesis of alkaline cements. It aimed to present adequate curing regime for volcanic ash based alkaline cement synthesis necessary to achieve optimum mechanical properties and durability. Further, it also aimed to test new agro-waste in alkaline activation chemistry in order to encourage the use of very low reactive volcanic ash (reactive phase content  $\leq 18\%$ ) as a primary precursor in the synthesis of alkaline cement at ambient temperature for civil engineering purposes. On this, the thesis layout is presented into three chapters as follows:

- The first chapter is focused on literature review. It brings out relevant studies concerning the reactivity of some aluminosilicate raw materials including those of volcanic ash in alkaline medium. Also, it reports techniques used to enhance the reactivity of aluminosilicates as well as relevant implication of ashes of agro-wastes in the cement technology;

- The second chapter is presenting all the raw materials and the experimental procedures as well as analytical techniques and measurements used along the realization of this thesis;
- The third chapter presents results and detailed discussions issued from experiments carried out in chapter two. This chapter is divided into 4 subparts as follows:
  - The first subpart is consecrated to the characterization of raw materials;
  - The second one is based on the effect of curing regimes on the mechanical strength and durability of low reactive volcanic ash based alkaline cements;
  - The third subpart shows the behaviour of cassava peel ash when alkali activated in various alkaline medium;
  - The fourth subpart reveals the impact of incorporating cassava peel ash in the alkaline activation of low reactive volcanic ash.
- At last, a general conclusion and outlooks are presented.

## **Chapter I: Literature review**

This first chapter will present a literature review concerning alkaline cement and its synthesis. It will also report methods used for the enhancement of reactivity of aluminosilicate raw materials in alkaline medium as well as the implication of agro-waste in the cement sector.

### **I.1. Alkaline cements**

#### **I.1.1. Definition and historical aspect**

Alkaline cement is a general name given to a class of binder system derived by the reaction of an alkali metal source (solid or dissolved) with a solid aluminosilicate powder either at ambient or slightly elevated temperatures [14]. The alkali sources used can include alkali hydroxides, silicates, carbonates, sulphates, aluminates or oxides, essentially any soluble substance which can supply alkali metal cations, raise the pH of the reaction mixture and accelerate the dissolution of the solid precursor [15]. Alkaline cement is a new generation of materials possessing either an amorphous or a semi-crystalline structure in which silicon and aluminium atoms are interconnected via oxygen atoms. The tetrahedral coordination of Al atoms generates negative charges which are balanced by the presence of alkali ions ( $\text{Na}^+$ ,  $\text{K}^+$ ,  $\text{Ca}^{2+}$  and  $\text{H}_3\text{O}^+$ ) in the framework. This cement is presented as an eco-friendly cement as well as a prominent alternative to Portland cement regarding the climatic concern in which Portland cement industries are noticed to be among the highest emitters of greenhouse gases (carbon dioxide in particular) into the atmosphere. For many decades now, Alkaline cement attracts a lot of attention since it is respectful to the environment (i.e. it has low Carbon footprint) and presents interesting durability properties.

The major development of this cement started around 1940 with Purdon who activated blast furnace slag with sodium hydroxide. According to him, it was a two steps process in which silica aluminium and calcium hydroxide are liberated and later on followed by the formation of silica and alumina hydrates as well as the regeneration of sodium hydroxide. Almost twenty-five years later, in research of alternative solutions against cement shortages experienced by former Soviet Union and China, Glukhovsky came in with a new binder he named "Soil-cement" obtained by mixing ground aluminosilicates with alkalis industrial wastes. The term "soil" was due to the fact that it looks like ground rock while that of "cement" was because it bears cementitious capacity. This author made crucial investigations about the alkaline activation of blast furnace slag. He

identified hydrated products as being composed of calcium silicate hydrates and calcium and sodium aluminosilicate hydrates, and also noticed that, clay minerals formed aluminium silicate hydrates when submitted to alkali activation. On his investigation, he classified alkali activators under six groups where M is an alkali ion: alkali (MOH); weak acid salts ( $M_2CO_3$ ,  $M_2SO_3$ ,  $M_3PO_4$ , MF); silicates ( $M_2O \cdot nSiO_3$ ); aluminates ( $M_2O \cdot nAl_2O_3$ ); aluminosilicate ( $M_2O \cdot Al_2O_3 \cdot (2-6)SiO_3$ ) and strong acid salt ( $M_2SO_4$ ). Years after Glukhosvky, researches on alkali activated cement went out of minds. After the firing that occurred in France between 1970 and 1973, a French researcher known as Davodovits undertook research on numerous aluminosilicates based on formulations and came out with the term “geopolymer”. The investigations of this French author gave to the alkaline cement, an exponential interest along the scientific community. Since 1990, alkali activation research has grown dramatically in all corners of the globe, with more than 100 active research centres (academic and commercial) now operating worldwide, and detailed research and development activity taking place on every inhabited continent. Much of these work have been based around the development of materials with acceptable performance, based on the particular raw materials which are available in each location. There are a very large number of technical publications available in the literature which report the basic physical and / or microstructural properties of alkaline binders derived from specific combinations of raw materials and alkaline activators [15,16].

### **I.1.2. Types of alkaline cement**

Alkaline cements are divided into two major categories: geopolymers and alkali activated materials. This distinction causes some ambiguities among scientists. The RILEM society (International Union of Testing and Research Laboratories for Materials and Structures) consider geopolymers as subset of alkali activated materials meanwhile the Geopolymer Institute along with some scientists assert that geopolymers are not alkali activated materials [15,17,18]. Whatsoever, by just relying on the type of starting materials (aluminosilicate raw material and alkaline solution) and procedure used for both synthesis, geopolymer and alkali activated material can be considered as one. However, the main difference is located on the end products.

- Geopolymers are said to be ceramic like inorganic polymer produced at low temperature, generally below 100 °C. They are mainly consisting of amorphous or semi-disordered tri-dimensional aluminosilicate network structure. Obtained through alkaline or acid activation, they



possess zeolite like structure resulting from the polycondensation of either various alkali-aluminosilicates or phosphate-aluminosilicates. Thus, geopolymers comprise several molecular units: silico-oxide (Na,K)-(-Si-O-Si-O-) for (Na,K)-poly(silicate) or (Na,K)-poly(siloxonate), silico-aluminate (Na,K)-(-Si-O-Al-O) for (Na,K)-poly(sialate), ferro-silico-aluminate (Na,K)- (-Fe-O-Si-O-Al-O-) or (Na,K)-poly(ferro-sialate), alumino-phosphate(-Al-O-P-O-) for poly(alumino-phosphate), that can be formed in a geopolymerization process [19]. The binding phase present is almost exclusively aluminosilicate and highly coordinated. Thus, to form such network structure, it is essential to use low calcium aluminosilicate raw materials. The high coordination in geopolymer materials provides the latter with high resistance to leaching effects in aggressive environments and to fire.

- Unlike above, alkali activated materials are obtained by the reaction between alkali metal source with a calcium rich aluminosilicate powder. The presence of high calcium content enables the formation of chain-like-structures rather than a pseudo-zeolitic one. Therefore, the binding phases formed in alkali activated materials consist of hydrated products such as C-A-S-H (calcium aluminosilicate hydrate) and/or C-S-H (calcium silicate hydrate) [15].

### **I.1.3. Chemistry of alkaline cement**

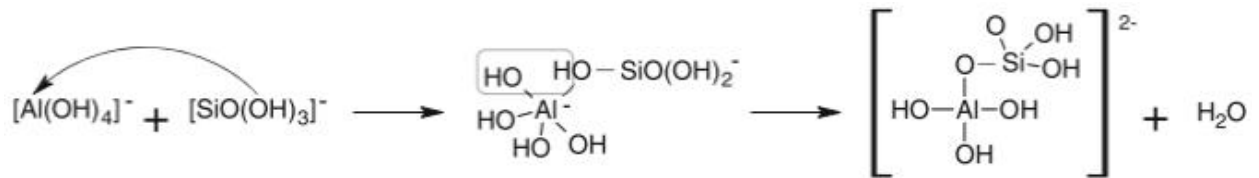
The process used for the synthesis of alkaline cement is known as the soil-gel process. This is a method which enables the synthesis of materials from molecular precursors in aqueous medium at ambient temperature. There exists a wide range of aqueous medium which can be used for the purpose. However, the activation of solid precursors in the reactive medium requires high pH in order to achieve an alkaline cement material with remarkable properties. So, the choice of an appropriate alkaline activator is necessary. Sodium hydroxide or a mixture of sodium hydroxide and silicate are highly recommended for the synthesis of alkaline cement. In general, the reaction mechanism involved in alkaline cement synthesis is similar to the knowledge achieved on zeolite and is known to be divided into three steps which are as follows:

- (1) Dissolution of solid precursors: this step is the major one among all and starts when solid precursors present in aluminosilicate raw material get in contact with alkaline solution. It consists of liberating the polymer forming species in the reaction medium through the breakdown of Ca-O, Mg-O, Si-O-Si, Si-O-Al and Al-O-Al bonds present in the reactive

phase. This breakdown is assured by the hydroxyl ions, and it is easily and highly achieved at higher pH.



- (2) Coagulation-polycondensation: the accumulation of dissolved ion precursors causes their interaction among them followed by the condensation process to form oligomers. Within this step, ion precursors condense depending on the pH and the stability of different precursors in order to obtain a more stable oligomers according to the Si / Al ratio. In this step, water molecules consumed during dissolution are released.



- (3) Polycondensation and crystallization: this is the last step which consists in the polymerization between oligomers and monomers followed by their reticulation and networking formation or crystallization in bigger molecules of polysialate with the 3 D framework.

Though this synthesis mechanism is general to all starting materials, some specificities concerning the structure and composition of the final binding phases characterising the type of alkaline cement formed, whether geopolymers or alkali activated materials. The difference resides on the choice of the aluminosilicate raw material which is either calcium rich or free aluminosilicates. Thus, the resultant binding products can either be calcium rich hydrated product bearing low crosslinking within the phase (alkali activated materials) or can just be siloxo-aluminate phase with high connectivity (geopolymers) depending on the precursor.

The synthesis of alkali activated materials requires calcium rich precursors such as blast furnace slag, class C fly ash, cement kiln dust and bottom ash. The main binding product formed is C-A-S-H (calcium aluminosilicate hydrate) or C-(N)-A-S-H (calcium sodium aluminosilicate hydrate) type gels with a disordered tobermorite-like type structure (Figure 1). This is accompanied by the formation of various types of C-S-H (calcium silicate hydrate) gels which are precipitated as

secondary products [20,21]. Sometimes, other secondary products such as hydrotalcite, aluminoferrite-mono phase (AFm) and zeolites (gibbsite and garronite), whose precipitation depend, in one way, on the type of activator, and in the other way, on the SiO<sub>2</sub>, Al<sub>2</sub>O<sub>3</sub> and MgO contents in the reactive medium, are also formed [20,22]. The C-A-S-H type gel is poorly crystalline when the starting material is activated with silicate solution than with sodium hydroxide [21]. Regarding Engelhardt description which best presents the connectivity in alkaline cement through the Q<sup>n</sup>(mAl) notation where Q represents a tetrahedral site with Si atom at the centre, n= 1 to 4 the coordination number of the Si centred while m and (n – m) are numbers of neighbouring Al and Si respectively, it has been revealed using the <sup>29</sup>Si and <sup>27</sup>Al Mass NMR analyses that the main binding phases in alkali activated materials have site connectivities ranging from Q<sup>1</sup> to Q<sup>3</sup> and varying degree of Al substitutions. The most preponderate are the Q<sup>2</sup> and Q<sup>3</sup> sites as presented in Figure 1 [15].

Contrary to the above paragraph, the synthesis of geopolymers requires as starting materials, low or free calcium aluminosilicate such as calcined clay, class F fly ash and mineral wastes with high silica and alumina contents. So, the geopolymer binder structures are constituted of silicon-oxo-aluminate units (abbreviated “sialate”), a combination of only SiO<sub>4</sub> and AlO<sub>4</sub> compounds tetrahedral linked by sharing of the oxygen atoms. This combination of tetrahedrons leaves room for the formation of a highly disordered and cross linked tri-dimensional polymer in which water molecules are trapped within the network. Some authors identify this main reaction product in geopolymer as sodium aluminosilicate hydrate (N-A-S-H) [21,23]. However, this appellation is full of contradiction since water is not a major structural component. Unlike alkali activated materials, the nuclear magnetic resonance revealed that geopolymer structures are predominated by Q<sup>4</sup> (m Al)-type of environments (Figure 2) in which the distribution of m values depends on the Si / Al ratio of the gel. The concentration of Q<sup>3</sup> sites is low in well-cured binders with hydroxide or low- or moderate-modulus silicate activators. A higher silicate concentration is required before these sites are notable in well-cured materials, although they are certainly present at early age at all Si / Al ratios [21]. These indicate the high degree of connectivity in geopolymer, and thus, reason of its high resistance to fire and to leaching in aggressive medium. Depending on the Si / Al ratio, Davidovits identified several geopolymer binder types such as polysialate (Si / Al = 1), polysialate-siloxo (Si / Al=2), polysialate disiloxo (Si / Al = 3) and polysialate multisiloxo (Si / Al > 3) [24]. Recently, it has been shown that in some circumstances, Fe atoms can replace Al atoms

in binder structure in certain extent, to form a polysialate binder type having ferro-silico-aluminate units [9,23,25,26].

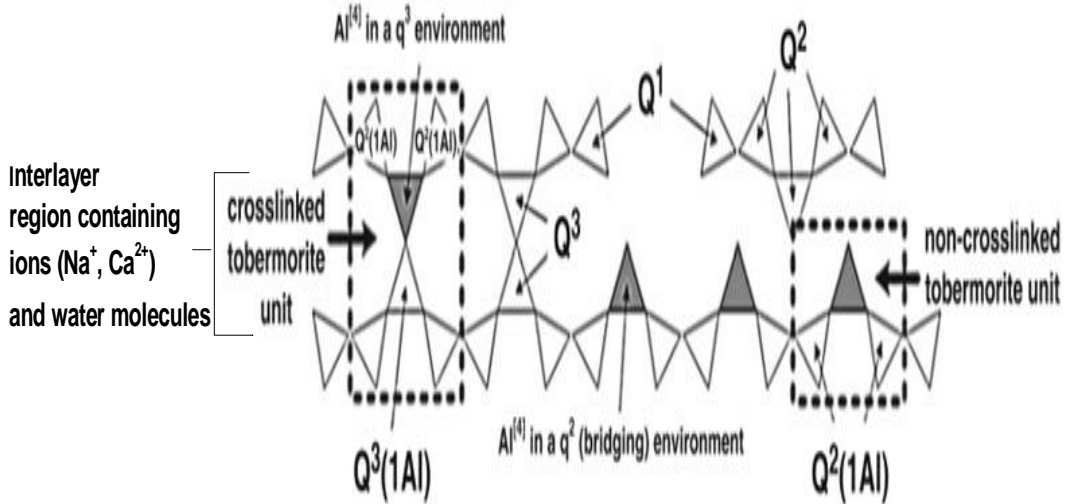


Figure 1: Schematic representation of cross linked and non-cross linked tobermorite structures which represent the generalised structure of the C-(N)-A-S-H type [15].

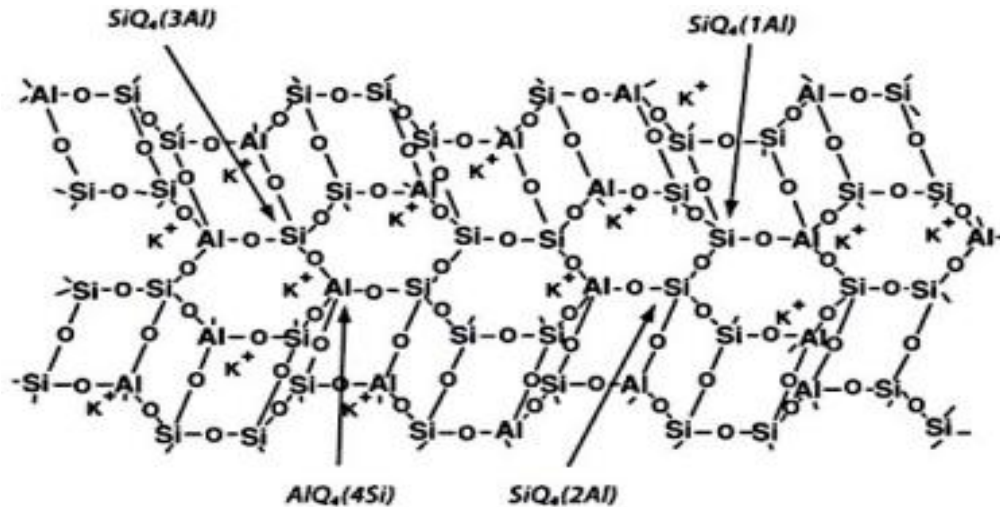


Figure 2: 3D geopolymer network [17]

#### I.1.4. Raw materials and their reactivity in alkaline medium

Generally, all materials containing large amount of  $\text{SiO}_2$  and  $\text{Al}_2\text{O}_3$  entities can be a potential raw material for the synthesis of alkaline cement. However, the latter oxides must be capable of undergoing dissolution in reactive medium. Additional oxides such as  $\text{CaO}$  and  $\text{Fe}_2\text{O}_3$ , if present

in the reactive phase of the starting materials, also contribute in the development of cementitious properties (setting, mechanical strength, and durability) in alkali activated cement synthesis. From this point of view, a wide range of geological rocks, mineral by-products and industrial wastes are potential raw materials. So far, a great number of raw materials have been investigated for alkaline cement synthesis around the world. In general, these raw materials are commonly known as aluminosilicate raw materials. It is worth noting that, beside the chemical composition, the choice of aluminosilicate raw materials for alkaline cement synthesis is based on local availability, even though their reactivity in alkaline medium remains the major parameters to be considered. The degree of reactivity of aluminosilicate raw materials relies on their dissolution capacity in alkaline medium. Some raw materials possess dissolution facilities than others either at ambient temperature or slightly elevated which may vary from one alkaline solution source to another. Many studies have presented the diversity that exist as far as sources of aluminosilicate raw materials are concerned, their origins and their implications in alkaline cement synthesis. However, in this thesis, review will be focused on the most prominent raw materials used in alkaline activation. In general, regarding their origins, aluminosilicate raw materials can be categorized into two groups which are natural and synthetic aluminosilicates

#### **I.1.4.1. Natural aluminosilicates**

These are natural occurring raw materials obtained through natural phenomena (alteration, volcanism, erosion, etc.). The most commonly used in the synthesis of alkaline cements are:

##### **a) Kaolin and kaolinite clay**

These are terms used to describe a group of relatively common clay minerals dominated by kaolinite mineral. However, Kaolin is said to be whiter, sandier and less plastic than kaolinite clay. Regardless of latter difference, both are mainly composed of fine-grained plate-like particles. They are formed when the anhydrous aluminium silicates which are found in feldspar-rich rocks, like granite, are altered by weathering or hydrothermal processes. The process which converts the hard granite into the soft matrix found in kaolin pits is known as "kaolinisation". The quartz and mica of the granite remain relatively unchanged whilst the feldspar is transformed into kaolinite.

Kaolin or kaolinite clay uses are multiple and diversified. Their whiteness and plasticity make them extremely suitable for their extensive use in the cosmetics, pharmaceutical, paint, paper, rubber, plastics and ceramic industries. In the cement industry, they are used among others as a precursor in the synthesis of clinker, the main component of Portland cement. Their high  $\text{Al}_2\text{O}_3$  and  $\text{SiO}_2$  contents make them suitable for alkaline cement synthesis, but, their degree of crystallinity influences their dissolution in alkaline medium. This is observed through long setting time, low strength and low durability. The synthesis of kaolin or kaolinite clay based alkaline cement at ambient temperature is almost not feasible, thus justifies the low number of publications on the domain. Some studies like that of C. Heah et al. (2011) revealed that increased in temperature favours strength development in Kaolin based geopolymer products. Furthermore, they also noticed that prolonged curing time enhanced geopolymerization process and yielded more strength [27]. The same trend is achieved while increasing the concentration of sodium hydroxide solution (6-12 mol / L) [28]. To palliate the low reactivity of kaolin and kaolinite clay, some curing conditions such as high curing temperature, pre-treatment (mechanical activation, thermal activation, etc.) are necessary to enhance their low dissolution [27–29].

#### **b) Volcanic ashes**

These are by-products of volcanic eruption. They are fragments of pulverized rocks, minerals and volcanic glass. Commonly known as natural pozzolana, volcanic ashes are multi-form particles that possess porous structure and various colours depending on their chemical composition. The bulk chemical composition of volcanic ash is characterised by high amounts of  $\text{SiO}_2$ ,  $\text{Al}_2\text{O}_3$ ,  $\text{Fe}_2\text{O}_3$  and  $\text{CaO}$ , associated with minor quantities of  $\text{MgO}$ ,  $\text{Na}_2\text{O}$ ,  $\text{K}_2\text{O}$ ,  $\text{TiO}_2$  and trace quantities of many other elements [4]. Obtained from natural phenomenon, this ash presents some negative effects on human beings. When inhaled, they cause serious damage in lungs and can be deadly for people suffering from asthma and chronic lung diseases. Therefore, the massive use of this ash will be beneficial for the reduction of environmental issues and the rapid reconstruction of devastated area caused by volcanic eruption.

Volcanic ash has a wide range of applications. In agriculture, they are used as conditioner to increase soil porosity. When mixed with soil, it helps in the retention of moisture, and acts as a feeding regulator for liquid fertilizers. The agricultural applications of volcanic ash range from small flowerpots to commercial farms and fruit groves. Moreover, they are used in tanks for the

hydroponic cultivation of vegetables in greenhouses. Also, it is used as an abrasive for cosmetic skin buffing stone washing fabric hand soap [4]. Beside the aforementioned, volcanic ash is hugely used in the construction sector, rather as aggregates in concrete or as an admixture in blended cement. Regarding their ability to react with CaO to form a binding phase (C-S-H gel), volcanic are used as substituent to clinker (30-35% wt) in order to lower the cost of production of Portland cement. Simultaneously, this leads to the reduction of clinker production and greenhouse gas emission [30]. However, this practice seems not enough to impact on pollution issues. Hence, there is a need to develop alternative cement which is more respectful to the environment. Many reported studies have proven the used of volcanic ashes as a potential raw material in the synthesis of alkaline cement due to their high silica and alumina content. Depending on the source, some of their cement based products express acceptable cementitious properties as far as setting time, compressive strength and durability are concerned. Volcanic ash expresses optimum reactivity when activated with a mixed solution of sodium silicate and sodium hydroxide (12M) in which the silicic modulus ( $\text{SiO}_2 / \text{Na}_2\text{O}$ ) is equal 1.4 [3,9] to produce alkaline cement, but in some circumstances, requires high concentration of sodium hydroxide solution (15M), high temperature (60 or 80°C) and a calcium rich source to produce alkali activated materials [31]. Hence, the reactivity of volcanic ash in alkaline medium vary from one volcanic source to another, and in general, it is very low compared to synthetic raw materials (metakaolin, blast furnace slag, etc.). This must be majorly related to varied glassy phase content and composition [8,9]. Moreover, other parameters such as specific surface area of particles, clay content, silicic modulus and curing temperature, also affect this reactivity [3,32]. Djobo et al. (2016) studied the reactivity of volcanic ash by determining the amount and composition of the glassy phase along with total heat released using ICP-OES and isothermal conduction calorimetry (ICC) analyses respectively. They reported low reactivity of volcanic ash which was expressed by low dissolution capacity of the latter in alkaline solution as well as low heat released during geopolymerization [9]. In order to alter this low reactivity, some authors successfully suggested several scientific processes (alkaline fusion, blending and mechanical activation) which were just applied to volcanic ashes with reactive phase content  $\leq 30$  % by mass [5,31,33,34]. Most of these processes are energy depending and costly. Later on, Djon Li Ndjock et al. (2017) studied the rational utilization of volcanic ashes in alkaline activation by using diverse sources of volcanic ash. Upon their study, the authors came out with the conclusion that the amount of glassy phase and  $\text{SiO}_2 / \text{Al}_2\text{O}_3$  molar ratio of glassy phase were

the criteria to be taken in to consideration when choosing volcanic ash for alkaline cement technology [8]. Based on that, they suggested a scale of selection as shown in Figure 3 (**A** = volcanic ash that can be used for alkaline cement synthesis, whereas **B** = volcanic ash that must be used as filler). Regardless of the reactivity, volcanic ash possesses environmental and economic assets as far as climatic and socioeconomic aspects are concerned and that, due to its natural aspect and availability. Thus, it will be worthy to lay more interest on this raw material, mostly in developing countries.

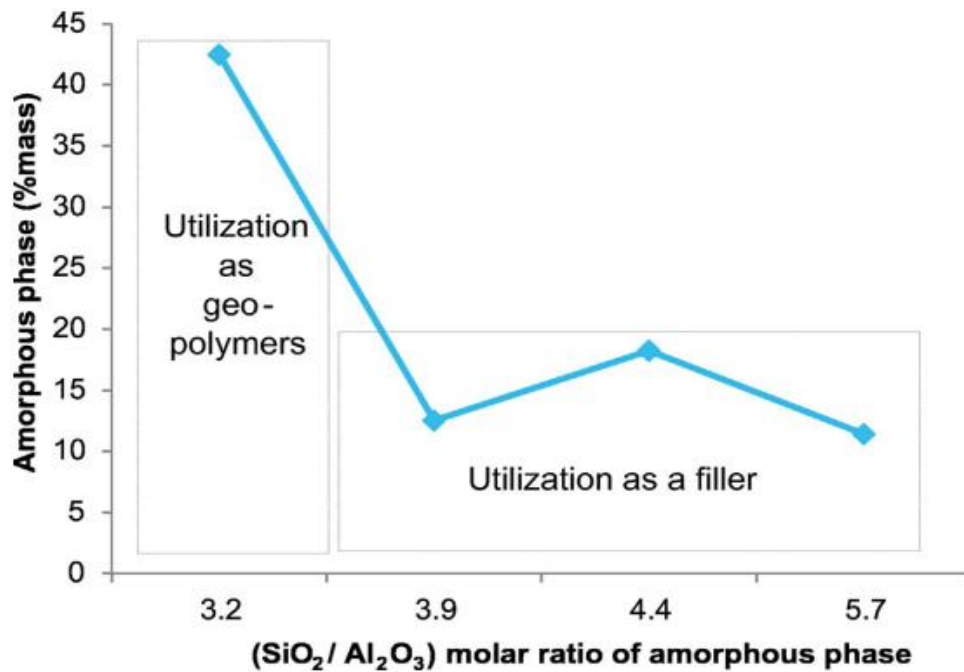


Figure 3: Chart summarising the rational utilisation of volcanic ashes [8].

### c) Laterites

Laterite is an iron rich aluminosilicate raw materials made from kaolinite in which high amount of Al<sup>3+</sup> ions are replaced by Fe<sup>2+</sup> or Fe<sup>3+</sup> ions. In general, they are formed in areas of high fluctuation humidity and temperature, where soils with kaolinite in the presence of iron minerals undergo gradual corrosion to form hardened matrices generally called indurated matrices [35,36]. These indurated matrices are typified according to their alumina (gibbsite and boehmite) and iron minerals (goethite and hematite) content mixed with disordered or less crystallized kaolinites [36,37]. Some impurities such as amorphous silica and quartz are generally present. Laterite soil is highly abundant in tropical and subtropical regions such as Africa, South America and Australia [38]. Due to this abundance and its ability to hardening upon exposure to wetting and drying, the





Mainly constituted of aluminium and silicon oxides, many authors have observed that in the distorted structure of metakaolin, aluminium atoms possess 4, 5 and 6 coordination while silicon atoms are either in the form of amorphous silica ( $Q^4$  site) or in a mixed form of  $SiO_4$  linking the tetrahedrons to 1 or 2 aluminium atoms ( $Q^4(1Al)$  site). In some cases, some silicon atoms still possess hydroxyl groups. All these observations were done when kaolinite was subjected to heat treatment at different temperatures [42]. This implies that the degree of disorder in metakaolin structure vary and depends on the transformation parameter (i.e. temperature of calcination). Thus, this impacts its degree of reactivity in alkaline medium. Many authors suggested 700 °C and temperature rate increase of 1°C / min as the appropriate parameter to obtain a well disordered metakaolin [43,44]. Because of its high pozzolanic activity, metakaolin is most at time used in civil engineering as a partial substituent to Portland cement in order to reduce the  $CO_2$  emission generated by the production of Portland cement. Its incorporation in cement mixtures favours the hydration of anhydrous cements. It brings in the formation of closed porosity favourable for mechanical strength and durability of cement matrix due to the high amount of C-S-H gel formed and lack of interconnected pore [45,46].

The research for an alternative binder to Portland cement has revealed interesting characteristics of metakaolin when used in alkaline activation. In the alkaline cement technology, metakaolin can be used as the main raw material. Compared to other aluminosilicate raw materials, up to now, this raw material seems to be the best for alkaline cement synthesis, in particularly for geopolymer since it is Al and Si rich and possesses high dissolution in alkaline medium [21]. This high dissolution is more pronounced in NaOH than in KOH [47]. Also, metakaolin provides a synthesis medium for geopolymer cement at ambient temperature. Its high Al content provides short setting time to the cement pastes and favours the early strength development. The fact that metakaolin is almost composed of Al and Si atoms with the absence of Ca atoms, it is an adequate raw material for geopolymer synthesis since its Al atoms content assures a good cross-linking within the binding gel. Raison to this, they are used, in some circumstance, as additive to other raw materials to enrich the reactive medium and to fight against efflorescence [5,48].

#### **b) Blast Furnace slag (BFS)**

Blast Furnace Slag is a by-product of the manufacturing of iron in a blast furnace where iron ore, limestone and coke are heated up to 1500 °C. When these materials melt in the blast furnace, two

products are produced molten iron, and molten slag. The molten slag is lighter and floats on the top of the molten iron. Thus, it is been collected and cooled. The cooling system quenches the molten slag and solidifies it to form particles with diameter generally not larger than 5 mm. The resulting slag is either highly or lowly crystalline depending on the cooling method and comprises of silicates and alumina from the original iron ore, combined with some oxides from the limestone [49]. BFS is constituted of a quaternary system of CaO-MgO-Al<sub>2</sub>O<sub>3</sub>-SiO<sub>2</sub>, with additional oxides of Ti, S and Mn depending on the chemical composition of the iron ore. Different forms of slag products are produced depending on the method used to cool the molten slag. These products are as follows:

- Air-cooled blast furnace slag (ACBFS) commonly known as blast furnace rock slag obtained from air cooling system at ambient temperature;
- Expanded or foamed slag obtained from a cooling and solidifying system with controlled amount of water and air or steam;
- Pelletized blast furnace slag (PBFS), the molten slag is cooled and solidified with water and air quenched in a spinning drum, pellets.
- Granulated blast furnace slag (GBFS) obtained from water quenching process.

Among the above mentioned slags, granulated blast furnace slag (GBFS) is most widely used for the production of alkali activated materials due to its composition and its high vitreous phase content with little or non-crystalline phase. Thus, when ground, GBFS possesses more cementitious properties than the rest, which make it a suitable admixture to Portland cement [50]. It provides some advantages when partially replaced to Portland cement such as good workability, increase in setting time with reduced bleeding and high resistance to sulphate attack and alkali-silica reaction [51].

In alkaline cement technology, ground granulated blast furnace is presented as one of the best raw material for alkali activated materials. GBFS based alkali activated materials present fast setting time and high compressive strength with a binding structure, most of the time, composed of C-S-H, C-A-S-H and hydrotalcite-like phases (Mg<sub>6</sub>Al<sub>2</sub>CO<sub>3</sub>(OH)<sub>16</sub>·4H<sub>2</sub>O) [20,22,52]. Whatever, this composition largely depends on GBFS composition and glassy content. Certain investigations revealed that MgO and Al<sub>2</sub>O<sub>3</sub> contents in the latter play a major role in strength development in alkali activated materials. According to many authors, increase in MgO content to about 18% in

GBFS results to faster reaction and to high compressive strength as a consequence of the formation of hydrotalcite type product when GBFS is activated with  $\text{Na}_2\text{SiO}_3$  solution. However, when activated with NaOH solution, only a slight change in compressive strength was observed in relation to MgO content. Moreover, the increase in MgO content lowered Al uptake by C-S-H to form C-A-S-H [22]. On the other hand,  $\text{Al}_2\text{O}_3$  content in GBFS behave reversely, in exception to NaOH activation where no influence is noticed. Increasing  $\text{Al}_2\text{O}_3$  content (from 7 to 17 % wt) in GBFS leads to decrease in Mg/Al ratio of hydrotalcite, along with the formation of strätlingite ( $\text{C}_2\text{ASH}_8$ ) due to Al incorporation in the C-A-S-H type product. This variation slows down the hydration process and causes a drop in early strength. Besides that, after 28 days of curing,  $\text{Al}_2\text{O}_3$  variation in slag is found to have no significant impact on the late compressive strength of the  $\text{Na}_2\text{SiO}_3$  activated slags [20]. Like metakaolin, GBFS is also used as adjuvant to low reactive aluminosilicate raw materials in the synthesis of alkaline cement [6].

### c) Fly ash

Fly ash is a heterogeneous and complex residue resulting from coal combustion in coal fired power plant. Its morphology is characterized by solid or hollow spheres, consisting essentially of a vitreous phase and a few minority of crystalline phases such as quartz (5%–13%), mullite (8%–14%) and magnetite (3%–10%) [53]. Fly ash is composed of  $\text{SiO}_2$  as the major oxide, and  $\text{Al}_2\text{O}_3$ , CaO,  $\text{Fe}_2\text{O}_3$ ,  $\text{TiO}_2$ , MgO,  $\text{K}_2\text{O}$  and  $\text{Na}_2\text{O}$  as secondary oxides. Anyway, this composition varies depending on the type of coal (anthracite, bituminous, subbituminous and lignite) used and the incineration process in place at the power plant. Its colour vary from light bronze to grey to black, depending on the amount of unburned carbon in the ash. The colour reflects the carbon content in fly ash, the lighter the colour of fly ash, the lower the content of carbon. Also, The specific gravity of fly ash usually ranges from 2.1 to 3.0 [54]. Based on Ca content, fly ash is categorized into two classes known as class C for Ca rich fly ash (produced from lignite and subbituminous coals) and class F for low Ca fly ash (mostly produced from bituminous coal) [55]. These ashes find their application in civil engineering. Fly ash has dominantly been the primary contributor to the cement industry because it is used either as a raw material or as an additive in cement manufacturing. Due to its inherent pozzolanic characteristics, it is used to partially replace clinkers in ordinary Portland cement [56,57]. Moreover, it is used as a soil stabiliser owing to its ability to reduce soil's affinity to absorb water and thus prevent soil swelling [58].

Recent developments have shown the potentiality of fly ash as a raw material for alkaline cement synthesis. Like all aluminosilicate raw materials, its reactivity in alkaline medium varies according to the activation solution. Even though, its amorphous phase composition is more concerned since the crystalline phases remain inert in alkaline solution. In general, fly ashes possess a very stable amorphous phase which renders its dissolution in alkaline medium very slow at ambient temperature, then resulting to low compressive strength at early ages. To overcome this, curing temperatures ( $\geq 75$  °C) are always needed. On the other hand, Ca rich fly ash (class C) exhibits very short setting time while that of class F is too long. The setting characteristic of fly ash based alkaline cement can be adjusted by using other pozzolana such as ground granulated blast furnace slag [59]. Also, this can be done with accelerators or retarders. Lee and van Deventer (2002) observed that Ca and Mg salts can accelerate the setting time of KOH / Na<sub>2</sub>O·SiO<sub>2</sub>-activated Class F fly ash pastes through solid dissolution. The authors also found that K salts delayed setting only when the initial activating solution was low in soluble silicate. Furthermore, the right composition of Cl, CO<sub>3</sub><sup>2-</sup> and NO<sub>3</sub><sup>-</sup> salts could also retard the setting [60]. Some accelerators and retarders used for Portland cement systems are also applicable to Class C fly ash-based alkaline cement systems. Addition of gluconate efficiently delays the setting time of Class C fly ash paste with no adverse effect on strength. An addition of 1% and 2% sucrose could delay final setting time from 130 min to 210 and 230 min, respectively [61].

#### **d) Calcined laterite**

Regarding the low reactivity of untreated laterites in alkaline medium due to high crystallinity, the latter is preferentially subjected to thermal treatment so as to enhance the degree of disorder in their structure. Recently, several studies have presented the potentiality of calcined laterite as a raw material in alkaline cement synthesis, and at the same time, have revealed the implication of iron oxide in the building of a tri-dimensional binding structure poly(ferro-silico-aluminate)[25,26,62]. Among numerous studies are the investigations of Kaze et al. (2017 and 2018) which revealed the optimum conditions in which laterites can be served as an excellent raw material in the synthesis of geopolymer cement. On that, the authors achieved reduction in setting time and highest flexural strength with calcined laterite (500 °C) when mixed with alkaline solution constituted of NaOH (8M) solution and sodium silicate (volume ratio 1:1), and thereafter observed the insertion of Fe<sup>3+</sup> ion in the geopolymer network to form a ferro-sialate [23].

Afterward, the authors assessed the effect of silicate modulus ( $\text{SiO}_2/\text{Na}_2\text{O} = 0.75, 0.92$  and  $1.04$ ) on properties of geopolymers synthesized from calcined laterite at  $600\text{ }^\circ\text{C}$  [63]. Their study revealed that the shorting of setting time and the increase of compressive strength vary with the decrease in silicate modulus with  $0.75$  as the best  $\text{SiO}_2/\text{Na}_2\text{O}$  molar ratio. During this assessment, they noticed the partial dissolution of some iron rich minerals (ilmenite, maghemite, and hematite) in alkaline medium followed by the formation of new crystalline phase such as fayalite, siderite and thermonatrite. Next to this, Kaze et al. (2018) tried to equilibrate Al/Si and Fe/Si molar ratios in laterite based geopolymer cured at  $90\text{ }^\circ\text{C}$  with the help of rice husk ash in order to improve their engineering properties. On this, the high mechanical properties obtained were associated to the formation of mixed phases such as iron silicate, polysialate and ferro-sialates [64]. Based on all these investigations and the abundance of laterite soil in the world, laterite seems to be high potential supplementary raw material for the synthesis of eco-friendly low cost building materials.

## **I.2. Techniques for increasing reactivity of aluminosilicate raw materials**

### **I.2.1. Mechanical activation**

It is a disintegration process whereby high solid materials are broken-down to fine particles in order to satisfy technology requirements. This is done with high energy milling without any change in chemical composition. In case the activation leads simultaneously to change in composition, this will be known as mechanochemical activation. In other words, mechanical treatment is a method that increases the reactivity of solid material by increasing the disordering of crystal phases and by generating defects or other metastable forms that cause decrease in activation energy barrier for the process. The primary effect of mechanical activation is the reduction in particle sizes, causing changes in physical properties such as particle size distribution, specific surface area, surface energy and phase composition. The mechanism of transformation occurring during mechanical activation of materials can be divided into three main stages, which depend on the degree of dispersion and grinding time. These stages are as follows [65]:

- At stage 1, grinding process takes place relatively quickly leading to particle size reduction and increase in specific surface area. The energy consumed during grinding is proportional to the particle surface area produced. This stage is referred to as Rittinger's stage.
- At stage 2, as grinding continuous, the number of small particles increases. The number of flaws and pores decreases and the grinding resistance of the material increases.

Simultaneously, the particles begin to adhere to surfaces of grinding media and mill, as well as to each other. The energy used for size reduction is no longer proportional to the increase in surface area. Despite this nonlinearity, the increase in dispersion can still be remarkable. This is considered to be the aggregation stage.

- At stage 3, after reaching a certain fineness, further grinding leads to decrease in the degree of dispersion in certain materials. This stage is known as agglomeration and it is mostly characterized by crystal structural and mechanochemical changes.

This activation can be performed using mills, which are of different characteristics. However, the efficiency of the activation process relies on many factors such as type of mill, types of grinding media such as balls, rods or other shapes, material of milling media (stainless steel, tungsten carbide, zirconium oxide, aluminium oxide, silicon nitride), grinding atmosphere (air, inert gas, reductive gas, wet or dry milling atmosphere), fill level of the milling chamber, ball-to-powder ratio (BPR), grinding temperature, speed of the mill and grinding time [66].

Mechanical activation has shown its positive impact in many research studies as far as enhancement of the reactivity of low reactive raw materials for cement synthesis is concerned. For instance, the use of mechanically activated fly ash, volcanic ash and kaolin for alkaline cement synthesis have shown prominent improvement of properties in final products. Many authors revealed a high degree of reactivity of low reactive raw aluminosilicate materials when mechanically activated [29,67]. With fly ash, Kumar et al. observed that the increase in reactivity is related to the reduction in median particle size to less than 5-7  $\mu\text{m}$  [68]. According to Musci et al. (2015), the reactivity of mechanically activated lignite fly ash in stirred media mill depends on the milling time up to a certain fineness. They noticed that extreme fineness, due to a prolonged duration of grinding, decreases mechanical properties [69]. Besides that, Djobo et al. (2016), while mechanically activating low reactive volcanic ash, observed a change in crystallinity followed by mechanochemical reaction between volcanic ash grains and atmospheric carbon dioxide. Moreover, the authors, in non-conformity to other studies, observed that the degree of reaction is more pronounced at ambient curing temperature than at elevated temperature [33]. Furtherly, on more soft raw material such as Kaolin whose hardness according to Mohs scale is lesser than 4, mechanical activation was less efficient [29]. Nevertheless, mechanical activation may be

considered as a suitable method for improving the reactivity of low reactive aluminosilicate raw materials.

### **I.2.2. Physical separation**

Activation by physical separation of particles is a technique used to maximise reactive content in solid precursors by reducing the amount of unreactive particles. This method is achieved with the help of techniques such as air classifier, flotation, sieving, sorting, clarification and magnetic separation, and is highly used in mineral processing [70,71]. In cement technology, it has shown that precursor can be tailored in order to achieve desired properties. For instance the use of sieving and magnetic separation on fly ash particles in order to improve cementitious properties of blended Portland cement [70,72,73]. On the other hand, many attempts on activation by separation method in the synthesis of alkaline cement have also been reported by many authors. On these, separation method yielded modifications such as bulk chemical and mineralogical compositions, pH and particle size distribution [74]. So, it has been revealed that among separated particles of calcium rich fly ash in alkaline medium, finer ones expressed low setting time and improved compressive strength and drying shrinkage [75]. Similar trend was observed by Kumar et al while working on low calcium fly ash. On theirs, they noticed low quartz content in fine particle and thermonatrite formation compared to coarse particles [76]. Whatsoever, according to comparative study, the latter technique seems less efficient than mechanical activation in alkali activation [77].

### **I.2.3. Thermal activation**

Thermal activation is a process whereby low reactive aluminosilicate raw materials are subjected to heat treatment (calcination) at high temperature in order to increase its reactivity in a particular medium. Generally, aluminosilicate raw materials are high crystalline materials. These materials possess very low degree of dissolution in alkaline medium. Therefore, in order to increase this dissolution, the latter are calcined at precise temperature to change their crystalline structure to an amorphous one. This method is mostly applied to aluminosilicate raw materials rich with hydroxylated crystalline phases or minerals. A good example is kaolinite with its sheet structure within which structural water is present. When subjected to thermal treatment, Kaolinite loses this structural water to obtain a disordered structure known as metakaolinite. Many successful



studies have been carried out among which the investigation done by Elimbi et al. (2011) who proved that 700 °C is the best temperature to obtain a well disordered metakaolin necessary for alkaline cement synthesis [43]. Additionally, the degree of disordering was also dependent of the rate of calcination which was to be 1 °C/min for Kaolinite [44]. Moreover, other aluminosilicate raw materials which require thermal treatment before alkaline activation are laterite and halloysite at 500 and 600-750 °C respectively [23,78,79].

#### **I.2.4. Chemical activation**

Chemical activation refers to the use of admixtures to impact the properties of cement based products. In general, this deals with the incorporation of chemical in material system in order to modify the reactivity of cementing materials. The used of admixtures leads to the improvement of cementitious properties such as workability, acceleration or retardation of setting time, strength development and durability of concretes. In cement technology, the chemical activation can be regarded base on two aspects such as the type of admixture and the route of administration:

➤ Type of admixture

a) Cement admixtures

These are materials other than cement, aggregates and water, which are generally used in low proportions as a single functionality additive in order to improve specific properties such as setting, mechanical strength, permeability, workability and durability. For many decades, several types of admixtures are been used in concrete technology, and are broadly categorized as chemical and mineral admixtures.

- Chemical admixture

Chemical admixtures refer to manufactured products added to concrete mixing with the aim to modify specific properties of fresh or hardened concretes or in, some cases, both. They are generally water soluble and are effective at low dosage in concrete. Such products are categorized into five groups depending on their contribution which can occur at the early age of the hardening processes or later. The categorization is as follows [80]: accelerators (admixture used to increase the setting rate of cementing materials); retarders (admixture used to slow down the hardening process of cementing materials); plasticizer or superplasticizer (it reduces water consumption and increases the workability of fresh cement pastes and mortars); and Air-entraining admixture

(pore-forming agents used to facilitate the development of stable air-void system within concrete in order to improve their durability to freezing and thawing cycles).

- Mineral admixture

Mineral admixtures are natural occurring additives, industrial and other waste by-products used in cement technology to obtain specific engineering properties of cement mortars and concretes: increase in strength, reduction in water demand, permeability, low heat of hydration, improved durability, correcting deficiencies in aggregate gradation (as fillers). They are principally constituted of  $\text{SiO}_2$ ,  $\text{Al}_2\text{O}_3$  and  $\text{CaO}$  necessary for their binding properties. Also known as supplementary cementing materials (SCM), they attract a lot of attention due to the economic benefit and environmental assets. Unlike chemical admixtures, these admixture are available in abundance at a much lower cost and are used in relatively large amounts as replacement of cement and/or of fine aggregate in concrete. Mineral admixtures are mostly pozzolanic materials and some even possess self cementitious properties in addition to being pozzolanic [55]. Based on that, these materials are grouped into five classes such as: cementitious (mineral additive, when finely grind, possess the ability to self-harden in the presence of moisture); cementitious and pozzolanic (Calcium rich materials that have both the capacity to self-compact and to undergo pozzolanic reaction when mixed with cement in the presence of moisture); highly pozzolanic (materials consisting essentially of pure silica in non-crystalline form); normally pozzolanic (materials rich with silicate glass containing Aluminium, iron and alkalis. Like highly pozzolanic, they possess no cementitious properties when exposed to moisture); and weak pozzolanic (materials consisting essentially of crystalline silicates minerals, and only small amount of non-crystalline matter).

It is important to highlight that the above classification is mainly related to Portland cement chemistry. For the moment, there exist no similar specific classification based on alkaline cement chemistry. Nevertheless, regarding the chemical compositions and studies conducted on almost all the raw materials that fit the latter classification, it is highly noticed that all the latter are suitable for the synthesis of alkali activated cement.

➤ Route of administration

The use of admixture in the synthesis of alkaline cement is of a wide range related on expected outcome which thereby depends on the route of utilization. Many studies have reported the use of the latter in the synthesis of alkaline cements along with their effects on cementitious properties [5,61,81–85]. It will be wrong to just highlight the type of admixture without mentioning the different ways they are used. Based on studies reported, there exist two routes of utilisation of admixture in the synthesis of alkaline cement depending on the type of the admixture which can be either chemical or mineral as mentioned earlier above. Hence, the different routes are alkali fusion and blending.

a) Alkali fusion

This is a pre-treatment method based on the decomposition of an aluminosilicate raw material in the presence of chemical admixture through thermal treatment at high temperature in order to increase the reactive content of a low reactive material. Among others bases, NaOH pellets remain the most commonly used admixture. In general, the procedure of alkali fusion consists of mixing aluminosilicate raw material with NaOH pellets and submitting the mixture to heat treatment at temperature of about 550 °C [34,86,87]. The method is generally used in the synthesis of zeolites. In alkaline cement, many studies have presented the positive impact of this method in different low reactive aluminosilicate raw materials. Many authors revealed that alkali fusion alter the reactivity of low reactive materials by increasing amorphous content. Using various raw materials, they got to the conclusion that alkali fusion improve properties of alkaline cement such as setting time, mechanical strength and sustainability [34,86,88]. On volcanic ash with amorphous content of about 29 % by mass, Tchakoute et al. realized that resulting properties of fused volcanic ash based geopolymer mainly depends on the  $\text{Al}_2\text{O}_3 / \text{Na}_2\text{O}$  molar ratio of the fused mixture where  $\text{Na}_2\text{O}$  content is provided by NaOH pellets, and  $\text{Al}_2\text{O}_3$  content by aluminosilicate. By varying the  $\text{Al}_2\text{O}_3 / \text{Na}_2\text{O}$  molar ratio within the range 0.06-0.77, they noticed that the highest amorphous content (76 % by mass) was achieved at  $\text{Al}_2\text{O}_3 / \text{Na}_2\text{O}$  molar ratio equal to 0.13. The latter provided an alkaline cement that possesses low setting time and shrinkage as well as high compressive strength [34]. In the same tendency, Tchadjié et al. (2015) tried to disorder granite structure for an eventual synthesis of granite based alkaline cement, and realized that amorphous content increases with increase in NaOH content.. Though NaOH of 60% by mass of granite generated the 54 % by

mass of amorphous, but it was not enough to obtain the highest compressive strength. Furthermore, they also noticed that high amorphous content in fused granite was not sufficient to obtain sustainable mortars after water stability evaluation [86]. Also, it is important to highlight besides the fact that alkali fusion process requires relatively lower calcination temperature (550 °C) than that of the formation of metakaolin and all the likes, the latter process makes use of excess of sodium hydroxide which must be consumed by adding another more reactive aluminosilicate raw material such as metakaolin [32,34,86].

#### b) Blending

In cement technology, blending refers to a conventional method used for the synthesis of mixed cementing material in order to influence cementitious properties. This method is applied depending on several reasons which can be economical, socio-political or chemical. Blending is a method that involves the combination of aluminosilicate raw material and admixture(s) by mixing two or more substances without pre-treatment such as alkaline fusion. Its application induces changes in bulk chemical composition of aluminosilicate raw material and thereby, leads to modifications of cementitious properties. In other words, this technique is used to adjust the chemical composition of reactive entities present in raw materials in order to acquire desired properties. In a more precise manner, this chemical modification mainly involves  $\text{SiO}_2$ ,  $\text{Al}_2\text{O}_3$ ,  $\text{CaO}$  and  $\text{Fe}_2\text{O}_3$  oxides contents since they are essential constituents of the binding phase in alkaline cement. Unlike alkali fusion, blending approach is an eco-friendly method commonly used due to its facility to be carried out at low or no energy demand. Furthermore, this approach favours the use of diversified sources of raw materials among which are: natural raw materials and waste products. Several successful attempts in alkaline cement have been reported on the beneficial effect of developing blending cement. In order to improve the strength of alkali activated binder developed by utilizing these high-calcium GBFS and high-silica ultrafine palm oil fuel ash (POFA), Yusuf et al. (2014) tested the incorporation of aluminium hydroxide in this mixture. They realized that the blending led to change in  $\text{SiO}_2 / \text{Al}_2\text{O}_3$ ,  $\text{H}_2\text{O} / \text{Na}_2\text{O}$  and  $\text{Ca} / \text{Si}$  ratio, and eventually, to the formation of distinctive products: calcium-silicate-hydrate (C-S-H) and Ca / Na-alumino-silicate-hydrate (C / N-A-S-H). Moreover, they observed that  $\text{Al}(\text{OH})_3$  dosage value of 4 wt% yielded the highest 3-day compressive strength [81]. Also, Songpiriyakij et al. (2010), evaluated the effect of  $\text{SiO}_2 / \text{Al}_2\text{O}_3$  molar ratio within a wide range (4.03-1035) on the compressive strength and degree of reaction of

rice husk-bark ash and fly ash based geopolymers. They came out with the conclusion that the optimum  $\text{SiO}_2 / \text{Al}_2\text{O}_3$  ratio to obtain the highest compressive strength was 15.9 and that fly ash was more reactive than RHBA. Furthermore, they added that besides the reactivity of both source materials, the quality of the achieved matrix also contributes in the enhancement of compressive strength of the alkaline cement paste [89]. Elsewhere, Kaze et al. suggested the incorporation of rice husk ash in geopolymer synthesis from iron rich precursor in order to equilibrate the Si / Al and Si / Fe molar ratios. This incorporation led to the formation of ferro-sialates (Fe / Al-S-H) and ferrisilicate gels in addition to polysialate phases (N-A-S-H) which significantly impact the engineering properties of laterites based geopolymer [64]. Concerning volcanic ash, some assessments were done. Tchakoute et al. (2012) assessed the effect of adding alumina oxide to volcanic ash and metakaolin based alkaline cement. The authors concluded that the limits dosage of  $\text{Al}_2\text{O}_3$  addition for the better improvement of compressive strength are 20% and 40% respectively in metakaolin and volcanic ash based alkaline cement [85]. Besides that, Djobo et al. (2014 and 2016) aimed compensating the low reactive content of volcanic ash in geopolymer synthesis by incorporating metakaolin, bauxite and calcined oyster shell. They realized that these incorporations are beneficial to mechanical strength and setting time as well as the prohibition of efflorescence [5,90]. Moreover, the impact of the incorporation of slag in low reactive volcanic ash based alkaline cement was also assessed. The authors revealed that slag has good effect on both setting time and compressive strength achieved by the development of coexistence gels (C-A-S-H / N-A-S-H) [4,6]. All the above studies done up to now on diverse volcanic ash sources in alkaline cement synthesis are interesting, but additional work still needs to be carried out in order to complete the gap of knowledge compared to those done on fly ash, slag and metakaolin based alkaline cement.

### **I.2.5. Curing regimes**

Depending on the processing conditions, cement based materials can exhibit a wide variety of properties and characteristics. This is due to the varied reactivity of solid precursor in the reactive medium, which leads to the formation of binding phases. With the aim to achieve good properties such as high mechanical strength and durability, cement based materials are subjected to treatment conditions, among which curing regime is found to be a crucial parameter. Curing regime is a parameter which involves control of humidity in the curing milieu necessary to achieve a high

degree of binding phase formation. Such parameter includes sealed curing in polyethylene bag, chamber containing constant carbon dioxide concentration or vapour-proof membrane [11,91], unsealed curing and wet curing in water or saline water [92]. All these curing conditions can be done either at ambient or slightly elevated temperature [93,94]. In the cement technology, sealing curing is the most wide-spread technique due to their good output as far as cementitious properties are concerned. This curing approach enables the prevention of moisture loss. In general, water is the key substance necessary for the dissolution and hydration of cement components. A good example is that of Portland cement in which inadequate water content will lead to low cementitious properties. So, a constant sealing to avoid moisture loss is generally recommended for the curing of specimens to achieve optimum hydrated binding phases. Similar curing is applied on alkaline cement specimens since water takes part in the formation of the inorganic polymer as well as associated hydrated phases (C-A-S-H and C-S-H) [95–97]. Unlike Portland, the role of water in alkaline cement is mainly for dissolution and reaction purposes. However, a certain quantity is found to be retained by the binding phase [96,98]. The quantity retained is proportionate to the amount of reactive phase and constituents present in solid precursor. In fly ash based alkaline cement, this value is about 10.74 % by mass of the whole water [95], and 17 % by mass in metakaolin based alkaline cement [99]. Thus, in alkaline cement synthesis, the management of water content in the reactive medium seems to be a crucial parameter to be considered in order to acquire desired properties. The literature reveals that water conservation in the curing system can be favourable in some circumstances, and harmful in others, in the synthesis of alkaline cement [99]. According to Lee et al.(2016), sealing in polyethylene bags followed by curing at ambient atmosphere of the laboratory is more appropriate to fly ash based geopolymers than unsealing and curing [12], while the reverse is true for Xie and Kayali (2013) [10]. The above studies show that, in alkaline cement, the curing regime process vary from one activated source to another in order to achieve good cementitious properties. No matter the proven effect of curing regimes, low interest is given to this parameter which seems important in the development of cementitious properties in alkaline cement. To the best of our knowledge, there are not yet existing scientific data on the effect of the latter on the synthesis of low reactive volcanic ash based alkaline cement.

### **I.3. Agricultural wastes as a resource in the cement technology**

For many decades till now, the growing population around the world imposes an increase in agri-products supply, which in turn leads to huge production of waste products. These wastes are either obtained from domestic or industrial activities. Some of the major industrial crops produced are cereal (from wheat, rice, maize, barley, oats, sorghum and millet), groundnut, sugarcane, cassava tubers, palm oil, coconut, and cocoa. In areas of huge production and transformation, the latter produce a lot of wastes known as agro-wastes. In case there is lack of adequate waste management systems, like in developing countries, these agro-wastes are generally dumped in the environment and/or incinerated. Elsewhere, in some industries, these wastes are instead used as source of energy in order to reduce the energy demand. This process of waste transformation to energy generates ashes which are usually landfilled. Hence, for environmental protection and sustainable development, extensive studies are done to valorise agro-wastes and their by-products.

In the cement technology, some agro-wastes are used as fillers for the production of lightweight building materials for structural load-bearing, acoustic and insulation purposes [100,101] while their by-products, with regard to their chemical compositions (high  $\text{SiO}_2$ ,  $\text{Al}_2\text{O}_3$  and  $\text{CaO}$ ) are used as partial substituent to cement [102–104]. A wide range of studies exist with Portland cement in which numerous agro-wastes have been used, and interesting results have been achieved. However, in this work, the review will be focused on the impact of using by-products (ashes) in the alkaline cement technology. Several studies have been reported on the matter. Among others, commonly used ashes in the latter domain are: rice husk ash (RHA); sugarcane bagasse ash (SBA); and palm oil fuel ash (POFA). Their choice is mostly due to both their availability and high amorphous silica content. However, when used as alone raw precursors, they present low reactivity in alkaline medium thereby yielding cement products with long setting time and low mechanical properties [105,106]. Most often, they are subjected to blending with high reactive aluminosilicate raw materials and / or to heat curing in order to improve their reactivity in alkaline medium [64,105,107–109]. Sore et al. (2016) showed that the incorporation rice husk ash in metakaolin based geopolymer enhances the mechanical strength. Along their study, they observed that beside the formation of new mineral phases, the mechanical strength increases with increase in curing temperature (from 30 to 90 °C) [110]. Almost similar strength development was obtained by Kaze et al. (2018) using laterite as the solid precursor and RHA as an adjuvant [64]. Moreover,

Kaur et al. (2018) noticed that RHA reactivity increases with increase in molarity of the alkali activator solution [105]. In the same manner, but at ambient temperature (25 °C), blast furnace slag based alkaline cement products synthesized with various activator solutions yielded the highest strength when SBA content of 25 % by mass of precursor was incorporated. Furtherly, the authors observed that the presence of SBA in the latter has no significant influence in their durability [111]. Suddenly, the same SBA content was also needed in fly ash alkaline cement cured either at 20 or 60 °C [112]. Like RHA and SBA, according to Yusuf et al (2014), strength development in granulated blast furnace slag based alkaline cement can be achieved by incorporating both PFOA and  $\text{Al}(\text{OH})_3$  [81].

On the other hand, by-products of other agro-wastes are also used in alkaline cement synthesis, but for other purposes than the one mentioned in the previous paragraph. This concerns the use of ashes either as a source of alkali in one-part alkaline cement synthesis or as an alternative to commercial silicate. In the first case (as alkali source), the aim is to ease the manipulation of alkaline cement as that of ordinary cement. So, some authors assessed the utilisation of alkali rich ashes (from cotton, maize and oak) as alkaline activators for the synthesis of metakaolin based alkaline cement. This consisted of mixing the concerned ashes with metakaolin, followed by the addition of water. Along their assessment, they noticed that the highest pH (13-14) was achieved after mixing Maize stalk and maize cob ashes and water. Of these two, the maize cob ashes showed a higher reactivity and reaction extent when mixed with water and metakaolin thereby yielding a strength of 27 MPa. Microstructurally, this reactivity was also demonstrated by the shifting of Si-O-T band, fingerprint of alkaline cement [113]. Concerning the use of by-products of agro-wastes as a source of silica to replace commercial silicate, new approach is used in order to reduce energy demand and pollution related to the synthesis of alkaline cement. This consist of dissolving a silica rich waste (rice husk and sugar bagasse ashes) in sodium hydroxide with respect to  $\text{SiO}_2 / \text{T}_2\text{O}$  ratio where T = alkali metal (K and Na) in order to obtain silicate solution necessary for the synthesis of alkaline cement. The existing studies revealed that this novel approach give results which are quite comparable to those obtain with commercial silicate [114–116]. It is important to highlight that majority of ashes of agro-wastes yet used in alkaline cement synthesis originate from crops that grow above the soil, and their incorporations in the latter synthesis are of worth interest, but applications are limited on high reactive aluminosilicate raw materials in alkaline medium.



Thus, it will be also interesting to investigate the suitability of other sources of agro-waste such as cassava peel ash.

Cassava peel ash is a sub-product of cassava peels obtained via thermal treatment. Its implication in alkaline cement synthesis is not yet known. Nevertheless, in Portland cement technology, it is highly assessed as a supplementary cementitious material due to its high pozzolanic activity. Several studies reveal that the partial replacement of Portland cement by cassava peel ash in concretes produces comparable setting time, mechanical and durability properties with those concretes free of cassava peel ash [13,117,118]. Looking at its rich oxides ( $\text{SiO}_2$ ,  $\text{Al}_2\text{O}_3$ ,  $\text{CaO}$ ,  $\text{Fe}_2\text{O}_3$  and  $\text{K}_2\text{O}$ ) content, its application in alkaline cement synthesis can be of worth interest.

#### **I.4. Summary and motivations of the thesis**

The review of investigation carried out on the enhancement of cementitious properties of low reactive aluminosilicate based alkaline cement presented herein revealed that:

- There exist a wide variety of aluminosilicate raw materials available for the synthesis of alkaline cement. Among others, volcanic ash remains the only natural occurring material that, without any pre-treatment, possesses a certain degree of reactivity in alkali medium at ambient temperature. Though, its reactivity is relatively low compared to those of synthetic raw materials, however, the latter natural raw material is highly abundant in countries of known volcanism. Several techniques such as mechanical activation, alkali fusion and blending have shown worthy results concerning the enhancement of the reactivity of volcanic ash in alkaline medium. Nevertheless, the assessments were limited on volcanic ash with amorphous  $\geq 30$  % by mass. Below this value, low reactive volcanic ash (amorphous content  $\leq 26$  % by mass) are recommended to be used as filler than cement precursor. Regarding the level of poverty in less developed countries, it will be worth interesting to bring out new methods to improve cementitious properties of low reactive volcanic ash based eco-friendly cement for a sustainable development. This will further encourage the use of volcanic ash in the synthesis of alkaline cement

- The curing regime has a considerable influence on properties of cement products. It can either positively or negatively affect strength development in alkaline cement products. So, its application vary from one raw material to another. There are lack of research data on the effect of this parameter on mechanical strength and durability in alkaline cement, in general, and in volcanic

ash based alkaline cement, in particular. Varying this crucial parameter might enable novel appreciation of the reactivity of low reactive volcanic ash in alkaline medium.

- Incorporation of ashes of agro-wastes in the synthesis of alkaline cement has given interesting properties as far as the development of mechanical strength and durability is concerned. The various sources of ashes yet used are known and limited, and their blending is limited to high reactive aluminosilicate raw material due to their low reactivity in alkaline medium at ambient temperature. Thus, there exist low data on the enhancement of the reactivity of low reactive aluminosilicate raw materials in alkaline medium at ambient temperature by the incorporation of ashes of agro-wastes. The assessment of new by-product of agro-waste capable of challenging the highlighted limit experienced by former ashes will be of great interesting. Cassava peel ash has shown prominent results when partially substituted to Portland cement due to its good  $\text{Al}_2\text{O}_3$ ,  $\text{SiO}_2$  and  $\text{CaO}$  content [119,120]. Despite the latter chemical content which seems favourable for alkaline cement, and the abundance of cassava peel wastes in some areas of the world, to the best of our knowledge, there exist no research data concerning the implication of its ash in the synthesis of alkaline cement. So, it seems interesting to evaluate its reactivity in alkaline medium as well as its influence in the alkaline activation of low reactive volcanic ash.

The above relevant points present, in a certain manner, the questioning that this thesis will try to elucidate. This will, in one way, enable the valorisation of an additional agro-waste material and, in another way, help to encourage the use of low reactive volcanic ash as a main raw material in the synthesis of alkaline cement for engineering application.

## Chapter II: Materials and experimental methods

This chapter presents the different raw materials either natural or synthetic needed for the realization of this work. Also, it presents all the experimental procedures, characterization techniques and physical measurements applied in the laboratory to enable the assessment of both raw materials and synthesized products. At the end of this chapter, a summary of the experimental procedures carried out is also given.

### II.1. Materials

#### II.1.1. Solid materials

##### II.1.1.1. Volcanic ash

Two types of volcanic ash were used as sources of aluminosilicate raw materials. They were collected in two regions of Cameroon alongside the “Cameroon volcanic line”. The first sample denoted “**Vn**” originated from the locality of Vina situated in the adamawa region of Cameroon whereas the other sample denoted “**Ma**” originated from the locality of Manjo situated in the littoral region of Cameroon. As presented in Figure 4, sample Vn has a grey coloration while Ma has a red coloration. This different coloration might be related to their organic matter and iron contents.

Prior to use, the collected volcanic ash samples were pulverized with ball mill and later passed through 100  $\mu\text{m}$  sifter. The powder obtained were conserved in closed PVC container before any utilisation.



Figure 4: Volcanic ash powders used.

### II.1.1.2. Cassava peels and cassava peel ash

Cassava (*Manihot esculenta* Crantz), also known as *manioc*, is a staple food in tropical countries and provides more than 10 percent of the daily dietary caloric intake to about 300 million people in 15 African countries and in Paraguay. It is the fourth supplier of dietary energy in the tropics (after rice, sugar and maize) and the ninth world-wide. Its cultivation and processing provide household food security, income and employment opportunities for 500 million people in Africa, Asia and the Americas [121]. According to the FAOSTAT (1997), in 1995, about 164 million tons of cassava roots were produced. Slightly more than the half of this amount was produced in Africa with a production in Cameroon of about 1.3 million tons [121]. These values keep on increasing with years and were found to be about 277.1 million tons for the world production and 5.4 million tons for Cameroon production in 2018 [122]. Cassava is a carbohydrate rich crop obtained from cassava roots which is comprised of cassava peels (outer section with a deep brown colour), central pith (middle section with a white colour) and starchy flesh (inner section) as presented by the transversal section of the root in Figure 5a. The processing of these roots either for consumption or industrial purposes yields a lot of peels (*Manihot utilisima*) as waste. This waste constitute about 15% of the weight of the cassava root [121]. Made up of two layers, the outer one known as the periderm (brownish red) and the inner one as the cortex (white), cassava peels are usually not considered suitable for human consumption but can be used for feeding of pigs. Most of the time, these waste materials are dumped into the environment. In this work, cassava peels used were collected in the locality of Sombo (department of Nyong-Ekelle, Centre Region of Cameroon). Its collection was done in a family processing firm where cassava tubers are harvested and peeled for production of fermented cassava paste for commercial purposes. The resulting peels were collected, washed and dried at opened atmospheric air until achievement of crackled peels. With the aid of an electrical mixer, the crackled peels were grind and subjected to analyses such as TGA / DSC and FTIR before being thermally treated at 580 °C in an electric furnace branded Nabertherm, model LH 60 / 14 (Figure 6) using a rate of calcination of 5 °C / min following the calcination program below (Figure 7) in order to eliminate organic matter. Afterward, the ash obtained was sieved thanks to a 50µm sifter, and the resulting powder denoted “C<sub>A</sub>” was conserved in a PVC container before being used. Some grams of the later powder were subjected to XRD, FTIR, chemical composition, leaching test and particle size analysis.



Figure 5: (a) Whole cassava root and peeled pieces; (b) Washing and drying of cassava peels; (c) Cracked cassava peels and (d) Cassava peel ash used.



Figure 6: Electrical furnace (Nabertherm, model LH 60/14) used.

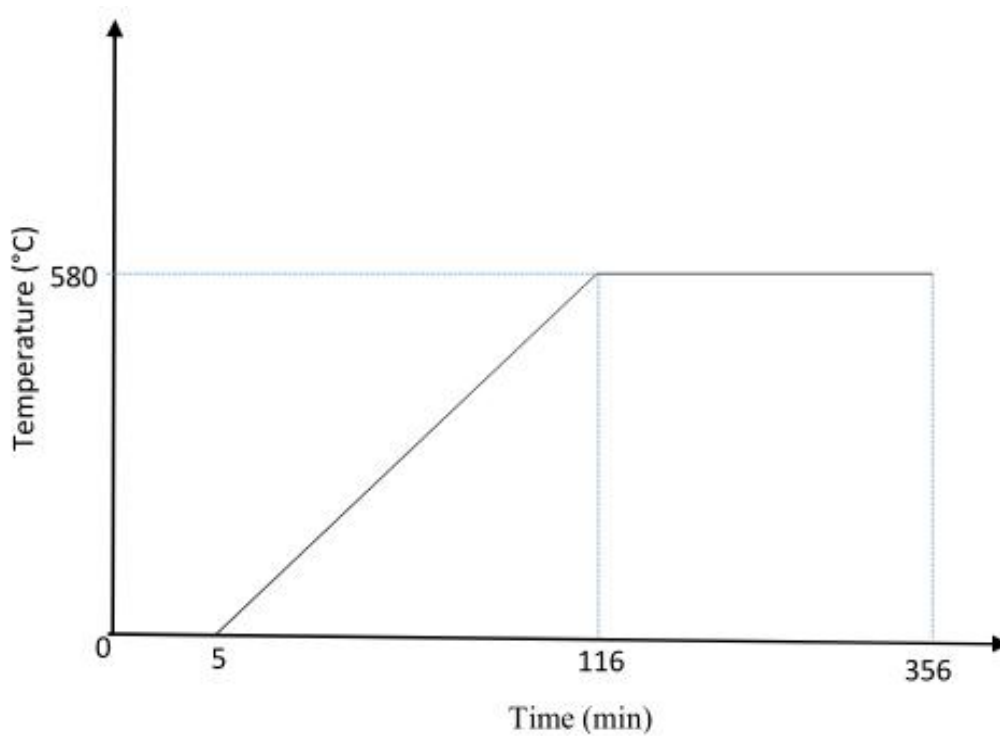


Figure 7: Calcination program of cassava peels used.

### II.1.2. Alkaline solution

According to research targets, different types of alkaline solutions were used to achieve results. These solutions were either a unique solution of sodium hydroxide or a mixture of sodium hydroxide and commercial sodium silicate solution. The latter were used based on the task to be

carried out. The tasks can be grouped into two sections (i.e. the quantification of reactive phase contents in solid precursors, and the synthesis of alkaline cements).

The quantification of reactive phase content was done on both volcanic and cassava peel ashes. The first step consisted of evaluating the reactive phase content ( $R_C$ ) in the latter raw materials by leaching each ash in sodium hydroxide solution (8 M), followed by the same action in hydrochloric acid (1 M). The second step consisted of using sodium hydroxide solution at different concentrations (i.e. 4 M, 8 M, and 12 M) as leaching solutions to assess the degree of dissolution of cassava peel ash ( $C_A$ ) in alkaline media.

Concerning the alkaline cement synthesis, two situations were involved. The first one consisted of synthesizing cassava peel ash based alkaline cements with various mixtures of sodium hydroxide and commercial sodium silicates solutions. These mixtures were prepared with respect to  $SiO_2/Na_2O$  molar ratio equal to: 2.8, 1.8 and 1.5. The other step consisted of using an alkaline solution (12 M sodium hydroxide solution and commercial sodium silicate solution) of  $SiO_2/Na_2O$  molar ratio equal to 1.4 to synthesize volcanic ash and composites of volcanic ash-cassava peel ash based alkaline cements.

## **II.2. Mix design and experimental procedures**

### **II.2.1. Curing regime on mechanical strength and durability properties of inorganic polymers from alkali activated low reactive volcanic ash.**

At this stage, powders of two samples of volcanic ash (Manjo “Ma” and Vinala “Vn”) were used to carry out the curing regime assessment. Each powder sample was mixed with alkaline solution at a liquid/solid ratio of 0.34 for Ma and 0.33 for Vn in an electric mixer for 5 minutes. The pastes obtained were cast in PVC cylindrical moulds (diameter: 25 mm and height: 50 mm) and vibrated on a vibrating table for 3 minutes to remove the trapped air. Later on, the cast pastes were conserved in a closed plastic container at ambient temperature of the laboratory. Depending on the setting time of each sample, Ma specimens were demoulded after 72 h while those of Vn were done after 24 h. The latter were cured in three different regimes for 28 days before experimental testing as follows: oven drying specimens for 48H at 60°C and later on sealing in a polyethylene bag at ambient temperature (ODS60); maintaining specimens in open atmospheric air of the laboratory (SOA25); and sealing specimens in polyethylene bag at ambient temperature of the

laboratory (SSP25). Note that, the laboratory temperature was about  $25 \pm 5$  °C. For identification purposes, depending on the sample, the synthesized products were denoted with a prefix of M for Ma based samples and V for Vn based samples, attached to the curing regime (ODS60, SOA25, and SSP25) as presented in Table I. After 28 days of curing, the obtained products were subjected to some measurements such as: quantification of water loss, compressive strength and durability tests, as well as TGA / DSC, XRD, FTIR and SEM analyses.

Table I: Mix design and curing conditions of synthesis procedure.

Code	Sample	Liquid to solid ratio	Curing regime
MSSP25	Ma	0.34	Polyethylene bag
MSOA25	Ma	0.34	Atmospheric air
MODS60	Ma	0.34	60°C (48 h)
VSSP25	Vn	0.33	Polyethylene bag
VSOA25	Vn	0.33	Atmospheric air
VODS60	Vn	0.33	60°C (48 h)

### II.2.2. Alkali activation of cassava peel ash

The objective of this stage was to assess the behaviour of cassava peel ash powder ( $C_A$ ) in alkaline medium as a potential aluminosilicate raw material for alkaline cement synthesis. In order to achieve this objective:

- First of all,  $C_A$  was subjected to leaching test using three concentrated solution of sodium hydroxide (i.e. 4M, 8M, and 12M) were used. This consisted of mixing 3 g of  $C_A$  with 90 mL of each NaOH solution (i.e. 4, 8 and 12M) for 1 h at 80°C. Afterward, the undissolved particles were separated from the leaching solution and rinsed with distilled water till neutral pH and Later on, dried in an oven at 105 °C till constant mass. Then, with the aid of the initial mass, the residual



mass was used to quantify the degree of dissolution of  $C_A$  in respective alkaline medium ( $D_C$  in % wt) as shown in the paragraph reserved to leaching test (Chapter II.3.1.).

- The second step consisted of synthesizing  $C_A$  based alkaline cement with alkaline solutions containing  $SiO_2 / Na_2O$  molar ratio equal to: 2.3; 1.8 and 1.5 respectively. This cement synthesis was done by mixing a definite mass of  $C_A$  powder with alkaline solution of specific  $SiO_2 / Na_2O$  molar ratio with respect to liquid-to-solid mass ratio of 1.12. For mortar purpose, sand was added to part of the cement pastes with respect to the sand-to- $C_A$  mass ratio of 2.5 and Later on, cast in cubic moulds of size 25 x 25 x 25 mm. Both mortars and pastes cured at ambient temperature ( $25 \pm 5$  °C) for 28 days before being subjected to compressive strength measurement, XRD, FTIR and SEM / EDX analyses respectively while the fresh pastes were subjected to initial setting time measurement. Note that, the synthesized cement products were denoted: AAC<sub>2.3</sub>, AAC<sub>1.8</sub> and AAC<sub>1.5</sub> with respect to the composition of the activator solutions. Table II summarizes the mix design of the activated products.

Table II: Summary of the mix design of alkali activated products.

Code	$C_A$ (%)	L / S	NaOH	$SiO_2 / Na_2O$	Sand / $C_A$
AAC <sub>2.3</sub>	100	1.12	4M	2.3	2.5
AAC <sub>1.8</sub>	100	1.12	8M	1.8	2.5
AAC <sub>1.5</sub>	100	1.12	12M	1.5	2.5

L / S: Liquid to Solid mass ratio,

### II.2.3. Partial replacement of low reactive volcanic ash by cassava peel ash during alkali activation of volcanic ash

The aim of this section was to assess the effect of cassava peel ash in low reactive volcanic ash based alkaline cement. For this reason, powders of volcanic ash ( $Ma$ ) and cassava peel ash ( $C_A$ ) were used as aluminosilicate raw materials. Alkaline cement pastes were obtained by mixing  $Ma$  with known proportions of  $C_A$  and alkaline activating solution in a Hobart mixer (M & O model

N50-G). This firstly involved dry mixing of volcanic ash and cassava peel ash for 5 minutes. Afterward, this was followed by addition of activating solution and the whole was mixed for 5 other minutes. Mixing of Ma and C<sub>A</sub> was done by partially replacing volcanic ash by cassava peel ash in the following proportions: 10, 20 and 30 % by mass. For good workability purpose, the liquid-to-solid mass ratios used were as presented in Table III. After mixing a given formulation, one part of paste was used for the determination of initial setting time while the other was cast in cylindrical PVC moulds (diameter 25 mm; height 50 mm). Once cast, the cylinders were vibrated for 5 minutes on an electrical vibrating table (M & O, type 202. N° 106) in order to remove trapped air bubbles. Except cylindrical specimens free of cassava peel ash whose demoulding was done after 72 h, the hardened cylinder specimens were demoulded 24 h later. After demoulding, almost the specimens were kept in a polyethylene bag and cured at ambient temperature of the laboratory for 28 days before carrying out physical measurements (compressive strength and mass and strength loss after immersion in acid for 30 days) or chemical characterizations (XRD, FTIR, SEM/EDX/ELEMENTAL MAPPING), while one specimen of each formulation was exposed to atmospheric air of the laboratory for 90 days for efflorescence observation. The different geopolymer specimens were labelled as GMC<sub>0</sub>, GMC<sub>10</sub>, GMC<sub>20</sub> and GMC<sub>30</sub> respectively. Table III summarizes the mixed proportions of different formulations.

Table III: Mix proportions of volcanic ash (Ma), cassava peel ash (C<sub>A</sub>) and alkaline solution.

Sample proportions (% by mass)				Composition of Raw materials (molar mass)			Mixture compositions (molar mass)		
Codes	Ma	C <sub>A</sub>	L / S	H <sub>2</sub> O / S	SiO <sub>2</sub> / Al <sub>2</sub> O <sub>3</sub>	CaO / SiO <sub>2</sub>	SiO <sub>2</sub> / Al <sub>2</sub> O <sub>3</sub>	Na <sub>2</sub> O / Al <sub>2</sub> O <sub>3</sub>	CaO / SiO <sub>2</sub>
GMC <sub>0</sub>	100	0	0.34	0.22	4.96	0.22	5.81	0.61	0.19
GMC <sub>10</sub>	90	10	0.37	0.24	4.59	0.23	5.49	0.64	0.19
GMC <sub>20</sub>	80	20	0.43	0.28	4.24	0.25	5.26	0.73	0.20
GMC <sub>30</sub>	70	30	0.47	0.30	3.91	0.27	4.99	0.77	0.21

L / S = Liquid to Solid mass ratio; H<sub>2</sub>O / S = Water to Solid mass ratio.

## II.3. Analytical measurements

### II.3.1. Leaching test

The leaching test is a quantitative measurement used to evaluate the reactive phase content (amorphous phase or mixture of amorphous /crystalline phases) present in an aluminosilicate raw material. In this study, it was determined through dissolution in NaOH-HCl solution. The method relies on the modified French standard XP P18-594 which consists of attacking reactive species (SiO<sub>2</sub>, Al<sub>2</sub>O<sub>3</sub>, CaO, etc. present in raw materials) in both alkaline and acidic media. This was carried out in two steps. Firstly, 3 g of each powdered aluminosilicate raw material was mixed with 90 mL of (8M) NaOH solution for 1 h at 80°C. Afterward, the undissolved particles were separated from the leaching solution and rinsed. The second step consisted of dissolving precipitated oxides present in residue of step 1 in (1M) HCl solution at 0°C for 30 minutes. The resulting residue was rinsed with distilled water till neutral pH. Later on, the residue was dried in an oven at 105 °C till constant mass, then the residual mass was used to determine the quantity of the reactive phase ( $R_C$  in % wt) as shown on the equation below:

$$R_c = \frac{M_{sample} - M_{residue}}{M_{sample}} * 100\%$$

In some cases, the final residue obtained after oven-drying until constant mass was subjected to XRD analysis in order to visualize microstructural changes occurred during leaching.

This leaching test was carried out in the laboratory of applied inorganic chemistry (option: physico-chemistry of mineral materials) of the University of Yaoundé 1.

### II.3.2. Particle size distribution

The laser particle size analyser (Malvern Mastersizer 2000, UK) was used to determine the particle size distribution of powders of volcanic ashes and cassava peel ash used in this work. The technique of laser diffraction is based on the principle that particles passing through a laser beam will scatter light at an angle that is directly related to their size: large particles scatter at low angles, whereas small particles scatter at high angles. The method involved passing of dilute well-dispersed slurry of the powdered sample to be analysed through a flow cell positioned in the path

of the laser beam to generate a scattering pattern. In our study, water was used as a dispersant, and ultrasonic vibration for 2 min was applied to avoid agglomeration.

This measurement was carried out in the laboratory of geology (AGEs) of the University of Liège, Belgium.

### **II.3.3. Chemical composition**

The chemical compositions of samples were determined by inductively coupled plasma and optical emission spectroscopy (ICP-OES) using an Optima™ 7000 DV ICP-OES (Perkin Elmer) equipped with a CCD sensor. This device is used to determine, qualitatively and quantitatively, the elements present in a given sample. Its principle relies on the excitation of atoms of elements present in a sample by a plasma energy. Later on, this excited atoms return to low energy position and emit rays (spectrum rays) corresponding to the photon wavelengths which are measured. The element type is determined based on the position of the photon rays, and the content of each element is determined based on the rays' intensity.

In order to carry out this analysis, the sample must be completely dissolved in a solution. In ICP OES instrument, sample is transported as a stream of liquid sample. With the help of a nebulizer, this liquid sample is converted to into an aerosol and then transported to the plasma where it is desolvated, vaporized, atomized and / or ionized. The excited atoms or ions emit their characteristic radiations which are detected and turned to an electronic signal that can be converted to usable information. In this research work, each sample was subjected to fusion reaction with lithium metaborate followed by their dissolution in concentrated nitric acid before being subjected to ICP OES analysis. The analysis was carried out in the LMDC / INSA of Toulouse, France.

### **II.3.4. X-ray diffraction**

X-ray diffraction is a non-destructive analytical technique used to study the crystal structures and atomic spacing. It is based on constructive interference of monochromatic X-rays and a crystal sample. X-rays produced by cathode ray tube are filtered to produce monochromatic radiation, collimated to concentrate and directed toward the sample. In contact with the sample at specific angles, these incident rays are either diffracted when they meet a lattice plane or transmitted. The interaction between the monochromatic X-rays and the sample yields both constructive and destructive interferences. With respect to the Bragg's law (2), constructive interference produces

X-ray diffraction peaks. Also, the peak intensities are determined by the distribution of atoms within the lattice.

$$n\lambda = 2d\sin\theta \quad (2)$$

$n$  = integer

$\lambda$  = wavelength of X-rays

$d$  = interplanar spacing generating the diffraction

$\theta$  = diffraction angle

There exist two types of X-rays diffraction: single crystal and powder X-ray diffractions. The first one permits the study of the crystal structure while the second, powder X-ray diffraction, is used to identify crystalline phases present in unknown material. All over this study, it is powder X-ray diffraction that was used to study the mineralogical content of raw materials and synthesized products. Thanks to the Bruker D8 advance diffractometer having Bragg-Brentano configuration and Copper radiation. The acquisitions were made between  $4^\circ$  and  $70^\circ 2\theta$ , with a step size of  $0.02^\circ$  and an acquisition time of 48 s per step in order to obtain acceptable resolution for a quantitative study. In this study, this analysis was carried out in the LMDC / INSA of Toulouse, France.

### **II.3.5. Fourier transform infrared spectroscopy**

Fourier Transform Infrared (FTIR) spectroscopy is an analytical technique that permit the identification of infrared-active molecules in organic or inorganic solid, liquid or gas samples. It is a rapid and non-destructive technique which measures the absorption of infrared radiation by the sample material versus the wavelength. That is, infrared radiation is passed through a sample. Some of the infrared radiation is absorbed by the sample and some of it is transmitted. With the help of an interferometer and a decoder (Fourier transformation), the information received from these absorption and transmission generates an infrared spectrum. The resulting spectrum represents a fingerprint of a sample with absorption peaks which correspond to the frequencies of vibrations between the bonds of the atoms making up the sample. In our studies, FTIR analysis was performed on a Bruker IR Alpha-p spectrophotometer scanning within the range of 400 to  $4000 \text{ cm}^{-1}$ . This analysis was carried out in the laboratory of applied physical and analytical chemistry (option: analytical chemistry) of the University of Yaoundé 1.

### II.3.6. Thermal analysis

The thermal analyses used in the realization of this thesis are thermogravimetry analysis (TGA) and differential scanning calorimetry (DSC).

TGA is a technique of measurement that allows the mass variation of a sample to be followed when increasing the temperature. Therefore, the results are given in terms of mass changed versus temperature, provides information on the decomposition of the sample. In the other hand, DSC is based on differences of heat exchange between a sample and a reference (e.g. alumina, but may also be air). Its resulting curve shows the heat emitted or absorbed by the material versus the temperature, thereby providing information linked on phase transitions: glass transition temperature, the melting and crystallization temperatures, enthalpies of reaction and decomposition. The two analyses are complementary to each other.

In our studies, these analyses were carried out in the laboratory of applied inorganic chemistry (option: physico-chemistry of mineral materials) of the University of Yaoundé 1. The device used for their realization is named LINSEIS STA PT-1000, operating from ambient temperature to 1000 °C in self-generated air atmosphere at heating and cooling rates of 10 and 20 °C / min respectively, using  $\alpha$ -alumina as crucibles (Figure 8).



Figure 8: Thermal analysis device (LINSEIS STAPT-1000) used.

### II.3.7. Scanning electron microscopy and energy dispersive spectroscopy

The scanning electron microscopy (SEM) is an analytical technique use to reveal the detailed surface characteristics of a solid sample and provide information related to its tri-dimensional structure. SEM is the most widespread technique available in analytical laboratory destined to

characterize physical properties such as morphology, shape, and size of materials at the micro and nanoscale. Its principle relies on the use of accelerated beam of high energy electrons to strike the surface of a sample in order to generate electron-sample interactions. These interactions lead to production of secondary electrons and backscattering electrons which are detected and amplified to create an image corresponding to the surface topography of the specimen. The secondary electrons provide information related to the morphology of the sample while back-scattered electrons provide information about the distribution of different elements in the sample. Besides that, scanning electron microscope is also capable of performing analyses of selected point locations on a sample with the aid of an auxiliary technique known as energy dispersive X-rays spectroscopy (EDX). EDX is used to provide information about the elemental composition of a sample. Its principle is related to the emission of X-rays from a sample through electron-sample interaction. When the electron beam removes an inner shell electron from a sample, causing a higher energy electron to fill the shell and release X-rays. These characteristic X-rays are used to identify the composition, and measure the abundance of elements in a sample. As each element has a unique X-ray spectrum, the elemental composition can be determined on the basis of detected X-rays.

Sample preparation for SEM analysis involves polishing and securing a specimen on to a metal support 'stub' and, if the sample is non-conducting, coating the surface with a conducting thin layer of metal. The analysis was carried out in the LMDC / INSA of Toulouse, France.

### **II.3.8. Quantification of water loss**

Quantification of water loss consists of evaluating the amount of water sent away by the cement specimen during the curing period and under specific condition. Besides, it also helps to estimate the amount of water retained in a material. This evaluation can be carried out in different ways. In this study, the quantification was simply done using the weighing approach. It consisted of weighing each specimen, using an electronic balance, at a particular time interval: just after demoulding (day 0); 48 h after demoulding (day 2) and 672 h after the demoulding (day 28). Note that, this assessment was carried out on 6 specimens per curing condition in order to assure the reproducibility of values and the measurements were done in the laboratory of applied inorganic chemistry (option: physico-chemistry of mineral materials) of the University of Yaoundé 1.

### II.3.9. Compressive strength

Compressive strength test is a mechanical test measuring the maximum amount of compressive load a material can bear before fracturing. In cement chemistry, this measurement is an essential point used to evaluate the degree of reactivity of cementitious material after a given period of time. Several studies have used this measuring parameter to reveal the reactivity of aluminosilicate raw materials in alkaline activation. Compressive strength is a uniaxial measurement in which the test pieces, usually in the form of a cube, prism, or cylinder, are compressed between the platens of a compression-testing machine by a gradually applied load. The formula to calculate the compressive strength is:

$$CS = F / A \quad (3)$$

F represents the force applied (in KN) on the sample;

A represents the cross sectional area (in mm<sup>2</sup>) of sample;

CS is the compressive strength (in MPa).

In order to carry out the testing, an electrohydraulic press M &O, type 11.50, N° 21 (Figure 9) was used with respect to the French standard NF EN 196-1 where definite specimens are being subjected to gradual load until fracture. Note that, tests are being done on three specimens to assure the reproducibility of values and were carried out in the laboratory of applied inorganic chemistry (option: physico-chemistry of mineral materials) of the University of Yaoundé 1.



Figure 9: Electro-hydraulic press used.



### II.3.10. Setting time

This is the time taken for a cement paste to start hardening and losing its plasticity. Its timing begins from the mixing (preparation period of the cement paste) to when it starts hardening. The instrument required to undertake initial setting time measurement is the VICAT apparatus (Figure 10), and the technique procedure used was based on the French standard NF EN 196-3. This consists of releasing the plunger and allowing it to sink into the test mould filled of cement paste. Afterward, observe the penetration of the plunger from the bottom of mould indicated on the scale. The same experiment at different positions on the mould until the plunger should stop penetrating at a distance of 1.13 mm from the bottom of the test mould of 40 mm high. Note that, this test is been done at a temperature of  $20 \pm 3$  °C and was carried out in the laboratory of applied inorganic chemistry (option: physico-chemistry of mineral materials) of the University of Yaoundé 1.

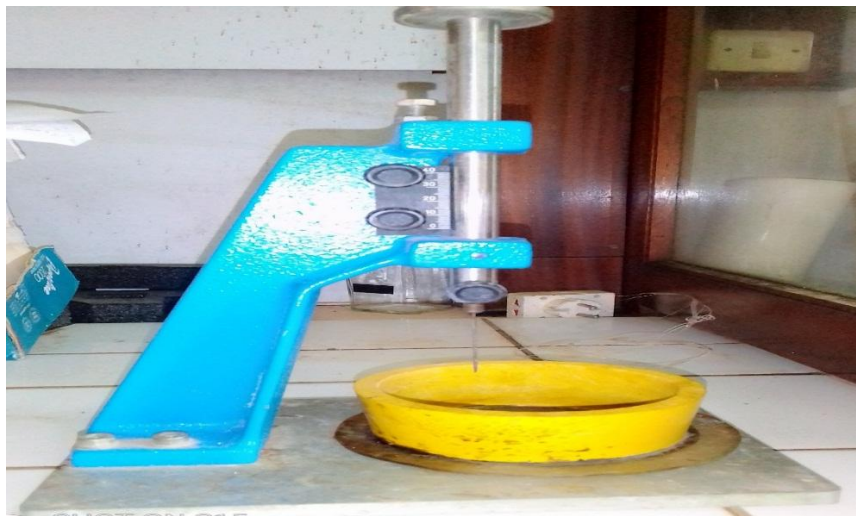


Figure 10: VICAT apparatus used.

### II.3.11. Durability

Durability can be defined as the ability of a material to remain serviceable in the surrounding environment during the useful life without damage or unexpected fracture. It is an important parameter considered in applied science in order to avoid or limit the occurrence of unexpected events that can lead to disasters. Thus, it helps to predict limits and conditions of usage of materials. In civil engineering, durability of cementitious materials expresses its ability to exist for long without significant deterioration by resisting the effects of heavy use, drying, wetting, heating,

freezing, thawing, corrosion, oxidation, volatilization, etc. On these, there exist numerous experimental techniques for the assessment of durability related to an eventual application of the material to be tested. However, in this thesis, three experimental approaches, undertaken in the laboratory of applied inorganic chemistry (option: physico-chemistry of mineral materials) of the University of Yaoundé 1, were used to assess the evolution of the durability of synthesized alkaline cement materials. That is:

- Acid attacks

This is a method used in cement chemistry to evaluate the stability of cementitious materials in aggressive medium. It consists of immersing cementitious materials in acid solution of known concentration for particular time. In our studies, the acid attack was assessed in 5% by mass of sulphuric acid solution for 28 and 90 days. Later on, the resulting cementitious specimens were subjected to mass loss and compressive strength tests.

- Water stability

Water stability is used to see for how far a material can behave when immerge in water for a long period of time. Also, it helps to predict if a certain material can be used in humid areas. Its methodology is simple and consists of immersing synthesized cementitious materials in water for 28 days at ambient temperature of the laboratory. Afterward, the resulting specimens is subjected to visual and compressive strength test in order to assess changes occurred.

- Efflorescence test

Generally, cement materials contain alkali metals, and sometimes, some of these alkali metals are soluble in water, thus making their migration to the surface of the materials possible. When that happens, the migrated alkalis react with atmospheric carbon dioxide to form a whitish layer (characteristic of efflorescence) common known as trona. Efflorescence is highly observed in alkaline cements due to their alkali metal ions high content. The level of the latter phenomenon in alkaline cements, in some circumstances, reveals the degree of reactivity that has taken place as well as the contribution of aluminium atom in the building of polycondensed network structure. To undertake this assessment, the harden cement paste or mortar is exposed to atmospheric air for a given period of time in order to permit the formation of a whitish layer. In this study, the different alkaline cement specimens were exposed to atmospheric air for 90 days.

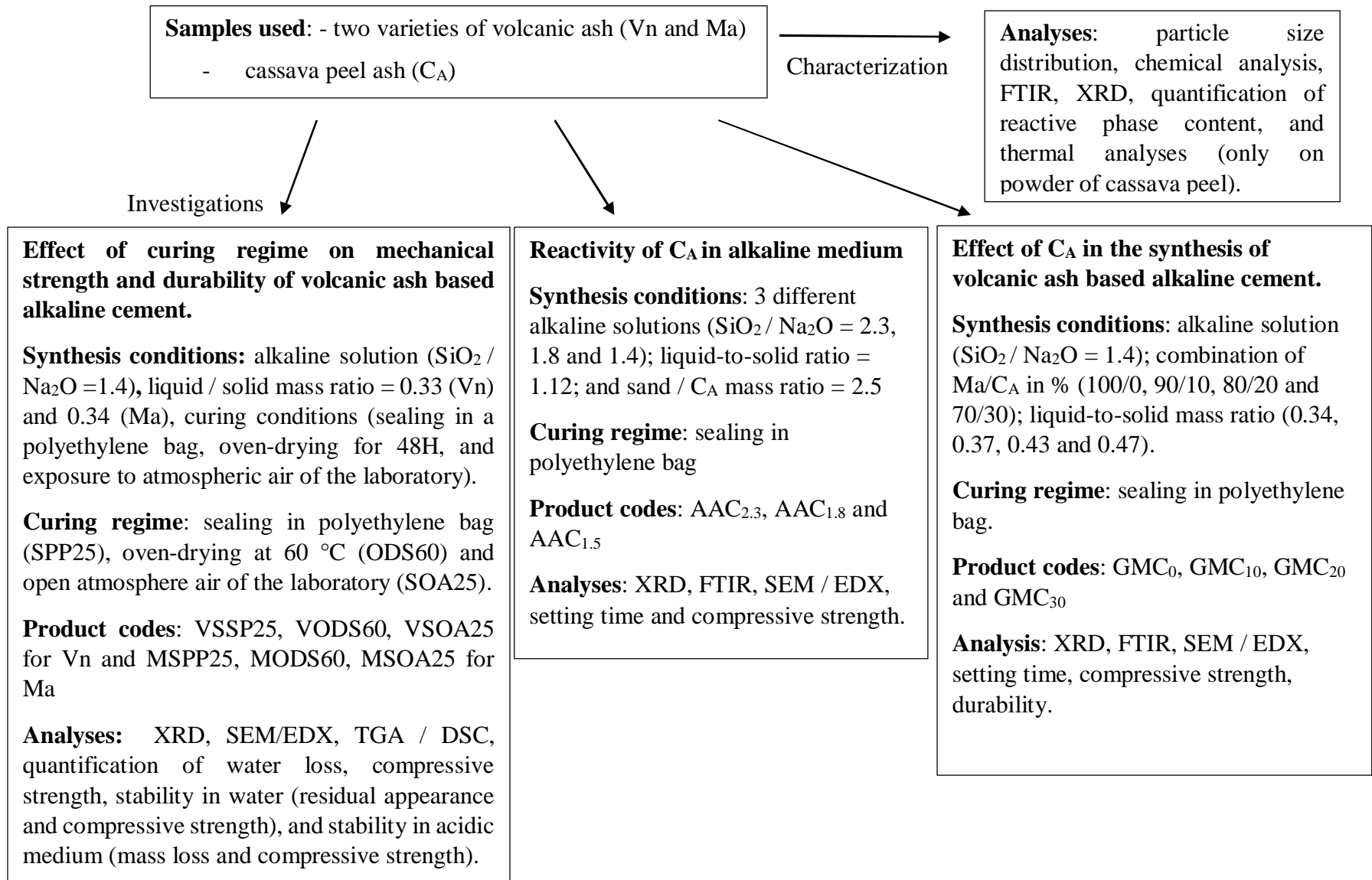


Figure 11: Summary of the experimental work carried out.

## Chapter III: Results and discussion

The third section of this thesis presents the outcome of the investigations carried out as described in Chapter 2 above. Firstly, it reports detailed information about the raw materials used in this thesis. Secondly, it sheds light on the impact that has water management systems (curing regimes) in the development of cementitious properties during the synthesis of volcanic ash based alkali activated cement. Moreover, it presents results and detailed discussions on the behaviour of cassava peel ash in alkaline media as well as its influence on the alkaline activation of low reactive volcanic ash.

### III.1. Characterization of raw materials

#### III.1.1. Particle size distribution

Figure 12 presents the particle size distribution with respect to the volume occupied by particles of volcanic ashes (Ma and Vn) and cassava peel ash ( $C_A$ ). Next to this, is the Table IV showing the specific surface area and maximum diameter corresponding to 10 % ( $d_{10}$ ), 50 % ( $d_{50}$ ) and 90 % ( $d_{90}$ ) of the cumulative volume of particles. The results reveal that the grain size of the three powder samples ranges between 0.1 and 50  $\mu\text{m}$ . For volcanic ashes, the particle size distribution is almost identical at a percentage distribution of 10 % (0.96  $\mu\text{m}$  for Vn and 0.94  $\mu\text{m}$  for Ma), but a slight difference is observed at  $D_{50}$  and  $D_{90}$  with 3.59 and 15.57  $\mu\text{m}$  for Vn and 5.43 and 21.55  $\mu\text{m}$  for Ma respectively. In the other hand, the particle distribution in  $C_A$  powder is observed to be respectively 1.89, 11.17 and 31.08  $\mu\text{m}$  for  $D_{10}$ ,  $D_{50}$  and  $D_{90}$ . Moreover,  $C_A$  expresses the lowest specific surface area of about 1.28  $\text{m}^2 / \text{g}$  against 2.64  $\text{m}^2 / \text{g}$  and 2.41  $\text{m}^2 / \text{g}$  for Vn and Ma respectively. It can be highlighted that the observed values of specific surface area correlate with those of particle size distribution where it is well noticed that the finer the particles the larger their surface area. According to many authors, these parameters have an influence on the reactivity of aluminosilicate raw material in alkaline medium [3]. The larger the specific surface area the higher the reactivity of the solid precursor in the reactive medium. Based on this previous statement, it is expected that the reactivity of Vn and Ma powder in the reaction medium will be higher than that of  $C_A$  powder. However, there exists just a slight difference of about 0.23  $\mu\text{m}$  between the specific

surface area of Vn and Ma powder samples. This therefore suggests that Vn may have almost similar or slightly elevated reactivity in alkaline medium than Ma.

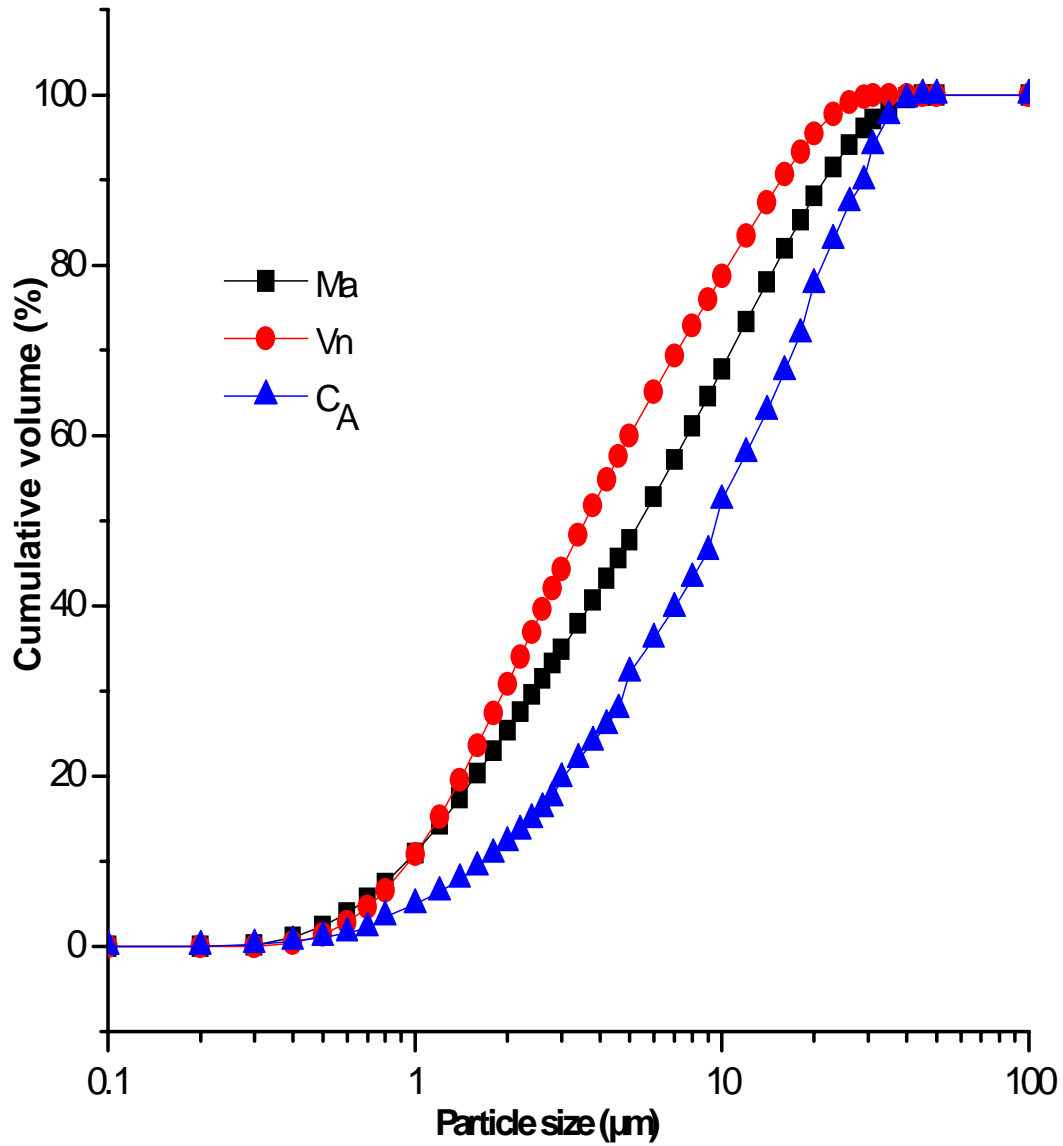


Figure 12: Particle size distribution of volcanic ashes and cassava peel ash.

Table IV: Particle sizes and specific surface area.

Sample	D <sub>10</sub> (μm)	D <sub>50</sub> (μm)	D <sub>90</sub> (μm)	specific surface area (m <sup>2</sup> /g)
Vn	0.96	3.59	15.57	2.64
Ma	0.94	5.43	21.55	2.41
C <sub>A</sub>	1.89	11.17	31.08	1.28

### III.1.2. Chemical composition

The chemical composition of volcanic ashes (Ma and Vn) and cassava peel ash (C<sub>A</sub>) are presented on Table V. This result is expressed in terms percentage by mass of oxides of elements constituted in samples. On this table below, silicon oxide and aluminium oxides are majors entities present in the three samples with a sum of 58.16 % for Ma, 61.44 % for Vn and 42.27 % for C<sub>A</sub>. Secondary oxides such as Fe<sub>2</sub>O<sub>3</sub>, CaO and MgO, in the descending order, are present in volcanic ashes. Their proportions vary from one volcanic ash to another (i.e. 14.19, 8.80 and 7.70 % by mass for Ma and 11.52, 7.77 and 5.17 % by mass for Vn respectively). In cassava peel ash, the third most predominant oxide is K<sub>2</sub>O with a value of 14.20 % by mass. Potassium is one of the most essential element in plant cells for optimal growth and productivity [123–125]. The latter oxide is followed by CaO (10.10 %), Fe<sub>2</sub>O<sub>3</sub> (9.67 %), SO<sub>3</sub> (4.78 %) and MgO (2.52 %) respectively. Additional oxides such as Na<sub>2</sub>O, TiO<sub>2</sub>, MnO, and P<sub>2</sub>O<sub>5</sub> are also present in all the samples and in low quantities. The above chemical composition of C<sub>A</sub> joins the results obtained by Vassilev et al. (2014) on 86 varieties of biomass [126]. Moreover, it is noticed that cassava peel ash expresses the highest loss on ignition (LOI) of 13.40 % by mass. The high LOI value in C<sub>A</sub> can be suggested to be due to the presence of residual organic matter and carbonate, sulphate and phosphate compounds in the ash. Concerning volcanic ashes, the LOI values are 3.87 and 1.79 % by mass for Vn and Ma respectively. The high value in Vn sample can be assigned to the presence of high organic matter and/or hydroxylated minerals content in Vn than in Ma. Globally, regarding the respective chemical composition of all the samples, it can be assumed that the latter are suitable in the synthesis of alkali activated cement [4,86].

Table V: Chemical composition (% by mass) of volcanic ashes (Ma and Vn) and cassava peel ash (C<sub>A</sub>).

Oxides	SiO <sub>2</sub>	Al <sub>2</sub> O <sub>3</sub>	BaO	CaO	Cr <sub>2</sub> O <sub>3</sub>	Fe <sub>2</sub> O <sub>3</sub>	K <sub>2</sub> O	MgO	MnO	Na <sub>2</sub> O	P <sub>2</sub> O <sub>5</sub>	SO <sub>3</sub>	SrO	TiO <sub>2</sub>	F	LOI	Total
Ma	43.32	14.84	0.06	8.80	0.16	14.19	1.52	7.70	0.20	3.04	0.74	0.01	0.10	3.15	-	1.79	99.80
Vn	44.56	16.88	0.11	7.77	0.03	11.52	2.19	5.17	0.20	2.93	0.67	0.06	0.13	2.69	-	3.87	98.81
C <sub>A</sub>	22.60	19.67	-	10.10	0.02	9.67	14.20	2.52	0.11	0.39	1.71	4.68	-	1.34	0.03	13.40	99.90

LOI : loss on ignition

### III.1.3. Thermal analysis of cassava peels

Prior to use, cassava peels were first subjected to thermal analysis in order to acquire valuable information regarding its thermal behaviour at different temperatures so as to obtain an appropriate temperature necessary to remove organic matter and to obtain an amorphous and reactive ash which can undergo high dissolution in alkaline medium. Figure 13 presents the thermal behaviour of cassava peel subjected to thermogravimetry and differential scanning calorimetry analyses. On this figure, three thermal phenomena can be observed. On TGA curve, the latter are characterized by two mass loss: one at 58-155 °C and the broadest one at 207-560 °C. while on DSC curve, one endothermic peak at 101°C characterizing the loss of humidity, and two exothermic peaks identified at 318 and 528 °C characterizing the combustion of cellulose and lignin respectively are observed. Similar phenomena were observed by other authors [127,128]. Regarding the above results, 580 °C was chosen as an adequate temperature to assure the complete removal of organic matter in the cassava peel as well as the obtainment of low crystallized ash.

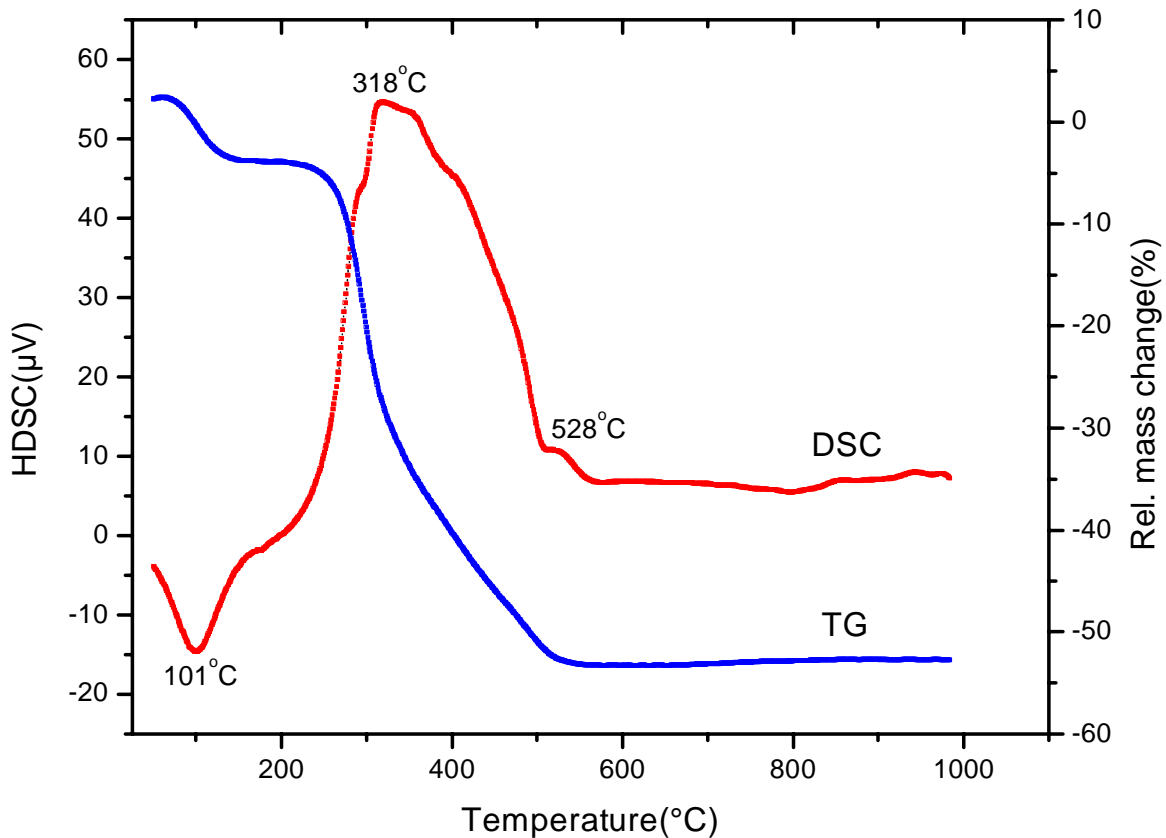


Figure 13: Thermal analyses of cassava peel.



### III.1.4. Fourier Transform Infrared spectroscopy analysis

Figure 14 presents the Fourier Transform Infrared spectra of Cassava peel (CP), cassava peel ash ( $C_A$ ) and volcanic ashes (Ma and Vn). On the spectrum of CP, the vibration bands at 3275 and 1636  $\text{cm}^{-1}$  correspond to the existence of free and intermolecular bonded O-H groups [129]. Those at 2927, 1459, 1337 and 760  $\text{cm}^{-1}$  are attributed to the stretching and bending vibrations of the C-H bond of the aliphatic group respectively [129,130]. A band at about 1245, 1152, 1078 and 998  $\text{cm}^{-1}$  indicate the vibration of the C-O-C bonds present in the cellulose and hemicellulose. [131,132]. Additionally, the band at 924  $\text{cm}^{-1}$  is assigned to the stretching vibration of the O-H bond of the cellulose [133]. Finally, the strong absorption band at 1000  $\text{cm}^{-1}$  is assigned to the C-OH stretching vibration [131]. It is important to highlight that all the above mentioned absorption bands, present on CP spectrum, are absent on the spectrum of its calcined version ( $C_A$ ). This suggests that all the organic entities present in CP were removed when the latter was subjected to thermal treatment at 580 °C. The resulting product was the required ash.

Looking at the Fourier Transform Infrared spectra of the three ashes ( $C_A$ , Vn and Ma), most of the absorption bands present on each Fourier Transform Infrared spectrum can be classified into three groups. Firstly, the absorption bands located at about 3449-3422 and 1653-1640  $\text{cm}^{-1}$  which correspond to the stretching and bending vibration of water molecules [114,134]. The second group is assigned to the absorption bands located at about 997-968 and 560-510  $\text{cm}^{-1}$ . Both intervals are respectively attributed to asymmetric and symmetric stretching vibration of the Si-O-Si and Si-O-Al bonds [44]. The fact that the absorption bands of the latter bonds (Si-O-Si and Si-O-Al) differ from one sample to another may be linked to their various aluminium and calcium contents [114,135]. The last group is assigned to the absorption bands located at about 916-919  $\text{cm}^{-1}$  which are attributed to the vibration of the 6-fold coordinated  $\text{Al}_{(\text{VI})}\text{-O}$  [3]. It can be highlighted that, among the three samples (ashes), this third group of bands is unique to volcanic ashes. Besides the above mentioned, it is well noticed that  $C_A$  possesses extra absorption bands. Among these bands are: those located at about 1417, 875 and 712  $\text{cm}^{-1}$  which are attributed to the vibration modes of carbonate (i.e. asymmetric stretching, out-of and in-plane vibrations respectively) [136,137]; the one located at 1114  $\text{cm}^{-1}$  which is assigned to the stretching vibration of the Si-O bond; and finally the band at about 616  $\text{cm}^{-1}$  is attributed to the out-of-plane vibration of Si-O or Al-O bond [114,134].

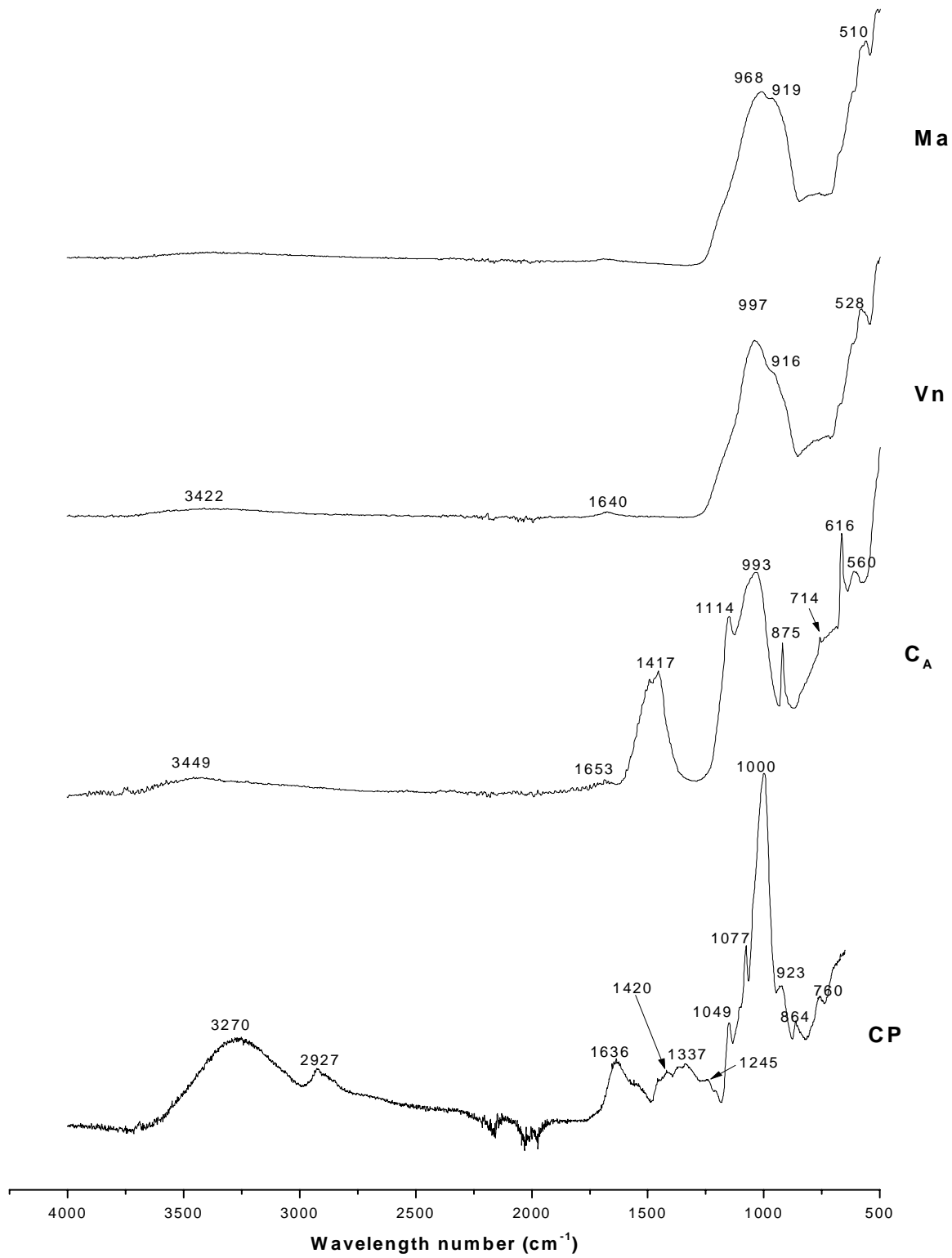


Figure 14: FTIR spectra of raw materials (CP: cassava peel, C<sub>A</sub>: cassava peel ash, Ma and Vn: volcanic ashes).

### III.1.5. X-ray diffraction analysis

Figure 15 below presents the X-ray diffraction patterns of volcanic ashes (Vn and Ma) and cassava peel ash ( $C_A$ ) powders respectively. It reveals similarities and differences that exist between the latter samples as far as mineralogical content is concerned. Concerning volcanic ash, no matter the hundred kilometres that separates the two sites of collection, both samples (Vn and Ma) possess some common mineral phases such as anorthite  $[(Na_{0.45}Ca_{0.55})(Al_{1.55}SiO_{2.45}-O_8)$ : PDF 71-0748], augite aluminian  $[Ca(Mg,Fe,Al)(Si,Al)_2O_6$ : PDF 41-1483], hematite  $[\alpha-Fe_2O_3$ : PDF 89-2810], maghemite  $[\gamma-Fe_2O_3$ : PDF 04-0755], fosterite ferroan  $[(Mg_{0.879}Fe_{0.2121})(Mg_{0.881}Fe_{0.119})(SiO_4)$ : PDF 83-0645]. These mineral phases are almost common to volcanic ash. Nevertheless, there exists some differences between Ma and Vn. In Ma, there are mineral phases such as muscovite  $[(Na_{0.07}K_{0.90}Ba_{0.01})(Al_{1.84}Ti_{0.04}Fe_{0.07}Mg_{0.04})(Si_3O_2Al_{0.98})O_{10}(OH)_2$ : PDF 82-2450] and diopside  $[CaMg(SiO_3)_2$ : PDF 19-0239], while in Vn, the presence of mineral phases such as kaersutite  $[NaCa_2(Mg,Fe+2)_4Ti(Si_6Al_2)O_{22}(OH)_2$ : PDF 44-1450] and diopside ferrian  $[Ca(Mg_{0.82}Fe_{0.18})(Si_2O_6)$ : PDF 87-0699] is noticed. Furthermore, on the same figure, the X-ray diffraction pattern of  $C_A$  reveals mineral phases such as arcanite  $[K_2SO_4$ : PDF 05-0613]; calcite  $[CaCO_3$ : PDF 83-0578] and quartz  $[SiO_2$ : PDF 86-1629]. Based on the intensities of their peaks, the latter mineral phases are identified as major mineral phases present in  $C_A$ . However, there are also minor minerals such as beusite calcian  $[(Mn^{2+}, Fe^{+2}, Ca)(PO_4)_2$ : PDF 16-1353]; Potassium phosphate  $[\alpha-K_2P_3O_{10}$ : PDF 45-0209]; anatase  $[TiO_2$ : PDF 86-1157] and Magnesium oxide  $[MgO_2$ : PDF 76-1363]. Additionally, besides the identified crystalline phases, the presence of a broad hump can be noticed on the three X-ray diffraction patterns mentioned above. The latter is located at  $2\theta = 18-35$  on the X-ray diffraction of both volcanic ashes and at  $2\theta = 14-38$  on that of  $C_A$ . This hump reveals the presence of amorphous phase necessary in alkaline activation. Focusing on the volume of the latter, it can be noticed that sample  $C_A$  possesses the largest hump followed by samples Vn and Ma respectively. The previous statement therefore suggests that  $C_A$  possesses the high content of amorphous phase, followed by Vn and later on by Ma. Also, it is important to highlight that oxides such as  $Al_2O_3$  and  $Fe_2O_3$  present in the chemical composition of  $C_A$  (Table V) are significantly absent among crystalline phases (Figure 14) which may suggest their existence in its amorphous phase.

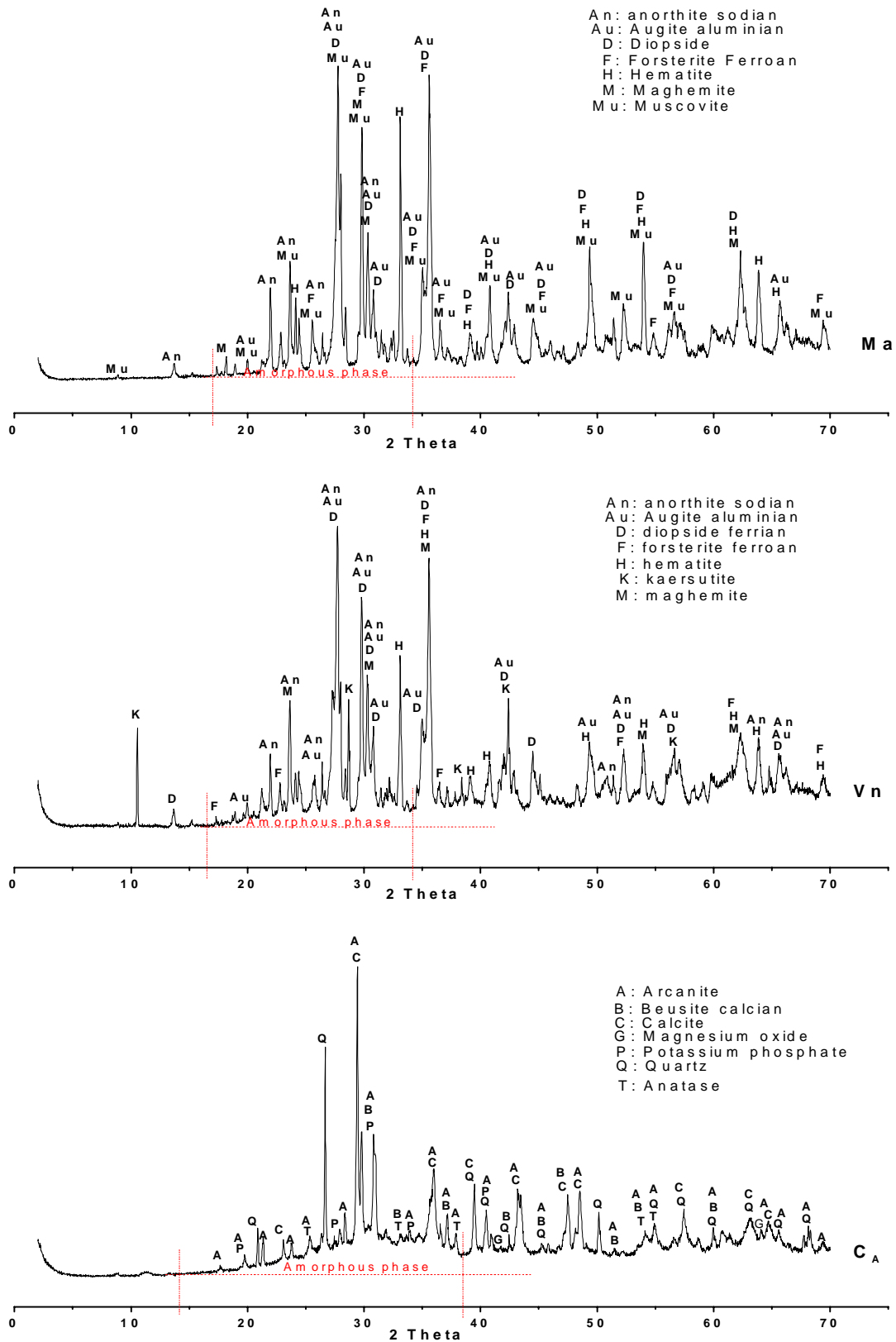


Figure 15: XRD patterns of raw materials (Vn and Ma: volcanic ashes, CA: cassava peel ash).

### III.1.6. Reactive phase content

Table VI below gives the reactive phase content ( $R_C$ ) of volcanic ashes (Vn and Ma) and cassava peel ash ( $C_A$ ) quantified by leaching each sample in both sodium hydroxide and Hydrochloric acid solutions. It can be highlighted that the reactive phase content in most cases is majorly consisted of the amorphous phase present in the raw material. However, in some circumstances, the latter can also be associated to the dissolved crystalline phases. From Table VI, it can be noticed that  $C_A$  sample possesses the highest  $R_C$  of about 72 % by mass, followed by Vn and Ma samples whose values are about 26 and 18 % by mass respectively. The latter results are in accordance with the observation done on X-ray diffraction patterns (Figure 15) as far as the presence of a hump is concerned. On this, relying on former research studies conducted by other authors [3,5,8] which related reactive phase content and reactivity, the above results suggest that the reactivity of the three powder samples in alkaline medium may follow this order:  $C_A > Vn > Ma$ .

With regard to the high reactive phase content of  $C_A$ , the resulting residue of the latter, after leaching, was subjected to X-ray diffraction analysis in order to visualize the mineralogical changes that had occurred in  $C_A$ . The resulting X-ray diffraction pattern is presented in Figure 16, and shows that in exception to quartz, majority of crystalline phases as well as the amorphous phase have been leached out by the solutions. Moreover, peaks of residual calcite are also identified. This may be due to insufficient quantity of leaching solution and/or time to enable its complete dissolution. Thus,  $C_A$  expresses high dissolution in both alkaline and acid solution.

Table VI: Reactive phase content ( $R_C$ ) in each raw material.

Sample	Ma	Vn	$C_A$
$R_C$ (% by mass)	18	26	72

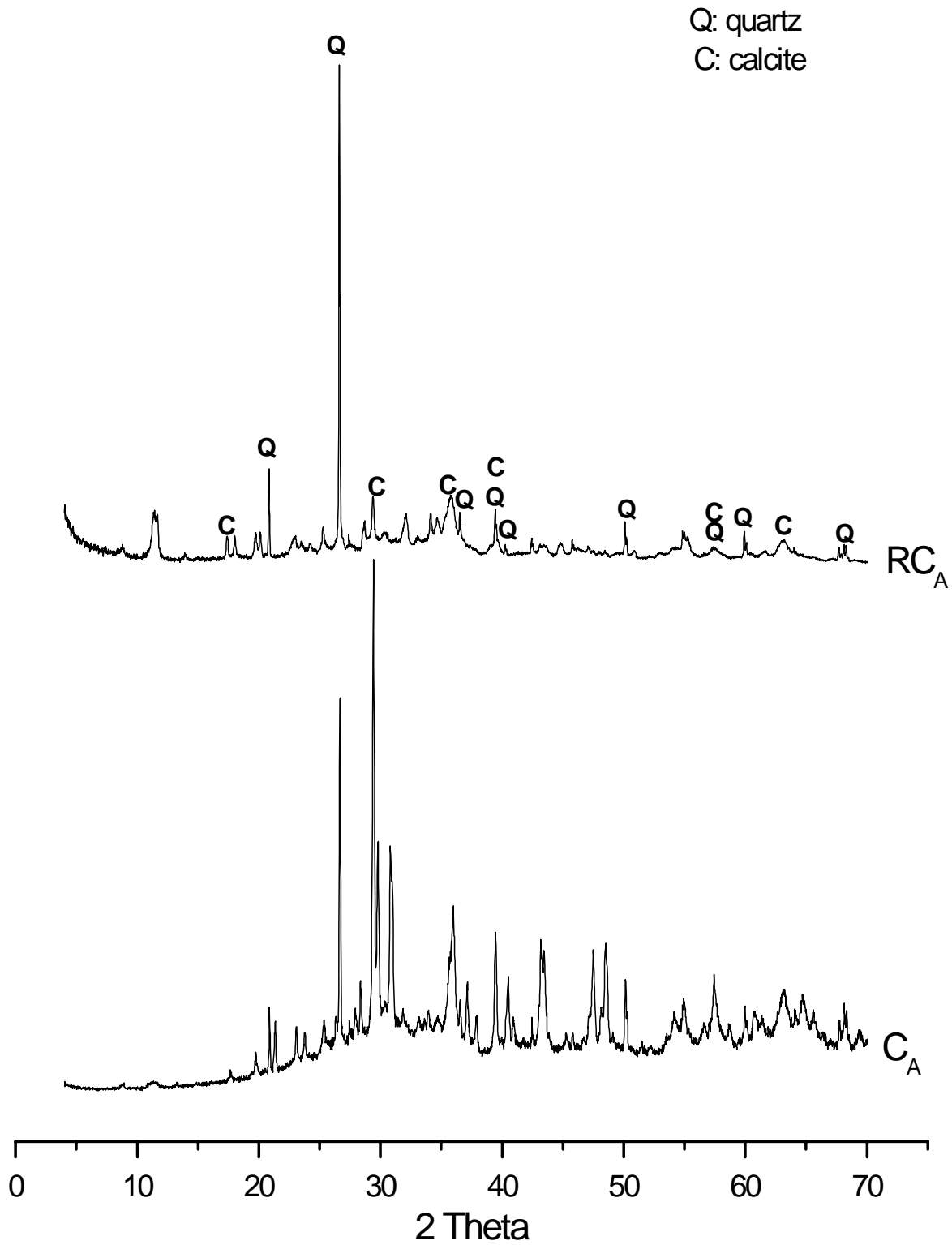


Figure 16: XRD pattern of cassava peel ash residue (RC<sub>A</sub>) and Cassava peel ash (C<sub>A</sub>).

## **III.2. Effects of curing regime on mechanical strength and durability of low reactive volcanic ash based alkaline cement.**

### **III.2.1. Water loss and microstructure**

#### **a) Water loss content during curing of volcanic ash based alkaline cement.**

Table VII gives the variation of water loss in volcanic ash based alkaline cement with respect to the curing regimes. According to the latter table, no matter the sample and curing days, the trend of water loss in volcanic ash based alkaline cement specimens increases from sealing curing (SSP25) to oven curing (ODS60) with open atmospheric air curing (SOA25) as an intermediate. As it could be foreseeable, ODS60 curing regime expresses the highest water loss of about 87-88 % by mass of total water content after 2 days against 35-39 and 1-2 % by mass for SOA25 and SSP25 respectively. Moreover, the above loss is continuous with SOA25 and SSP25 even after 28 days of curing, whereas in ODS60, the reverse is achieved (i.e. After 28 days of curing, mass increase of about 9 and 7 % for Ma and Vn specimens respectively). The latter increase can be assigned to the precipitation of sodium carbonate resulting from the reaction between free sodium ions present in hardened alkaline cement pastes and atmospheric Carbon dioxide. Furthermore, comparing both samples (Ma and Vn) under SSP25 curing regime, it can be highlighted that Vn specimens express more water retention than Ma specimens. This must be due to the presence of high quantity of hydrated mineral (kaersutite) and / or organic matter in Vn than in Ma which might form hydrogen bond with water molecules thereby limiting its slackening. According to Park S. and Pour-Ghaz M. (2018), the presence of hydroxylated surface in the alkaline cement structure favours the retention of water molecules [96].

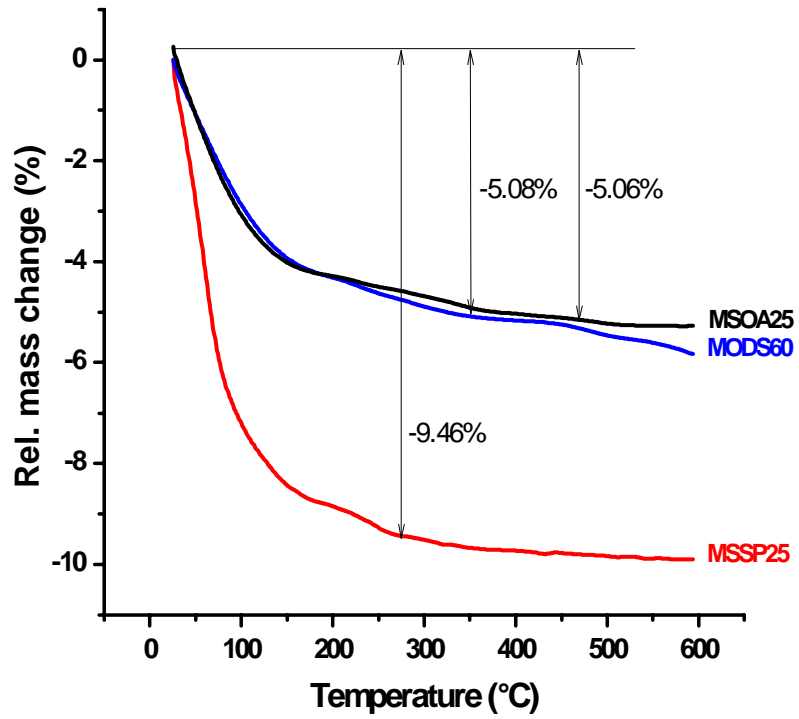
In order to visualise analytically the water loss, powders of 28 days cured specimens were subjected to thermal analyses (TGA and DSC) and the resulting thermographs are depicted in Figures 17 and 18. As obvious, ODS60 expresses the least water loss followed by SOA25 and SSP25 respectively. This trend is inverse and in accordance to that of Table VII, thereby confirming the viability of the latter results. On the other hand, it seems worth interesting to highlight that the temperature at which maximum water is lost revealed by an endothermic peak on the DSC curves located between 0 and 200 °C seems to depend on the curing regime. Figures 17 and 18 show that maximum water loss is achieved at: 64 and 81 °C (ODS60); 59 and 71 °C

(SOA25) and 58 and 49 °C (SSP25) for Ma and Vn based alkaline cement respectively. Moreover, regardless to the water content in cement product, the broadness of this endothermic peak increases from SPP25 (25-78 °C) to ODS60 (25-150 °C) regime, with SOA25 regime (25-135 °C) as the intermediate. This difference in temperature might be related to the degree of polycondensation that has occurred in respective specimens. In fact, alkaline cement obtained from a more reactive raw material such as metakaolin, usually expresses maximum loss at temperature beyond 100 °C with a broad endothermic peak that lies between 25 and 180 °C characterising both free and chemically bound water from the inorganic polymer network [138]. The above temperature variation suggests that the trend of polycondensation follows this order: ODS60 > SOA25 > SSP25. Furthermore, the optimum water loss temperatures in VODS60 (81 °C) and VSOA25 (79 °C) suggest that the polycondensation process is more pronounced in Vn based alkaline cement than in Ma based alkaline cement (64 °C for MODS60 and 59 °C for MSOA25) as expected regarding  $R_c$ . Whereas the reverse is true between VSSP25 (49 °C) and MSSP25 (58 °C) due to the high retention of water molecules expressed by Vn sample despite its high reactive phase content. Thus, the higher the degree of polycondensation, the higher the temperature required to release the water molecules contained in the inorganic polymer framework.

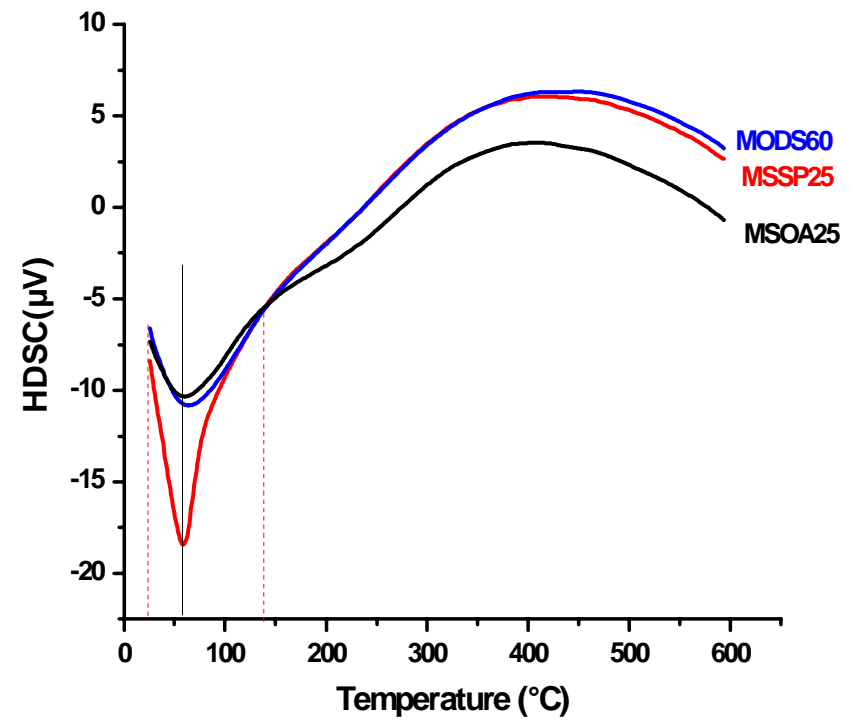
Table VII: Water loss (% by mass) versus the curing regime of alkaline cement.

		2 days	28 days
Ma	SSP25	2.2 ± 0.1	22.3 ± 0.1
	SOA25	35.4 ± 0.1	71.8 ± 0.1
	ODS60	87.1 ± 0.1	79.5 ± 0.1
Vn	SSP25	0.7 ± 0.1	4.7 ± 0.1
	SOA25	38.7 ± 0.1	72.1 ± 0.1
	ODS60	88.3 ± 0.1	82.5 ± 0.1



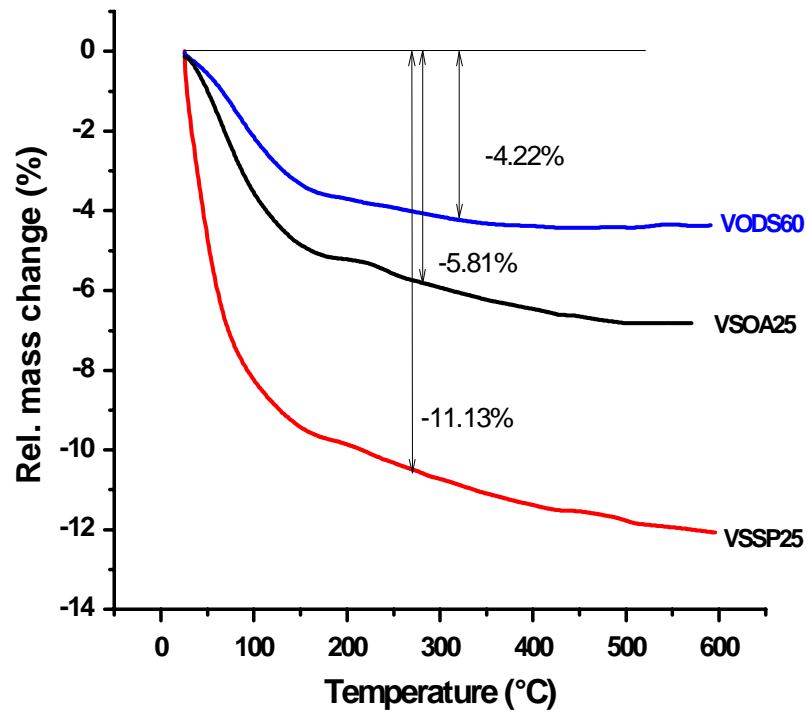


(a)

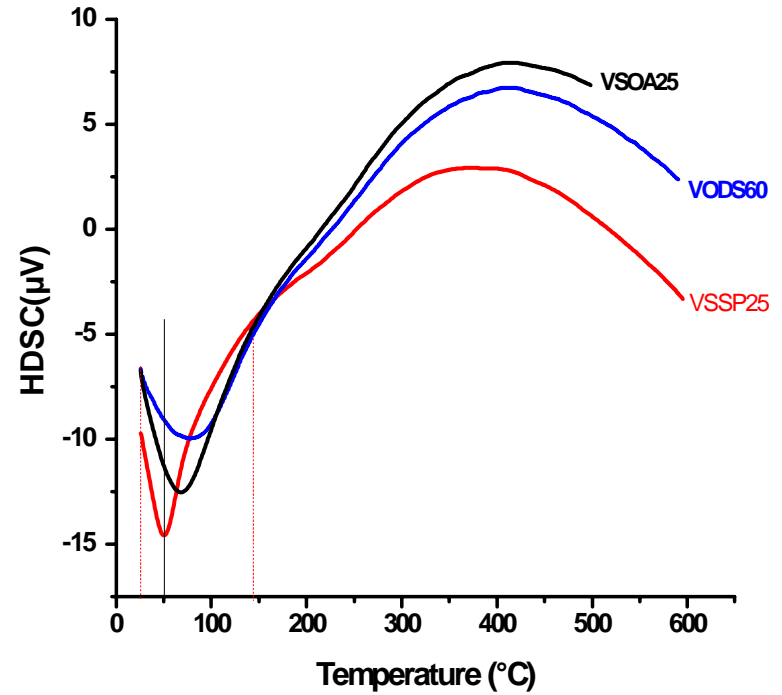


(b)

Figure 17: Thermographs of Ma based alkaline cement aged 28 days (a: TG and b: DSC).



(a)



(b)

Figure 18: Thermographs of Vn based alkaline cement aged 28 days (**a**: TG and **b**: DSC).

## **b) Microstructure**

### **- X-ray diffraction**

Figures 19 and 20 show the mineralogical modifications that have occurred in volcanic ash based alkaline cement maintained under various curing regimes. On these figures, it can be noticed that all the minerals identified in raw materials are present in cement products. Whereas, besides the amorphous phase, some minerals such as muscovite, kaersutite, diopside, maghemite and hematite seem to have undergone a certain degree of dissolution in alkaline medium depending on the curing regime. This is noticeable by comparing the intensities of their respective peaks at different curing regimes as revealed by the dissolution index of some mineral phases (DIM) in Table VIII. The partial dissolution in alkaline medium of some of the latter minerals (diopside and muscovite) were earlier identified by Knauss et al. (1992) and Ojo et al. (2019) respectively [139,140]. Kaze et al. (2018) also indicated slight dissolution of some iron minerals (ilmenite, maghemite and hematite) in laterite based geopolymer cured under opened atmosphere, and suggested their implication in the formation of binding phases [63]. In the present study, it is noticed that the partial dissolution of some mineral phases is highly expressed in specimens sealed in polyethylene bag at ambient temperature of the laboratory (SSP25) followed by those cured in an oven at 60 °C (ODS60) and in open ambient atmospheric air of the laboratory (SOA25) respectively. The above variations can be assigned to the influence of water content and temperature. According to some authors, the role of water in the synthesis of alkaline cement is to provide a medium for dissolution and reaction [96,98,141]. In fact, in SSP25 curing regime, the rate of water loss is very slow (almost negligible) at ambient temperature as observed in Table VII and Figures 17 and 18. Thus, the captured water molecules at higher pH induces partial dissolution of some mineral phases. In SSP25, this mineral dissolution is marked by an increase in the broadness of the hump located between 5 and 40 ° (2 theta) on the XRD patterns characterising an increase in amorphous phase content (Figures 21). Whereas, in ODS60 and SOA25, the latter phenomenon is respectively less pronounced due to rapid water loss. However, in ODS60, slightly elevated curing temperature also favoured partial dissolution of some mineral phases, but to a certain level. Besides the aforementioned, it can also be noticed that mineral dissolution is more pronounced in Vn specimens than in Ma specimens sealed in polyethylene bag at ambient temperature of the laboratory, and this due to: the high water retention (Table VII and Figures 17 and 18) and the high content of hydroxylated mineral in Vn. Thus, the higher the water retention in an alkaline medium, the greater the dissolution of

amorphous phase as well as some mineral phases. Based on the above level of dissolutions, the degree of polycondensation in synthesized product maintained under various curing regime is expected to follow this trend: SSP25 > ODS60 > SOA25. This suggested trend is in contradiction with the one done based on results of thermal analyses (Figures 17 and 18) and enables to notice that high amorphous phase content in the reaction medium under certain curing regimes does not necessary lead to high degree of polycondensation.

Table VIII: dissolution index of some mineral phases based on XRD patterns of alkali activated volcanic ashes suggested to various curing regimes.

Sample	Alkali activated Cement	Kaersutite	Diopside	hematite	Maghemite	Muscovite
Vn		1.00	1.00	1.00	1.00	
	MSSP25	0.42	0.81	0.84	0.84	-
	MODS60	0.80	0.91	0.95	0.93	-
	MSOA25	0.69	0.98	0.92	0.92	-
Ma			1.00	1.00	1.00	1.00
	VSSP25	-	0.90	0.85	0.84	0.98
	VODS60	-	0.86	0.81	0.85	0.91
	VSOA25	-	0.96	0.91	0.90	1.00

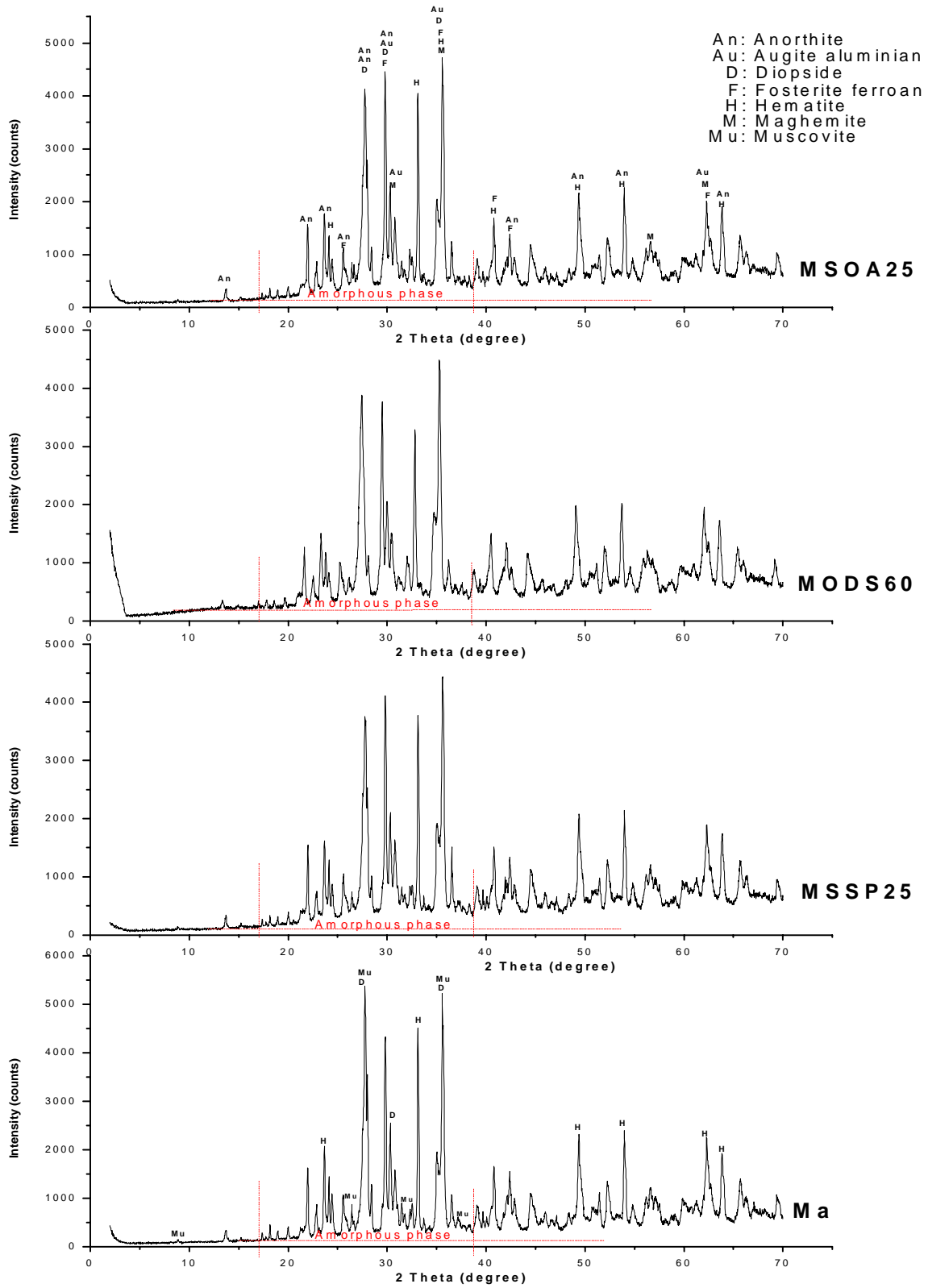


Figure 19: XRD patterns of Ma based alkaline cements aged 28 days preserved under various curing regimes.

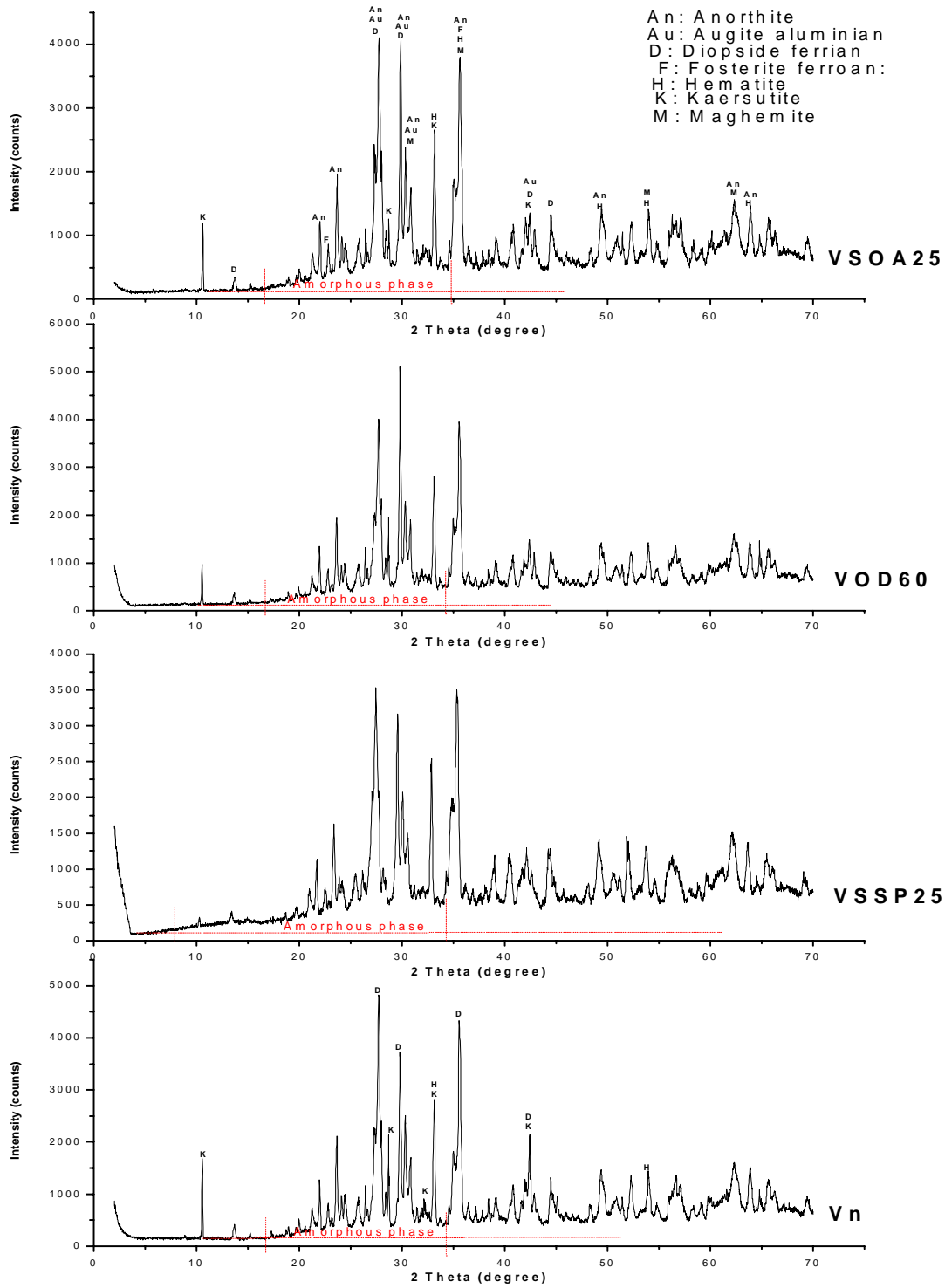


Figure 20: XRD patterns of Vn based alkaline cements aged 28 days preserved under various curing regimes.

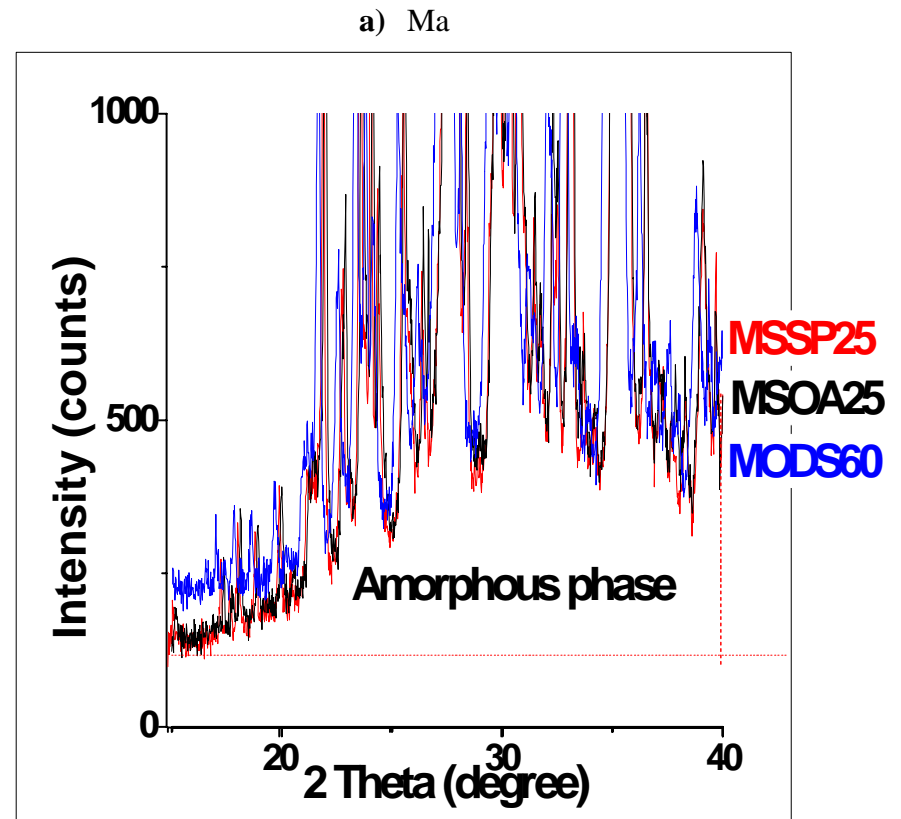
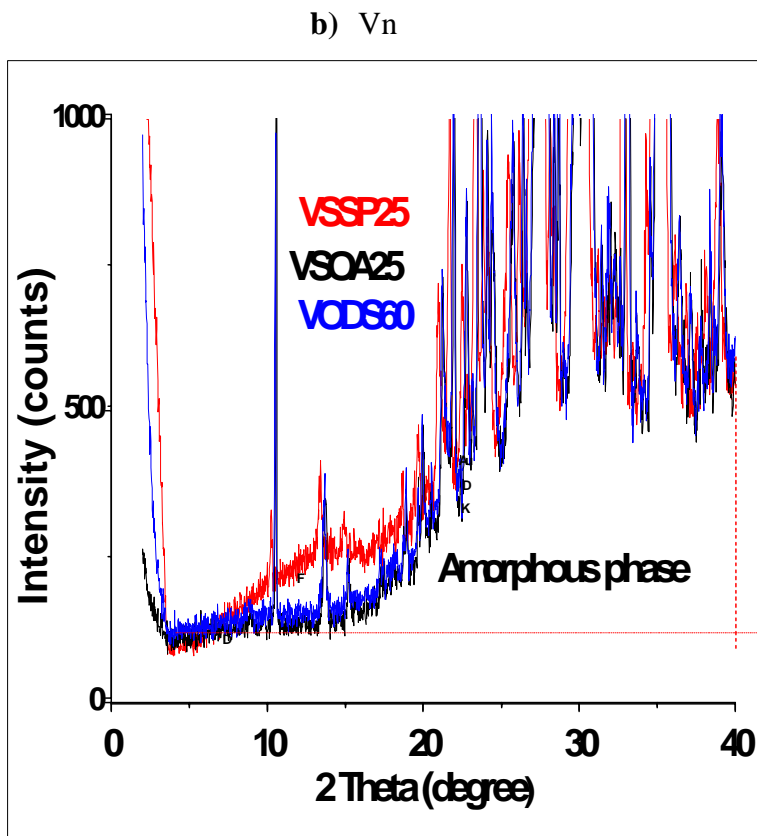
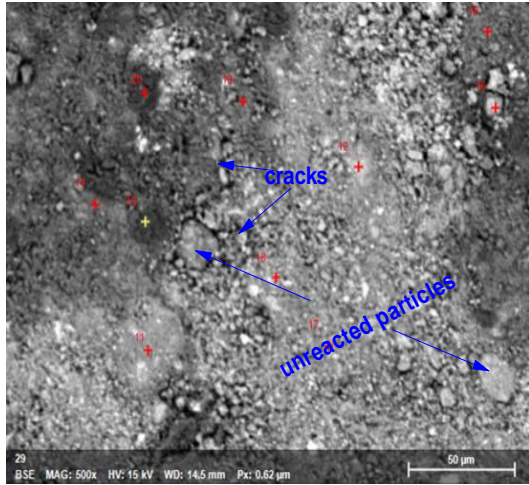


Figure 21: Merged XRD pattern (from 0 to 40 ° 2 $\theta$ ) of volcanic ash based alkaline cements aged 28 days subjected to various curing regimes.

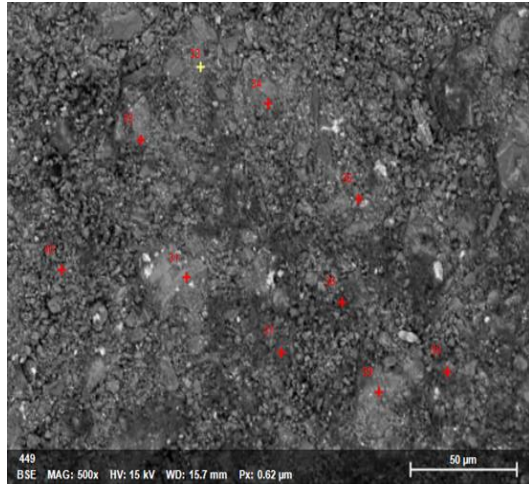
### - Scanning Electron Microscopy

Figure 22 shows Scanning Electron Microscopy images of volcanic ash based alkaline cement specimens cured for 28 days in various curing regimes. On this figure, a heterogeneous morphology is observed on each image among which, the presence of Na rich phase is observed. The latter phase is identified as an efflorescence area due to its very high Na<sup>+</sup> ions content, which in contact with atmospheric CO<sub>2</sub>, will lead to the formation of a whitish layer identified as efflorescence. Moreover, the aforementioned phase is more pronounced in SSP25 cured specimens and seems to decrease from SOA25 to ODS60 cured ones. This trend reveals a progressive level of consumption of sodium ions in the cured specimens and can also translate the degree of polycondensation in respective specimens maintained under various curing regimes. This suggests that the level of polycondensation in SSP25 might be lower than those in SOA25 and ODS60 respectively. In this regard, it is well observed that SSP25 products present the least compactness and possess numerous cracks and unreacted particles, whereas ODS60 ones present the highest compactness and the least cracks. SOA25 products seem to be at the intermediate position. The latter confirms that sealing curing regime delays the polycondensation process in low reactive volcanic ash based alkaline cement, while oven drying and open atmospheric air curing regimes seem to have a favourable response to polycondensation reaction since they led to more compactness. This highlighted difference can be attributed to water management during the polycondensation process. According to Zuhua et al., if too much water exist around reactive species, polycondensation will be hindered [99]. In SSP25 curing regime, the rate of water loss is too slow (Table VII). The fact that the reactive phase content in studied volcanic ashes is very low, the high water content retained by the SSP25 curing regime might have spaced out the reactive entities in the reaction medium thereby hindering their polycondensation. The effect is more significant in VSSP25 specimen than elsewhere, thus justifying the presence of more cracks and the least compactness observed. However, in ODS60 and SOA25 curing regimes, the gradual or rapid loss of water in the reaction medium permits the interaction of reactive entities thereby favouring their polycondensation. The scanning electron microscope results are in opposition with the expectations drawn from X-ray diffraction results above (Figures 19 and 20), and therefore show that high dissolution does not necessary lead to high compactness under certain curing system.

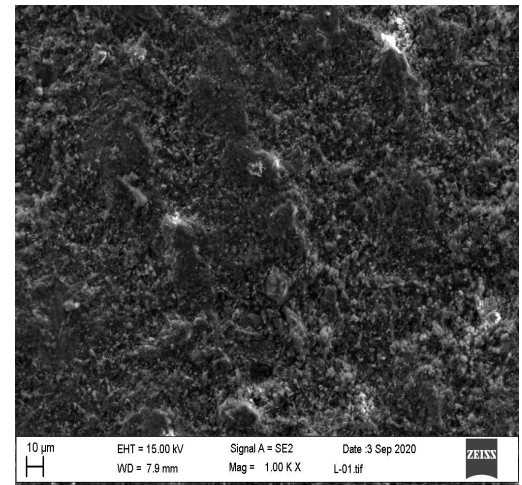




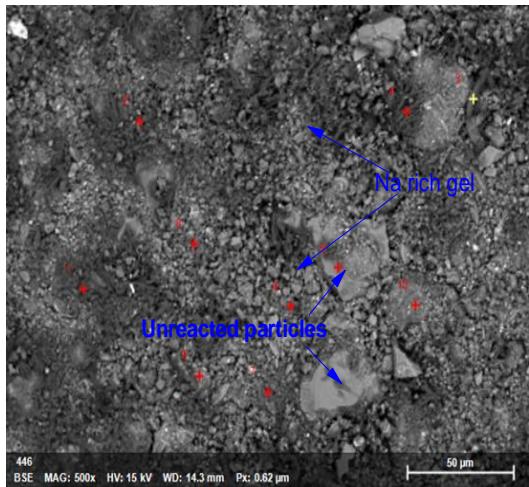
a) MSSP25



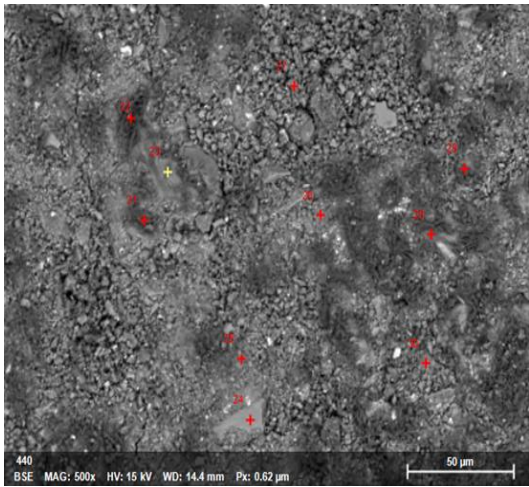
b) MSOA25



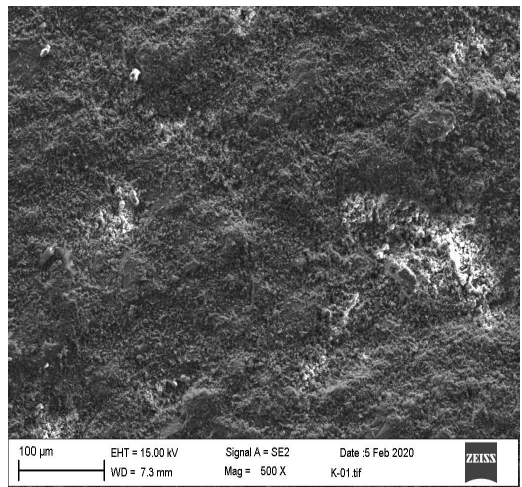
c) MODS60



d) VSSP25



e) VSOA25



f) VODS60

Figure 22: SEM images of volcanic ash based alkaline cement specimens aged 28 days.

### III.2.2. Compressive strength

Figure 23 shows the variation of 28 days compressive strength of volcanic ash based alkaline cement versus curing regime. This figure reveals that no matter the volcanic ash sample, the compressive strength of the cement products increases from SSP25 (with 3.0 MPa for Ma and 1.8 MPa for Vn) to ODS60 (with 16.2 MPa for Ma and 36.1 MPa for Vn) and SOA25 (with 17.1 MPa for Ma and 37.9 MPa for Vn). This strength variation shows how the three curing regimes affect the mechanical properties of cement products, and seems to reveal that oven drying and open atmospheric air curing regimes are adequate regimes for the synthesis of low reactive volcanic ash based alkaline cement. The 28 days compressive strength trend seems to be in accordance with the observations done on scanning electron microscope micrographs revealed earlier above in Figure 22, and supports the fact that water retention in the reaction medium affects the properties of low reactive volcanic ash based alkaline cement. In general, the compressive strength reveals the degree of consolidation that has occurred in cement products. The higher the consolidation, the higher the compressive strength. In alkaline cement chemistry, the level of consolidation translates degree of polycondensation that has taken place in the cement product. In this sense, low strength achieved with SSP25 reflects the low level of consolidation (polycondensation) that has occurred whereas high strength achieved with SOA25 and ODS60 reflects the high level of consolidation. This is as a result of various water contents provided by the curing regimes. Similar observations were done by other authors who realized that moisture content in curing system has effects on properties of alkaline cement products, and concluded that water retention in a closed curing system lowers the compressive strength than that in a water escape system [10,99]. Comparing volcanic ash samples, Vn based specimens demonstrate higher strength than Ma ones and this, due to its high reactive phase content (Table VI). Nevertheless, it is noticed that Vn based alkaline cement expresses lower strength than Ma based alkaline cement when preserved under SSP25 condition. This must be as a result of higher retention of water molecules in Vn based alkaline cement than in Ma as revealed earlier in Table VII. Hence, low water loss in a curing system of low reactive volcanic ash based alkaline cement hinders the polycondensation process thereby lowering the compressive strength.

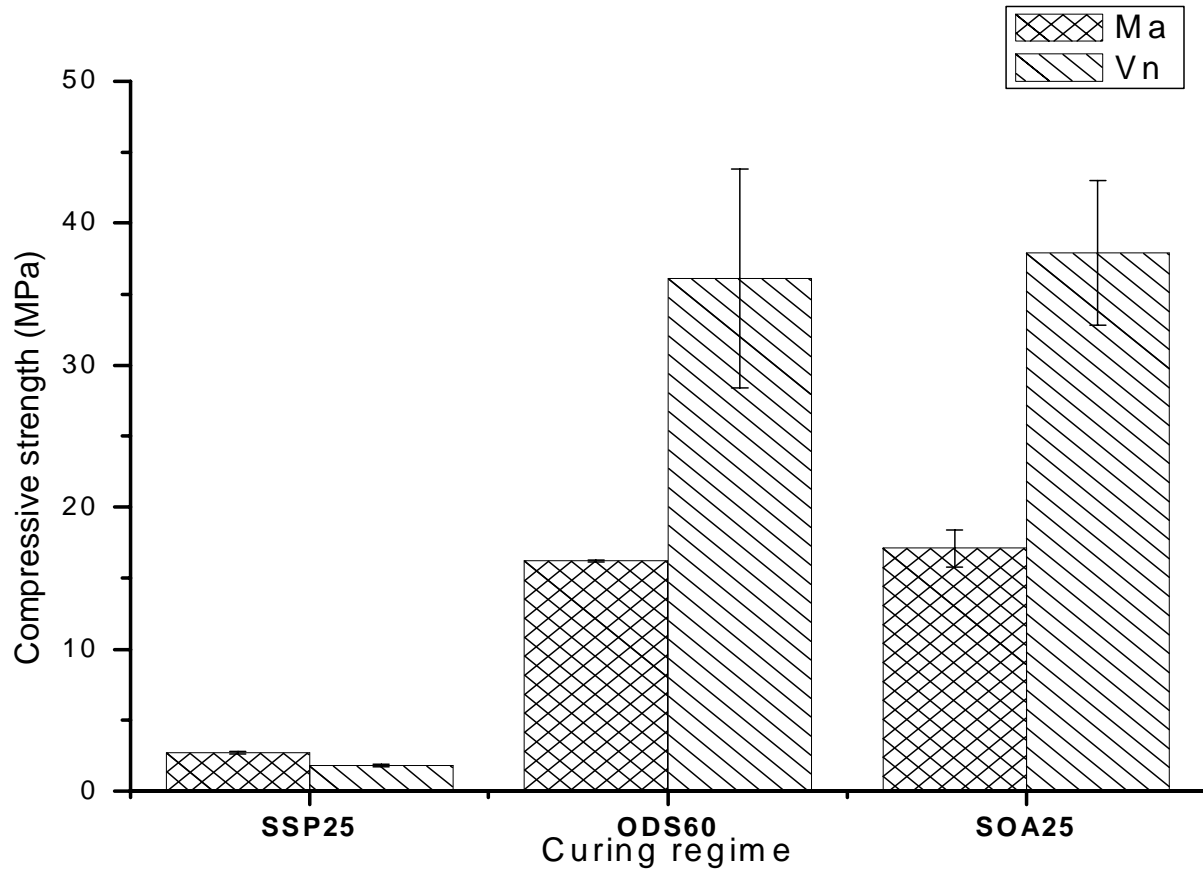


Figure 23: 28 days compressive strength of volcanic ash based alkaline cements.

### III.2.3. Durability

#### III.2.3.1. Sulphuric acid soaking

##### a) Mass loss

Figure 24 presents the mass loss of volcanic ash based alkaline cement specimens aged 28 days immersed in 5 % sulphuric acid for 30 days. According to the latter figure, SSP25 expresses the highest mass loss of about 11.23 % by mass for Ma and 15.40 % by mass for Vn, followed by SOA25 (4.59 % by mass for Ma and 6.09 % by mass for Vn), and later by ODS60 (2.91 % by mass for Ma and 4.35 % by mass for Vn). The above trend shows that oven drying and open atmospheric air curing regimes yield cement products that are more stable in acid medium than those obtained from sealing curing. In fact, the higher the consolidation of a cement specimen, the higher the stability of the latter in an aggressive environment. In this way, it can be deduced that

ODS60 and SOA25 cement specimens are more consolidated than SSP25 ones. Additionally, the observed trend in Figure 24 is in accordance with scanning electron microscope and compressive strength results (Figures 22 and 23 respectively) and thus gives additional certitude to the fact the degree of polycondensation in low reactive volcanic ash based cement increases following the curing regime order as follows: SSP25 < SOA25 < ODS60. Hence, the higher the water retention in low reactive aluminosilicate based cement, the lower will be its stability in aggressive medium. Furthermore, while comparing sample at each curing regime, it can be noted that Vn based alkaline cement products express higher mass loss than those of Ma. This can be due to the fact that Ma possesses lower reactive phase content ( $R_C$ ) than Vn, which makes the availability of unreacted alkaline solution more significant in its respective cement products, which must have interacted with acid solution, thereby reducing its effect.

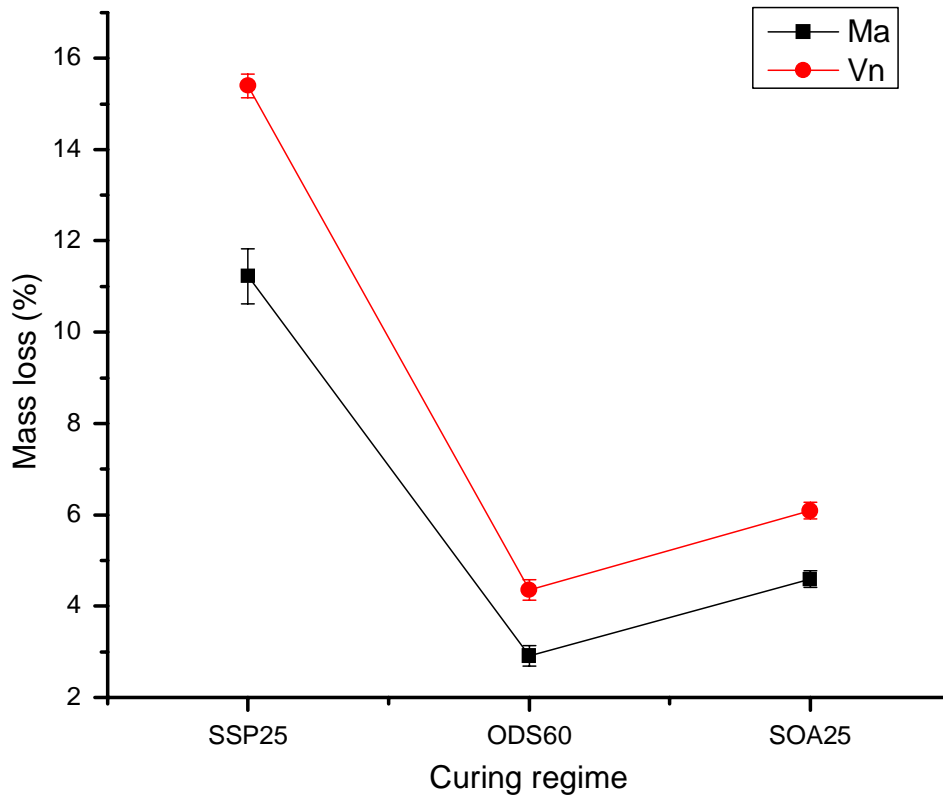


Figure 24: Mass loss (%) of volcanic ash based alkaline cement aged 28 days, immersed in 5% by mass of sulphuric acid for 30 days.

## b) Compressive strength

The residual strengths obtained from immersed specimens in acid medium for 30 and 90 days presented in Figures 25 and 26 show antagonistic trend from one sample to another, but are in accordance with the trend of mass loss observed above between Vn and Ma based specimens. Ma based specimens demonstrate an increase in strength when immersed in acid medium while the reverse is observed with Vn based specimens. That is, after 30 and 90 days of immersion, Ma based alkaline cement products recorded respective residual strengths of 4.9 and 5.4 MPa for MSSP25, 18.1 and 26.2 MPa for MODS60 and 26.2 and 28 MPa for MSOA25 whereas for Vn based alkaline cement products, the recorded strengths were 5.4 and 6.8 MPa for VSSP25, 18.1 and 9 MPa for VODS60 and 34.3 and 28 MPa for VSOA25. These correspond to strength increase of: 81 and 100 % for MSSP25; 11 and 62 % for MODS60; 53 and 64 % for MSOA25 (Figure 25) and 201 and 276 % for VSSP25, and to strength decrease of: 50 and 75 % for VODS60 and 10 and 26 % for VSOA25 (Figure 26). The above increase in strength can be due to high availability of unreacted silicate in Ma based specimens than in Vn based specimens. In fact, the very low reactive phase content in Ma sample renders unreacted silicate available in the reactive medium compared to Vn sample which expressed high reactivity in alkaline medium. This unreacted silicate when exposed to acid medium, forms silica gel which may have helped in reinforcing the residual strength. According to many authors, the exposure of sodium meta-silicate in acid medium causes the formation of silica gel [142–144]. On the other hand, in exception to VSSP25 specimens, the drop in residual strength expressed by Vn based specimens as mentioned earlier in this paragraph can be attributed to the depolymerisation of the binding phase. Furthermore, it can be noted that the latter drop in residual strength is more pronounced in VODS60 specimens than in its counterpart VSOA25. In one way, this can be attributed to low amount of free silicate in VODS60 than in VSOA25. In other way, this might be due to the presence of micro pores in VODS60 generated by rapid loss of water molecules under oven drying regime. According to many authors, the presence of micro pores in alkaline cement product subjected to acid attack, permits a high level of penetration of acid solution in the structure, which can lead to high depolymerisation of the inorganic polymer framework [145–147].

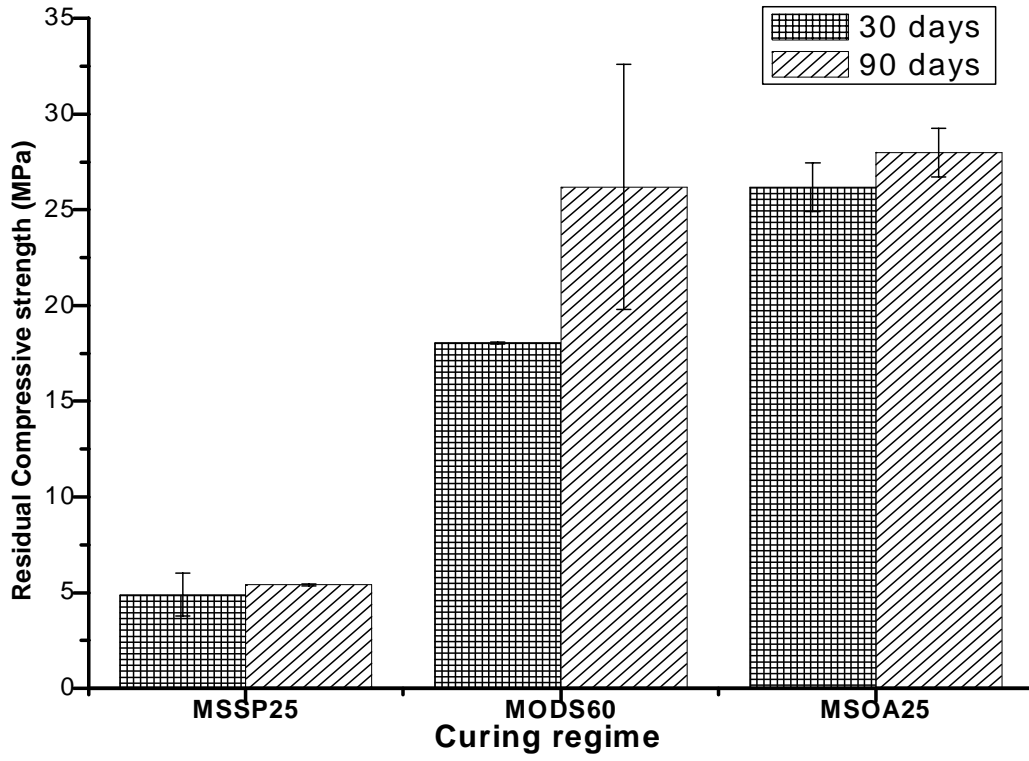


Figure 25: Residual of strength of Ma based alkaline cement after immersion in 5 % by mass of sulphuric acid.

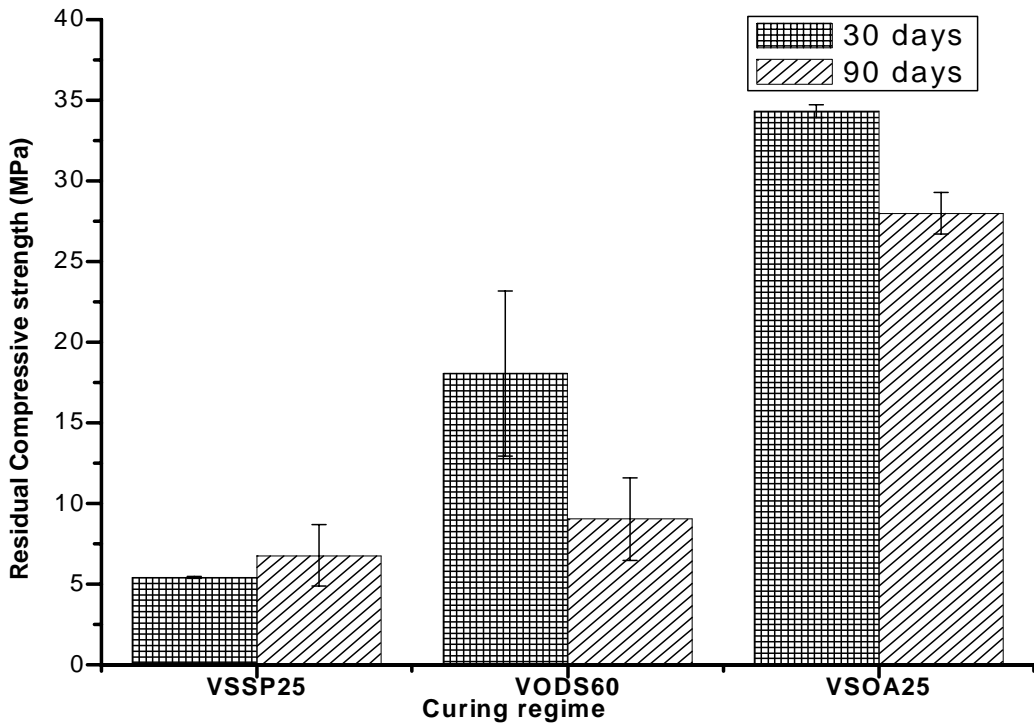
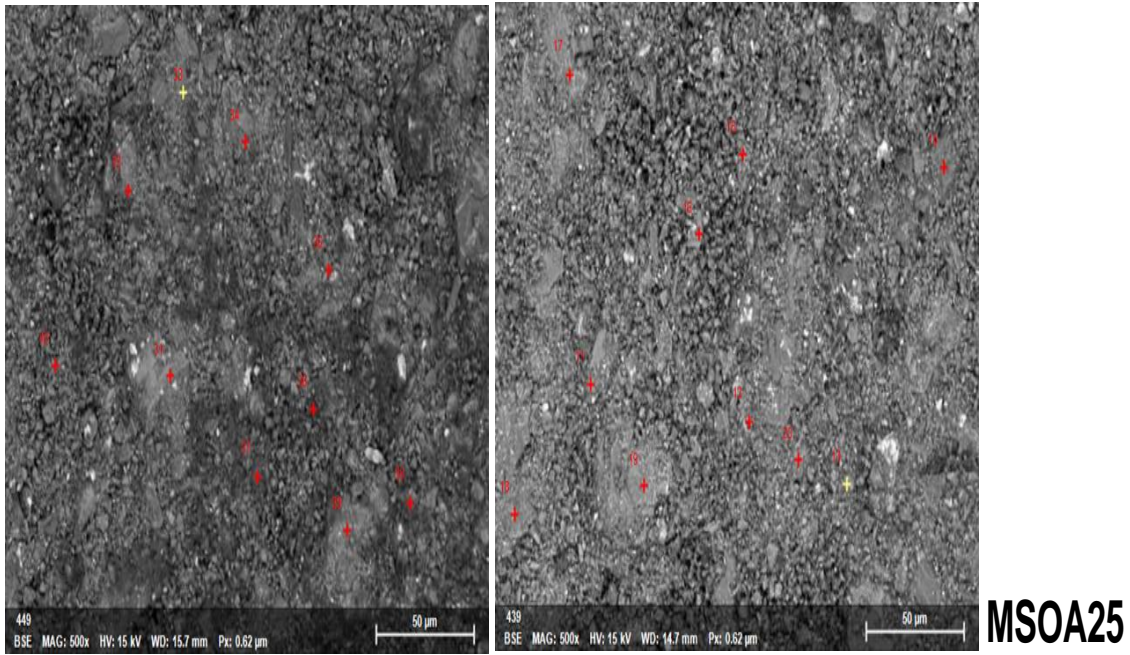


Figure 26: Residual strength of Vn based alkaline cement after immersion in 5 % by mass of sulphuric acid.

### c) Microstructure

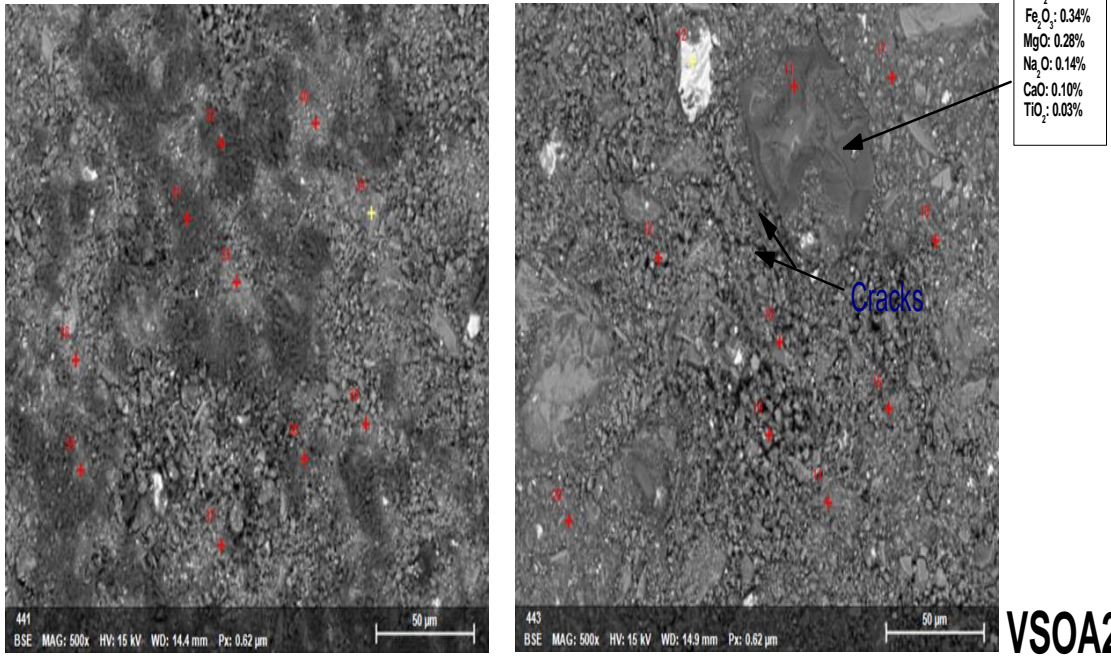
Figure 27 presents the microstructural changes that have occurred on SOA25 cement specimens when subjected to sulphuric acid attacks for 30 days. On these scanning electron microscope images, it can be well observed that the Na rich phase present in either MSOA25 or VSOA25, is completely absent in their respective acid soaked specimens. This suggests that the Na rich phase, due to its basic character, has been leached out from the specimens by the acid solution. Additionally, the compactness of MSOA25 soaked specimen is found to be more pronounced than its non-soaked one. This, therefore, confirms that the interaction that has taken place between the unreacted silicates in Ma based cement products and the acid solution has given place to a new product that has contributed to enhance the compactness of Ma based cement product. On the other hand, the compactness of VSOA25 specimens reduces when subjected to acid attacks. From the SEM images, this can be assigned to the appearance of cracks and new phase identified as Al rich phase thanks to EDX results. The presence of Al rich phase might be the resultant of the depolymerisation process mentioned earlier above. The above observations are in accordance with the results obtained on residual strength (Figures 25 and 26) and thus, reveal the higher stability of Ma (reactive phase content  $\leq 18$  % by mass) based alkaline cement specimens compared to those of Vn (reactive phase content  $\geq 26$ ) in acid medium.



Non-soaked

Soaked

**MSOA25**



Non-soaked

Soaked

**VSOA25**

Figure 27: SEM images of volcanic ash based alkaline cement specimens cured on open atmospheric air (SOA25) for 28 days before and after subsection to sulphuric acid attack.



### III.2.3.2. Water soaking

#### a) Compressive strength

The variation of residual strength of specimens soaked in distilled water for 30 days versus the curing regime is presented in Figure 28. The results obtained show that the stability of volcanic ash based alkaline cement specimens in water increases from SSP25 to ODS60 curing regime with SOA25 curing regime as the intermediate. SSP25 curing regime recorded a residual strength of 0 MPa for Ma and 0.9 MPa for Vn, followed by SOA25 with 2.7 MPa for Ma and 10.2 MPa for Vn; and finally ODS60 with 7.2 MPa for Ma and 13.8 MPa for Vn. In fact, the immersion of cement product into water is to assess whether there are water soluble phases present in the latter which in turn can weaken the cement product. Thus, regarding the above results, it is obvious that ODS60 curing regime favours the highest degree of polycondensation in alkaline activation of low reactive volcanic ash. Nevertheless, SOA25 curing regime is not to be neglected.

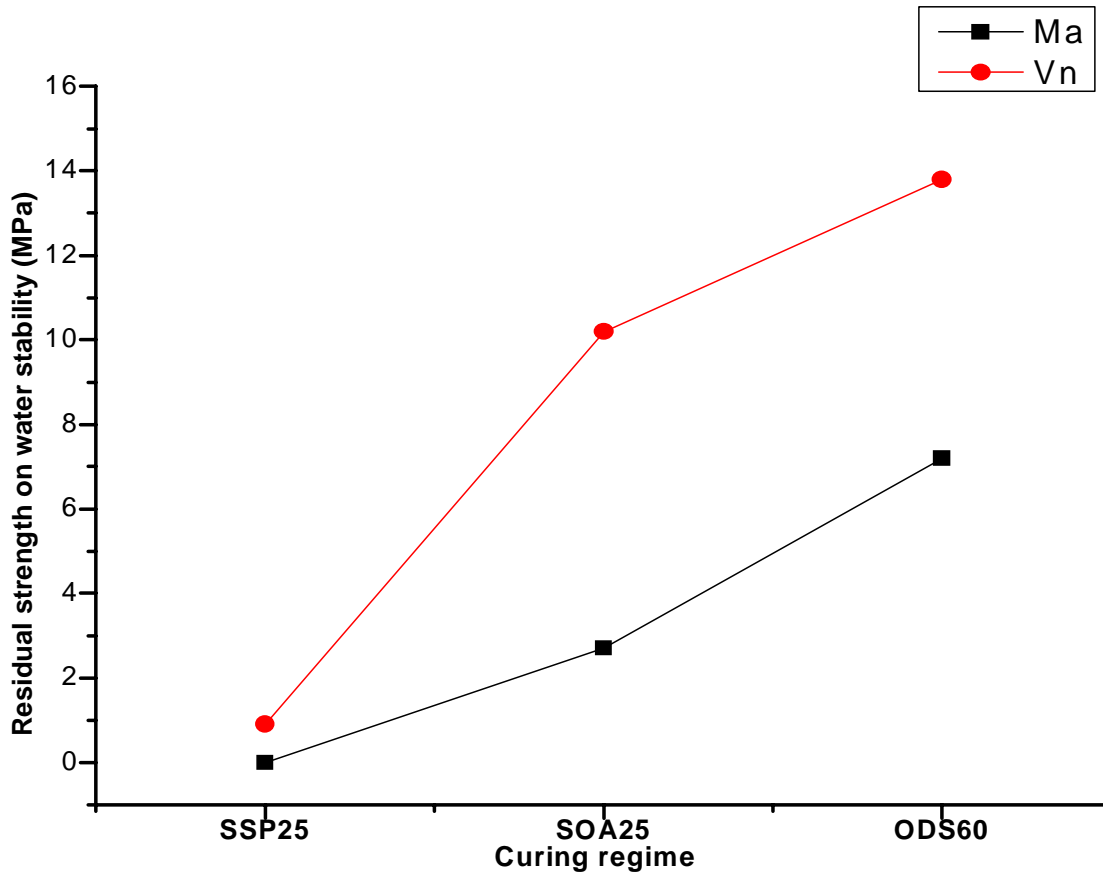


Figure 28: Residual compressive strength of alkali activated volcanic ashes immersed in water for 30 days.

### b) Visual aspect of specimens after immersion in water for 30 days

Regarding the increase in residual strength of Ma based alkaline cement products soaked in acid medium for 30 days (Figure 23), it seemed interesting to compare the stability in water of the latter to those kept away from acid medium. To do that in order to favour ambient curing, only MSOA25 cured specimens were used. The visual aspect of immersed specimens (MSOA25 acid and MSOA25 normal) in distilled water for 30 days is shown in Figure 29. On these picture, it is well observed that cement products merged in acid medium do not undergo visual deterioration when soaked in water. Hence, acid cured specimen (MSOA25 acid) shows high stability in water than its counterpart (MSOA25 normal). Moreover, this is further confirmed by residual strength presented in Table IX where it is noticed that MSOA25 acid recorded 19.0 MPa against 2.7 MPa for MSOA25 normal after 30 days of immersion in water. This corresponds to strength decrease of about 28 and 84 % for MSOA25 acid and MSOA25 normal respectively. The latter reveals the significant contribution of acid curing on the development of strength and stability in low reactive volcanic ash based alkaline cement. On this regard, acid curing seems necessary to the alkaline activation of low reactive volcanic ash with reactive content  $\leq 18$  % by mass.



**MSOA25 normal**



**MSOA25 acid**

Figure 29: Visual aspect of Ma based alkaline cement specimens immersed in water for 30 days.

Table IX: Residual strength of specimens after 30 days of immersion in water.

Residual strength (MPa)	
MSOA25 normal	2.7
MSOA25 acid	19.0

MSOA25: normal cured specimens, MSOA25 acid: acid cured specimens.

### III.2.4. Conclusion

The use of low reactive volcanic ash as alone raw material in alkaline activation seems to be of low interest due to its low reactivity in alkaline medium. In order to encourage its use, the present study tries to provide curing regimes necessary to enhance the mechanical and durability properties of low reactive volcanic ash based alkaline cement. Thus, it is noted that sealing curing regime fosters amorphous phase dissolution as well as proportions of some mineral phases, but hinders polycondensation reaction. This led to the production of cement products with low compressive strength and poor durability. Thus, the latter regime is found not suitable for the alkaline activation of low reactive materials. However, oven drying and open atmospheric air curing regimes provide low reactive volcanic ash based alkaline cement: high mechanical properties and good durability. Besides that, alkaline cement derived from volcanic ash with reactive phase content  $\leq 18$  % by mass and cured in open atmospheric air possesses low stability in water. The later seems to be enhanced when the specimens is beforehand soaked in acid medium. Therefore, the curing regime is an essential parameter in the development of cementitious properties of low reactive volcanic ash based alkaline cement.

### III.3. Reactivity of cassava peel ash ( $C_A$ ) in alkaline medium

#### III.3.1. Dissolution capacity of $C_A$ in different concentrated alkaline solutions.

The Table X below shows the percentage of  $C_A$  particles dissolution varies with respect to the concentration of NaOH solution. From this table, it can be noticed that the amount of dissolved particles increases from 42.96 to 52.52 % by mass when the NaOH concentration of the leaching solution increases from 4M to 12M respectively, with 45.08 % by mass for 8M as an intermediate value. This reveals the influence of the pH of the leaching solution on the dissolution capacity of  $C_A$  despite its high alkali content, and joins other studies which reported that the higher the pH of the leaching solution, the higher the dissolution capacity of aluminosilicate [9,47]. Looking at the X-ray diffraction patterns of solid residues of the leaching tests presented in Figure 30, the broad hump, located at  $2\theta = 14 - 38^\circ$  on X-ray diffraction of  $C_A$  (Figure 15), characterising the existence of an amorphous phase is absent. This confirms the dissolution of the latter phase independent to the NaOH concentration of the leaching solutions. Moreover, some major crystalline phases such calcite and arcanite seem to have also dissolved. However, their dissolution increases with increase in sodium hydroxide concentration. Thus, the below results (Table X and Figure 30) show that  $C_A$  is sensitive to alkaline solution and requires high concentrated alkaline medium for high dissolution.

Table X: Dissolution capacity ( $D_C$ ) of  $C_A$  versus the concentration of NaOH solution.

Concentration of NaOH solution	Amount of dissolved particles in alkaline solution (% by mass of $C_A$ )
4M	42.96
8M	45.08
12M	52.52

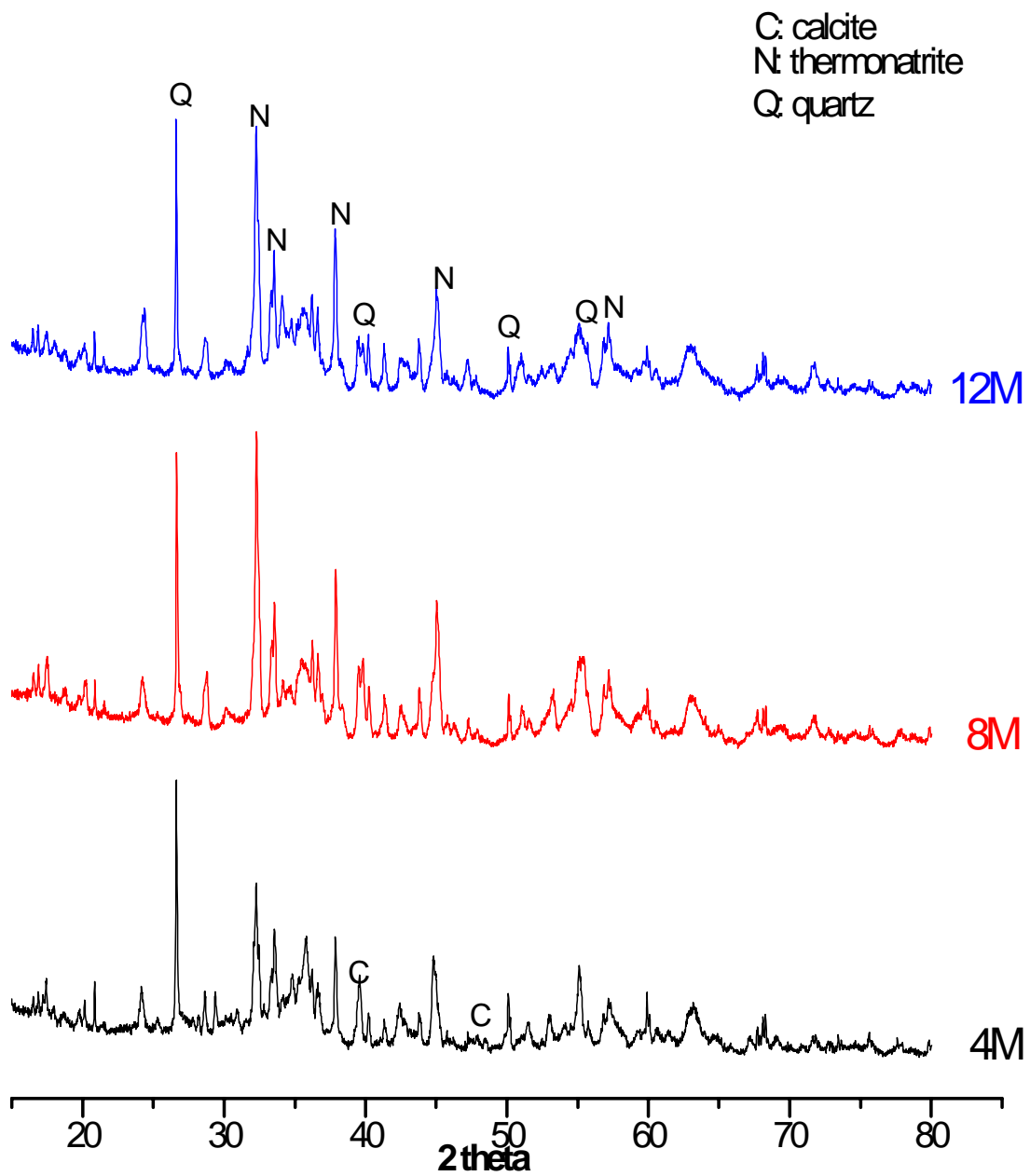


Figure 30: XRD patterns of residues of leached cassava peel ash in different NaOH solutions.

### III.3.2. Characterization of cassava peel ash based alkaline activated materials

#### III.3.2.1. Microstructure

- **Fourier Transform Infrared spectroscopy**

Figure 31 presents the Fourier Transform Infrared spectra of  $C_A$  based alkali activated products compared to that of  $C_A$ . On this figure, it is well remarked that the vibration bands located at 1112 and 1004  $\text{cm}^{-1}$  present on  $C_A$  spectrum, corresponding respectively to the stretching of the Si-O bond and to the asymmetry stretching vibrations of Si-O-Si and Si-O-Al bonds, are now absent in the alkali activated products. These two bands must have fused and shifted to a lower wavelength number band at 988  $\text{cm}^{-1}$  which corresponds to the vibration of Si-O-T (T: Si or Al) bonds of the newly formed aluminosilicate gel after alkaline activation [31,87]. Moreover, this newly formed band (988  $\text{cm}^{-1}$ ) gradually increases in size as the  $\text{SiO}_2 / \text{Na}_2\text{O}$  molar ratio of the alkaline solution decreases from 2.3 to 1.5 (Figure 31b). All these reveal the formation of a polycondensed structure in alkali activated cassava peel ash as observed by other authors using other aluminosilicates raw materials [9,79]. Also, the progressive broadness of the latter band points out the high degree of polycondensation ordered by the decrease in  $\text{SiO}_2 / \text{Na}_2\text{O}$  molar ratio. The bands at 1419  $\text{cm}^{-1}$  is attributed to the vibration of carbonates. This band associated with 875 and 714  $\text{cm}^{-1}$  corresponding to the vibration of C-O bonds of calcite in  $C_A$ . On the other hand, the latter band (1419  $\text{cm}^{-1}$ ) can also be attributed sodium carbonate usually present alkali activated materials due to free mobile sodium ions [48]. Due to the presence of calcite, it is difficult to confirm whether sodium carbonate is present in  $C_A$  based alkali activated products. However, it can be highlighted that the absorbance peaks of carbonate diminish as the  $\text{SiO}_2 / \text{Na}_2\text{O}$  molar ratio decreases, and hence, suggest a high dissolution of calcite content. Similarly, the bands at 3362 and 1643  $\text{cm}^{-1}$  corresponding to the vibration of water molecules in alkaline activated products [5,44,87] seem to follow the same trend as C-O bands. This suggests that AAC<sub>2.3</sub> specimens retain more water molecules than those of AAC<sub>1.5</sub>. In general, in exception to the amorphous polycondensed structure which retain water molecule, other phases such calcium silicate hydrate, sodium carbonate and hydrotalcite, usually present in alkali activated materials, are water consuming phases [148]. This means that besides the inorganic polymer, there might be other phases formed in AAC<sub>2.3</sub> which are responsible for the high retention of water molecules.

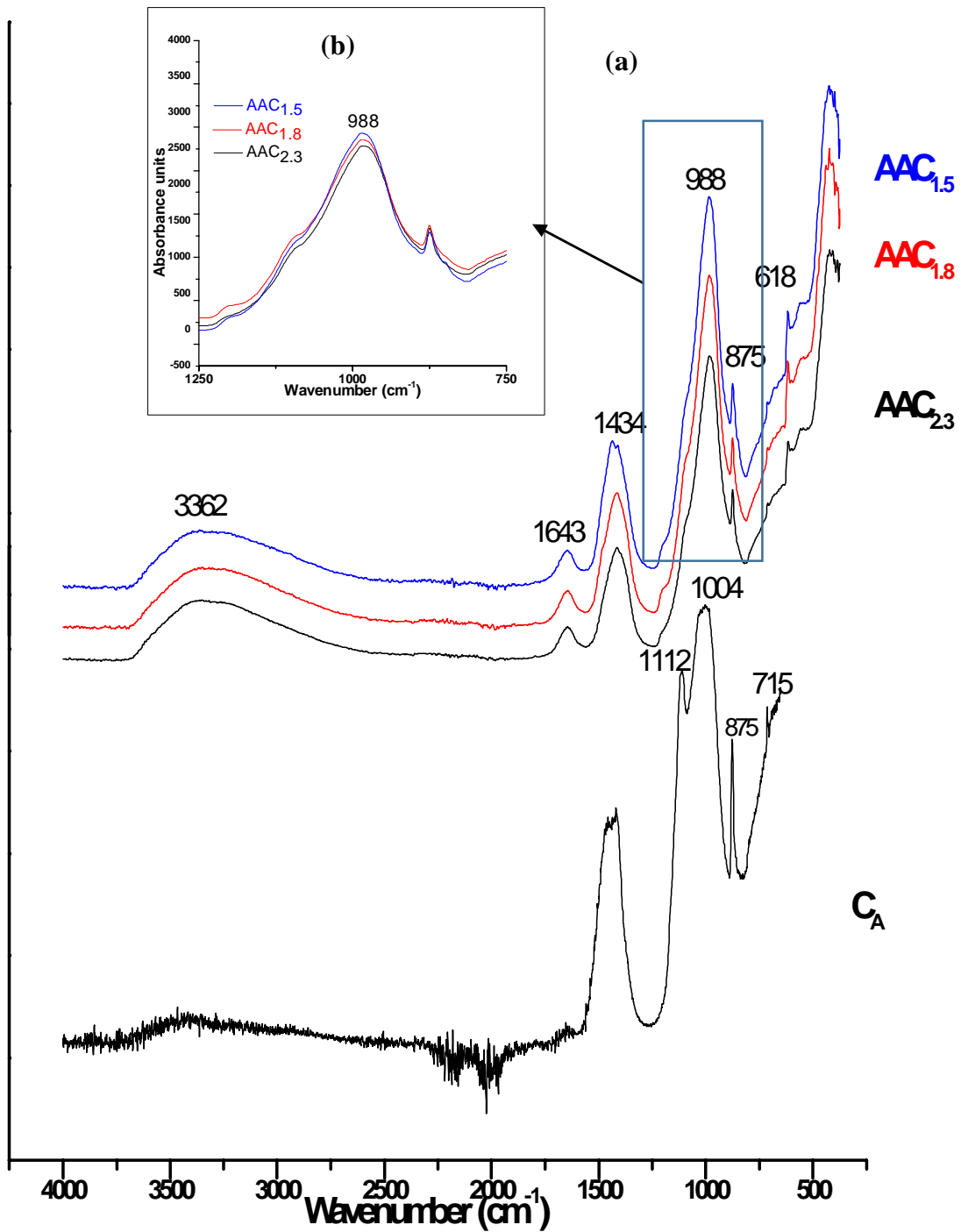


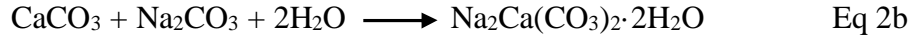
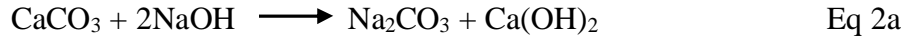
Figure 31: FTIR spectra of cassava peel ash based alkali activated pastes.

- **X-ray diffraction**

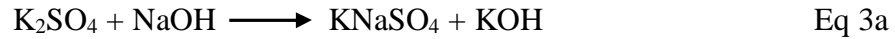
The X-ray diffraction patterns of alkali activated cassava peel ash (AAC) and that of its raw material ( $C_A$ ) are presented in Figure 32. In exception to arcanite, major minerals such calcite, quartz and beusite calcian identified in the raw materials are also present in alkali activated products. However, calcite content seems to vary as we go across the patterns (from AAC<sub>2.3</sub> to AAC<sub>1.5</sub>). This is noticeable through the intensities of peaks attributed to this mineral which decrease as the  $SiO_2 / Na_2O$  molar ratio decreases. Besides that, the presence of new peaks corresponding to newly formed minerals such as pirssonite [ $(Na_2Ca(CO_3)_2$  : PDF 24-1065], Calcium silicate hydrate [ $Ca_2SiO_4 \cdot 0.30H_2O$ : PDF 15-0584] and apthitalite [ $(K_3Na(SO_4)_2$ : PDF 20-0928] are also identified. On this, it is important to note that, calcium silicate hydrate (C-S-H) is formed in AAC<sub>2.3</sub> and AAC<sub>1.5</sub> specimens, and that due to the various degree of dissolution of reactive entities of  $C_A$  in respective alkaline solutions. At high  $SiO_2 / Na_2O$  molar ratio (i.e. at low alkaline medium), calcium entities are predominantly dissolved thereby promoting the formation of C-S-H gel [15]. Differently, as the latter molar ratio decreases, several entities (Si, Al, Fe and Ca) are highly dissolved which can inhibit the formation of C-S-H. Concerning pirssonite and apthitalite, these are mineral phases resulting from the reaction of sodium ions with calcite and arcanite respectively as proposed in equations 2(a-b) and equation 3(a-b). Calcite transformation to pirssonite was reported by several authors [148–150], and seems to be more pronounced at  $SiO_2 / Na_2O$  molar ratio equal to 1.8 when we compare the intensities of its respective peaks along different  $SiO_2 / Na_2O$  molar ratios. Referring to equation 2a, during this pirssonite formation, calcium hydroxide is been produced. However, its presence in activated products is not revealed by the X-ray diffraction patterns. This, therefore, suggests that the latter is either amorphous or has been transformed to a more stable compound. According to some authors, the presence of reactive calcium in a carbon dioxide rich medium can favour the formation of calcium carbonate [91,151,152]. The latter idea seems judicious here since there might be free carbonate ions present in the reactive medium which result from the dissolution of original calcite whose  $Ca^{2+}$  ion may have participated in the formation of binding phase(s). Hence, this might explain why the existence of calcite content persist despite its multitude contributions in the reaction medium (pirssonite and binding phase formations). Besides the above, it can also be highlighted that apthitalite formation makes available the presence of potassium ions in the reactive medium (equation 3a) which might participate in the polycondensation reaction. Furthermore, regarding the absence of peaks



attributed to arcanite on the X-ray diffraction patterns of  $C_A$  based alkali activated products, it can be concluded that the latter mineral phase is totally transformed to apthitalite.



Pirssonite



Apthitalite

Concerning minor crystalline phases (potassium phosphate and magnesium oxide) earlier identified on the X-ray diffraction pattern of  $C_A$ , it is very difficult to suggest that either the latter phases reacted or remained inert in the reaction medium due to abundance of peaks on the X-ray diffraction pattern. On the other hand, a broad hump as observed on  $C_A$  pattern, is still visible on the patterns of activated products (AAC). Nevertheless, the latter is well modified, and seems to have shrunk in width to about  $08^\circ (2\theta)$  (from  $14 - 38^\circ (2\theta)$  for  $C_A$  to  $22 - 38^\circ (2\theta)$  for AAC) followed by a slight increase in height when compared to that of  $C_A$ . This hump modification seems to increase with decrease  $\text{SiO}_2 / \text{Na}_2\text{O}$  molar ratio. In many reported studies, the hump modification is most often identified as a hump shift which is one of the characteristic of a formed polycondensed structure [3,24,153]. But here, the observed shrinkage must be related to the composition of the amorphous binding phases present in the hump. Whatsoever, the altering of the  $C_A$  hump under alkaline activation is in accordance with the band formed at  $998 \text{ cm}^{-1}$  on the Fourier Transform Infrared spectra (Figure 31), and thus, confirms the formation of a polycondensed structure.

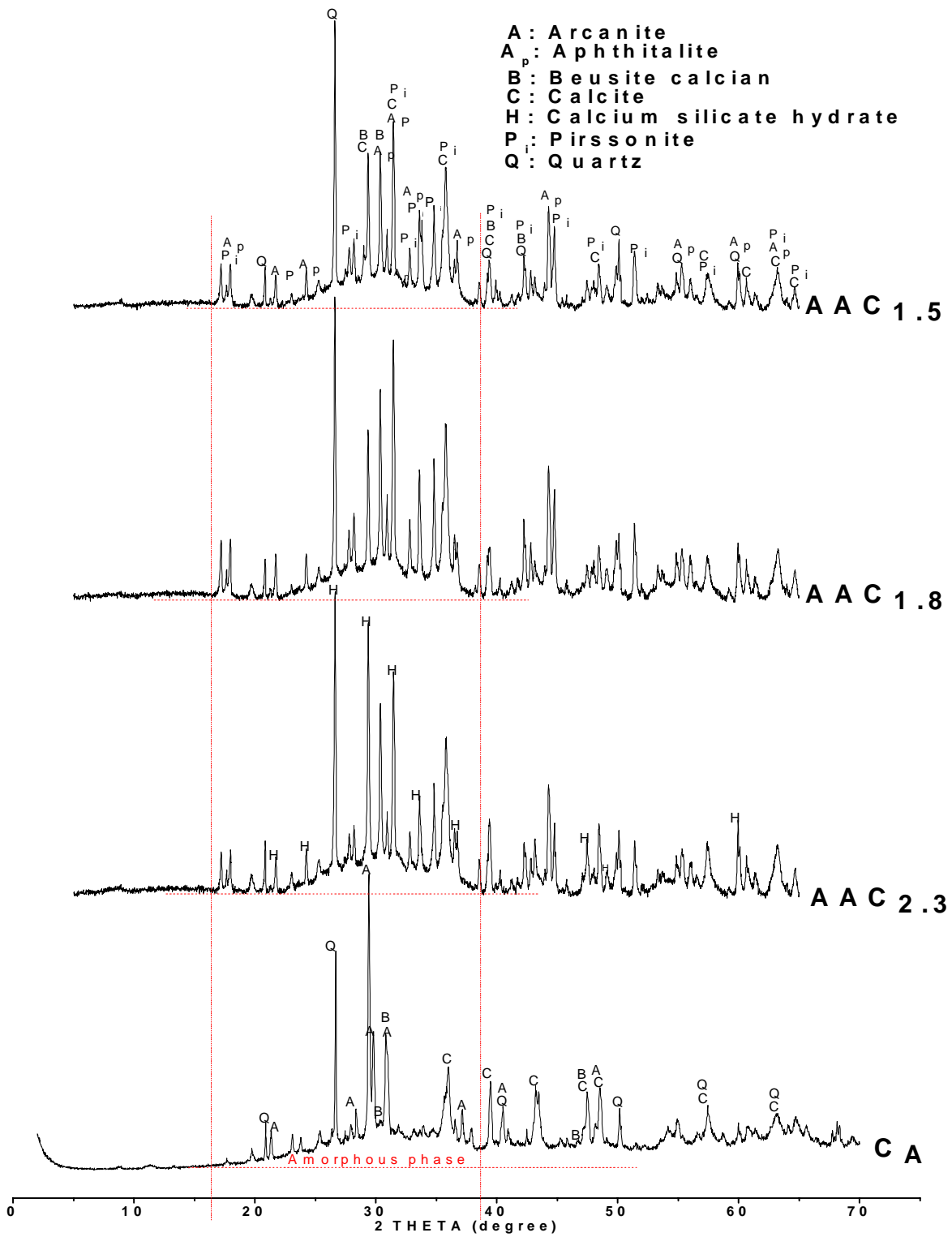
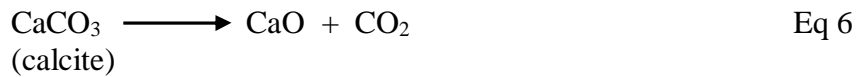
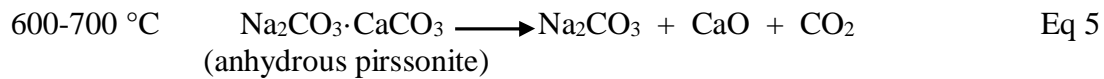
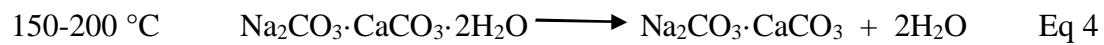


Figure 32: XRD patterns of cassava peel ash based activated pastes.

- **Thermal analysis**

Figure 33 below shows respectively the TGA (a) and DSC (b) curves of the  $C_A$  based alkali activated products subjected to thermal analysis from ambient temperature to 700 °C. On both curves, four thermal phenomena characterized by mass loss and endothermic peaks on TGA and DSC curves respectively can be identified. The first phenomenon occurs within the temperature interval 50 – 110 °C, followed by the second one located between 150 and 200 °C. The third and fourth phenomena are respectively located within 400 – 520 °C and 600 – 700 °C. The first phenomenon is attributed to the departure of free water molecules. Within this first range, AAC<sub>2,3</sub> expresses water loss by two endothermic peaks centred at 68 and 91 °C on the DSC curves (Figure 33b). The first peak (at 68 °C) is attributed to the liberation of water molecules contained in sodium carbonate while that at 91 °C is attributed to the loss of water molecules contained in the pores of the binding phase of the  $C_A$  based alkali activated cement. As the  $SiO_2/Na_2O$  molar ratio decreases, the two latter peaks give way to a large unique peak centred at 76 °C (AAC<sub>1,5</sub>) which indicates an increase in binding phase content to the detriment of sodium carbonate formation. The above changings suggest that as the pH increases, binding phase content increases thereby inhibiting the formation of sodium carbonate. The second mass loss (150 - 200 °C) for which an endothermic peak centred at 170 °C is presented on the DSC curve, is assigned to the dehydration of the pirssonite (equation 4) and C-S-H gel. The intensity of the latter peak is found to reduce when the DSC curves are compared (from AAC<sub>2,3</sub> to AAC<sub>1,5</sub>). This drop is mainly attributed to the inhibition of C-S-H gel formation as the basicity of the reaction medium increases. This result joins the observation done on the X-ray diffraction patterns of AAC<sub>1,8</sub> and AAC<sub>1,5</sub> where the absence of crystalline C-S-H was noticed (Figure 32). Between 400 and 520 °C, there is a third thermal phenomenon assigned to the dehydration of calcium aluminosilicate hydrate gel [154]. Moreover, it can also attributed to the decomposition of calcium hydroxide if present. Additionally, within the same temperature interval (400-520 °C), it is important to highlight that other phenomenon must have taken place without any modification of mass. This concerns a solid-solid phase transition of anhydrous pirssonite from one polymorphic form to another [155]. The last thermal phenomenon observed corresponds to the decomposition of calcium carbonate present in both anhydrous pirssonite and unreacted calcite to form sodium carbonate and calcium oxide respectively as shown in equations 5 and 6 [155,156]. It is noticeable on TGA curves (Figure 33a), within the temperature interval 400-700 °C, that the mass loss is more pronounced in AAC<sub>1,8</sub>, than

elsewhere. This suggests that one of the phases decomposing within this temperature interval must be in high amount in AAC<sub>1.8</sub> specimens compared to other products. In fact, if the Ca(OH)<sub>2</sub> yielded by pirssonite formation is present in the amorphous form and/or in the form of calcium carbonate in C<sub>A</sub> based alkali activated products as suggested earlier in comments related to X-ray diffraction results of C<sub>A</sub> based alkali activated products (Figure 32), in this case, AAC<sub>1.8</sub> might be considered as having the highest Ca(OH)<sub>2</sub> and / or CaCO<sub>3</sub> contents in view of its pirssonite content which seems to be the highest. Consequently, this might be the main reason why mass loss is higher in AAC<sub>1.8</sub> than in other products at this temperature range.



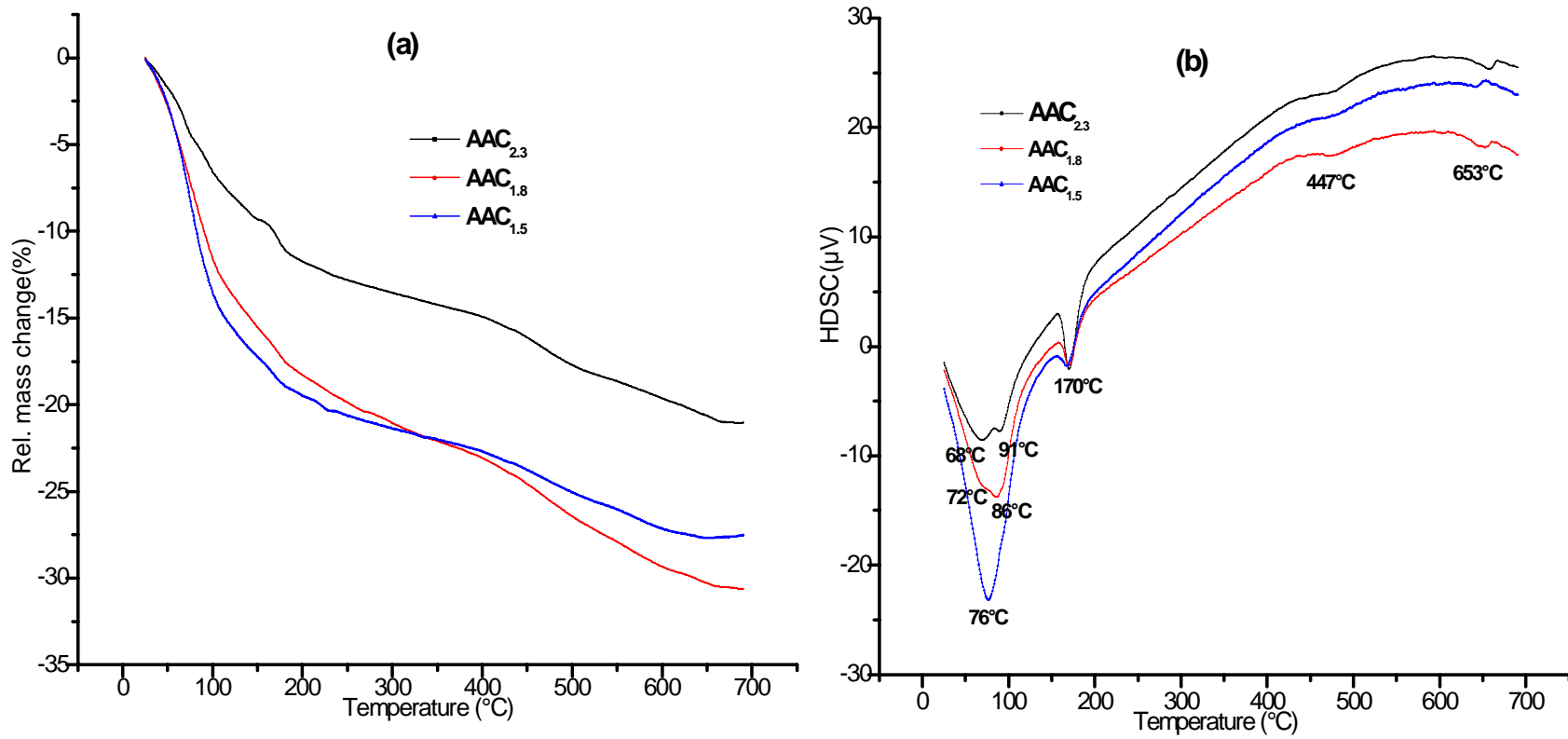


Figure 33: TGA (a) and DSC (b) curves of alkali activated cassava peel ash.

- **Scanning Electron Microscopy**

The micrographs of scanning electron microscope of  $C_A$  based alkali activated products are presented in Figure 34. On this figure, it is observed that the surfaces of specimens present a heterogeneous morphology which seems compact and highly constituted of laminar type structure throughout the specimens. Comparing the micrographs, it is worthwhile to note that the heterogeneity of the surface increases as  $SiO_2 / Na_2O$  molar ratio increases. This can be revealed by the presence of two layers in  $AAC_{1.5}$ : laminar type structure (zone 1) and smooth compact layer (zone 2). The laminar type structures are ascribed to apthitalite and pirssonite phases present in the specimens. Their size and distribution along the surface of specimens seems to increase with respect to the increase in  $Na_2O$  content (i.e.  $SiO_2 / Na_2O$  decreases from 2.3 to 1.8). The previous statement is in accordance with the increase in intensities of peaks of both minerals (pirssonite and apthitalite) observed on X-ray diffraction patterns in Figure 32. This therefore suggests that as the  $Na_2O$  content increases, more and more Na atoms are consumed by calcite and arcanite to form pirssonite and apthitalite respectively. Moreover, relying on the elemental mapping which reveals the distribution of element all over the surface of cement specimens, the observed laminar type structures are suggested to be either mixed with the binding phase(s) or covering the binding phase(s). The idea of having both suggestions in the specimens is not left behind. Whatsoever, both phases are present in specimens. Besides that, on the micrograph of  $AAC_{2.3}$ , bowl type structures can also be noticed. Regarding its elemental mapping (Figure 35), these bowl type structures are identified as sodium carbonate, and seem to disappear as the  $SiO_2 / Na_2O$  molar ratio decrease to 1.5 (Figure 36). This variation suggests that in  $AAC_{2.3}$  specimen, some  $Na^+$  ions are free and mobile which render them susceptible to chemical reaction with carbonate ions present in the reaction medium or with atmospheric carbon dioxide in order to form sodium carbonate. The latter phenomenon was expected to be more pronounced (i.e. high formation of sodium carbonate) in  $AAC_{1.8}$  and  $AAC_{1.5}$  regarding the increasing  $Na_2O$  content. Instead, the reverse is observed. This, therefore, suggests that in  $AAC_{2.3}$ , in exception to pirssonite and apthitalite phases which are formed by significant consumption of  $Na^+$  ions, the degree of dissolution of reactive entities (particularly Al and Si) was low thereby making the availability of  $Na^+$  ions possible, which later led to the formation of sodium carbonate. As the  $SiO_2 / Na_2O$  molar ratio declines due to increase in Na, the degree of dissolution of reactive species is enhanced thereby enabling the formation of sodium consuming phases (pirssonite, apthitalite and the binding phase). Furthermore, looking at

the distributions of different elements through the elemental mappings of Alkali activated cement products presented in Figures 35 and 36, further knowledge can be achieved on the formed phases. On these figures, particularly in AAC<sub>2.3</sub> (Figure 35), the distribution of potassium atoms seems to mainly depend to those of sulphur, whereas in AAC<sub>1.5</sub>, besides sulphur atoms, the distribution of potassium atoms is also depending to those of Ca, Al and Si (Figure 36). This shows that, in AAC<sub>1.5</sub> (high alkaline medium), there is a high degree of interaction between reactive entities than in AAC<sub>2.3</sub> (low alkaline medium) caused by high dissolution induced by the high pH of reaction medium. To support the previous statement, observing the distribution of Ca, Al, Si, Fe, Na and K atoms, in AAC<sub>2.3</sub>, the elemental mapping reveals the present of a calcium sodium aluminosilicate hydrate gel. While in AAC<sub>1.5</sub>, besides the latter phase, a new binding gel known as potassium calcium ferroaluminosilicate gel is present. It is important to highlight that other binding phases might be present, but, regarding the spreading out of phases such as pirssonite and apthitalite, it is difficult to suggest any eventual additional binding phase(s).

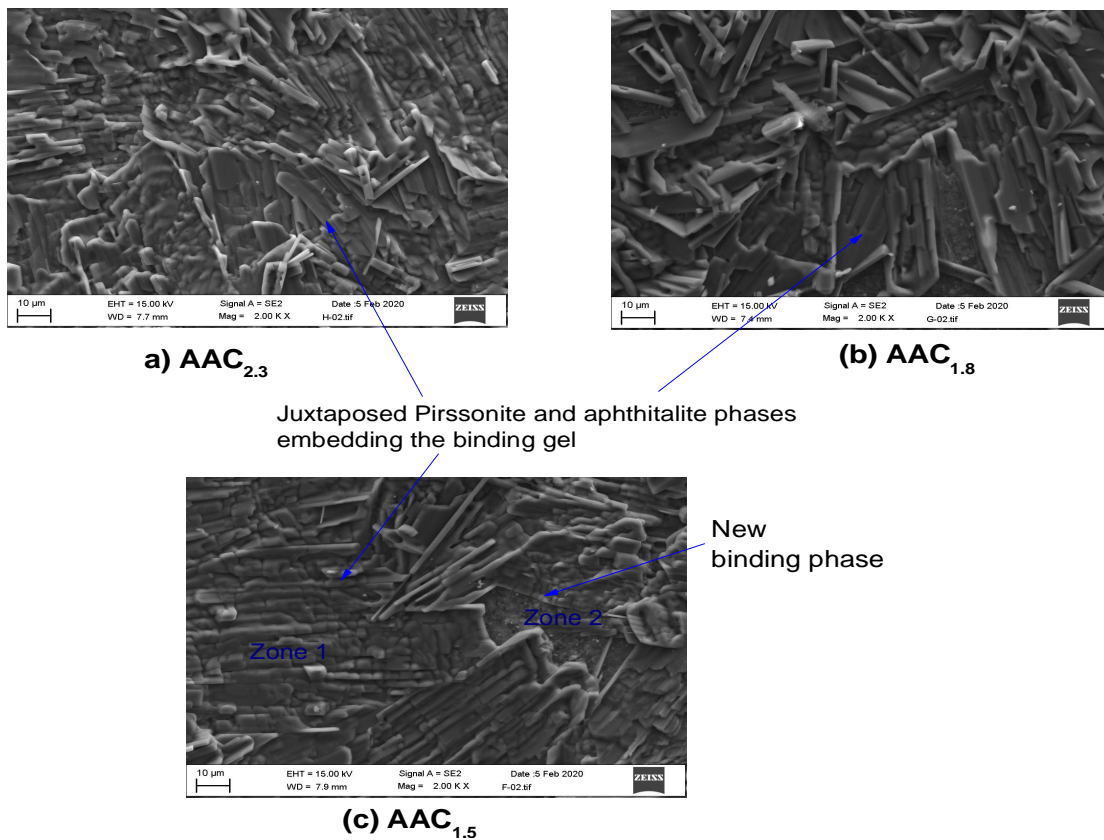


Figure 34: SEM images of alkali activated cassava peel ash aged 28 days

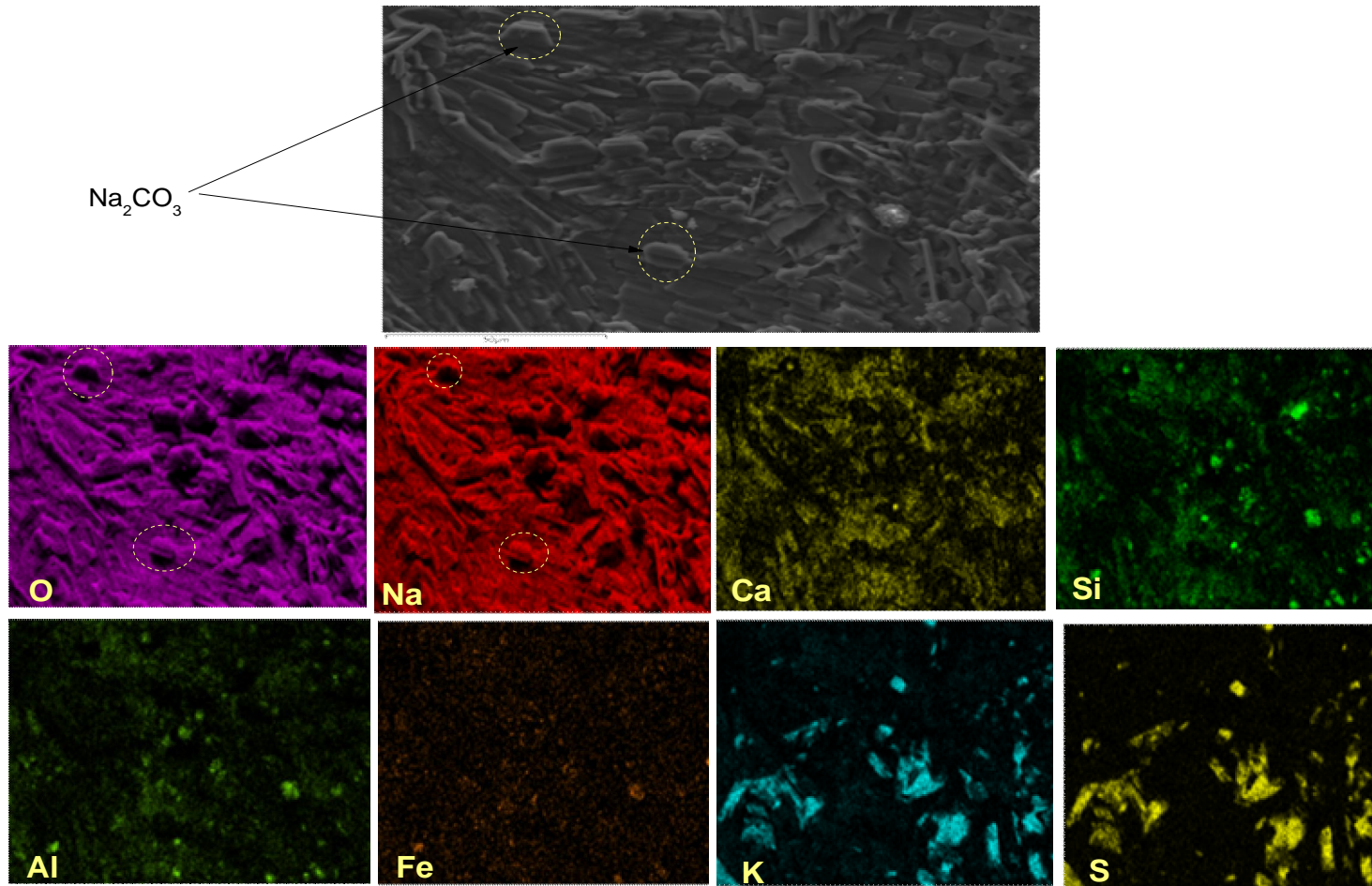


Figure 35: Elemental mapping of cassava peel ash based alkali activated pastes (AAC<sub>2.3</sub>) aged 28 days.



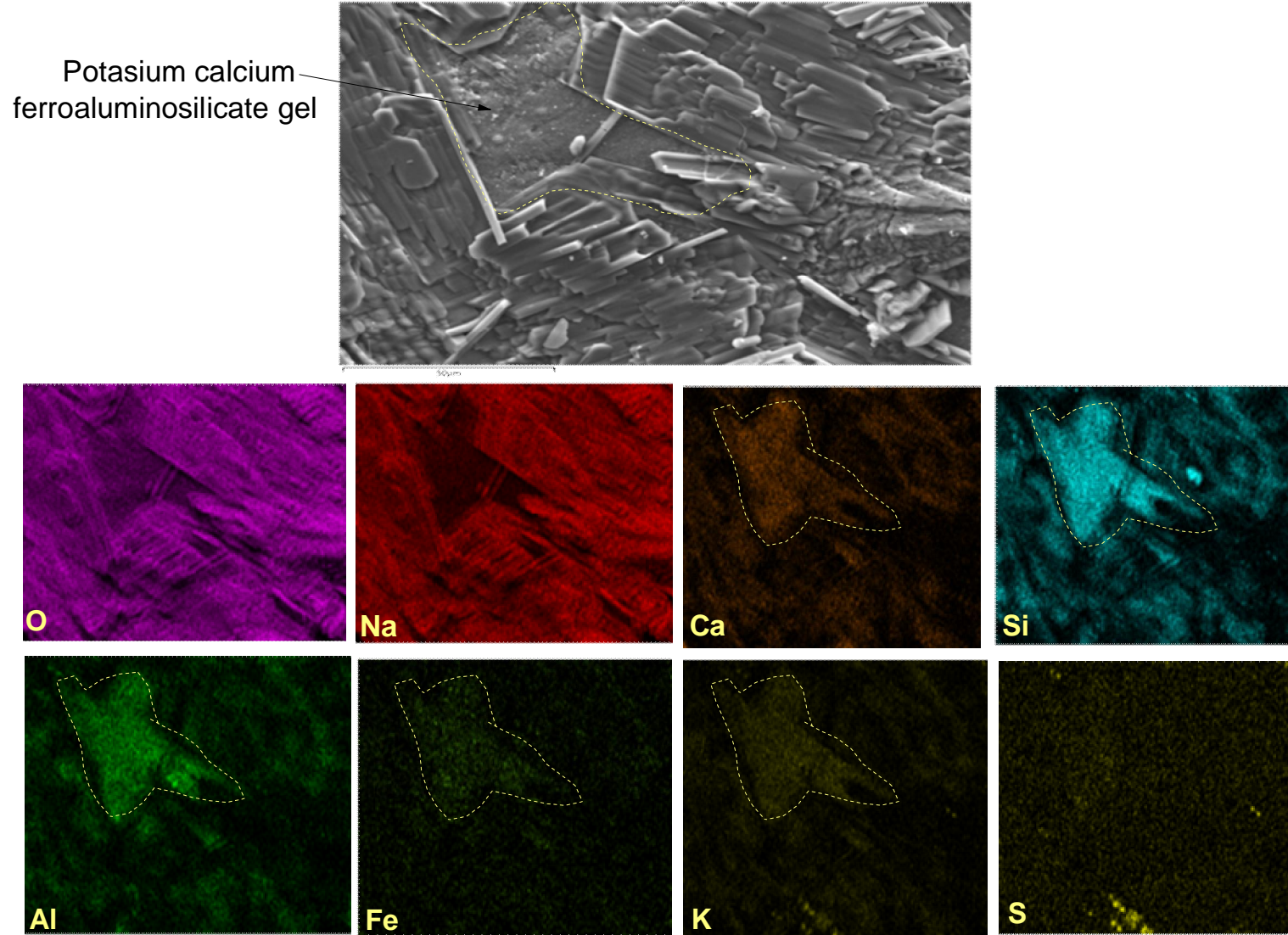


Figure 36: Elemental mapping of cassava peel ash based alkali activated pastes ( $AAC_{1.5}$ ) aged 28 days.

### III.3.2.2. Setting time and compressive strength

Table XI shows the variations of the initial setting time and the 28 days compressive strength of  $C_A$  based alkali activated products activated in various alkaline media. The results obtained show that the initial setting time fresh  $C_A$  based alkali activated pastes increases as the  $SiO_2/Na_2O$  molar ratio decreases from 2.3 to 1.8 (i.e. 74 min for  $AAC_{2.3}$  and 251 min for  $AAC_{1.8}$ ), and later on, decreases slightly when the latter ratio attains 1.5 (208 min). This variation corresponds to an initial setting retardation of 239 % (between  $AAC_{2.3}$  to  $AAC_{1.8}$ ) and 181 % (between  $AAC_{2.3}$  and  $AAC_{1.5}$ ). Regarding the low dissolution capacity of  $C_A$  in low alkaline medium noted in Table X, it was expected that the trend of the initial setting time will be the contrary of the above results. The opposite results obtained enable us to realize that in fact, the low value of initial setting time obtained with  $AAC_{2.3}$  paste is not mainly governed by the quantity of reactive content, but instead by the quality (constituents) of the reactive content. In fact, in low alkaline medium ( $SiO_2/Na_2O = 2.3$ ), reactive calcium is highly present in the reaction medium due to further decrease in alkalinity of the activation solution through the consumption of Na ions by the formation of apthitalite and pirsonnite,. This led to fast precipitation of hydrated phase such calcium silicate hydrate, thereby provoking a faster setting. Moreover, the precipitation of apthitalite and pirsonnite may have also contributed in the reduction of the initial setting time. When the  $SiO_2/Na_2O$  molar ratio increases, the pH of the activation solution increases. Thus, the dissolution capacity of  $C_A$  increases. This high dissolution of the reactive phase content in  $C_A$  favoured the formation of a polycondensed network structure thereby reducing or inhibiting the formation of C-S-H gel. Indeed, the formation of a polycondensed network structure possesses higher setting time than that of calcium silicate hydrate [157]. Therefore, the delayed initial setting time observed on  $AAC_{1.8}$  and  $AAC_{1.5}$  cement pastes suggests that the polycondensed network must be the major binding phase present in the latter cement pastes [158].

On the other hand, the variation of the compressive strength is different to that of the initial setting time. In Table XI, it is well observed that as the  $SiO_2/Na_2O$  molar ratio decreases from 2.3 to 1.5, the compressive strength of  $C_A$  alkali activated mortars increases from 9 to 14 MPa. This results are in concordance with the results of dissolution capacity and observations done on scanning electron microscopy images presented in Table X and Figure 33 respectively. In fact, the low strength generated by  $AAC_{2.3}$  mortars is attributed to the low content of C-(N)-A-S-H gel formed

due to low dissolution of reactive entities. As the pH of the activation solution increases, the dissolution capacity of reactive entities present in solid precursor increases. This leads to a stronger binding phase(s) formation than in AAC<sub>2.3</sub> as observed earlier in scanning electron microscopy images / elemental mapping results (Figures 32, 33 and 34). Furthermore, the incorporation of potassium atoms in the binding phases might have also contributed to enhance the compressive strength. In fact, according to Pereira et al., potassium based alkali cement produces higher mechanical strength than sodium one [111].

Table XI: Initial setting time and 28 day compressive strength.

Formulations' codes	Initial setting time (min)	Compressive strength (MPa)
AAC <sub>2.3</sub>	74	9
AAC <sub>1.8</sub>	251	11.4
AAC <sub>1.5</sub>	208	14.4

### III.3.3. Conclusion

The reactivity of cassava peel ash in alkaline medium as a potential raw material for the synthesis of cement was evaluated in this section of this research study. Results obtained revealed that sodium ions are mainly consumed by the formation new mineral phases such as pirssonite and apthitalite through the dissolution of calcite and arcanite respectively. This helped to reduce the formation of sodium carbonate in cassava peel ash based alkali activated products obtained under high pH. Moreover, no matter the alkali content of cassava peel ash, high alkaline solution is needed to provide high dissolution of its reactive entities. Thus, the reactivity of cassava peel ash is found to increase with decrease in SiO<sub>2</sub>/ Na<sub>2</sub>O molar ratio of the activation solution (from 2.3

to 1.5). The latter is expressed by an increase in compressive strength which is assured by both the coexistence of calcium sodium aluminosilicate hydrate and potassium calcium ferroaluminosilicate hydrate gels. Thus, cassava peel ash can be considered as an additional raw material for the synthesis of alkali activated binder.

### **III.4. Effect of cassava peel ash in alkaline activation of low reactive volcanic ash.**

#### **III.4.1. Initial setting time**

Figure 37 shows the effect of partial replacement of cassava peel ash ( $C_A$ ) on initial setting time of volcanic ash based geopolymers cured at ambient temperature ( $20 \pm 5$  °C) of laboratory. It is clearly established that, when volcanic ash is used alone as precursor material for geopolymer synthesis, initial setting time is long (i.e. 1184 min = 19.7 H). This is attributed to low reactive phase content in Ma as observed in Table VI. Conversely, the latter initial setting time gradually decreases to 631, 513 and 424 min with partial replacement of volcanic ash by 10, 20 and 30 % by mass of cassava peel ash respectively. These correspond to percentage drop of 46, 57 and 64 % for GMC<sub>10</sub>, GMC<sub>20</sub> and GMC<sub>30</sub> respectively. This variation may result of increasing amount of reactive phase brought by  $C_A$ . In fact,  $C_A$  contains more reactive phase than Ma as seen earlier in Table VI. So, its incorporation through partial replacement of Ma in the synthesis of geopolymers increases the reactive phase content of the mixture. Besides that, according to Table I, replacement of Ma by  $C_A$  in the mixtures leads to the reduction of SiO<sub>2</sub> / Al<sub>2</sub>O<sub>3</sub> molar ratio, hence increase in alumina content of the mixtures. The lessening of initial setting time is in accordance with alumina content in reactive phase as previously revealed (Table V and Figure 14). In fact, as reported by several authors [90,153,159], in geopolymer synthesis, the increase in reactive alumina leads to the decrease of setting time. Also, during alkaline activation of aluminosilicates, dissolution of reactive alumina is more rapid than reactive silica, which results in faster Al-O-Si bonds formation than Si-O-Si ones [41,43]. Moreover, the presence of calcite in  $C_A$  may have contributed to the reduction of initial setting time. In fact, Djobo et al. [90] and W.K.W. Lee and J.S.J. van Deventer [60] used calcined oyster shell and inorganic salts respectively to observe that increase of calcite content in alkaline medium accelerates the initial setting time of geopolymer pastes.

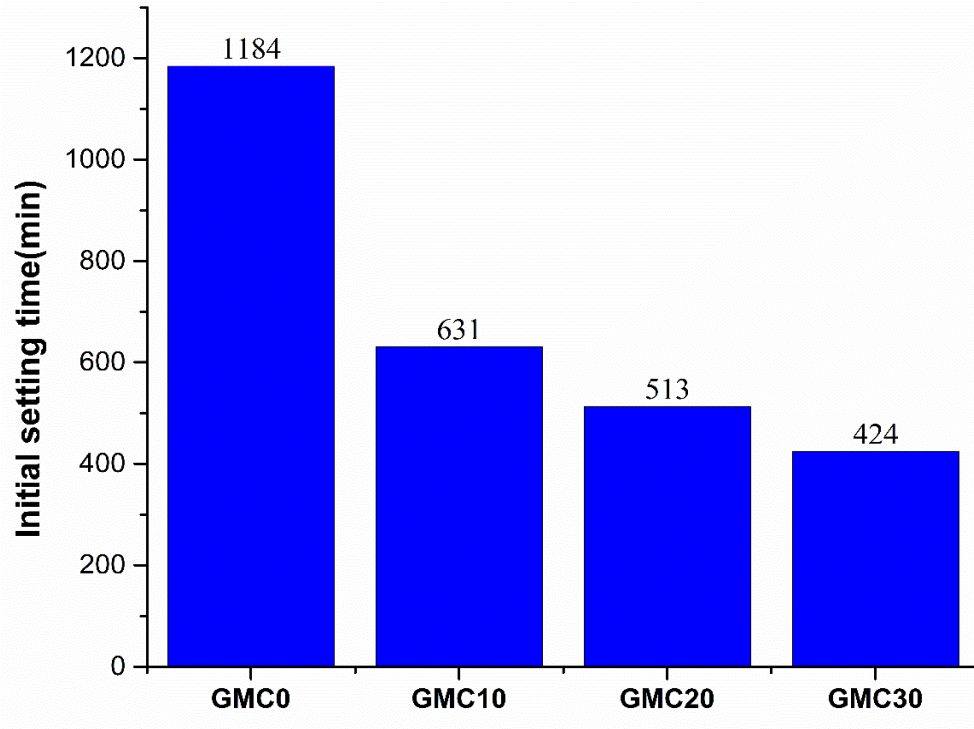


Figure 37: Initial setting of geopolymer pastes.

### III.4.2. Microstructure

#### III.4.2.1. Fourier Transform Infrared spectroscopy

Figure 38 presents Fourier Transform Infrared spectra of the geopolymers. Except the vibration band at  $1406\text{ cm}^{-1}$  which refers to incoming carbonate (efflorescence), all the absorption bands on the spectrum of Ma (Figure 14) are also present on that of GMC<sub>0</sub>. This highlights the low reactivity of Ma during alkaline activation. The band at  $971\text{ cm}^{-1}$  which corresponds to asymmetric stretching vibration of Si-O-Si and Si-O-Al bonds gradually become sharper with the replacement of Ma by C<sub>A</sub> (Figure 38). This is attributed to the shifting of the vibration bands at  $1004$  and  $1112\text{ cm}^{-1}$  of the spectrum of C<sub>A</sub> (Figure 14) to a unique and low wave number ( $988\text{ cm}^{-1}$ ) on the spectra of the geopolymers. This induces the disappearance of the stretching vibration of the 6-fold coordinated Al (VI) -O located at  $913\text{ cm}^{-1}$ . According to Djobo et al.[5], this sharpness characterizes a high degree of polycondensation. Thus, the previous findings highlight the participation of cassava peel ash in the network formation of the geopolymers.

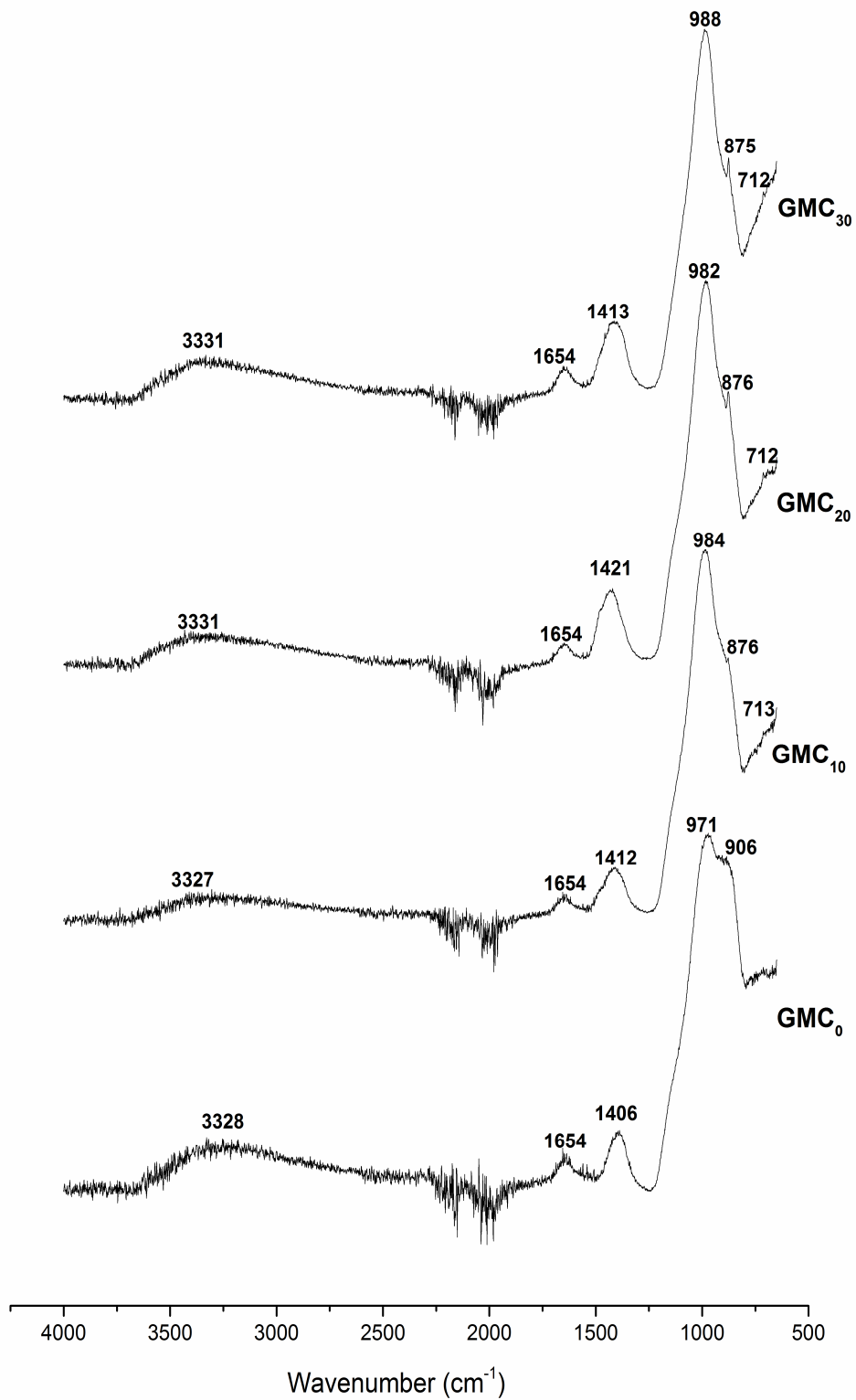


Figure 38: FTIR spectra for geopolymer pastes aged 28 days.

### III.4.2.2. X-ray diffraction

The X-ray diffraction patterns of geopolymers cured at ambient temperature for 28 days of laboratory are given in Figure 39. Except muscovite, diopside, hematite, arcanite and calcite, all the minerals initially present in Ma and C<sub>A</sub> are not affected by alkaline activation. The reactivity of muscovite and calcite in alkaline medium was already observed by other authors [5,32,160]. The partial dissolution of muscovite, diopside and hematite marked by the drop of its peak intensities is simultaneously followed by slight increase of the hump between 18 and 38° (2θ) on the X-ray pattern of GMC<sub>0</sub> (Figure 39) when compared to that of Ma (Figure 15). These noted dissolutions are influenced by the water content present in the reaction medium as revealed earlier above by the curing regime study. Unfortunately, these dissolutions were not enough to prevent the formation of efflorescence on the surface of GMC<sub>0</sub>. This is confirmed by new peaks present at 9.04°, 29.04°, 33.87° and 37.18° (2θ) respectively on the X-ray pattern of GMC<sub>0</sub> and which are ascribed to sodium hydrogen carbonate hydrate [Na<sub>3</sub>H(CO<sub>3</sub>)<sub>2</sub> · 2H<sub>2</sub>O: PDF 76–0739]. Conversely, peak intensities of the latter gradually decrease with respect to C<sub>A</sub> replacement. This is also accompanied by the transformation of arcanite (K<sub>2</sub>SO<sub>4</sub>) to apthitalite (K<sub>3</sub>Na(SO<sub>4</sub>)<sub>2</sub>), suggesting that addition of cassava peel ash may help to reduce the formation of sodium hydrogen carbonate hydrate (efflorescence). Similar transformation was observed earlier above while using C<sub>A</sub> as alone precursor in alkaline activation. Despite the reactivity induced by C<sub>A</sub> replacement during the geopolymer synthesis of Ma, calcite peaks were still significantly observed on the X-ray diffraction patterns of geopolymers, which confirms its low dissolution in alkaline medium as observed by other authors [90,160]. It is also interesting to highlight that the crystalline phase (pirssonite) observed on X-ray diffraction patterns of cassava peel ash based alkali activated products (AAC<sub>2.3</sub>, AAC<sub>1.8</sub> and AAC<sub>1.5</sub>) in Figure 32 is completely absent on those of cassava peel ash-volcanic ash based geopolymer composites (GMC<sub>10</sub>, GMC<sub>20</sub> and GMC<sub>30</sub>) in Figure 39. It was earlier revealed that pirssonite formation was as a result of the dissolution of calcite in the alkaline medium. So, its absence confirms the low dissolution of calcite in the reaction medium in presence of volcanic ash. The latter observations and suggestions reveal and confirm the contribution of volcanic ash in the synthesized alkali activated composite. Therefore, this suggests that, along with the alkaline solution, there was sufficient reactive entities in low reactive volcanic ash to interact with those present in cassava peel ash. This amount of reactive entities were sufficient to inhibit the formation of pirssonite induced by the dissolution calcite present in C<sub>A</sub>.

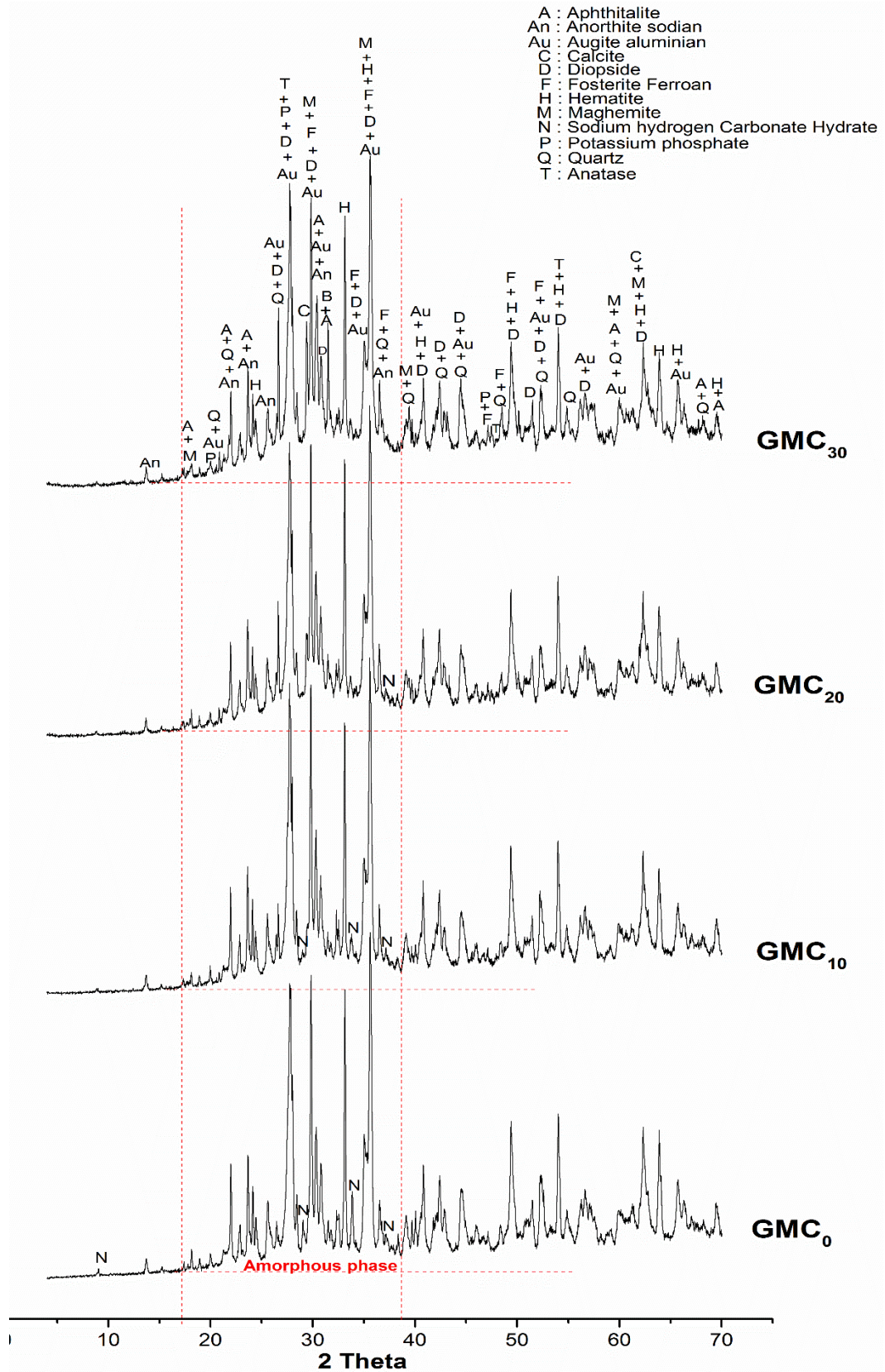


Figure 39: XRD patterns of geopolymers aged 28 days.



### III.4.2.3. Thermal curves (TGA and DSC) of GMC<sub>0</sub> and GMC<sub>30</sub>

The monitoring of thermal behaviour of volcanic ash based inorganic polymer composites containing 0 and 30% by mass of cassava peel ash is shown on TGA and DSC curves in Figure 40. Both samples show two thermal accident within the temperature ranges: 50-200 °C and 220-700 °C. The first interval with a maxima at 58 and 76 °C (DSC curves) for GMC<sub>0</sub> and GMC<sub>30</sub> respectively is assigned to the loss of free water molecules adsorbed in pores of the polymer network while the second is attributed to the water molecules bounded to the inorganic polymer. The different temperatures maxima (58 °C for GMC<sub>0</sub> and 76 °C for GMC<sub>30</sub>) show the degree of retention of water molecules in cement products, which intend may predict the degree of polycondensation that has occurred. On this, it can be observed that C<sub>A</sub> rich volcanic ash based alkaline cement retains more water molecule than C<sub>A</sub> free ones. This is merely confirmed by the mass loss registered on TGA curves expressed in terms of endothermic peaks revealing a thermal accident (Figure 40). Here, it is noticed that GMC<sub>30</sub> expresses higher mass loss than GMC<sub>0</sub> (i.e. a total mass loss of 17.30 % for GMC<sub>30</sub> against 7.86 % for GMC<sub>0</sub>). This highest mass loss suggests the presence of high binding phase content in volcanic ash based geopolymer containing cassava peel ash. The latter suggestion follows the hump's trend observed on X-ray diffraction pattern above (Figure 39) which characterises the amorphous phase content and indirectly the degree of polycondensation. The higher the amorphous phase content in an alkaline cement product, the higher will be the mass loss observed on the TGA curve. GMC<sub>30</sub> has the highest amorphous phase content than GMC<sub>0</sub>, reason of its higher mass loss. Moreover, it is also important to note that the presence of aphtitalite phase, due to its salty nature, may have also contributed in the enhancement of water retention in the geopolymer specimens as the C<sub>A</sub> content increases. On the other hand, as observed in X-ray diffraction pattern above (Figure 39), the absence of exothermic peaks at 170, 447 and 653 °C, fingerprints of pirssonite decomposition, is noticed on DSC curve of GMC<sub>30</sub> no matter the C<sub>A</sub> content. This indeed confirms the non-formation of pirssonite. So, pirssonite mineral formed in alkali activated cassava peel ash (Figure 32) is completely absent in GMC<sub>30</sub> despite the presence of calcite. This, once more, shows that the reactive phase content in volcanic ash seems to have sufficiently reacted with reactive entities present in cassava peel ash thereby preventing calcite from interacting with the reactive medium in order to form pirssonite as observed earlier in alkaline activation of cassava peel ash.

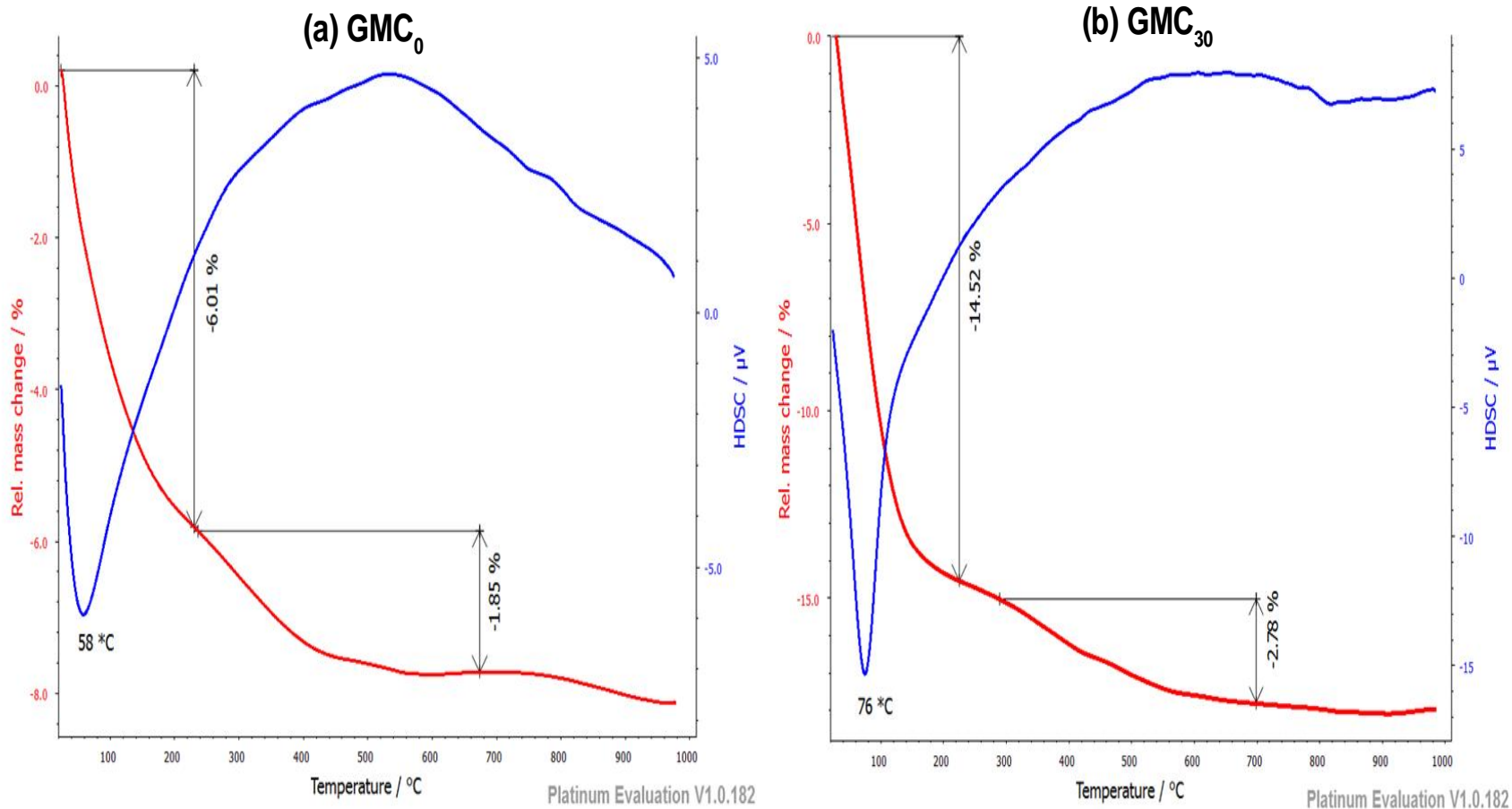


Figure 40: Thermograms (TGA and DSC) of GMC<sub>0</sub> and GMC<sub>30</sub>.

#### III.4.2.4. Scanning Electron Microscopy

Figures 41 and 42 show respectively the micrographs of the scanning electron microscopy and the elemental energy dispersive X-ray maps of the geopolymers aged 28 days. On Figure 41, heterogeneous and porous aspects are observed on geopolymers free of cassava peel ash; but the latter seem to decrease while going through Figure 41 on which homogeneous products are gradually observed as the cassava peel ash content increases. This indicates that replacement of volcanic ash by cassava peel ash has an impact on the morphology of geopolymers. The aforementioned heterogeneity is well observed by the existence of three main layers identified as L<sub>1</sub>, L<sub>2</sub> and L<sub>3</sub>. Looking at their respective physical aspects and chemical compositions thanks to energy dispersive X-ray analysis (Table XII), L<sub>1</sub>, L<sub>2</sub> and L<sub>3</sub> are suggested to correspond respectively to unreacted particles, sodium- rich geopolymer gel and efflorescence areas. Also, when comparing the chemical composition of layer L<sub>2</sub> at different proportions of cassava peel ash replacement (Table XII), it is observed that when the amount of cassava peel ash increases, Na / Al molar ratio decreases within the spreading sodium- rich geopolymer gel and this gets close to 1, with Si/Al molar ratio found within 2.1 and 2.7 interval. This is visualized on the elemental energy dispersive X-ray maps (Figure 42) on which it is noticed that, with increasing amount of cassava peel ash, sodium atoms with respect to aluminium and silicon ones are gradually and homogeneously distributed all over the geopolymer structure. This suggests the reduction of free sodium ions in the geopolymer structure and corroborates the observations done on the reduction of efflorescence. In fact, according to some authors [161], the high level of aluminium atoms during the geopolymer synthesis favours the cross linking of gels, thereby reducing sodium ions mobility. Also, Hong and Glasser [162] concluded that the presence of reactive alumina enhances alkali binding by turning C-S-H gel into C-A-S-H one. In case, it would have been a partial dissolution of calcium rich component in the reaction medium, the latter conclusion may be the reason of absence of C-S-H gel on the X-ray diffraction patterns of Figure 39 despite the presence of calcium in reaction medium. But, an opposite suggestion (i.e. non-dissolution of calcium rich component) can also justify the latter absence. Moreover, the above mentioned Si / Al molar ratio joins the conclusion drawn by Piegang He et al. [163] that geopolymers with Si / Al molar ratio  $\leq 2.5$  are chemically stable in air thereby producing no efflorescence. Hence, it is obvious that cassava peel ash brings a synergistic effect during geopolymerization of volcanic ash.

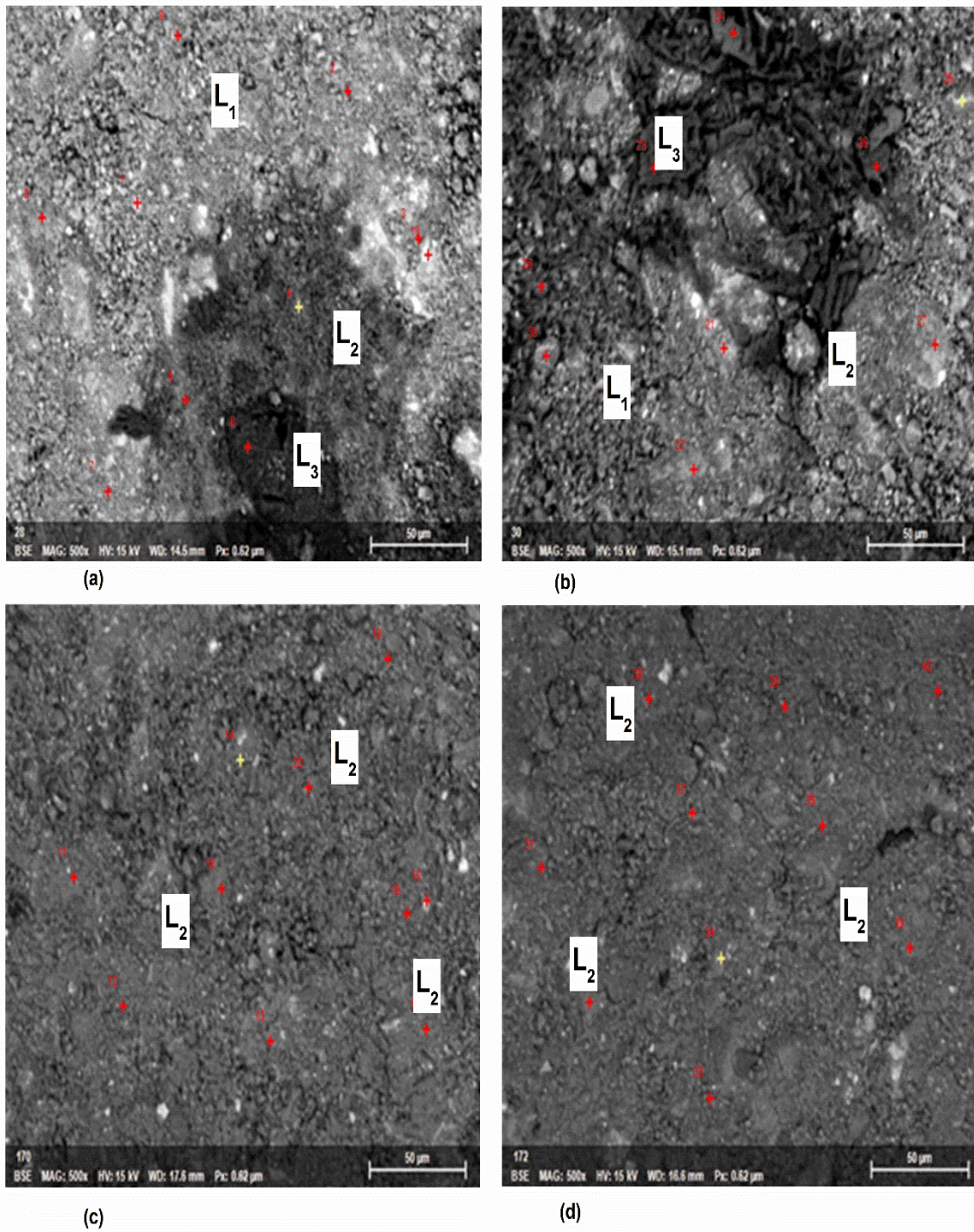


Figure 41. SEM images of volcanic ash based geopolymers aged 28 days containing various percentage of cassava peel ash (a: GMC<sub>0</sub>; b: GMC<sub>10</sub>; c: GMC<sub>20</sub> and d: GMC<sub>30</sub>).

Table XII: Elemental composition of chosen areas on geopolymer pastes aged 28 days.

Sample	Area	Element concentration (wt %)										Molar ratio		
		Na	K	Ca	Al	Si	Fe	P	Ti	Mg	O	Si/Al	Na/Al	Ca/Si
GMC <sub>0</sub>	L <sub>1</sub>	11.3	2.4	6.9	6.2	23.3	9.5	0.0	1.8	2.6	35.7	2.9	2.1	0.1
	L <sub>2</sub>	16.8	0.7	7.0	10.3	23.7	0.9	0.0	0.1	0.1	40.4	2.0	1.9	0.2
	L <sub>3</sub>	63.5	1.0	1.4	1.2	2.3	1.2	0.2	0.2	0.0	29.0	2.4	62.1	0.3
GMC <sub>10</sub>	L <sub>1</sub>	5.2	0.3	8.3	7.8	18.9	4.0	0.4	1.2	4.6	49.3	2.9	0.8	0.2
	L <sub>2</sub>	7.4	0.3	7.2	12.4	21.3	2.2	0.1	0.4	0.8	47.9	1.8	0.7	0.2
	L <sub>3</sub>	68.3	0.0	0.3	0.9	3.0	0.2	0.0	0.0	0.2	27.1	2.5	89.1	0.1
GMC <sub>20</sub>	L <sub>2</sub>	12.7	2.1	7.0	7.4	16.7	10.0	0.0	1.9	1.9	40.3	2.1	1.1	0.3
	L <sub>2</sub>	9.7	4.5	5.0	7.4	23.3	4.3	0.0	0.9	1.6	43.3	3.0	1.5	0.2
	L <sub>2</sub>	7.3	6.7	10.0	6.7	16.7	9.5	0.0	1.5	0.8	40.8	2.5	1.3	0.4
GMC <sub>30</sub>	L <sub>2</sub>	7.0	5.2	4.5	7.8	21.9	7.5	0.2	1.6	1.2	42.7	2.7	1.1	0.1
	L <sub>2</sub>	9.5	3.3	4.6	10.2	21.8	4.2	0.4	1.1	0.8	43.5	2.1	1.1	0.1
	L <sub>2</sub>	6.7	3.6	4.8	9.2	22.4	5.9	0.1	1.5	1.9	43.6	2.4	0.9	0.2

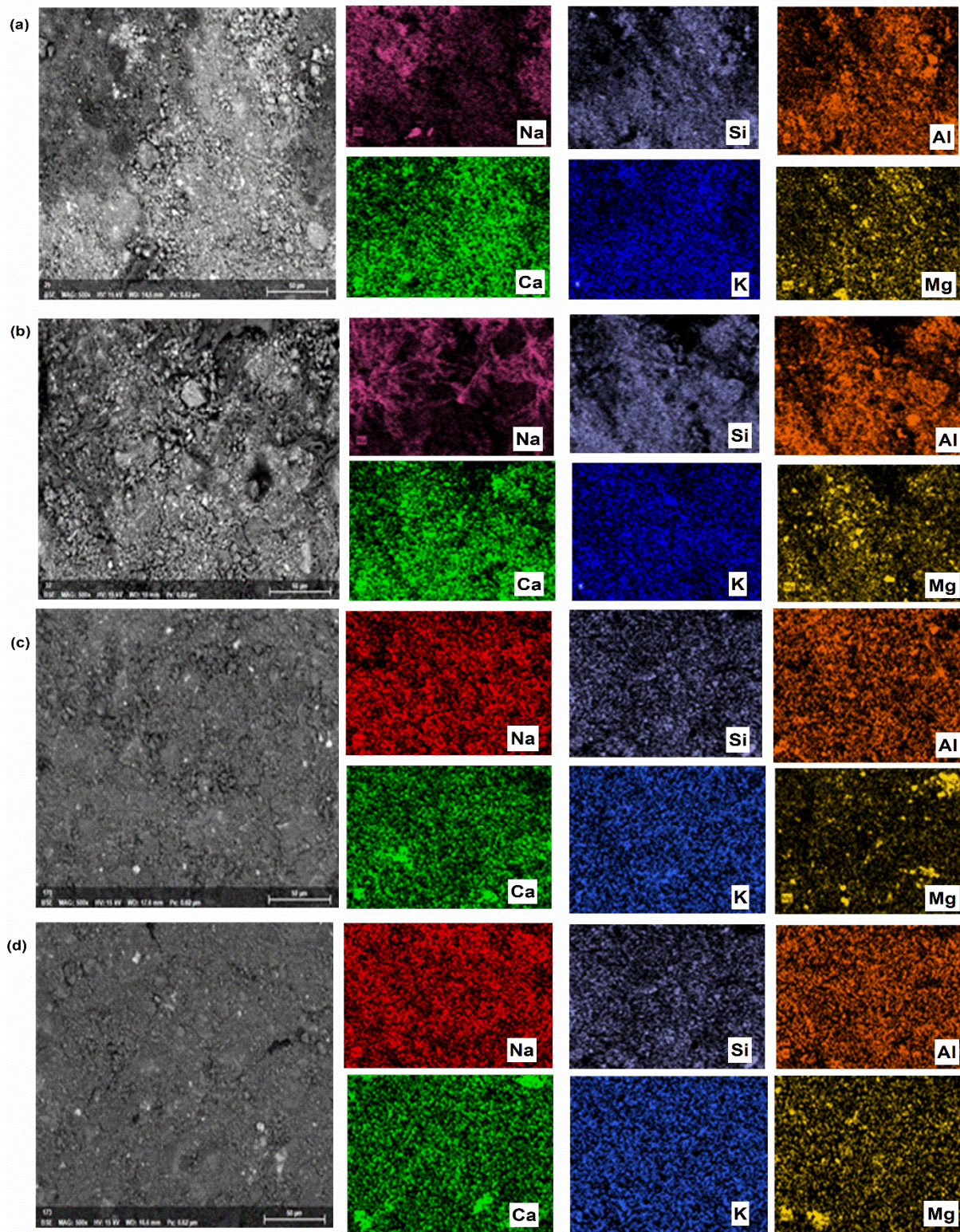


Figure 42: Elemental mapping of geopolymer aged 28 days (a: GMC<sub>0</sub>; b: GMC<sub>10</sub>; c: GMC<sub>20</sub> and d: GMC<sub>30</sub>).

### III.4.3. Compressive strength

The result of 28 days compressive strength versus cassava peel ash of geopolymer paste specimens cured at ambient temperature of laboratory is given in Figure 43. The latter figure reveals a significant compressive strength increase from 3.0 MPa (specimen GMC<sub>0</sub>) to 25.0 MPa (specimen GMC<sub>30</sub>) with 17 MPa (specimen GMC<sub>10</sub>) and 21 MPa (specimen GMC<sub>20</sub>) as intermediates. The latter trend corresponds to a percentage increase of about 467, 600 and 733 % for GMC<sub>10</sub>, GMC<sub>20</sub> and GMC<sub>30</sub> respectively. This enhancement of the compressive strength is in accordance with the observations done on Figure 41 confirmed by the compactness brought about by cassava peel ash in geopolymer morphology. Mechanical strength of geopolymer is among other governed by the reactive phase content of aluminosilicate and the degree of formation of new tri-dimensional network of Si-O-Al. All of these mainly depend on SiO<sub>2</sub> / Al<sub>2</sub>O<sub>3</sub> molar ratio of reactive phase along with its ability to be dissolved in alkaline medium [164]. The low compressive strength exhibited by GMC<sub>0</sub> is assigned in one way to its low reactive phase content, and in the other way, to the presence of high water content resulting from the fact of undertaken sealing curing as observed earlier above in the study based on the effect of curing regime. Hence, high SiO<sub>2</sub> / Al<sub>2</sub>O<sub>3</sub> molar ratio (Table III) and high water retention which lead to low degree of geopolymerization. Conversely, replacement of volcanic scoria ash by gradual increasing amount of cassava peel ash allows getting geopolymer specimens with increasing amount of reactive phase (Table VI) which lowers the SiO<sub>2</sub> / Al<sub>2</sub>O<sub>3</sub> molar ratio by increasing the alumina content, and enable the consumption of water molecules as observed on thermal curves (Figure 40). This increases polycondensation thus optimizes the densification of geopolymers. According to Tchakoute et al. [85], addition of appropriate amount of amorphous alumina oxide to an aluminosilicate material increases the geopolymerization extent resulting in the increase of compressive strength. Also, the presence of calcite and iron oxide in cassava peel ash are an asset which may favour compressive strength increase because both can behave as network formers [26,160].

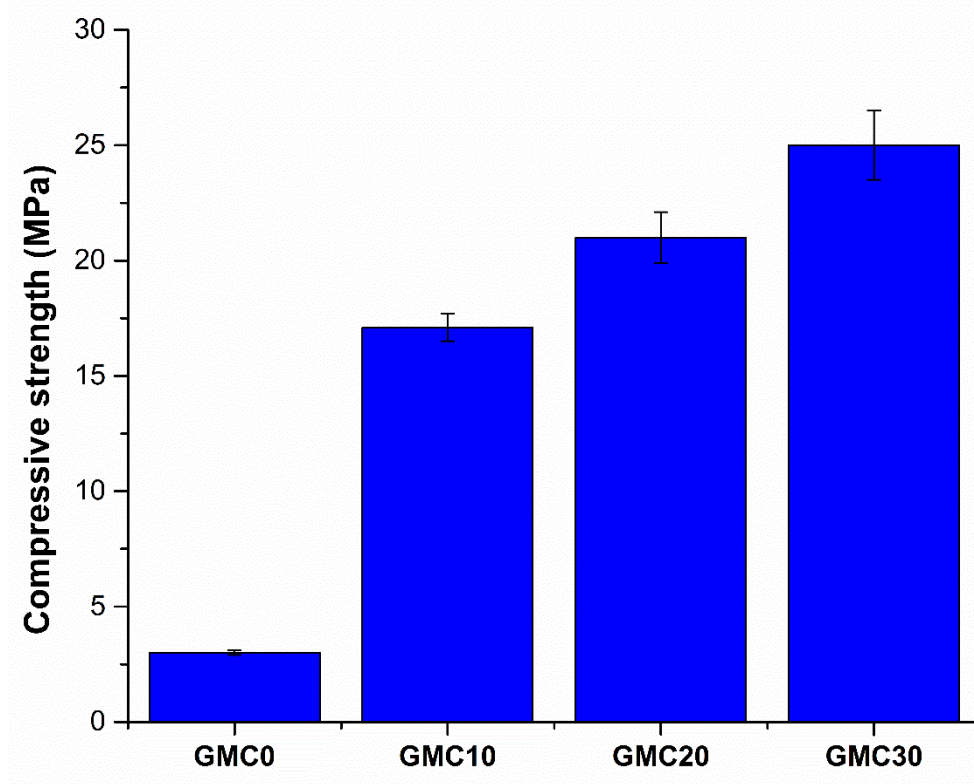


Figure 43: Compressive strength of geopolymer pastes aged 28 days.

#### III.4.4. Efflorescence and durability

Figure 44 shows the appearance of hardened geopolymer paste specimens initially covered with thin film of polyethylene for 24 h and later on exposed for 90 days at atmospheric air of the laboratory. The latter figure reveals the presence of efflorescence which is marked here by the presence of whitish layer on the surface of geopolymer specimens. Among the different geopolymer specimens, GMC<sub>0</sub> exhibits the highest extent of efflorescence. Replacement of Ma by gradual increasing amount of cassava peel ash reduces the magnitude of efflorescence from the specimen GMC<sub>10</sub> to the specimen GMC<sub>30</sub>. This whitish layer is identified as sodium hydrogen carbonate hydrate as revealed by X-ray diffraction patterns (Figure 39). In alkaline medium, efflorescence is the result of availability and mobility of sodium ions which react with CO<sub>2</sub> from atmospheric air. However, sodium ions availability depends among other on the presence of low reactive phase content of aluminosilicate [48]. The high extent of efflorescence in GMC<sub>0</sub> is attributed to its low reactive phase content. Cassava peel ash replacement compensates the deficiency in reactive phase whose increasing amount gradually reduces the extent of efflorescence. Also, replacement of Ma by increasing amount of cassava peel ash allows the



consumption of available sodium ions by arcanite [ $K_2SO_4$ ] to get aphthitalite [ $K_3Na(SO_4)_2$ ], hence reduction of the formation of efflorescence.

To get an idea on the durability of geopolymers fabricated from partial replacement of volcanic ash by cassava peel ash, specimens  $GMC_0$  and  $GMC_{30}$  were separately soaked for 28 days in 5% by mass of sulphuric acid solution. The results obtained from the latter evaluation are presented in Table XIII and reveal that specimens  $GMC_0$  experienced mass loss of 2.76 % and residual strength of about 4.51 MPa meanwhile specimens  $GMC_{30}$  experienced mass loss of 7.59 % and residual strength of about 9.41 MPa. The pronounced mass loss in specimens  $GMC_{30}$  is ascribed to the chemical reaction which has occurred between calcite ( $CaCO_3$ ) present in the geopolymer (Figure 38) and sulphuric acid solution (equation 7). The latter reaction produces a gas (carbon dioxide) which, when escaping, generates small cracks on the wall of the specimens  $GMC_{30}$  as shown in Figure 45. This thereby causes the reduction of strength. Nevertheless, after 28 days of immersion in acid solution, the surface of all specimens seemed to remain structurally intact, implying that the obtained geopolymers are stable in acid medium.

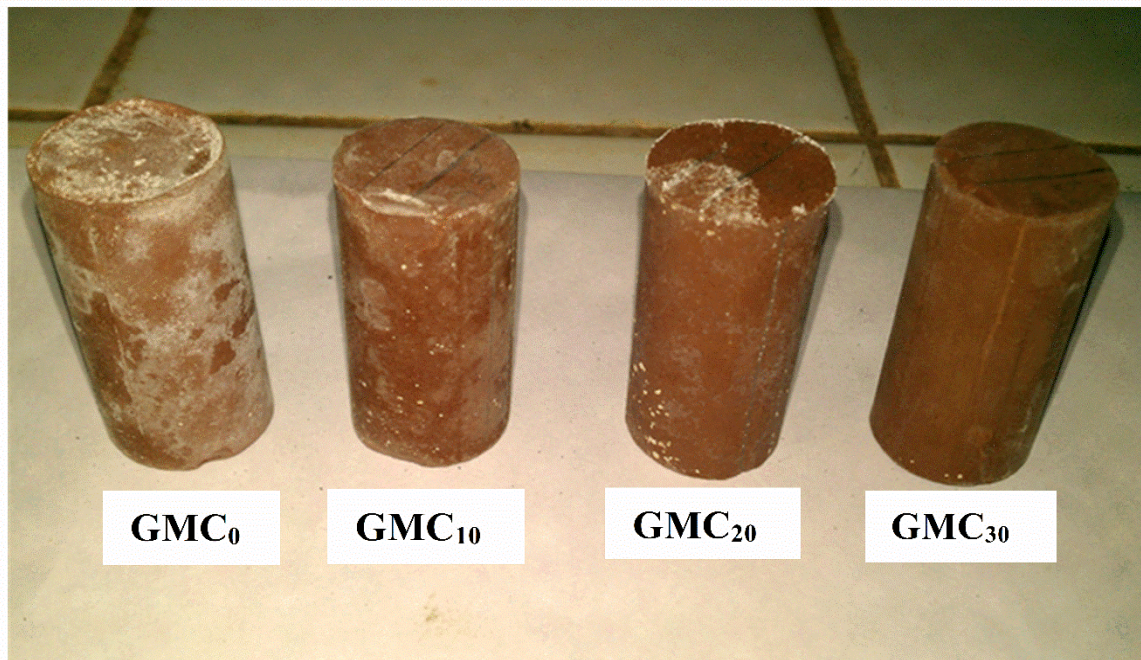
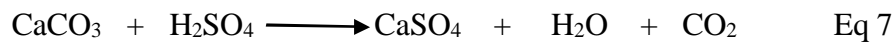


Figure 44: Efflorescence test for geopolymer pastes aged 28 days exposed at ambient temperature of the laboratory for 90 days.

Table XIII: Mass loss (%) and residual strength of geopolymers, aged 28 days, immersed in 5 % by mass of sulphuric acid.

	GMC <sub>0</sub>	GMC <sub>30</sub>
Mass loss (%)	-2.76	- 7.59
Residual strength (MPa)	4.52	9.41

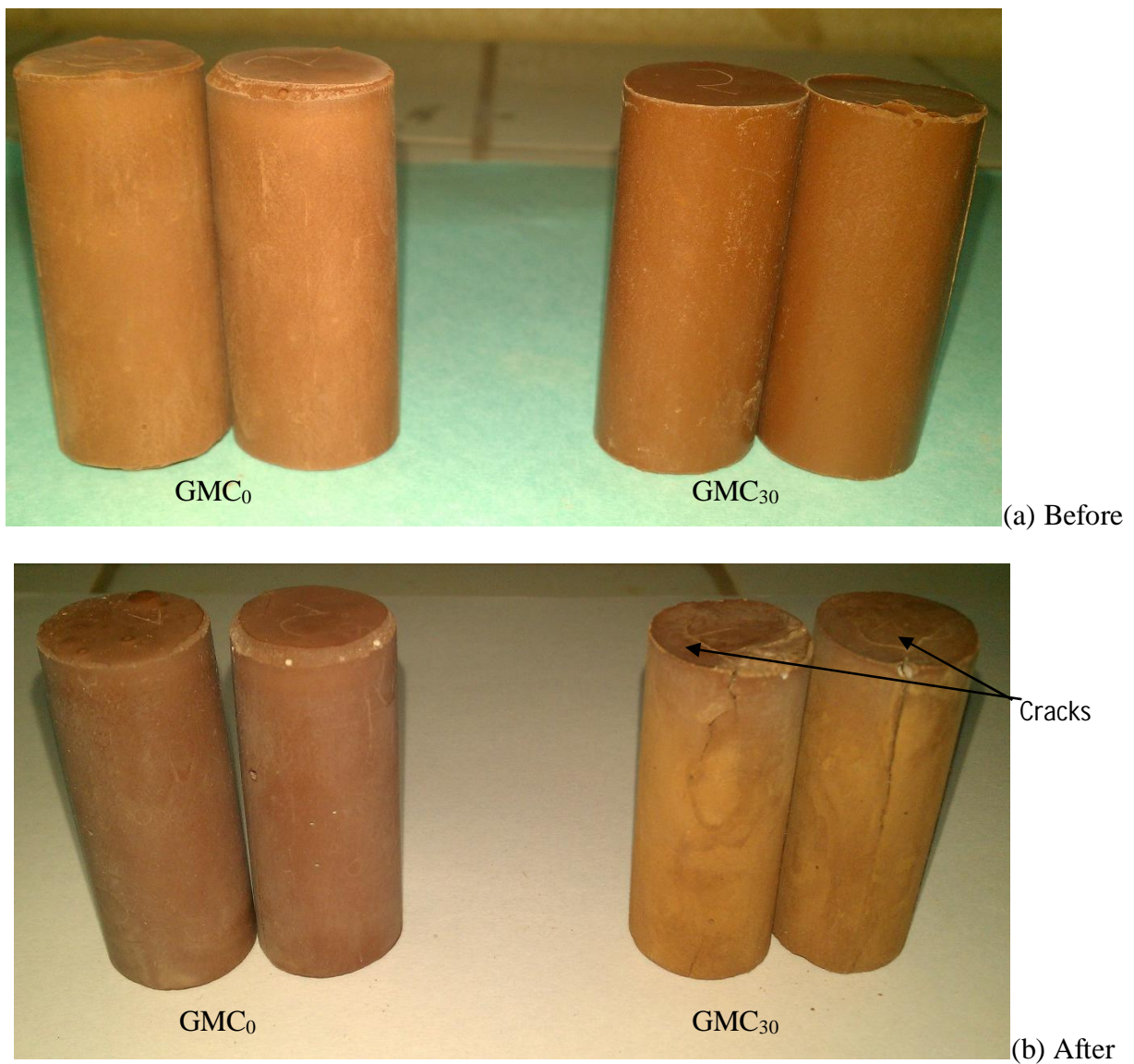


Figure 45: Visual aspect of inorganic polymer specimens before and after 30 days of immersion in acidic medium.

### III.4.5. Conclusion

Due to its high reactive phase content (72 % by mass), cassava peel ash was partially (0, 10, 20 and 30 % by mass) used to assess the effects of its replacement to low reactive volcanic ash (having reactive phase content of 18 % by mass) in the synthesis of volcanic ash based alkaline cement. This assessment led to positive effects on the obtained products. Thus, when used alone, volcanic ash showed low reactivity in alkaline medium, thereby making the handling of geopolymer specimens possible after 3 days. Afterward, the latter products yielded a compressive strength of 3.0 MPa after 28 days of curing under ambient temperature and abundant efflorescence on specimens exposed to atmospheric air of the laboratory for 90 days. Conversely, gradual replacement of volcanic ash by cassava peel ash enriches the reaction medium with significant amount of reactive phase within which considerable amount of alumina and calcite are present. The latter allowed to get geopolymer pastes with substantial reduced initial setting time for about 64 % and specimens aged 28 days with significant increase of compressive strength of about 733 % for 30 % by mass of cassava peel ash used. This behaviour was attributed to the degree of geopolymerization that was induced by the presence of cassava peel ash. Also, replacement of volcanic ash by cassava peel ash ( $\geq 20$  % by mass) led to compact enough products and homogeneous distribution of  $\text{Na}^+$  ions over the structure of geopolymer specimens along with reduction of magnitude of efflorescence. First of all, the lessening of efflorescence was ascribed to the presence of significant amount of aluminium atoms in the geopolymer network. Secondly, the latter was additionally attributed to the presence of arcanite ( $\text{K}_2\text{SO}_4$ ) in the replacement which helped to embed unreacted  $\text{Na}^+$  ions through the formation of apthitalite [ $\text{K}_3\text{Na}(\text{SO}_4)_2$ ]. Moreover, despite its low reactive content, volcanic ash was observed to have a synergistic effect with cassava peel ash thereby inhibiting the formation of pirssonite no matter the presence of calcite. Furthermore, after 28 days of immersion in 5 % by mass of sulphuric acid, the surface of all specimens remains structurally intact. Hence, cassava peel ash behaves as an additional precursor that brings synergistic effect to volcanic ash during alkaline activation.

## GENERAL CONCLUSION AND OUTLOOKS

The aim of this study was to suggest novel, low cost and local approach which can further encourage the use of volcanic ash, as a whole, and low reactive volcanic ash in particular, as a main precursor for the synthesis of alkaline cement especially in areas of the world where high abundance of this raw material is observed. Thus, in order to avoid undervaluation of the reactivity of volcanic ash in alkaline medium, the influence of three curing regimes on mechanical properties and durability of alkali activated volcanic ash were assessed. This was done to come out with an adequate curing condition necessary to obtain an efficient alkali activated material synthesized from low aluminosilicate raw material. Afterward, the improvement of reactive phase content was proposed as an alternative to the first solution for low reactive volcanic ash that could not fit the first approach.

To carry out the experimental studies linked to this thesis, two varieties of volcanic ash were collected in various localities along the Cameroon line. Added to this, was an agro-waste (cassava peels) obtained from a highly cultivated crop (cassava tubers) around the globe whose by-product (ash) was used.

First of all, the various solid raw materials used in this study were characterized using diverse analysing techniques such as X-ray diffraction, Fourier transform Infrared spectroscopy, Particle size distribution, Inductive Coupled Plasma Optical Emission Spectroscopy and leaching test. The results obtained show that the two volcanic ash samples (denoted: Ma and Vn) used along this study possess almost similar particle size distribution and chemical composition with major oxide such as silicon dioxide (43.32-44.56 % by mass), aluminium oxide (14.84-16.88 % by mass), iron oxide (11.52-14.19 % by mass) and calcium oxide (7.77-8.80 % by mass) which render them susceptible raw materials for alkaline activation. However, the reactive phase content and loss on ignition are respectively higher in Vn (26 and 3.87 % by mass) than Ma (18 and 1.79 % by mass). Contrary to volcanic ash, besides the above oxides, cassava peel ash ( $C_A$ ) also possesses potassium oxide as the third most abundant oxide. Its loss on ignition is almost 4times that of volcanic ash (Vn), principally due to its high carbonate content. Moreover,  $C_A$  possesses a very high amount of reactive phase content (72 % by mass) making it suitable for alkaline activation.

As a second objective, which was to assess the curing regime necessary for high degree of reactivity of low reactive volcanic ash in alkaline medium, synthesized volcanic ash based alkaline activated pastes were subjected to three curing regimes. The results obtained revealed that regarding the low reactive phase content in volcanic ashes, sealing curing is not a good curing regime for the development of mechanical properties. Due to water retention, this curing regime hinders polycondensation reaction despite the high degree of dissolution it induces. The water retention is higher in sample possessing more hydroxylated minerals (i.e. in sample possessing higher loss on ignition). Instead, oven drying at 60 °C and open atmospheric air at ambient temperature favour progressive water loss which leads to optimum polycondensation reaction. So, volcanic ashes considered as low reactive raw material in alkaline medium, in suitable curing regimes, expressed higher 28 days compressive strength (16.2-17.1 MPa for Ma and 36.1-37.9 MPa for Vn) than sealing curing (2.7 MPa for Ma and 1.8 MPa for Vn). Similar trend was observed as far as stability in water for 30 and 90 days are concerned. Whereas, specimens made from volcanic ash with reactive phase content  $\leq 18$  % by mass (Ma specimens) seem very stable in acidic medium compared to those containing a reactive phase  $\geq 26$  by mass (Vn specimens). Moreover, acid curing seems favourable to Ma specimens since it enhances their stability in water to about 599 %.

Regarding the low reactivity of Ma sample (amorphous content  $\leq 18$  % by mass) in alkaline medium at room temperature, by-product of a local waste (cassava peel) was assessed as a potential precursor in alkaline cement synthesis in order to raise a synergistic effect necessary to enhance cementitious properties of volcanic ash based alkaline cement. Results obtained through this investigation show that when used alone as precursor, cassava peel ash reacts with alkaline solution to form alkali activated materials with formation of new crystalline phases such as calcium silicate hydrate, pirssonite and apthitalite whose quantities vary depending on the  $\text{SiO}_2 / \text{Na}_2\text{O}$  molar ratio. High degree of reactivity of cassava peel ash in alkaline medium along with formation of new gel (calcium potassium ferroaluminosilicate hydrate gel) was achieved at  $\text{SiO}_2 / \text{Na}_2\text{O}$  molar ratio equal to 1.5. This was physically expressed by a high compressive strength of about 14 MPa. Afterward, its combination to low reactive volcanic ash, within the range 0-30 % by mass, in the synthesis of alkaline cement through sealing curing yielded alkaline cement products with low setting time (64 %) and high compressive strength (733 %) which satisfy the ASTM standard for construction [165]. Also, it helps to turn down the magnitude of efflorescence by assuring a

homogeneous distribution sodium ions through the formation of a geopolymer gel and aphthitalite. Hence, low reactive volcanic ash with reactive phase content  $\geq 26$  % by mass can be used as solid precursor in alkaline activation, but require specific curing regime such as open atmospheric air (SOA25) and oven drying at 60 °C (ODS60), in order to achieve satisfactory mechanical properties and durability. Furthermore, cassava peel ash can be used either as alone solid precursor for the synthesis of alkali activated material or as a good admixture in the synthesis of low reactive volcanic ash based alkaline cements.

For further work, we propose:

- Intense durability studies on low reactive volcanic ash based alkaline cements subjected to various acid curing in order to handle the cost and reliability of the method for potential applications;
- Intense durability test on volcanic ash-cassava peel ash based alkaline cement mortars and concretes in order to better handle their suitability as far as engineering applications are considered;
- The assessment of cassava peel ash as a source of alkali oxide for the synthesis of one-part alkaline cements.

## REFERENCES

- [1] G. Arku, Housing Policy in Developing Countries, *Int. Encycl. Hum. Geogr.* 7 (2020) 79–82. doi:10.1016/B978-0-08-102295-5.10395-6.
- [2] J. Davidovits, False values on CO<sub>2</sub> emission for geopolymer cement / concrete published in scientific papers, technical paper #24, Geopolymer Inst. Library, [Www.geopolymer.org](http://www.geopolymer.org). (2015) 1–9.
- [3] H.K. Tchakoute, A. Elimbi, E. Yanne, and C.N. Djangang, Utilization of volcanic ashes for the production of geopolymers cured at ambient temperature, *Cem. Concr. Compos.* 38 (2013) 75–81. doi:10.1016/j.cemconcomp.2013.03.010.
- [4] J.N.Y. Djobo, A. Elimbi, H.K. Tchakouté, S. Kumar, Volcanic ash-based geopolymer cements/concretes: the current state of the art and perspectives, *Environ. Sci. Pollut. Res.* 24 (2016) 4433–4446. doi:10.1007/s11356-016-8230-8.
- [5] J.N.Y. Djobo, L.N. Tchadjié, H.K. Tchakoute, B.B.D. Kenne, A. Elimbi, D. Njopwouo, Synthesis of geopolymer composites from a mixture of volcanic scoria and metakaolin, *J. Asian Ceram. Soc.* 2 (2014) 387–398. doi:10.1016/j.jascer.2014.08.003.
- [6] P.N. Lemougna, A. Nzeukou, B. Aziwo, A.B. Tchamba, K. Wang, U.C. Melo, X. Cui, Effect of slag on the improvement of setting time and compressive strength of low reactive volcanic ash geopolymers synthesized at room temperature, *Mater. Chem. Phys.* 239 (2020) 122077. doi:10.1016/j.matchemphys.2019.122077.
- [7] P. Cong, Y. Cheng, Advances in geopolymer materials : A comprehensive review, *J. Traffic Transp. Eng. (English Ed.)* 8 (2021) 283–314. doi:10.1016/j.jtte.2021.03.004.
- [8] B.I. Djon Li Ndjock, A. Elimbi, M. Cyr, Rational utilization of volcanic ashes based on factors affecting their alkaline activation, *J. Non. Cryst. Solids.* 463 (2017) 31–39. doi:10.1016/j.jnoncrysol.2017.02.024.
- [9] J.N.Y. Djobo, A. Elimbi, H.K. Tchakouté, and S. Kumar., Reactivity of volcanic ash in alkaline medium , microstructural and strength characteristics of resulting geopolymers

- under different synthesis conditions, *J. Mater. Sci.* 51 (2016) 10301–10317. doi:10.1007/s10853-016-0257-1.
- [10] J. Xie, and O. Kayali, Effect of initial water content and curing moisture conditions on the development of fly ash-based geopolymers in heat and ambient temperature, *Constr. Build. Mater.* 67 (2013) 1–9. doi:10.1016/j.conbuildmat.2013.10.047.
- [11] S. Pangdaeng, T. Phoo-ngernkham, V. Sata, and P. Chindaprasirt, Influence of curing conditions on properties of high calcium fly ash geopolymer containing Portland cement as additive, *J. Mater.* 53 (2014) 269–274. doi:10.1016/j.matdes.2013.07.018.
- [12] S. Lee, A. Van Riessen, and C. Chon, Benefits of sealed-curing on compressive strength of fly ash-based geopolymers, *J. Mater.* 9 (2016) 598. doi:10.3390/ma9070598.
- [13] O. Olatokunbo, E. Anthony, O. Rotimi, O. Solomon, A. Tolulope, and O. John, Assessment of strength properties of cassava peel ash-concrete, *Int. J. Civ. Eng. Technol.* 9 (2018) 965–974.
- [14] M.H. Samarakoon, P.G. Ranjith, T.D. Rathnaweera, and M.S.A. Perera, Recent Advances in Alkaline Cement Binders: A Review, *J. Clean. Prod.* 227 (2019) 70–87. doi:10.1016/j.jclepro.2019.04.103.
- [15] J.L. Provis, and J.S.J. van Deventer, Alkali Activated Materials State-of-the-Art Report, RiLEM TC 224-AAM, Springer, 2014. doi:10.1007/978-94-007-7672-2.
- [16] F. Pacheco-torgal, Alkali-activated binders: A review Part 1 . Historical background , terminology , reaction mechanisms and hydration products, 22 (2008) 1305–1314. doi:10.1016/j.conbuildmat.2007.10.015.
- [17] J. Davidovits, Why Alkali-Activated Materials ( AAM ) are NOT Geopolymers ?, *Tech. Pap. #25, Geopolymer Inst. Libr. Www.geopolymer.org.* (2018) 1–9. doi:10.13140/RG.2.2.34337.25441.
- [18] J. Liu, and Y. Fang, Study on the disposition of water in fly ash-based geopolymers using ATR – IR, in: 5th Int. Conf. Durab. Concr. Struct. Jun 30–Jul 1, 2016 Shenzhen Univ.



- Shenzhen, Guangdong Prov. P.R.China, 2016: pp. 163–170. doi:10.5703/1288284316126.
- [19] J. Davidovits, Geopolymers : Ceramic-Like Inorganic Polymers, *J. Ceram. Sci. Technol.* 350 (2017) 335–350. doi:10.4416/JCST2017-00038.
- [20] M. Ben Haha, B. Lothenbach, G. Le Saout, and F. Winnefeld, Influence of slag chemistry on the hydration of alkali-activated blast-furnace slag - Part II: Effect of Al<sub>2</sub>O<sub>3</sub>, *Cem. Concr. Res.* 42 (2012) 74–83. doi:10.1016/j.cemconres.2011.08.005.
- [21] J.L. Provis, and S.A. Bernal, Geopolymers and Related Alkali-Activated Materials, *Annu. Rev. Mater. Res.* 44 (2014) 299–330. doi:10.1146/annurev-matsci-070813-113515.
- [22] M. Ben Haha, B. Lothenbach, G. Le Saout, F. Winnefeld, Influence of slag chemistry on the hydration of alkali-activated blast-furnace slag - Part I: Effect of MgO, *Cem. Concr. Res.* 41 (2011) 955–963. doi:10.1016/j.cemconres.2011.05.002.
- [23] R.C. Kaze, L.M.B. Mougam, M.L.F. Djouka, A. Nana, E. Kamseu, U.F.C. Melo, C. Leonelli, The corrosion of kaolinite by iron minerals and the effects on geopolymerization, *Appl. Clay Sci.* 138 (2017) 48–62. doi:10.1016/j.clay.2016.12.040.
- [24] J. Davidovits, S. Quentin, GEOPOLYMERS Inorganic polymerie new materials, *J. Therm. Anal.* 37 (1991) 1633–1656. doi:10.1007/BF01912193.
- [25] J. Davidovits, and R. Davidovits, Ferro-sialate Geopolymers ( -Fe-O-Si-O-Al-O- ), *Geopolymer Inst. Libr.* (2020) 1–6. doi:10.13140/RG.2.2.25792.89608/2.
- [26] P.N. Lemougna, J.D. Mackenzie, G.N.L. Jameson, H. Rahier, U.F.C. Melo, The role of iron in the formation of inorganic polymers (geopolymers) from volcanic ash: a <sup>57</sup>Fe Mössbauer spectroscopy study, *J. Mater. Sci.* 48 (2013) 5280–5286. doi:10.1007/s10853-013-7319-4.
- [27] C.Y. Heah, H. Kamarudin, A.M.M. Al, M. Binhussain, M. Luqman, I. Khairul Nizar, C.M. Ruzaidi, Y.M. Liew, Effect of Curing Profile on Kaolin-based Geopolymers, *Phys. Procedia.* 22 (2011) 305–311. doi:10.1016/j.phpro.2011.11.048.
- [28] C.Y. Heah, H. Kamarudin, A.M.M. Al Bakri, M. Bnhussain, M. Luqman, I.K. Nizar, C.M.

- Ruzaidi, Y.M. Liew, Kaolin-based geopolymers with various NaOH concentrations, *Int. J. Miner. Metall. Mater.* 20 (2013) 313. doi:10.1007/s12613-013-0729-0.
- [29] A.D. Hounsi, G.L. Lecomte-nana, G. Djétéli, P. Blanchart, Kaolin-based geopolymers : Effect of mechanical activation and curing process, *Constr. Build. Mater.* 42 (2013) 105–113. doi:10.1016/j.conbuildmat.2012.12.069.
- [30] R. Siddique, Resources , Conservation and Recycling Effect of volcanic ash on the properties of cement paste and mortar, "Resources, Conserv. Recycl. 56 (2011) 66–70. doi:10.1016/j.resconrec.2011.09.005.
- [31] J.N.Y. Djobo, H.K. Tchakouté, N. Ranjbar, A. Elimbi, L.N. Tchadjié, D. Njopwouo, J. Biernacki, Gel Composition and Strength Properties of Alkali-Activated Oyster Shell-Volcanic Ash: Effect of Synthesis Conditions, *J. Am. Ceram. Soc.* 99 (2016) 3159–3166. doi:10.1111/jace.14332.
- [32] H.K. Tchakouté, S. Kong, J.N.Y. Djobo, L.N. Tchadjié, D. Njopwouo, A comparative study of two methods to produce geopolymer composites from volcanic scoria and the role of structural water contained in the volcanic scoria on its reactivity, *Ceram. Int.* 41 (2015) 1–10. doi:10.1016/j.ceramint.2015.06.073.
- [33] J.N.Y. Djobo, A. Elimbi, K.H. Tchakouté, S. Kumar, Mechanical activation of volcanic ash for geopolymer synthesis : effect on reaction kinetics , gel characteristics , physical and mechanical, *R. Soc. Chem. Adv.* 6 (2016) 39106–39117. doi:10.1039/C6RA03667H.
- [34] H.K. Tchakoute, A. Elimbi, B.B.D. Kenne, J.A. Mbey, D. Njopwouo, Synthesis of geopolymers from volcanic ash via the alkaline fusion method : Effect of Al<sub>2</sub>O<sub>3</sub> / Na<sub>2</sub>O molar ratio of soda – volcanic ash, *Ceram. Int.* 39 (2013) 269–276. doi:10.1016/j.ceramint.2012.06.021.
- [35] A.K. Kasthurba, M. Santhanam, H. Achyuthan, Investigation of laterite stones for building purpose from Malabar region , Kerala , SW India - Chemical analysis and microstructure studies, 22 (2008) 2400–2408. doi:10.1016/j.conbuildmat.2006.12.003.

- [36] F. Trolard and Y. Tardy, A model of Fe<sup>3+</sup>-kaolinite, Al<sup>3+</sup>-goethite, Al<sup>3+</sup>-hematite equilibria in laterites, *J. Clay Miner.* 24 (1989) 1–21.
- [37] G. Stoops, and V. Marcelino, 15 - Lateritic and Bauxitic Materials, in: *Interpret. Micromorphol. Featur. Soils Regoliths*, Elsevier B.V., 2018: pp. 691–720. doi:10.1016/B978-0-444-53156-8.00015-5.
- [38] R.P. Bourman, Perennial problems in the study of laterite : A review Perennial problems in the study of laterite : A review, *Aust. J. Earth Sci. An Int. Geosci. J. Geol. Soc. Aust.* 40 (1993) 387–401. doi:10.1080/08120099308728090.
- [39] C.A. Oyelami, and J.L. Van Rooy, A review of the use of lateritic soils in the construction/development of sustainable housing in Africa: A Geological Perspective, *J. African Earth Sci.* 119 (2016) 226–237. doi:10.1016/j.jafrearsci.2016.03.018.
- [40] R.C. Poudeu, C.J. Ekani, C.N. Djangang, P. Blanchart, Role of heat-treated laterite on the strengthening of geopolymer designed with laterite as solid precursor, *Ann. Chim. - Sci. Des Mater.* 43 (2019) 359–367. doi:10.18280/acsm.430601.
- [41] E.A. Obonyo, E. Kamseu, P.N. Lemougna, A.B. Tchamba, U.C. Melo, C. Leonelli, A sustainable approach for the geopolymerization of natural iron-rich aluminosilicate materials, *Sustainability.* 6 (2014) 5535–5553. doi:10.3390/su6095535.
- [42] D. Massiot, P. Dion, J.F. Alcover, F. Bergaya, <sup>27</sup>Al and <sup>29</sup>Si MAS NMR Study of Kaolinite thermal decomposition by controlled rate thermal analysis, *J. Am. Ceram. Soc.* 78 (1995) 2940–2944. doi:10.1111\_j.1151-2916.1995.tb09067.x.
- [43] A. Elimbi, H.K. Tchakoute, D. Njopwouo, Effects of calcination temperature of kaolinite clays on the properties of geopolymer cements, *Constr. Build. Mater.* 25 (2011) 2805–2812. doi:10.1016/j.conbuildmat.2010.12.055.
- [44] B.B.D. Kenne, A. Elimbi, M. Cyr, J.D. Manga, H.K. Tchakoute, Effect of the rate of calcination of kaolin on the properties of metakaolin-based geopolymers, *J. Asian Ceram. Soc.* 3 (2015) 130–138. doi:10.1016/j.jascer.2014.12.003.

- [45] E. Potapova, E. Dmitrieva, The effect of metakaolin on the processes of hydration and hardening of cement, *Mater. Today Proc.* 19 (2019) 2193–2196. doi:10.1016/j.matpr.2019.07.373.
- [46] H. El-diadamony, A.A. Amer, T.M. Sakkary, S. El-Hoseny, Hydration and characteristics of metakaolin pozzolanic cement pastes, *HBRC J.* 14 (2018) 150–158. doi:10.1016/j.hbrj.2015.05.005.
- [47] C. Panagiotopoulou, E. Kontori, T. Perraki, G. Kakali, Dissolution of aluminosilicate minerals and by-products in alkaline media, *J. Mater. Sci.* 42 (2007) 2967–2973. doi:10.1007/s10853-006-0531-8.
- [48] E. Najafi, A. Allahverdi, J.L. Provis, Efflorescence control in geopolymer binders based on natural pozzolan, *Cem. Concr. Compos.* 34 (2012) 25–33. doi:10.1016/j.cemconcomp.2011.07.007.
- [49] R. Siddique, Ground Granulated Blast Furnace Slag, in: *Waste Mater. By-Products Concr.*, 2008: pp. 1–39. doi:10.1007/978-3-540-74294-4\_1.
- [50] S.R. Rao, Metallurgical slags, dust and fumes, *Waste Manag. Ser.* 7 (2006) 269–327. doi:10.1016/S0713-2743(06)80093-0.
- [51] R.T. Flynn, J.M. Aldred, and P.G. Snow, Slag Cement in Concrete and Mortar Reported by ACI Committee 233, (2003) 1–19.
- [52] M. Ben Haha, G. Le Saout, F. Winnefeld, B. Lothenbach, Influence of activator type on hydration kinetics, hydrate assemblage and microstructural development of alkali activated blast-furnace slags, *Cem. Concr. Res.* 41 (2011) 301–310. doi:10.1016/j.cemconres.2010.11.016.
- [53] A.G. De Torre, A. Palomo, G. Lo, M.M. Alonso, M.A.G. Aranda, Quantitative determination of phases in the alkali activation of fly ash . Part I . Potential ash reactivity, 85 (2006) 625–634. doi:10.1016/j.fuel.2005.08.014.
- [54] A. Rai, M. Kumar, Y.K. Vajpai, Effects of fly ash and other ingredients to the strength and

- cost of “falgcds ” (flyash , lime , gypsum , cement , stone dust ) bricks, *Int. J. Eng. Tech. Res.* 3812 (2014) 244–250.
- [55] P.K. Mehta, *Mineral Admixtures.*, in: *Concr Admixtures Handb, Prop, Sci, Technol*, 1984: pp. 303–336.
- [56] V.G. Papadakis, Effect of fly ash on Portland cement systems Part I. Low-calcium fly ash, *Cem. Concr. Res.* 29 (1999) 1727–1736. doi:10.1016/S0008-8846(99)00153-2.
- [57] V.G. Papadakis, Effect of fly ash on Portland cement systems Part II. High-calcium fly ash, *Cem. Concr. Res.* 30 (2000) 1647–1654. doi:10.1016/S0008-8846(00)00388-4.
- [58] P. Indiramma, C. Sudharani, S. Needhidasan, Utilization of fly ash and lime to stabilize the expansive soil and to sustain pollution free environment – An experimental study, *Mater. Today Proc.* 22 (2020) 694–700. doi:10.1016/j.matpr.2019.09.147.
- [59] S. Saha, C. Rajasekaran, Enhancement of the properties of fly ash based geopolymer paste by incorporating ground granulated blast furnace slag, *Constr. Build. Mater.* 146 (2017) 615–620. doi:10.1016/j.conbuildmat.2017.04.139.
- [60] W.K.W. Lee, J.S.J. Van Deventer, The effect of ionic contaminants on the early-age properties of alkali-activated fly ash-based cements, *Cem. Concr. Res.* 32 (2002) 577–584. doi:10.1016/S0008-8846(01)00724-4.
- [61] U. Rattanasak, K. Pankhet, P. Chindapasirt, Effect of chemical admixtures on properties of high-calcium fly ash geopolymer, *Int. J. Miner. Metall. Mater.* 18 (2011) 364–369. doi:10.1007/s12613-011-0448-3.
- [62] P. Ninla, A. Balo, E. Kamseu, U. Chinje, M. Delplancke, H. Rahier, Influence of the processing temperature on the compressive strength of Na activated lateritic soil for building applications, *Constr. Build. Mater.* 65 (2014) 60–66. doi:10.1016/j.conbuildmat.2014.04.100.
- [63] C.R. Kaze, J.N. Yankwa, A. Nana, H.K. Tchakoute, E. Kamseu, U.C. Melo, and H. Rahier, Effect of silicate modulus on the setting, mechanical strength and microstructure of iron-

- rich aluminosilicate (laterite) based- geopolymer cured at room temperature, *Ceram. Int.* 44 (2018) 21442–21450. doi:10.1016/j.ceramint.2018.08.205.
- [64] R.C. Kaze, L. Myllyam, B. MOUNGAM, M. Cannio, R. Rosa, E. Kamseu, U.C. Melo, and C. Leonelli, Microstructure and engineering properties of Fe<sub>2</sub>O<sub>3</sub>(FeO)-Al<sub>2</sub>O<sub>3</sub>-SiO<sub>2</sub> based geopolymer composites, *J. Clean. Prod.* 199 (2018) 849–859. doi:10.1016/j.jclepro.2018.07.171.
- [65] L. Opoczky, Fine grinding and agglomeration of silicates, *Powder Technol.* 7 (1977) 1–7. doi:10.1016/0032-5910(77)85037-7.
- [66] P. Balaz, *Mechanochemistry in Nanoscience and Minerals Engineering*, Springer, 2008. doi:10.1007/978-3-540-74855-7.
- [67] J. Temuujin, R.P. Williams, A. Van Riessen, Effect of mechanical activation of fly ash on the properties of geopolymer cured at ambient temperature, *J. Mater. Process. Technol.* 209 (2009) 5276–5280. doi:10.1016/j.jmatprotec.2009.03.016.
- [68] S. Kumar, R. Kumar, Mechanical activation of fly ash : Effect on reaction, structure and properties of resulting geopolymer, *Ceram. Int.* 37 (2011) 533–541. doi:10.1016/j.ceramint.2010.09.038.
- [69] G. Mucsi, S. Kumar, B. Cs, R. Kumar, Z. Molnár, Á. Rácz, F. Má dai, Á. Debreczeni, Control of geopolymer properties by grinding of land filled fly ash, *Int. J. Miner. Process.* 143 (2015) 50–58. doi:10.1016/j.minpro.2015.08.010.
- [70] J. Payá, J. Monzó, M. V. Borrachero, E. Peris-Mora, Comparisons among magnetic and non-magnetic fly ash fractions: Strength development of cement-fly ash mortars, *Waste Manag.* 16 (1996) 119–124. doi:10.1016/S0956-053X(96)00034-7.
- [71] D.S. Rao, B. Das, Characterization and beneficiation studies of a Low grade bauxite ore, *J. Inst. Eng. Ser. D.* 95 (2014) 81–93. doi:10.1007/s40033-014-0050-8.
- [72] P. Chindapasirt, C. Jaturapitakkul, T. Sinsiri, Effect of fly ash fineness on microstructure of blended cement paste, *Constr. Build. Mater.* 21 (2007) 1534–1541.

doi:10.1016/j.conbuildmat.2005.12.024.

- [73] T. Sinsiri, P. Chindaprasirt, C. Jaturapitakkul, Influence of fly ash fineness and shape on the porosity and permeability of blended cement pastes, *Int. J. Miner. Metall. Mater.* 17 (2010) 683–690. doi:10.1007/s12613-010-0374-9.
- [74] H.W. Nugteren, V.C.L. Butselaar-Orthlieb, M. Izquierdo, G.J. Witkamp, M.T. Kreutzer, High strength geopolymers from fractionated and pulverized fly ash, 3rd World Coal Ash, WOCA Conf. - Proc. (2009) 1–9. <http://www.flyash.info/%0AHigh>.
- [75] P. Chindaprasirt, T. Chareerat, S. Hatanaka, T. Cao, High-strength geopolymer using fine high-calcium fly ash, *J. Mater. Civ. Eng.* 23 (2011) 264–270. doi:10.1061/(ASCE)MT.1943-5533.0000161.
- [76] S. Kumar, F. Kristály, G. Mucsi, Geopolymerisation behaviour of size fractioned fly ash, *Adv. Powder Technol.* 26 (2015) 24–30. doi:10.1016/j.appt.2014.09.001.
- [77] S. Kumar, R. Kumar, T.C. Alex, A. Bandopadhyay, S.P. Mehrotra, Influence of reactivity of fly ash on geopolymerisation, *Adv. Appl. Ceram.* 106 (2007) 120–127. doi:10.1179/174367607X159293.
- [78] C.R. Kaze, H. Tchakoute Kouamo, T.T. Mbakop, J.R. Mache, E. Kamseu, C. Melo, C. Leonelli, and H. Rahier, Synthesis and properties of inorganic polymers (geopolymers) derived from Cameroon-meta- halloysite, *Ceram. Int.* 44 (2018) 18499–18508. doi:10.1016/j.ceramint.2018.07.070.
- [79] B. Zhang, H. Guo, P. Yuan, Y. Li, Q. Wang, and L. Deng, Geopolymerization of halloysite via alkali-activation : Dependence of microstructures on precalcination, *Appl. Clay Sci.* 185 (2019) 105375. doi:10.1016/j.clay.2019.105375.
- [80] D. S Shah, M.P. Shah, J. Pitroda, Chemical admixtures: a major role in modern concrete materials and technologies, *Natl. Conf. “Trends Challenges Civ. Eng. Today’s Transform. World.”* (2014) 1–15.
- [81] M. Olalekan, M. Azmi, M. Johari, Z. Arifin, M. Maslehuddin, Effects of addition of

- Al(OH)<sub>3</sub> on the strength of alkaline activated ground blast furnace slag-ultrafine palm oil fuel ash (AAGU) based binder, *Constr. Build. Mater.* 50 (2014) 361–367. doi:10.1016/j.conbuildmat.2013.09.054.
- [82] T. Revathi, R. Jeyalakshmi, N.P. Rajamane, M. Sivasakthi, Evaluation of the role of Cetyltrimethylammoniumbromide (CTAB) and Acetylenicglycol (AG) admixture on fly ash based geopolymer, *Orient. J. Chem.* 33 (2017) 783–792.
- [83] A. Kusbiantoro, M.S. Ibrahim, K. Muthusamy, A. Alias, Development of sucrose and citric acid as the natural based admixture for fly ash based geopolymer, *Procedia Environ. Sci.* 17 (2013) 596–602. doi:10.1016/j.proenv.2013.02.075.
- [84] P. Rovnanik, Influence of C12A7 admixture on setting properties of fly ash geopolymer, *Ceram. Silikaty.* 4 (2015) 362–367.
- [85] H. Tchakoute Kouamo, A. Elimbi, J.A. Mbey, C.J. Ngally Sabouang, D. Njopwouo, The effect of adding alumina-oxide to metakaolin and volcanic ash on geopolymer products: A comparative study, *Constr. Build. Mater.* 35 (2012) 960–969. doi:10.1016/j.conbuildmat.2012.04.023.
- [86] L.N. Tchadjié, J.N.Y. Djobo, N. Ranjbar, H.K. Tchakouté, B.B.D. Kenne, A. Elimbi, D. Njopwouo, Potential of using granite waste as raw material for geopolymer synthesis, *Ceram. Int.* 42 (2016) 3046–3055. doi:10.1016/j.ceramint.2015.10.091.
- [87] H. Xu, Q. Li, L. Shen, M. Zhang, J. Zhai, Low-reactive circulating fluidized bed combustion (CFBC) fly ashes as source material for geopolymer synthesis, *Waste Manag.* 30 (2010) 57–62. doi:10.1016/j.wasman.2009.09.014.
- [88] M. Xun, P. Zheng, H. Wang, Synthesis, characterization and mechanisms of one-part geopolymeric cement by calcining low-quality kaolin with alkali, *Mater. Struct.* 48 (2014) 699–708. doi:10.1617/s11527-014-0350-3.
- [89] S. Songpiriyakij, T. Kubprasit, C. Jaturapitakkul, P. Chindapasirt, Compressive strength and degree of reaction of biomass- and fly ash-based geopolymer, *Constr. Build. Mater.* 24 (2010) 236–240. doi:10.1016/j.conbuildmat.2009.09.002.



- [90] Y.J.N. Djobo, A. Elimbi, J.D. Manga, I.B. Djon Li Ndjock, Partial replacement of volcanic ash by bauxite and calcined oyster shell in the synthesis of volcanic ash-based geopolymers, *Constr. Build. Mater.* 113 (2016) 673–681. doi:10.1016/j.conbuildmat.2016.03.104.
- [91] Y. Jun, S.H. Han, T.Y. Shin, J.H. Kim, Effects of CO<sub>2</sub> curing on alkali-activated slag paste cured in different curing conditions, *Materials (Basel)*. 12 (2019) 3513. doi:10.3390/ma12213513.
- [92] H.M. Giasuddin, J.G. Sanjayan, P.G. Ranjith, Strength of geopolymer cured in saline water in ambient conditions, *Fuel*. 107 (2013) 34–39. doi:10.1016/j.fuel.2013.01.035.
- [93] P.N. Lemougna, A. Adediran, J. Yliniemi, T. Luukkonen, M. Illikainen, Effect of organic resin in glass wool waste and curing temperature on the synthesis and properties of alkali-activated pastes, *Mater. Des.* 212 (2021) 110287. doi:10.1016/j.matdes.2021.110287.
- [94] H. El-Hassan, E. Shehab, A. Al-Sallamin, Effect of curing regime on the performance and microstructure characteristics of alkali-activated slag-fly ash blended concrete, *J. Sustain. Cem. Mater.* 10 (2021) 289–317. doi:10.1080/21650373.2021.1883145.
- [95] Y. Fang, O. Kayali, The fate of water in fly ash-based geopolymers, *Constr. Build. Mater.* 39 (2013) 89–94. doi:10.1016/j.conbuildmat.2012.05.024.
- [96] S. Park, M. Pour-ghaz, What is the role of water in the geopolymerization of metakaolin ?, *Constr. Build. Mater.* 182 (2018) 360–370. doi:10.1016/j.conbuildmat.2018.06.073.
- [97] S.J.K. Melele, H.K. Tchakouté, C. Banenzoué, E. Kamseu, C.H. Rüschler, F. Andreola, C. Leonelli, Investigation of the relationship between the condensed structure and the chemically bonded water content in the poly (sialate-siloxo) network, *Appl. Clay Sci.* 156 (2018) 77–86. doi:10.1016/j.clay.2018.01.029.
- [98] M. Lizcano, A. Gonzalez, S. Basu, K. Lozano, M. Radovic, Effects of water content and chemical composition on structural properties of alkaline activated metakaolin-based geopolymers, *J. Am. Ceram. Soc.* 9 (2012) 1–9. doi:10.1111/j.1551-2916.2012.05184.x.
- [99] Z. Zuhua, Y. Xiao, Z. Huajun, C. Yue, Role of water in the synthesis of calcined kaolin-

- based geopolymer, *Appl. Clay Sci.* 43 (2009) 218–223. doi:10.1016/j.clay.2008.09.003.
- [100] K.H. Mo, U.J. Alengaram, M.Z. Jumaat, A Review on the Use of Agriculture Waste Material as Lightweight Aggregate for Reinforced Concrete Structural Members, *Adv. Mater. Sci. Eng.* 2014 (2014) 9. doi:10.1155/2014/365197.
- [101] J. Kumar, S. Kumar, and S.S. Basarkar, Concrete using agro-waste as fine aggregate for sustainable built environment – A review, *Int. J. Sustain. Built Environ.* 5 (2016) 312–333. doi:10.1016/j.ijbe.2016.06.003.
- [102] E. Nimwinya, W. Arjharn, S. Horpibulsuk, T. Phoo-ngernkham, A. Poowancum, A sustainable calcined water treatment sludge and rice husk ash geopolymer, *J. Clean. Prod.* 119 (2016) 128–134. doi:10.1016/j.jclepro.2016.01.060.
- [103] P. Kumar, A.P. Singh, Studies on Partial Replacement of Cement by Bagasse Ash in Concrete, *Int. J. Civ. Struct. Eng. Res.* 3 (2015) 308–310.
- [104] C. Marthong, Effect of rice husk ash (RHA) as partial replacement of cement on concrete properties, *Int. J. Eng. Res. Technol.* 1 (2012) 1–3.
- [105] K. Kaur, J. Singh, M. Kaur, Compressive strength of rice husk ash based geopolymer : The effect of alkaline activator, *Constr. Build. Mater.* 169 (2018) 188–192. doi:10.1016/j.conbuildmat.2018.02.200.
- [106] A. Akbar, F. Farooq, M. Shafique, F. Aslam, R. Alyousaf, H. Abduljabbar, Sugarcane bagasse ash-based engineered geopolymer mortar incorporating propylene fibers, *J. Build. Eng.* 33 (2020) 101492. doi:10.1016/j.job.2020.101492.
- [107] R.H. Ash, Y.J. Patel, N. Shah, Enhancement of the properties of ground granulated blast furnace slag based self compacting geopolymer concrete by incorporating, *Constr. Build. Mater.* 171 (2018) 654–662. doi:10.1016/j.conbuildmat.2018.03.166.
- [108] B. Bhushan, P. Jangra, and A. Garg, Effects of ultra fine slag as mineral admixture on the compressive strength , water absorption and permeability of rice husk ash based geopolymer concrete, *Mater. Today Proc.* 32 (2020) 871–877. doi:10.1016/j.matpr.2020.04.219.

- [109] B. Abiodun, M. Azmi, M. Johari, Z. Ariffin, Impact of added water and superplasticizer on early compressive strength of selected mixtures of palm oil fuel ash-based engineered geopolymer composites, *Constr. Build. Mater.* 109 (2016) 198–206. doi:10.1016/j.conbuildmat.2016.01.033.
- [110] J. Rivera, F. Castro, A. Fernández, J. Nuno, Alkali - Activated Cements from Urban , Mining and Agro - Industrial Waste : State - of - the - art and Opportunities, *Waste and Biomass Valorization*. 12 (2021) 2665–2683. doi:10.1007/s12649-020-01071-9.
- [111] A. Pereira, J.L. Akasaki, J.L.P. Melges, M.M. Tashima, L. Soriano, M. V. Borrachero, J. Monzó, J. Payá, Mechanical and durability properties of alkali-activated mortar based on sugarcane bagasse ash and blast furnace slag, *Ceram. Int.* 41 (2015) 1–13. doi:10.1016/j.ceramint.2015.07.001.
- [112] V.N. Castaldelli, J.C.B. Moraes, J.L. Akasaki, J.L.P. Melges, J. Monzó, M. V. Borrachero, L. Soriano, J. Payá, M.M. Tashima, Study of the binary system fly ash/sugarcane bagasse ash (FA/SCBA) in SiO<sub>2</sub>/K<sub>2</sub>O alkali-activated binders, *Fuel*. 174 (2016) 307–316. doi:10.1016/j.fuel.2016.02.020.
- [113] A. Peys, H. Rahier, Y. Pontikes, Potassium-rich biomass ashes as activators in metakaolin-based inorganic polymers, *Appl. Clay Sci.* 119 (2016) 401–409. doi:10.1016/j.clay.2015.11.003.
- [114] H.K. Tchakouté, C.H. Rüscher, S. Kong, E. Kamseu, C. Leonelli, Geopolymer binders from metakaolin using sodium waterglass from waste glass and rice husk ash as alternative activators : A comparative study, *Constr. Build. Mater.* 114 (2016) 276–289. doi:10.1016/j.conbuildmat.2016.03.184.
- [115] H. Kouamo Tchakouté, C. Henning Rüscher, M. Hinsch, J.N. Djobo Yankwa, E. Kamseu, C. Leonelli, Utilization of sodium waterglass from sugar cane bagasse ash as a new alternative hardener for producing metakaolin-based geopolymer cement, *Chemie Der Erde*. 77 (2017) 257–266. doi:10.1016/j.chemer.2017.04.003.
- [116] H.K. Tchakouté, C.H. Rüscher, S. Kong, E. Kamseu, C. Leonelli, Thermal behavior of

- metakaolin-based geopolymer cements using sodium waterglass from rice husk ash and waste glass as alternative activators, *Waste and Biomass Valorization*. 8 (2016) 573–584. doi:10.1007/s12649-016-9653-7.
- [117] C. Ogbonna, M.M. Elvis, G.U. Alaneme, Characterisation and use of cassava peel ash in concrete production, *Comput. Eng. Phys. Model.* 2 (2020) 12–28. doi:10.22115/CEPM.2020.223035.1091.
- [118] E.E. Agbenyeku, F.N. Okonta, Green economy and innovation: compressive strength potential of blended cement cassava peels ash and laterised concrete, *African J. Sci. Technol. Innov. Dev.* 6 (2014) 105–110. doi:10.1080/20421338.2014.895482.
- [119] L.O. Ettu, U.C. Anya, J.I. Arimanwa, L. Anyaogu, K.C. Nwachukwu, Strength of binary blended cement composites containing corn cob ash, *Int. J. Eng. Res. Dev.* 6 (2013) 77–82.
- [120] A.E. Emmanuel, A.I. Frank, Prolonged curing of green concrete from domestically derived cassava peels ash (DDCPA) and laterite, 5 (2014) 900–905.
- [121] M. Bokanga, CASSAVA: Post-harvest Operations, Ibadan, 1999. <https://www.fao.org/3/au998e/au998e.pdf>.
- [122] FAO, 2018, Food Outlook - Biannual report on global food markets, Trade and Markets Division of FAO, Rome, n.d. <http://www.fao.org/giews/>.
- [123] W. Xiao-guang, Z. Xin-hua, J. Chun-ji, L.I. Chun-hong, C. Shan, W.U. Di, Effects of potassium deficiency on photosynthesis and photo- protection mechanisms in soybean ( *Glycine max* ( L .) Merr .), *J. Integr. Agric.* 14 (2015) 856–863. doi:10.1016/S2095-3119(14)60848-0.
- [124] D.M. Oosterhuis, D.A. Loka, E.M. Kawakami, and W.T. Pettigrew, The Physiology of Potassium in Crop Production, *Adv. Agron.* 126 (2014) 203–233. doi:10.1016/B978-0-12-800132-5.00003-1.
- [125] A. Hafeez, S. Ali, X. Ma, S. Atta, A. Noor, A. Liu, S. Ahmed, M. Sohaib, G. Yang, Industrial Crops & Products Potassium to nitrogen ratio favors photosynthesis in late-

- planted cotton at high planting density, *Ind. Crop. Prod.* 124 (2018) 369–381. doi:10.1016/j.indcrop.2018.08.006.
- [126] S. V Vassilev, D. Baxter, C.G. Vassileva, An overview of the behaviour of biomass during combustion : Part II . Ash fusion and ash formation mechanisms of biomass types, *FUEL*. 117 (2014) 152–183. doi:10.1016/j.fuel.2013.09.024.
- [127] C. De Faria, F. Carraro, C. Cristina, D.A. Loures, L. Martins, Characterization of cassava biomass using differential scanning calorimetry and thermogravimetry for energy purposes, *J. Therm. Anal. Calorim.* 138 (2019) 3811–3823. doi:10.1007/s10973-019-08905-2.
- [128] Y. Park, M. Lang, H. Su, H. Won, S. Hoon, S. Jung, S. Park, S. Seo, Wild reed of Suncheon Bay : Potential bio-energy source, *Renew. Energy.* 42 (2012) 168–172. doi:10.1016/j.renene.2011.08.025.
- [129] A. Natasia, J. Febrianto, J. Sunarso, Y. Ju, N. Indraswati, S. Ismadji, Sequestering of Cu ( II ) from aqueous solution using cassava peel ( *Manihot esculenta* ), *J. Hazard. Mater.* 180 (2010) 366–374. doi:10.1016/j.jhazmat.2010.04.040.
- [130] A. Kurniawan, A. Natasia, J. Febrianto, Y. Ju, J. Sunarso, N. Indraswati, S. Ismadji, Evaluation of cassava peel waste as lowcost biosorbent for Ni-sorption : Equilibrium, kinetics, thermodynamics and mechanism, *Chem. Eng. J.* 172 (2011) 158–166. doi:10.1016/j.cej.2011.05.083.
- [131] C.G. Mothé, I.C. De Miranda, Characterization of sugarcane and coconut fibers by thermal analysis and FTIR, *J. Therm. Anal. Calorim.* 97 (2009) 661–665. doi:10.1007/s10973-009-0346-3.
- [132] J.A. MBEY, Films Composites Amidon de Manioc-Kaolinite: influence de la dispersion de l'argile et des interactions argile-amidon sur les propriétés des films, PhD Thesis, Univ. Lorraine, Fr. (2013) 157.
- [133] R. Prithivirajan, S. Jayabal, S.K. Sundaram, V. Sangeetha, Hybrid biocomposites from agricultural residues: Mechanical, water absorption and tribological behaviors, *J. Polym. Eng.* 36 (2016) 663–671. doi:10.1515/polyeng-2015-0113.

- [134] J. Madejova, and P. Komadel, Baseline studies of the clay minerals society source clays : infrared methods, *Clays Clay Miner.* 49 (2001) 410–432. doi:10.1346/CCMN.2001.0490508.
- [135] E.L.M. Mielcarek, J.A. Wongpa, C.H.A.I. Jaturapitakkul, Silicate- , aluminosilicate and calciumsilicate gels for building materials : chemical and mechanical properties during ageing, *Eur. J. Mineral.* 23 (2011) 111–124. doi:10.1127/0935-1221/2010/0022-2070.
- [136] N.S. Trivedi, S.A. Mandavgane, S. Mehetre, and B.D. Kulkarni, Characterization and valorization of biomass ashes, *Environ. Sci. Pollut. Res.* 23 (2016) 20243–20256. doi:10.1007/s11356-016-7227-7.
- [137] F.B. Reig, J.V.G. Adelantado, M.C.M.M. Moreno, FTIR quantitative analysis of calcium carbonate ( calcite ) and silica ( quartz ) mixtures using the constant ratio method . Application to geological samples, *Talanta.* 58 (2002) 811–821.
- [138] H.K. Tchakoute, C.H. Ruscher, S. Kong, E. Kamseu, C. Leonelli, Thermal Behavior of Metakaolin-Based Geopolymer Cements Using Sodium Waterglass from Rice Husk Ash and Waste Glass as Alternative Activators, *Waste and Biomass Valorization.* 8 (2016) 573–584. doi:10.1007/s12649-016-9653-7.
- [139] E. Beckley, K. Mustapha, R.S. Teixeira, H. Savastano, Development of unfired earthen building materials using muscovite rich soils and alkali activators, *Case Stud. Constr. Mater.* 11 (2019) e00262. doi:10.1016/j.cscm.2019.e00262.
- [140] K.G. Knauss, S.N. Nguyen, H.C. Weed, Diopside dissolution kinetics as a function of pH , CO<sub>2</sub> , temperature , and time, *Geochim. Cosmochim. Acta.* 57 (1993) 285–294. doi:10.1016/0016-7037(93)90431-U.
- [141] H. Tomáš, Michaela, Steinerová-Vondráková, Investigation of dissolution of aluminosilicates in aqueous alkaline solution, *Ceramics-Silikáty.* 5 (2002) 97–103.
- [142] M. Hamdan, C. Rueda, L. Blanco, F. Tamimi, J. Torres, U. Gbureck, E. Lopez, *Acta Biomaterialia* Effect of silica gel on the cohesion , properties and biological performance of brushite cement, *Acta Biomater.* 6 (2010) 257–265. doi:10.1016/j.actbio.2009.06.010.

- [143] H.A. Ali, A. Chughtai, A. Sattar, Synthesis of quality silica gel ; Optimization of parameters Silica Sol Silica Gel, *J. Fac. Eng. Technol.* (2009) 1–14.
- [144] S. Musić, N. Filipović-Vinceković, L. Sekovanić, Precipitation of amorphous SiO<sub>2</sub> particles and their properties, *Brazilian J. Chem. Eng.* 28 (2011) 89–94.
- [145] F.N. Okoye, S. Prakash, N.B. Singh, Durability of fly ash based geopolymer concrete in the presence of silica fume, *J. Clean. Prod.* 149 (2017) 1062–1067. doi:10.1016/j.jclepro.2017.02.176.
- [146] J. Noël, Y. Djobo, A. Elimbi, H. Kouamo, S. Kumar, Mechanical properties and durability of volcanic ash based geopolymer mortars, *Constr. Build. Mater.* 124 (2016) 606–614. doi:10.1016/j.conbuildmat.2016.07.141.
- [147] T. Bakharev, Resistance of geopolymer materials to acid attack, *Cem. Concr. Res.* 35 (2005) 658–670. doi:10.1016/j.cemconres.2004.06.005.
- [148] S.A. Bernal, R.S. Nicolas, J.S.J. Van Deventer, J.L. Provis, Alkali-activated slag cements produced with a blended sodium carbonate / sodium silicate activator, *Adv. Cem. Res.* 28 (2016) 262–273. doi:10.1680/jadcr.15.00013.
- [149] H.A. Abdel-Gawwad, S.A. Abo-El-Enein, A novel method to produce dry geopolymer cement powder, *Hous. Build. Natl. Res. Cent.* 12 (2014) 13–24. doi:10.1016/j.hbrcj.2014.06.008.
- [150] J.F. Rivera, C.M. Group, R.M. De Gutierrez, J.M. Mejia, M. Gordillo, Hybrid cement based on the alkali activation of by-products of coal Cementos, *J. Constr.* 13 (2013) 31–39. doi:10.4067/s0718-915x2014000200004.
- [151] S. Monkman, Y. Shao, Assessing the Carbonation Behavior of Cementitious Materials, *J. Mater. Civ. Eng.* 18 (2006) 768–776. doi:10.1061/(asce)0899-1561(2006)18:6(768).
- [152] S.A. Bernal, R. Mejía, D. Gutierrez, J.L. Provis, V. Rose, Cement and Concrete Research Effect of silicate modulus and metakaolin incorporation on the carbonation of alkali silicate-activated slags, *Cem. Concr. Res.* 40 (2010) 898–907.

doi:10.1016/j.cemconres.2010.02.003.

- [153] P. Duxson, A. Fernández-Jiménez, J.L. Provis, G.C. Lukey, A. Palomo, J.S.J. Van Deventer, Geopolymer technology: The current state of the art, *J. Mater. Sci.* 42 (2007) 2917–2933. doi:10.1007/s10853-006-0637-z.
- [154] E.L. Hôpital, B. Lothenbach, K. Scrivener, D.A. Kulik, Alkali uptake in calcium alumina silicate hydrate ( C-A-S-H ), *Cem. Concr. Res.* 85 (2016) 122–136. doi:10.1016/j.cemconres.2016.03.009.
- [155] T. Zakir, Evaluation and Control of Pirssonite Scale Formation in Green Liquor Systems of the Kraft Process, University of Toronto, 2011.
- [156] S.A. Bernal, Microstructural changes induced by CO<sub>2</sub> exposure in alkali-activated slag / Metakaolin Pastes, *Front. Mater.* 3 (2016) 1–10. doi:10.3389/fmats.2016.00043.
- [157] S. Alonso, A. Palomo, Alkaline activation of metakaolin and calcium hydroxide mixtures : influence of temperature , activator concentration and solids ratio, *Mater. Lett.* 47 (2001) 55–62. doi:10.1016/S0167-577X(00)00212-3.
- [158] C.K. Yip, G.C. Lukey, J.S.J. Van Deventer, The coexistence of geopolymeric gel and calcium silicate hydrate at the early stage of alkaline activation, *Cem. Concr. Res.* 35 (2005) 1688–1697. doi:10.1016/j.cemconres.2004.10.042.
- [159] P. De Silva, K. Sagoe-Crenstil, V. Sirivivatnanon, Kinetics of geopolymerization: Role of Al<sub>2</sub>O<sub>3</sub> and SiO<sub>2</sub>, *Cem. Concr. Res.* 37 (2007) 512–518. doi:10.1016/j.cemconres.2007.01.003.
- [160] C.K. Yip, J.L. Provis, G.C. Lukey, J.S.J. van Deventer, Carbonate mineral addition to metakaolin-based geopolymers, *Cem. Concr. Compos.* 30 (2008) 979–985. doi:10.1016/j.cemconcomp.2008.07.004.
- [161] E. Najafi Kani, A. Allahverdi, J.L. Provis, Calorimetric study of geopolymer binders based on natural pozzolan, *J. Therm. Anal. Calorim.* 127 (2017) 2181–2190. doi:10.1007/s10973-016-5850-7.



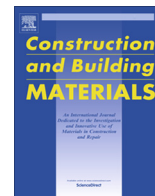
- [162] S.Y. Hong, F.P. Glasser, Alkali sorption by C-S-H and C-A-S-H gels: Part II. Role of alumina, *Cem. Concr. Res.* 32 (2002) 1101–1111. doi:10.1016/S0008-8846(02)00753-6.
- [163] P. He, M. Wang, D. Jia, S. Yan, J. Yuan, J. Xu, P. Wang, Y. Zhou, Effect of Si/Al ratio on the structure and properties of metakaolin based geopolymer, *J. Ceram. Int.* 42 (2016) 14416–14422. doi:10.1016/j.ceramint.2016.06.033.
- [164] B. Lee, G. Kim, R. Kim, B. Cho, S. Lee, C. Chon, Strength development properties of geopolymer paste and mortar with respect to amorphous Si / Al ratio of fly ash, *Constr. Build. Mater.* 151 (2017) 512–519. doi:10.1016/j.conbuildmat.2017.06.078.
- [165] National Concrete Masonry Association, TEK01-01F, ASTM specifications for concrete masonry units, *Fay Block Materials*. (2012) 1–9. <http://www.fayblock.com>.

## LIST OF PUBLICATION

Publication from the dissertation

1. **J. Baenla**, J.B. Bike Mbah, I.B. Djon Li Ndjock, A. Elimbi. Partial replacement of low reactive volcanic ash by cassava peel ash in the synthesis of volcanic ash based geopolymer. *Construction and Building Materials* 227 (2019) 116689.

**PUBLISHED ARTICLE**



# Partial replacement of low reactive volcanic ash by cassava peel ash in the synthesis of volcanic ash based geopolymer

J. Baenla<sup>a</sup>, J.B. Bike Mbah<sup>b</sup>, I.B. Djon Li Ndjock<sup>a</sup>, A. Elimbi<sup>a,\*</sup>

<sup>a</sup> Laboratory of Applied Inorganic Chemistry, Faculty of Science, P.O. Box 812, Yaoundé, University of Yaoundé 1, Cameroon

<sup>b</sup> Laboratoire de Matériaux et de Chimie Inorganique Industrielle, ENSAI BP 445, Ngaoundéré, Université de Ngaoundéré, Cameroon

## HIGHLIGHTS

- Cassava peel ash partially replaced volcanic ash in alkali activation of low reactive volcanic ash.
- Replacement reduced setting time and magnitude of efflorescence.
- Replacement increased compressive strength of specimens cured at ambient temperature.
- Replacement brings synergistic effect in alkali activation of volcanic ash.

## ARTICLE INFO

### Article history:

Received 22 January 2019

Received in revised form 17 July 2019

Accepted 7 August 2019

### Keywords:

Volcanic ash  
Cassava peel ash  
Replacement  
Geopolymer  
Synergistic effect  
Compressive strength  
Efflorescence

## ABSTRACT

This study assesses the replacement of low reactive volcanic ash by ashes of an agro-waste matter (cassava peel) within the range of 0–30% by mass in geopolymer synthesis. Gradual replacement of volcanic ash decreases the initial setting time and increases the compressive strength to about 64 and 733% respectively. Also, it turns down the magnitude of efflorescence. After immersion in 5% solution of sulphuric acid, the surface of all specimens remains structurally intact. Cassava peel ash behaves as an additional precursor that brings synergistic effect to volcanic ash during alkaline activation.

© 2019 Elsevier Ltd. All rights reserved.

## 1. Introduction

From many decades up to now, Portland cement remains the material of construction the most used in the world with current consumption of 1 m<sup>3</sup> per person per year [1]. Though its use remains topical, its production stands for big challenge to human activities. This because its production is a great energy consumer such as to get 1 tonne of cement, about 0.8–1 tonne of CO<sub>2</sub> is concomitantly emitted in the atmosphere, which contributes to greenhouse gas emission [2–4]. Thus, seeking for alternative construction binders with respect to our environment seems to be a concern. This is noticeable through several studies focused on synthesizing of eco-friendly cements [2,4–6]. Among promising ones, geopolymer seems to be a good alternative to Portland cement [2,6]. Geopolymers are tri-dimensional network structured

materials synthesized by alkaline activation of both reactive silica and alumina materials commonly known as aluminosilicates. Geopolymer structure is made up of silicon and aluminium atoms tetrahedrally linked by sharing of oxygen atoms. The negative charge generated by the tetra coordination of aluminium atom can be balanced by Na<sup>+</sup>, K<sup>+</sup>, Ca<sup>2+</sup> and Mg<sup>2+</sup> ions [7,8]. Engelhardt [9] best describes the connectivity in geopolymer through the Q<sup>n</sup>(mAl) notation where Q represents a tetrahedral site with Si atom at the centre, n = 4 the coordination number of the Si centre while m and (n – m) are numbers of neighbouring Al and Si respectively. The structure and properties of geopolymers largely depend on the composition and the reactivity of starting raw materials. Several studies showed various precursors for geopolymer synthesis with varied reactivities from one precursor to another [10–14]. Some are good precursors at ambient cured temperature (metakaolin) while others require slightly high temperature (fly ash, dairy of blast-furnace, kaolin, etc.). Recently volcanic ashes were used as precursor for geopolymer synthesis

\* Corresponding author.

E-mail address: [aelimbi2002@yahoo.fr](mailto:aelimbi2002@yahoo.fr) (A. Elimbi).

[7,10,15–17]. These are waste materials originating from volcanic eruption. Commonly known as natural pozzolana, they are multi-form particles that possess porous structure and various colours depending on their chemical composition. Found in areas of the earth with known volcanism, they present attractive potential since volcanic ashes do not need pre-treatment such as kaolin, thereby limit atmospheric pollution and energy demand. Besides its environmental asset, from one deposit to another, volcanic ashes possess varied reactivities under alkaline activation [7,10,15,18]. To overcome some of these varied reactivities, Tchakoute et al. [19,20] suggested the alkaline fusion method or alumina addition while Djobo et al. [21,22] suggested the addition of meta-kaolin or mechanical activation process. However, all these suggestions were good except the fact that they were examined on volcanic ashes with reactive phase content of more than 30% by mass. Djon Li Ndjock et al. [15] investigated the rational utilisation of volcanic ashes and concluded that sample with amount of reactive phase under 18% by mass is considered as a low reactive precursor for geopolymer synthesis and can be used as filler. The consequences of this low reactivity are geopolymers with long setting time, low mechanical properties and with presence of efflorescence [10]. Djobo et al. [23,24] partially replaced volcanic ash by bauxite and calcined oyster shell respectively in the synthesis of volcanic ash-based geopolymer. They observed decreasing of initial setting time (calcined oyster shell) and reduction of efflorescence (bauxite) along with positive effect on mechanical properties of geopolymer specimens. Also, attempts were made with ashes of agro-industrial wastes (rice husk ash, sugarcane bagasse ash, palm oil fuel ash, etc.) as additive to improve mechanical properties during the synthesis of geopolymers [25–28]. But, most of time, curing regime was at slightly high temperature. It is interesting to note that all the latter agro-industrial waste ashes experimented come from crops growing above the soil. Some are highly silica rich (rice husk ash, sugarcane bagasse ash, etc.) while others are calcium oxide rich (wood ash) [11,28,29]. In this study, a low reactive volcanic ash (18% by mass of reactive phase) was partially replaced by cassava peel ash (72% by mass of reactive phase) in the synthesis of volcanic ash-based geopolymers. For assessment of this work, efflorescence, XRD, FTIR, SEM, initial setting time, durability along with compressive strength were used as characterization and evaluation techniques.

## 2. Materials and experimental methods

### 2.1. Materials

#### 2.1.1. Volcanic ash

The present work made use of volcanic ashes collected from the locality of Manjo (4°50'31.1" Nord, 9°49'18.1" Est; altitude 526 m; Littoral Region of Cameroon). They are reddish multi-form particles mainly due to high iron content. Prior to be used, the collected material was oven-dried at 105 °C for 48 h, ground using a ball mill and then sieved thanks to the use of a 100- $\mu$ m sieve. The obtained powdered sample was referenced as Ma.

#### 2.1.2. Cassava peel ash

Cassava peel is a by-product of cassava processing for either consumption or industrial purpose. It is made up 15–20% of the total mass of tuber and represents the upper section covering the tuber that is mainly composed of carbohydrates. Made up of two layers, the outer is known as the periderm (brownish red) and the inner is the cortex (white). Cassava peels used in this work were collected at the locality of Sombo (Central Region of Cameroon). These peels were washed and dried then calcined at 580 °C in an electric furnace (Nabertherm, model LH 60/14) in order to

remove water and organic matter. This calcined temperature was chosen thanks to the thermal analysis of powder of cassava peel which showed the latest thermal phenomenon identified at 570 °C (Fig. 1). Prior to be used, the ash was sifted thanks to the use of a 50- $\mu$ m sieve. The obtained powder was labelled as C<sub>A</sub>.

#### 2.1.3. Alkaline activating solution

The activator was a mixture of sodium hydroxide solution (12 M) and commercial sodium silicate. The sodium hydroxide solution was obtained by dissolving sodium hydroxide pellets of 99% by mass purity in distilled water. The sodium silicate used was made up of (% by mass): SiO<sub>2</sub> (31.0), Na<sub>2</sub>O (12.8) and H<sub>2</sub>O (56.2). Shi and Day [30] showed that for activation of aluminosilicates, the utilization of alkaline activators is selective due to their variable activation effect. On this, they concluded that activator selection must be based on optimization testing. Hence, in this study, the SiO<sub>2</sub>/Na<sub>2</sub>O molar ratio of 1.4 was selected because according to many authors [7,10,21], the latter gives volcanic ash based geopolymer with best mechanical properties. Prior to be used, the alkaline activating solution was stored at ambient temperature of laboratory for at least 24 h in order to reach equilibrium.

## 2.2. Experimental methods

### 2.2.1. Geopolymer synthesis

Geopolymer pastes were obtained by mixing volcanic ash (Ma) and determined mass of cassava peel ash (C<sub>A</sub>) and alkaline activating solution in a Hobart mixer (M & O model N50-G). Firstly, dry mixing for 5 min was done with volcanic ash and cassava peel ash. This was followed by addition of activating solution and the whole was mixed for 5 other minutes. Mixing of Ma and C<sub>A</sub> was done by partially replacing volcanic ash by cassava peel ash. For good workability, the liquid-to-solid mass ratio was done according to Table 2. After mixing a given formulation, one part of paste was used for the determination of initial setting time while the other was cast in cylindrical PVC moulds (diameter 25 mm; height 50 mm). Once cast, the cylinders were vibrated for 5 min on an electrical vibrating table (M & O, type 202. N° 106) in order to remove trapped air bubbles. Except cylindrical specimens free of cassava peel ash whose demoulding was done after 72 h, the hardened cylinder specimens were demoulded 24 h later. After demoulding, all the specimens were kept in a polyethylene bag and cured at ambient temperature of the laboratory for 28 days before carrying out physical or chemical characterizations. Also,

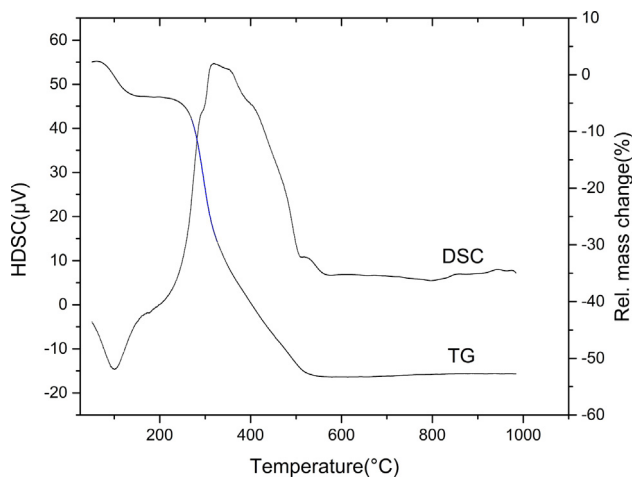


Fig. 1. Thermal analyses of cassava peel powder.

one specimen of each formulation was exposed to atmospheric air of the laboratory for 90 days for efflorescence observation. The different geopolymer specimens were labelled as GMC<sub>0</sub>, GMC<sub>10</sub>, GMC<sub>20</sub> and GMC<sub>30</sub> respectively (Table 1).

### 2.2.2. Characterization techniques

Thermal analyses (TG and DSC) were done thanks to a LINSEIS STA PT-1000 device operating from ambient temperature to 1000 °C in self-generated air of atmosphere at heating and cooling rates of 10 and 20 °C/min respectively. Inductive Coupled Plasma-Optical Emission Spectroscopy (Perkin Elmer Spectrometer Optima™ 7000 device) was used to determine chemical compositions of raw materials. Particle size distribution and specific surface area were performed using Malvern instruments Master sizer 2000 device. A modified method based on French Standard XP P18-594 [31] was used to quantitatively determine the reactive phase content of both raw materials (Ma and C<sub>A</sub>). It consisted of pouring a determined mass of raw material powder into sodium hydroxide solution (8 M) contained in a flask, then heating the whole at 80 °C in order to dissolve the amorphous phase [32]. This was followed by filtering and washing of the residue with hydrochloric acid (1 M) in order to dissolve the silica that had precipitated [33]. Later on, the resulted residue was rinsed with distilled water till neutral pH. The difference in mass between the raw material and the dried insoluble residue was used to determine the amount of reactive phase. For crystalline phase determination, powders of materials were submitted to X-ray diffraction thanks to the D8 Advance Bruker diffractometer, operating on the CuK<sub>α</sub> radiation while Fourier Transform Infrared Spectroscopy (Bruker Alpha-p IR spectrophotometer device) was carried out on powders of materials according to the KBr pellet method. An electro-hydraulic press (M & O, type 11.50, N° 21device) was used to measure compressive strength and the Vicat apparatus served for initial setting time assessment with respect to the norm EN 196-3. Scanning electron microscope (JOEL JSM-6380 Microscope) was used for microstructure observation of hardened products. Test on durability consisted of assessing the mass loss of specimens which were initially cured at ambient temperature of laboratory for 28 days and later immersed for extra 28 days in 5% by mass of sulphuric acid.

## 3. Results and discussion

### 3.1. Raw materials characterization

Chemical composition and reactive phase content of volcanic ash (Ma) and cassava peel ash (C<sub>A</sub>) are given in Table 2. SiO<sub>2</sub> and Al<sub>2</sub>O<sub>3</sub> are the major oxides in both ashes, primordial oxides for geopolymer synthesis [8,34]. Additional oxides such as Fe<sub>3</sub>O<sub>2</sub> and CaO which generally take part in alkali-activation [7,35] are also present in great amount. Also, K<sub>2</sub>O is the third most predominant oxide in C<sub>A</sub> since potassium is one of the most essential element in plant cells for optimal growth and productivity [36–38]. Loss on ignition is greater in C<sub>A</sub> than in Ma with values of 13.4 and

**Table 2**

Chemical composition (% by mass) of volcanic ash (Ma) and cassava peel ash (C<sub>A</sub>).

Oxides	Ma	C <sub>A</sub>
SiO <sub>2</sub>	43.32	22.60
Al <sub>2</sub> O <sub>3</sub>	14.84	19.67
BaO	0.06	–
CaO	8.80	10.10
Cr <sub>2</sub> O <sub>3</sub>	0.16	0.02
Fe <sub>2</sub> O <sub>3</sub>	14.19	9.67
K <sub>2</sub> O	1.52	14.20
MgO	7.70	2.52
MnO	0.20	0.11
Na <sub>2</sub> O	3.04	0.39
P <sub>2</sub> O <sub>5</sub>	0.74	1.71
SO <sub>3</sub>	0.01	4.68
SrO	0.10	–
TiO <sub>2</sub>	3.15	1.34
F	–	0.03
LOI	1.79	13.40
Total	99.80	99.90
R <sub>C</sub>	18.00	72.00

LOI: Loss on ignition R<sub>C</sub>: Reactive phase content.

1.79% by mass respectively. This may probably due to the presence of carbonate, sulphate and phosphate compounds in C<sub>A</sub>. Reactive phase content in C<sub>A</sub> is greater than the one in M<sub>A</sub> whose amounts are 72 and 18% by mass respectively, which accounts for its use in geopolymer synthesis. Particle size distribution of both samples ranges between 0.1 and 50 μm (Fig. 2). Ma proportionally possesses the smaller grain size particles than C<sub>A</sub> with an average particle size (d<sub>50</sub>) of 5.43 μm and 11.16 μm respectively. Inversely, C<sub>A</sub> exhibits lowest specific surface area (1.28 m<sup>2</sup>/g) compared to Ma whose value is 2.41 m<sup>2</sup>/g. Regarding the mineralogical composition (Fig. 3), Ma contains anorthite sodian[(Na<sub>0.45</sub>Ca<sub>0.55</sub>)(Al<sub>1.55</sub>SiO<sub>2.45</sub>O<sub>8</sub>); PDF 71-0748], augite aluminian [Ca(Mg,Fe,Al)(Si,Al)<sub>2</sub>O<sub>6</sub>; PDF 41-1483], fosterite ferroan [(Mg<sub>0.879</sub>Fe<sub>0.2121</sub>)(Mg<sub>0.881</sub>Fe<sub>0.119</sub>)(SiO<sub>4</sub>); PDF 83-0645], diopside [CaMg(SiO<sub>3</sub>)<sub>2</sub>; PDF 19-0239], hematite [α-Fe<sub>2</sub>O<sub>3</sub>; PDF 89-2810], maghemite [Fe<sub>2</sub>O<sub>3</sub>; PDF 04-0755] and muscovite [(Na<sub>0.07</sub>K<sub>0.90</sub>Ba<sub>0.01</sub>)(Al<sub>1.84</sub>Ti<sub>0.04</sub>Fe<sub>0.07</sub>Mg<sub>0.04</sub>)(Si<sub>3</sub>O<sub>2</sub>Al<sub>0.98</sub>O<sub>10</sub>(OH)<sub>2</sub>); PDF 82-2450]. C<sub>A</sub> contains arcanite [K<sub>2</sub>SO<sub>4</sub>; PDF 05-0613], calcite [CaCO<sub>3</sub>; PDF 83-0578], quartz [SiO<sub>2</sub>; PDF 86-1629], beusite calcian [(Mn<sup>2+</sup>, Fe<sup>2+</sup>, Ca)(PO<sub>4</sub>)<sub>2</sub>; PDF 16-1353], potassium phosphate [α-K<sub>2</sub>P<sub>3</sub>O<sub>10</sub>; PDF 45-0209], anatase [TiO<sub>2</sub>; PDF 86-1157] and magnesium oxide [MgO<sub>2</sub>; PDF 76-1363]. Moreover, there is a broad hump located between 14 and 38° (2θ) which indicates the amorphous fraction (R<sub>C</sub>) in C<sub>A</sub> and Ma necessary for geopolymerization [6,9]. The area which represents the broad hump in C<sub>A</sub> is larger than the one in Ma which corroborates the result obtained from leaching test (Table 2). Moreover, oxides such as Al<sub>2</sub>O<sub>3</sub> and Fe<sub>2</sub>O<sub>3</sub> in the chemical composition of C<sub>A</sub> (Table 2) are slightly present among crystalline phases (Fig. 3) which may suggest their existence in its reactive phase. The FTIR spectra of Ma and C<sub>A</sub> are given in Fig. 4. The absorption bands at 1004, 968 and

**Table 1**

Mix proportions of volcanic ash (Ma), cassava peel ash (C<sub>A</sub>) and alkaline solution.

Sample proportions (% by mass)			Composition of Raw materials (molar mass)			Mixture compositions (molar mass)			
Mix order	Ma	C <sub>A</sub>	L/S	H <sub>2</sub> O/S	SiO <sub>2</sub> /Al <sub>2</sub> O <sub>3</sub>	CaO/SiO <sub>2</sub>	SiO <sub>2</sub> /Al <sub>2</sub> O <sub>3</sub>	Na <sub>2</sub> O/Al <sub>2</sub> O <sub>3</sub>	CaO/SiO <sub>2</sub>
GMC <sub>0</sub>	100	0	0.34	0.22	4.96	0.22	5.81	0.61	0.19
GMC <sub>10</sub>	90	10	0.37	0.24	4.59	0.23	5.49	0.64	0.19
GMC <sub>20</sub>	80	20	0.43	0.28	4.24	0.25	5.26	0.73	0.20
GMC <sub>30</sub>	70	30	0.47	0.30	3.91	0.27	4.99	0.77	0.21

L/S = Liquid to solid mass ratio; H<sub>2</sub>O/S = water to solid ratio.

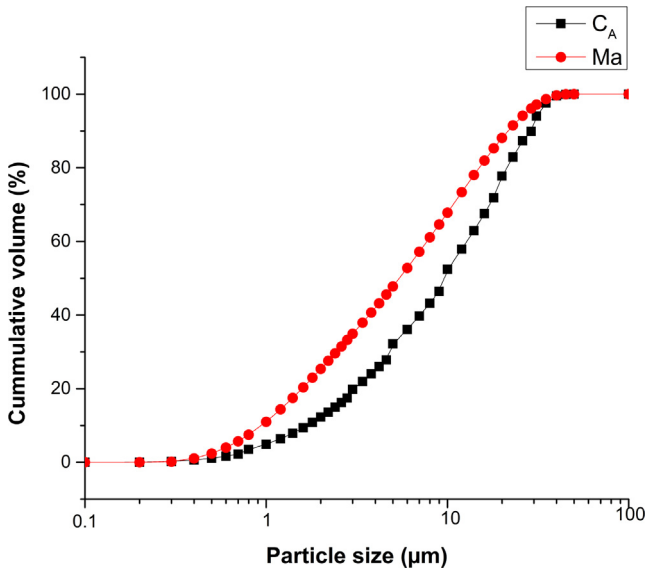


Fig. 2. Particle size distribution of powders of cassava peel ash ( $C_A$ ) and volcanic ash (Ma).

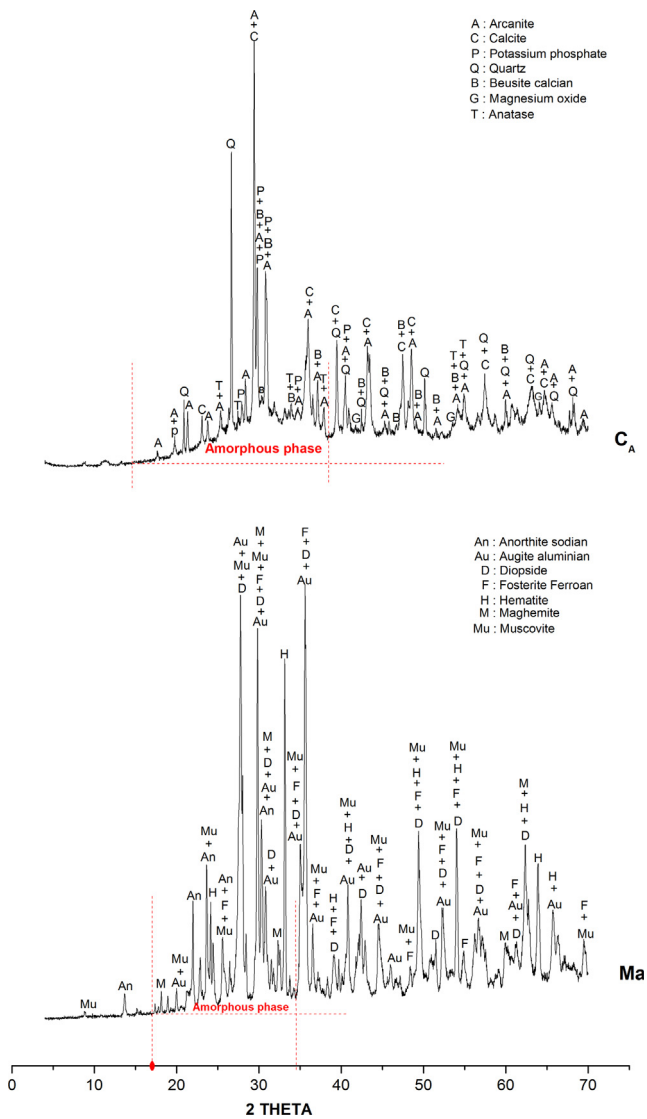


Fig. 3. X-ray diffractograms of volcanic ash (Ma) and cassava peel ash ( $C_A$ ).

913  $\text{cm}^{-1}$  are assigned to the asymmetric stretching vibrations of Si-O-Si and Si-O-Al bonds. In sugar cane bagasse and rice husk ashes, these peaks generally appear around 1099 and 1097  $\text{cm}^{-1}$  respectively [39,40]. This shift to lower wavelength numbers can be attributed to high alumina and calcium contents [20] in  $C_A$  and Ma. The peak at 1112  $\text{cm}^{-1}$  corresponds to the apical Si-O elongation vibration [21]. Moreover, carbonate vibration modes are responsible for the vibration bands at 1419, 875 and 714  $\text{cm}^{-1}$  corresponding to asymmetric stretch, out-of and in-plane vibrations respectively [22,23]. Peaks around 3433–3367 and 1646  $\text{cm}^{-1}$  are assigned respectively to stretching vibrations of O-H and bending vibrations of H-O-H of water molecules.

### 3.2. Characterization of geopolymers

#### 3.2.1. Initial setting time

Fig. 5 shows the effect of replacement of cassava peel ash on initial setting time of volcanic ash based geopolymers cured at ambient temperature ( $20 \pm 5 \text{ }^\circ\text{C}$ ) of laboratory. It is clearly established that, when volcanic ash is used alone as precursor material for geopolymer synthesis, initial setting is long. This is attributed to low reactive phase content in Ma as observed in Table 2. Conversely, initial setting time gradually decreases with replacement of volcanic ash by cassava peel ash. This may result of increasing amount of reactive phase brought by  $C_A$ . In fact, according to Table 1, replacement of Ma by  $C_A$  in the mixtures leads to the reduction of  $\text{SiO}_2/\text{Al}_2\text{O}_3$  molar ratio, hence increase in alumina content of the mixtures. The lessening of initial setting time is in accordance with alumina content in reactive phase as previously revealed (Table 2 and Fig. 3). In fact, as reported by several authors [23,41,42], in geopolymer synthesis, the increase in reactive alumina leads to the decrease of setting time. Also, during alkaline activation of aluminosilicates, dissolution of reactive alumina is

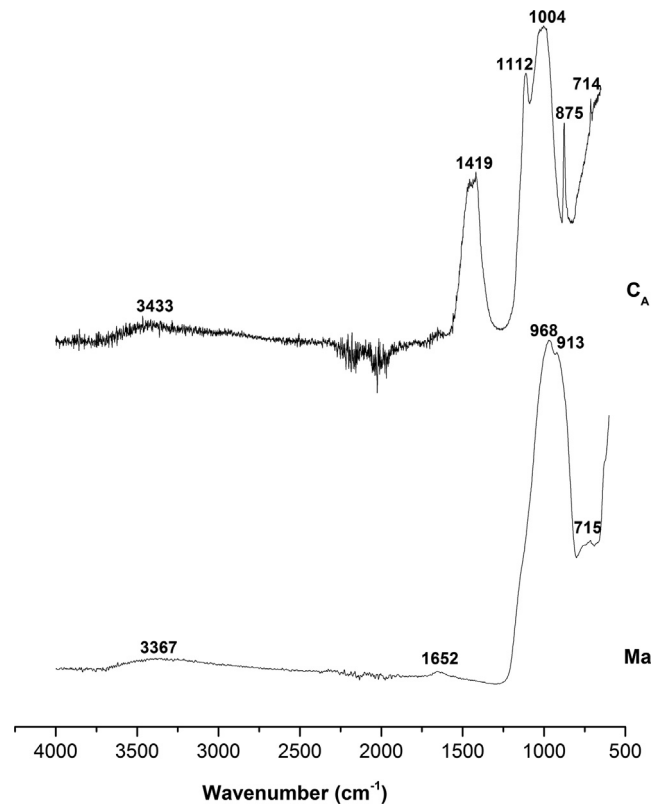


Fig. 4. FTIR spectra of volcanic ash (Ma) and cassava peel ash ( $C_A$ ).

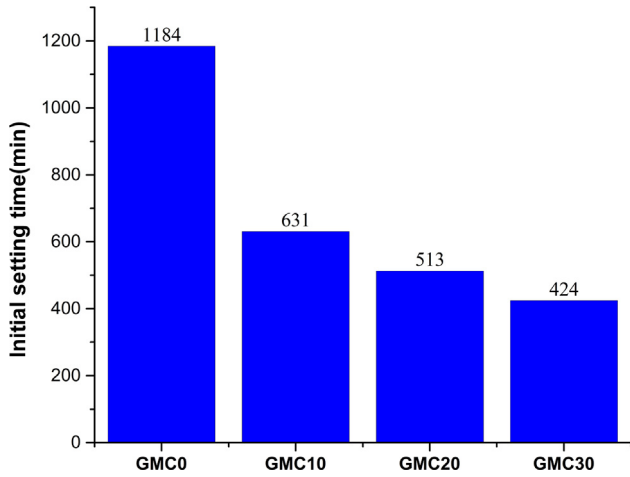


Fig. 5. Initial setting time of geopolymer pastes.

more rapid than reactive silica, which results in faster Al-O-Si bonds formation than Si-O-Si ones [41,43]. Moreover, the presence of calcite in  $C_A$  may have contributed to the reduction of initial setting time. In fact, Djobo et al. [23] and W.K.W. Lee and J.S.J. van Deventer [44] used calcined oyster shell and inorganic salts respectively to observe that increase of calcite content in alkaline medium accelerates the initial setting time of geopolymer pastes.

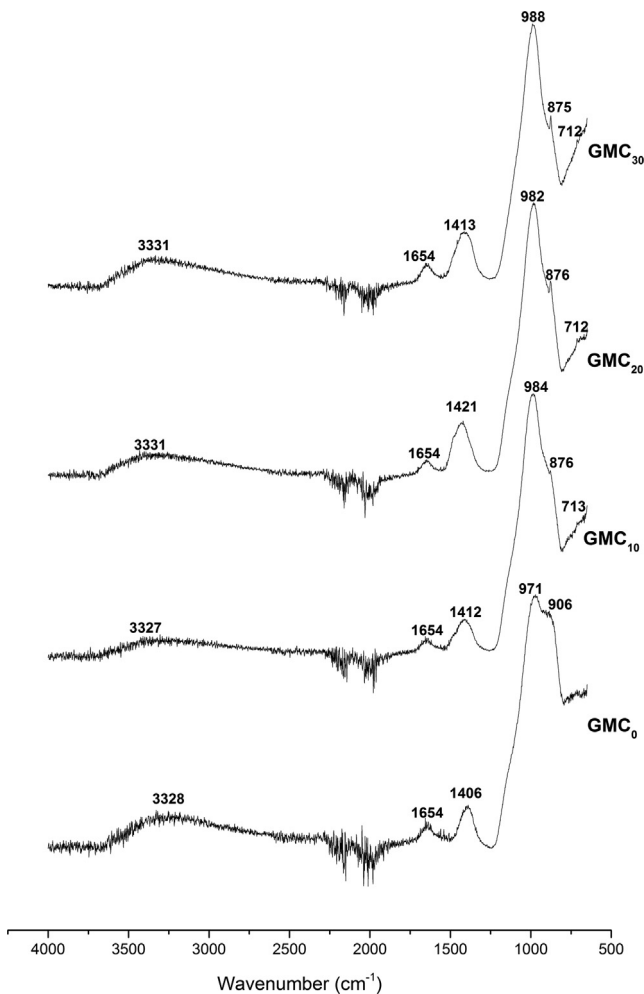


Fig. 6. Fourier Transform Infrared spectra of geopolymers aged 28 days.

### 3.2.2. Microstructure

Fig. 6 presents FTIR spectra of the geopolymers. Except the vibration band at  $1406\text{ cm}^{-1}$  which refers to incoming carbonate (efflorescence), all the absorption bands on the spectrum of  $Ma$  (Fig. 4) are also present on that of  $GMC_0$ . This highlights the low reactivity of  $Ma$  during alkaline activation. The band at  $972\text{ cm}^{-1}$  which corresponds to asymmetric stretching vibration of Si-O-Si and Si-O-Al bonds gradually become sharper with replacement of  $Ma$  by  $C_A$  (Fig. 6). This is attributed to the shifting of the vibration bands at  $1004$  and  $1112\text{ cm}^{-1}$  of the spectrum of  $C_A$  (Fig. 4) to a unique and low wave number ( $988\text{ cm}^{-1}$ ) on the spectra of the geopolymers. This induces the disappearance of the stretching vibration of the 6-fold coordinated  $Al_{(VI)}-O$  located at  $913\text{ cm}^{-1}$  [20]. According to Djobo et al. [21], this sharpness characterizes a high degree of polycondensation. Thus, the previous findings highlight the participation of cassava peel ash in the network formation of the geopolymers. The X-ray diffraction patterns of geopolymers cured at ambient temperature for 28 days of laboratory are given in Fig. 7. Except muscovite, arcanite and calcite, all the minerals initially present in  $Ma$  and  $C_A$  are not affected by alkaline activa-

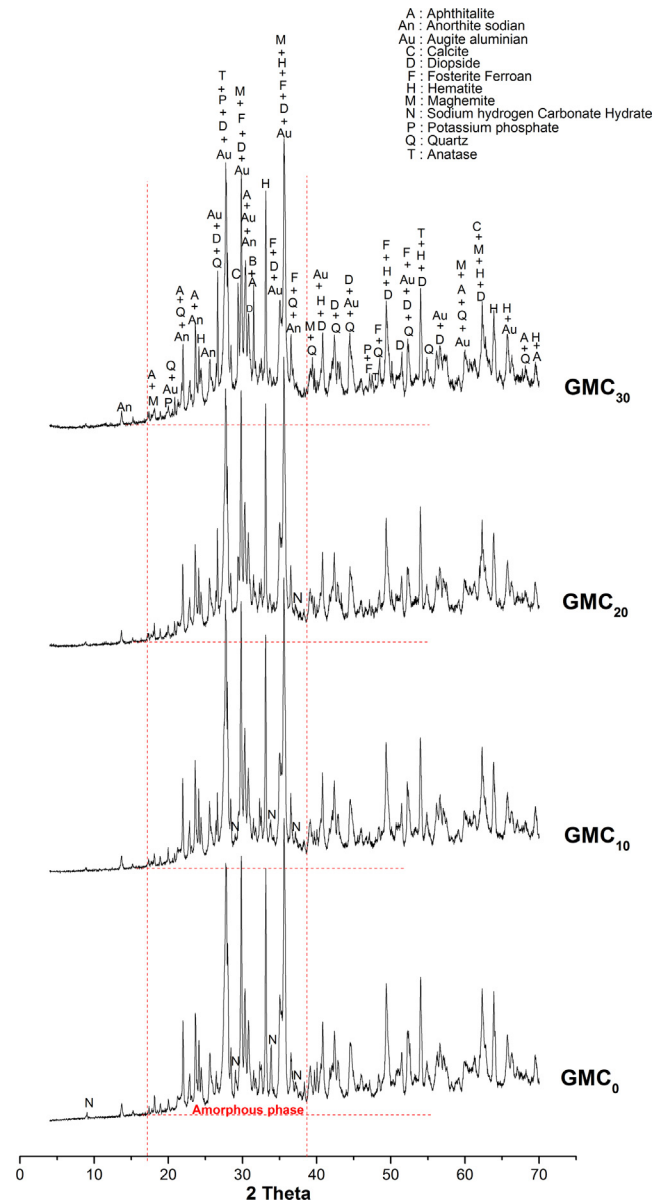


Fig. 7. X-ray diffractograms of geopolymers aged 28 days.



tion. The reactivity of muscovite and calcite in alkaline medium was already observed by other authors [17,21,39]. The dissolution of muscovite marked by the drop of its peak intensities is simultaneously followed by slight increase of the hump between 18 and 38° (2 $\theta$ ) on the X-ray pattern of GMC<sub>0</sub> (Fig. 7) when compared to that of Ma (Fig. 3). Unfortunately, this dissolution was not enough to prevent the formation of efflorescence on the surface of GMC<sub>0</sub>. This is confirmed by new peaks present at 9.04°, 29.04°, 33.87° and 37.18° (2 $\theta$ ) respectively on the X-ray pattern of GMC<sub>0</sub> (Fig. 7) and which are ascribed to sodium hydrogen carbonate hydrate [Na<sub>3</sub>H(CO<sub>3</sub>)<sub>2</sub>·2H<sub>2</sub>O: PDF 76–0739]. Conversely, peak intensities of the latter gradually decrease with respect to C<sub>A</sub> replacement. This is also accompanied by the transformation of arcanite (K<sub>2</sub>SO<sub>4</sub>) to apthitalite (K<sub>3</sub>Na(SO<sub>4</sub>)<sub>2</sub>), suggesting that addition of cassava peel ash may help to reduce the formation of sodium hydrogen carbonate hydrate (efflorescence). Despite the reactivity induced by C<sub>A</sub> replacement during the geopolymer synthesis of Ma, calcite peaks were still significantly observed on the XRD patterns of geopolymers, which confirms its low dissolution in alkaline medium as observed by other authors [23,39]. Figs. 8A and B show respectively SEM images and elemental EDX maps of the geopolymers aged 28 days. Heterogeneous and porous aspects are observed on geopolymers but the latter seem to decrease while going through Fig. 8A on which homogeneous products are gradu-

ally observed. This indicates that replacement of volcanic ash by C<sub>A</sub> has an impact on the morphology of geopolymers. The aforementioned heterogeneity is well observed by the existence of three main layers (L<sub>1</sub>, L<sub>2</sub> and L<sub>3</sub>). Looking at their respective chemical compositions thanks to EDX analysis (Table 3), L<sub>1</sub>, L<sub>2</sub> and L<sub>3</sub> are suggested to correspond respectively to unreacted particles, Na-rich geopolymer gel and efflorescence areas. Also, when comparing the chemical composition of layer L<sub>2</sub> at different proportions of C<sub>A</sub> replacement (Table 3), it is observed that when the amount of C<sub>A</sub> increases, Na/Al molar ratio decreases within the spreading Na-rich geopolymer gel and this gets close to 1, with Si/Al molar ratio found within 2.1 and 2.7 interval. This is visualized on the elemental EDX maps (Fig. 8B) on which it is noticed that, with increasing amount of C<sub>A</sub>, Na atoms with respect to Al and Si ones are gradually and homogeneously distributed all over the geopolymer structure. This suggests the reduction of free Na<sup>+</sup> ions in the geopolymer structure and corroborates the observations done on the reduction of efflorescence. In fact, according to some authors [20,40], the high level of Al atoms during the geopolymer synthesis favours the cross linking of gels, thereby reducing Na<sup>+</sup> ions mobility. Also, Hong and Glasser [45] concluded that the presence of reactive alumina enhances alkali binding by turning C-S-H gel into C-A-S-H one. This may be the reason of absence of C-S-H gel on the X-ray diffraction patterns of Fig. 7 despite the presence of calcium in

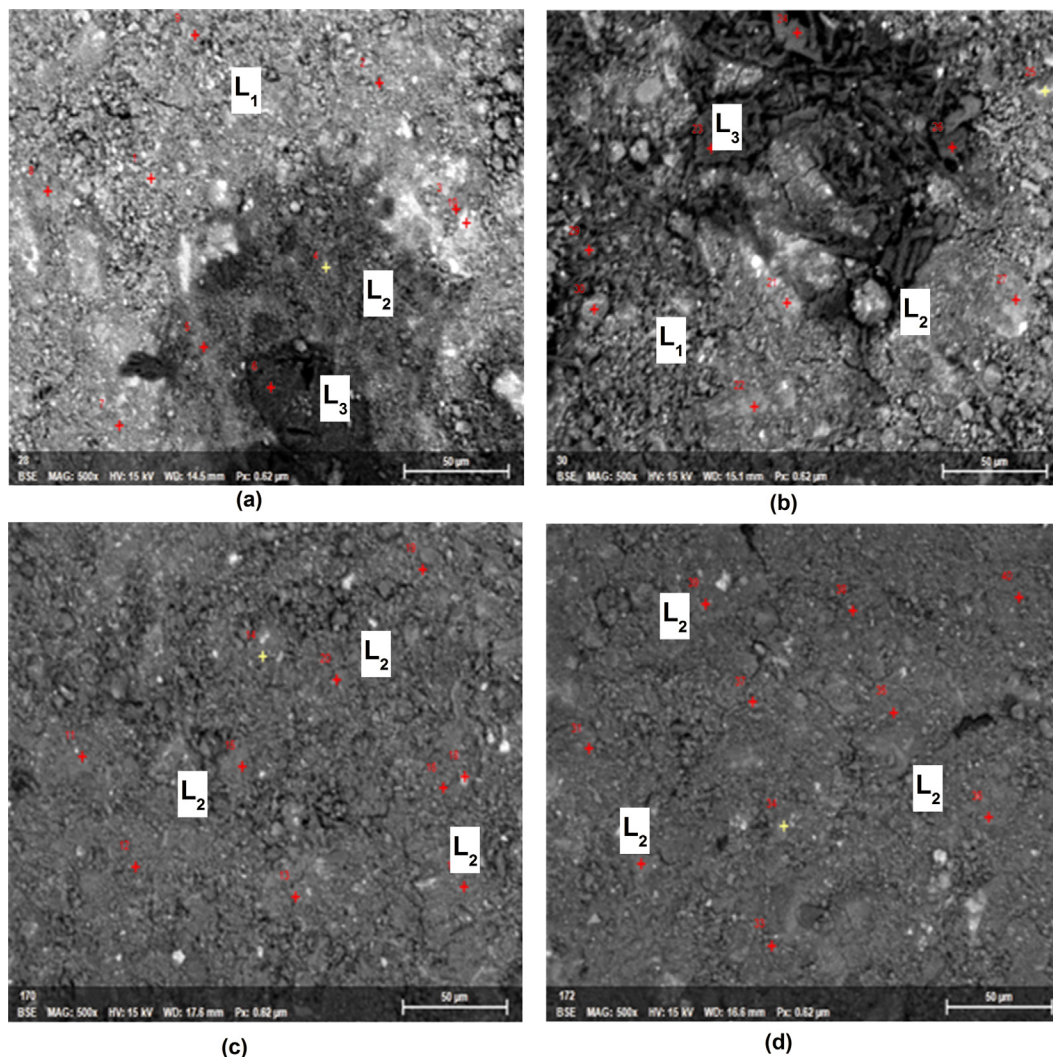
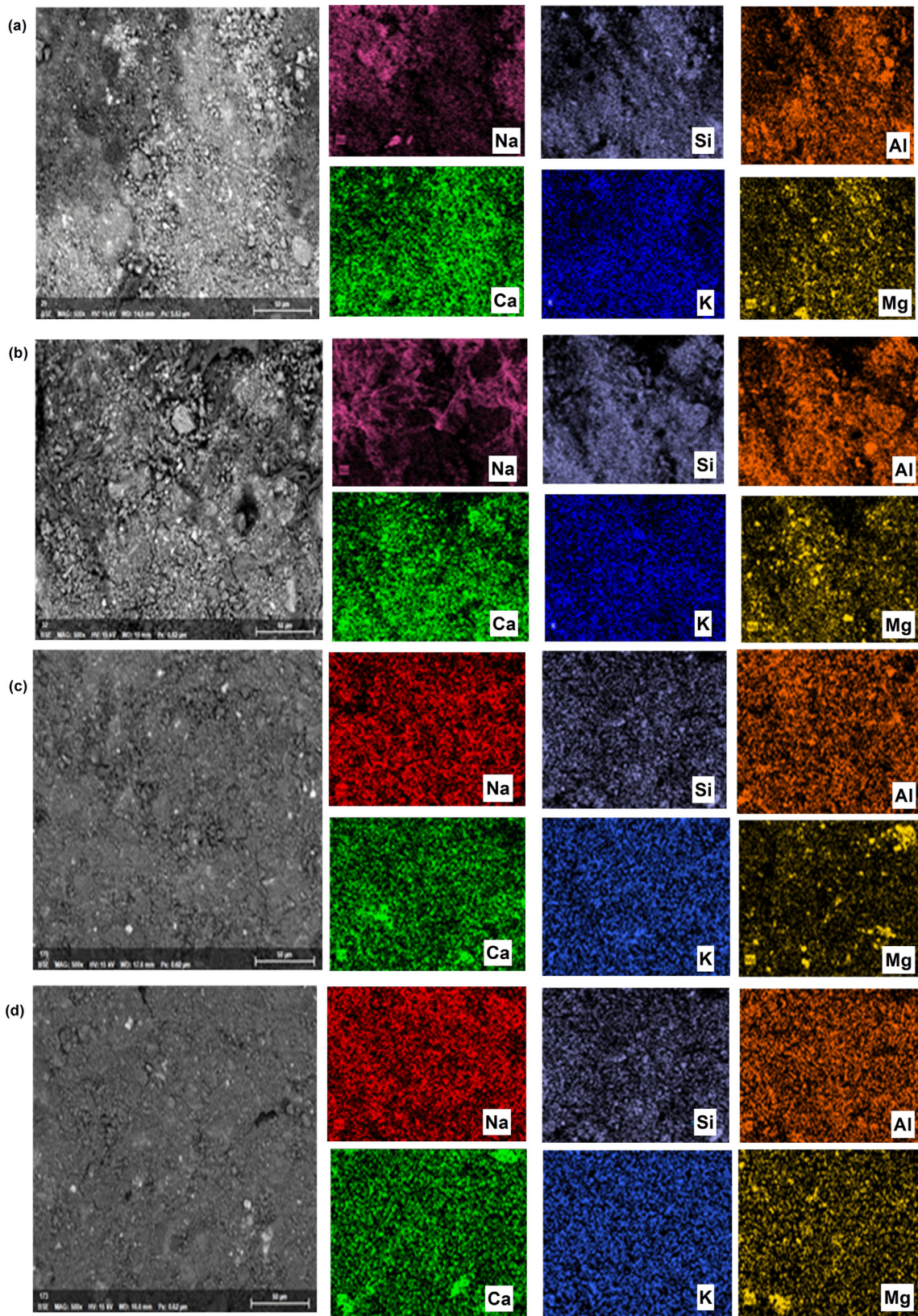


Fig. 8A. SEM images of geopolymers aged 28 days (a: GMC<sub>0</sub>; b: GMC<sub>10</sub>; c: GMC<sub>20</sub> and d: GMC<sub>30</sub>).



**Fig. 8B.** Elemental EDX maps of geopolymers aged 28 days (a: GMC<sub>0</sub>; b: GMC<sub>10</sub>; c: GMC<sub>20</sub> and d: GMC<sub>30</sub>).

the reaction medium. Moreover, the above mentioned Si/Al molar ratio joins the conclusion drawn by Piegang He et al. [34] that geopolymers with Si/Al molar ratio  $\leq 2.5$  are chemically stable in

air thereby producing no efflorescence. Hence, it is obvious that cassava peel ash brings a synergistic effect during geopolymerization of volcanic ash.

**Table 3**  
Elemental compositions of chosen areas on geopolymers aged 28 days.

Element concentration (wt%)		Molar ratio												
Sample	Area	Na	K	Ca	Al	Si	Fe	P	Ti	Mg	O	Si/Al	Na/Al	Ca/Si
GMC <sub>0</sub>	L <sub>1</sub>	11.3	2.4	6.9	6.2	23.3	9.5	0.0	1.8	2.6	35.7	2.9	2.1	0.1
	L <sub>2</sub>	16.8	0.7	7.0	10.3	23.7	0.9	0.0	0.1	0.1	40.4	2.0	1.9	0.2
	L <sub>3</sub>	63.5	1.0	1.4	1.2	2.3	1.2	0.2	0.2	0.0	29.0	2.4	62.1	0.3
GMC <sub>10</sub>	L <sub>1</sub>	5.2	0.3	8.3	7.8	18.9	4.0	0.4	1.2	4.6	49.3	2.9	0.8	0.2
	L <sub>2</sub>	7.4	0.3	7.2	12.4	21.3	2.2	0.1	0.4	0.8	47.9	1.8	0.7	0.2
	L <sub>3</sub>	68.3	0.0	0.3	0.9	3.0	0.2	0.0	0.0	0.2	27.1	2.5	89.1	0.1
GMC <sub>20</sub>	L <sub>2</sub>	12.7	2.1	7.0	7.4	16.7	10.0	0.0	1.9	1.9	40.3	2.1	1.1	0.3
	L <sub>2</sub>	9.7	4.5	5.0	7.4	23.3	4.3	0.0	0.9	1.6	43.3	3.0	1.5	0.2
	L <sub>2</sub>	7.3	6.7	10.0	6.7	16.7	9.5	0.0	1.5	0.8	40.8	2.5	1.3	0.4
GMC <sub>30</sub>	L <sub>2</sub>	7.0	5.2	4.5	7.8	21.9	7.5	0.2	1.6	1.2	42.7	2.7	1.1	0.1
	L <sub>2</sub>	9.5	3.3	4.6	10.2	21.8	4.2	0.4	1.1	0.8	43.5	2.1	1.1	0.1
	L <sub>2</sub>	6.7	3.6	4.8	9.2	22.4	5.9	0.1	1.5	1.9	43.6	2.4	0.9	0.2

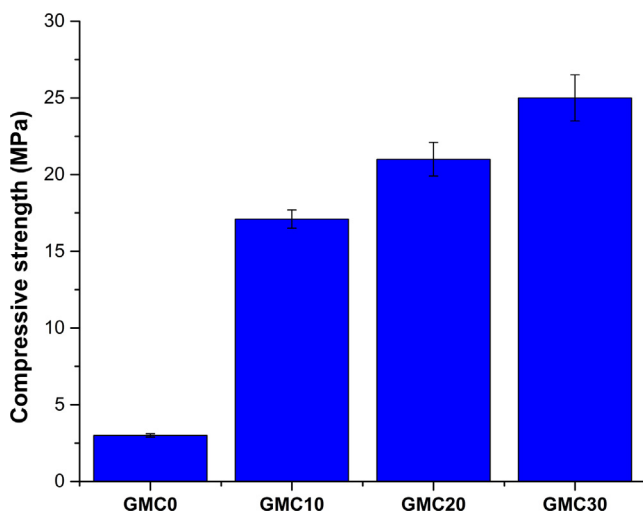


**Fig. 9.** 28 days compressive strength of geopolymers cured at ambient temperature of laboratory.

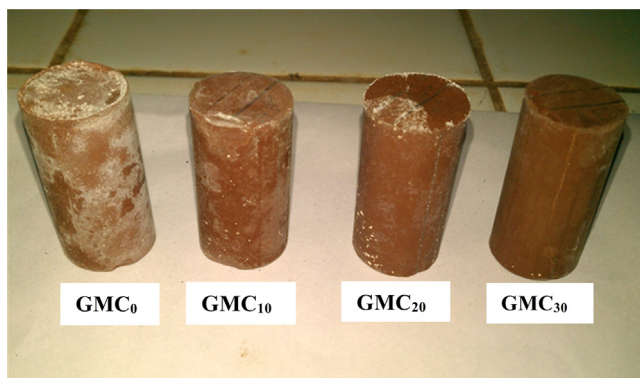


**Fig. 10.** Appearance of hardened geopolymer paste specimens exposed to atmospheric air of laboratory for 90 days.

### 3.2.3. Compressive strength

The result of 28 days compressive strength versus  $C_A$  of geopolymer paste specimens cured at ambient temperature of laboratory is given in Fig. 9. There is significant compressive strength increase from 3.0 MPa (specimen GMC<sub>0</sub>) to 25.0 MPa (specimen GMC<sub>30</sub>). This is in accordance with the observations done on Fig. 8A confirmed by the compactness brought about by  $C_A$  in geopolymer morphology. Mechanical strength of geopolymer is among other governed by the reactive phase content of aluminosil-

icate and the degree of formation of new tri-dimensional network of Si-O-Al [15,19]. All of these mainly depend on  $\text{SiO}_2/\text{Al}_2\text{O}_3$  molar ratio of reactive phase along with its ability to be dissolved in alkaline medium [46]. The low compressive strength exhibited by GMC<sub>0</sub> is assigned to its low reactive phase content, hence high  $\text{SiO}_2/\text{Al}_2\text{O}_3$  molar ratio (Table 3) which leads to low degree of geopolymerization. Conversely, replacement of volcanic scoria ash by gradual increasing amount of  $C_A$  allows getting geopolymer specimens with increasing amount of reactive phase (Table 2) which lowers the  $\text{SiO}_2/\text{Al}_2\text{O}_3$  molar ratio by increasing the alumina content. This increases polycondensation thus optimizes the densification of geopolymers. According to Tchakoute et al. [20], addition of appropriate amount of amorphous alumina oxide to an aluminosilicate material increases the geopolymerization extent resulting in the increase of compressive strength. Also, the presence of calcite and iron oxide in  $C_A$  are an asset which may favour compressive strength increase because both can behave as network formers [7,47].

### 3.2.4. Efflorescence and durability

Fig. 10 shows the appearance of hardened geopolymer paste specimens initially covered with thin film of polyethylene for 24 h and later on exposed for 90 days at atmospheric air of the laboratory. Efflorescence is marked here by the presence of whitish layer on the surface of geopolymer specimens. Among the different geopolymer specimens, GMC<sub>0</sub> exhibits the highest extent of efflorescence. Replacement of  $M_A$  by gradual increasing amount of  $C_A$  reduces the magnitude of efflorescence from the specimen GMC<sub>10</sub> to the specimen GMC<sub>30</sub>. This whitish layer is identified as sodium hydrogen carbonate hydrate as revealed by XRD patterns (Fig. 7). In alkaline medium, efflorescence is the result of availability and mobility of  $\text{Na}^+$  ions which react with  $\text{CO}_2$  from atmospheric air. However,  $\text{Na}^+$  ions availability depends among other of the presence of low reactive phase content of aluminosilicate [48]. The high extent of efflorescence in GMC<sub>0</sub> is attributed to its low reactive phase content.  $C_A$  replacement compensates the deficiency in reactive phase whose increasing amount gradually reduces the extent of efflorescence. Also, replacement of  $M_A$  by increasing amount of  $C_A$  allows the consumption of available  $\text{Na}^+$  ions by arcanite [ $\text{K}_2\text{SO}_4$ ] to get apththalite [ $\text{K}_3\text{Na}(\text{SO}_4)_2$ ], hence reduction of the formation of efflorescence. To get an idea on the durability of geopolymers fabricated from partial replacement of volcanic ash by cassava peel ash, specimens GMC<sub>0</sub> and GMC<sub>30</sub> were soaked for 28 days in 5% by mass of sulphuric acid solution. The results (Table 4) show that GMC<sub>0</sub> experienced mass loss of 2.76% meanwhile GMC<sub>30</sub> experienced mass loss of 7.59%. The pronounced mass loss in GMC<sub>30</sub> may mostly be ascribed to the chemical reaction between calcite ( $\text{CaCO}_3$ ) present in the geopolymer

**Table 4**

Mass loss (%) of geopolymers immersed in 5% by mass of sulphuric acid for 28 days.

	GMC <sub>0</sub>	GMC <sub>30</sub>
Mass loss	-2.76	-7.59

(Fig. 7) and sulphuric acid solution. Nevertheless, after 28 days of immersion in acid solution, the surface of all specimens seemed to remain structurally intact, implying that the obtained geopolymers are stable in acid medium.

#### 4. Conclusion

Due to its high amorphous phase content (72% by mass), cassava peel ash partially replaced low reactive volcanic ash during alkali activation of volcanic ash. This led to positive effects on the obtained products. Thus, when used alone, volcanic ash showed low reactivity in alkaline medium, thereby making the handling of geopolymers possible after 3 days, compressive strength of 3.0 MPa (specimens aged 28 days) and abundant efflorescence on specimens exposed to atmospheric air of the laboratory. Conversely, gradual replacement of volcanic by cassava peel ash allowed to get geopolymer pastes with reduced initial setting time (64%) and specimens aged 28 days with significant increase of compressive strength (733%). This behavior was attributed to additional reactive phase brought by the replacement of volcanic ash. Also, replacement of volcanic ash by cassava peel ash ( $\geq 20\%$  by mass) led to compact enough products and homogeneous distribution of Na<sup>+</sup> ions over the structure of alkali activated specimens along with reduction of magnitude of efflorescence. Lessening of efflorescence resulted among other to the presence of arcanite (K<sub>2</sub>SO<sub>4</sub>) in the replacement which helped to embed unreacted Na<sup>+</sup> ions through the formation of apththalite (K<sub>3</sub>Na(SO<sub>4</sub>)<sub>2</sub>). After 28 days of immersion in 5% by mass of sulphuric acid, the surface of all specimens remains structurally intact. Hence, cassava peel ash behaves as an additional precursor that brings synergistic effect to volcanic ash during alkaline activation.

#### Declaration of Competing Interest

The authors declare that they have no known competing financial interests or personal relationships that could have appeared to influence the work reported in this paper.

#### Acknowledgements

The authors address their thanks to the financial supports obtained from the "Bureau Afrique Centrale et des Grands Lacs de l'Agence Universitaire de la Francophonie (BACGL-AUF) under the grant NS0020//10406 and "The World Academy of Sciences" (TWAS) under the grant N 13-018 RG/CHE/AF/AC G—UNESCO FR: 3240277723 for having made available all facilities for carrying out this work.

#### References

- [1] E. Gartner, Industrially interesting approaches to "low-CO<sub>2</sub>" cements, *Cem. Concr. Res.* 34 (2010) 1489–1498, <https://doi.org/10.1016/j.cemconres.2004.01.021>.
- [2] J. Davidovits, Geopolymer Cement a review, published in *Geopolymer Science and Technics*, Technical Paper #21, Geopolymer Inst. Libr., 2013.
- [3] J. Davidovits, False Values on CO<sub>2</sub> Emission for Geopolymer Cement/Concrete published in *Scientific Papers*, Technical Paper #24, Geopolymer Inst. Libr., 2015.
- [4] R. Maddalena, J.J. Roberts, A. Hamilton, Can Portland cement be replaced by low-carbon alternative materials? A study on thermal properties and carbon emissions of innovative cements, *J. Clean. Prod.* (2018), <https://doi.org/10.1016/j.jclepro.2018.02.138>.
- [5] S.A. Walling, J.L. Provis, Magnesia-based cements: a journey of 150 years, and cements for the future?, *Chem. Rev.* (2015), <https://doi.org/10.1021/acs.chemrev.5b00463>.
- [6] L. Coppola, T. Bellezze, A. Belli, M.C. Bignozzi, F. Bolzoni, A. Brenna, M. Cabrini, S. Candamano, M. Cappai, D. Caputo, M. Carsana, L. Casnedi, R. Cioffi, O. Cocco, D. Coffetti, F. Colangelo, B. Coppola, V. Corinaldesi, F. Crea, E. Crotti, V. Daniele, S. De Gisi, F. Delogu, M.V. Diamanti, L. Di Maio, R. Di Mundo, L. Di Palma, J. Donnini, I. Farina, C. Ferone, P. Frontera, M. Gastaldi, C. Giosuè, L. Incarnato, B. Liguori, F. Lollini, S. Lorenzi, S. Manzi, O. Marino, M. Marroccoli, M.C. Mascolo, L. Mavilia, A. Mazzoli, F. Medici, P. Meloni, G. Merlonetti, A. Mobili, M. Notarnicola, M. Ormellese, T. Pastore, M.P. Pedferri, A. Petrella, G. Pia, E. Redaelli, G. Roviello, P. Scarfato, G. Scoccia, G. Taglieri, A. Telesca, F. Tittarelli, F. Todaro, G. Vilardi, F. Yang, Binders alternative to Portland cement and waste management for sustainable construction—part 1, *J. Appl. Biomater. Funct. Mater.* 16 (2018) 186–202, <https://doi.org/10.1177/2280800018782845>.
- [7] Jean Noël Yankwa Djobo, Antoine Elimbi, Hervé Kouamo Tchakouté, Sanjay Kumar, Reactivity of volcanic ash in alkaline medium, microstructural and strength characteristics of resulting geopolymers under different synthesis conditions, *J. Mater. Sci.* 51 (2016) 10301–10317, <https://doi.org/10.1007/s10853-016-0257-1>.
- [8] J. Davidovits, S. Quentin, GEOPOLYMERS inorganic POLYMERIE new materials, *J. Therm. Anal.* 37 (1991) 1633–1656, <https://doi.org/10.1007/BF01912193>.
- [9] G. Engelhardt, E. Lohse, U. Samoson, A. Mägi, M. Tarmak, M. and Lippmaa, dealuminated and ultrastable Y-zeolites, *ZEOLITES* 2 (1982) 59–62, [https://doi.org/10.1016/S0144-2449\(82\)80042-0](https://doi.org/10.1016/S0144-2449(82)80042-0).
- [10] H.K. Tchakoute, A. Elimbi, E. Yanne, C.N. Djangang, Utilization of volcanic ashes for the production of geopolymers cured at ambient temperature, *Cem. Concr. Compos.* 38 (2013) 75–81, <https://doi.org/10.1016/j.cemconcomp.2013.03.010>.
- [11] P. Sturm, G.J.G. Gluth, H.J.H. Brouwers, H.C. Kühne, Synthesizing one-part geopolymers from rice husk ash, *Constr. Build. Mater.* 124 (2016) 961–966, <https://doi.org/10.1016/j.conbuildmat.2016.08.017>.
- [12] B.B.D. Kenne, A. Elimbi, M. Cyr, J.D. Manga, H.K. Tchakoute, Effect of the rate of calcination of kaolin on the properties of metakaolin-based geopolymers, *J. Asian Ceram. Soc.* (2014) 1–9, <https://doi.org/10.1016/j.jascer.2014.12.003>.
- [13] S. Songpiriyakij, T. Kubprasit, C. Jaturapitakkul, P. Chindaprasirt, Compressive strength and degree of reaction of biomass- and fly ash-based geopolymer, *Constr. Build. Mater.* 24 (2010) 236–240, <https://doi.org/10.1016/j.conbuildmat.2009.09.002>.
- [14] S. Saha, C. Rajasekaran, Enhancement of the properties of fly ash based geopolymer paste by incorporating ground granulated blast furnace slag, *Constr. Build. Mater.* 146 (2017) 615–620, <https://doi.org/10.1016/j.conbuildmat.2017.04.139>.
- [15] B.I. Djon Li Ndjock, A. Elimbi, M. Cyr, Rational utilization of volcanic ashes based on factors affecting their alkaline activation, *J. Non. Cryst. Solids.* 463 (2017) 31–39, <https://doi.org/10.1016/j.jnoncrysol.2017.02.024>.
- [16] J.N.Y. Djobo, A. Elimbi, H. Kouamo, S. Kumar, Mechanical properties and durability of volcanic ash based geopolymer mortars, *Constr. Build. Mater.* 124 (2016) 606–614, <https://doi.org/10.1016/j.conbuildmat.2016.07.141>.
- [17] H.K. Tchakouté, S. Kong, J.N.Y. Djobo, L.N. Tchadjjié, D. Njopwouo, A comparative study of two methods to produce geopolymer composites from volcanic scoria and the role of structural water contained in the volcanic scoria on its reactivity, *Ceram. Int.* 41 (2015) 1–10, <https://doi.org/10.1016/j.ceramint.2015.06.073>.
- [18] J.N.Y. Djobo, A. Elimbi, H.K. Tchakouté, S. Kumar, Volcanic ash-based geopolymer cements/concretes: the current state of the art and perspectives, *Environ. Sci. Pollut. Res.* 24 (2017) 4433–4446, <https://doi.org/10.1007/s11356-016-8230-8>.
- [19] H.K. Tchakoute, A. Elimbi, B.B.D. Kenne, J.A. Mbey, D. Njopwouo, Synthesis of geopolymers from volcanic ash via the alkaline fusion method: effect of Al<sub>2</sub>O<sub>3</sub>/Na<sub>2</sub>O molar ratio of soda – volcanic ash, *Ceram. Int.* 39 (2013) 269–276, <https://doi.org/10.1016/j.ceramint.2012.06.021>.
- [20] H. Tchakoute Kouamo, A. Elimbi, J.A. Mbey, C.J. Ngaly Sabouang, D. Njopwouo, The effect of adding alumina-oxide to metakaolin and volcanic ash on geopolymer products: a comparative study, *Constr. Build. Mater.* 35 (2012) 960–969, <https://doi.org/10.1016/j.conbuildmat.2012.04.023>.
- [21] J.N.Y. Djobo, L.N. Tchadjjié, H.K. Tchakoute, B.B.D. Kenne, A. Elimbi, D. Njopwouo, Synthesis of geopolymer composites from a mixture of volcanic scoria and metakaolin, *J. Asian Ceram. Soc.* 2 (2014) 387–398, <https://doi.org/10.1016/j.jascer.2014.08.003>.
- [22] J.N.Y. Djobo, A. Elimbi, K.H. Tchakouté, S. Kumar, RSC Advances Mechanical activation of volcanic ash for geopolymer synthesis: effect on reaction kinetics, gel characteristics, physical and mechanical, *R. Soc. Chem. Adv.* 6 (2016) 39106–39117, <https://doi.org/10.1039/C6RA03667H>.
- [23] J.N.Y. Djobo, A. Elimbi, J.D. Manga, I.B.D. Li, Partial replacement of volcanic ash by bauxite and calcined oyster shell in the synthesis of volcanic ash-based geopolymers, *Constr. Build. Mater.* 113 (2016) 673–681, <https://doi.org/10.1016/j.conbuildmat.2016.03.104>.
- [24] J.N.Y. Djobo, H.K. Tchakouté, N. Ranjbar, A. Elimbi, L.N. Tchadjjié, D. Njopwouo, J. Biernacki, Gel composition and strength properties of alkali-activated oyster shell-volcanic ash: effect of synthesis conditions, *J. Am. Ceram. Soc.* 99 (2016) 3159–3166, <https://doi.org/10.1111/jace.14332>.
- [25] S. Detphan, P. Chindaprasirt, Preparation of fly ash and rice husk ash geopolymer, *Int. J. Miner. Metall. Mater.* 16 (2009) 720–726, [https://doi.org/10.1016/S1674-4799\(10\)60019-2](https://doi.org/10.1016/S1674-4799(10)60019-2).

- [26] N. Ranjbar, M. Mehrli, A. Behnia, U.J. Alengaram, M.Z. Jumaat, Compressive strength and microstructural analysis of fly ash/palm oil fuel ash based geopolymer mortar, *Mater. Des.* 59 (2014) 532–539, <https://doi.org/10.1016/j.matdes.2014.03.037>.
- [27] R.C. Kaze, L. Myllyam, B. Moungam, M. Cannio, R. Rosa, E. Kamseu, U.C. Melo, C. Leonelli, Microstructure and engineering properties of  $\text{Fe}_2\text{O}_3(\text{FeO})\text{-Al}_2\text{O}_3\text{-SiO}_2$  based geopolymer composites, *J. Clean. Prod.* 3 (2018), <https://doi.org/10.1016/j.jclepro.2018.07.171>.
- [28] A. Pereira, J.L. Akasaki, J.L.P. Melges, M.M. Tashima, L. Soriano, M.V. Borrachero, J. Monzó, J. Payá, Mechanical and durability properties of alkali-activated mortar based on sugarcane bagasse ash and blast furnace slag, *Ceram. Int.* 41 (2015) 1–13, <https://doi.org/10.1016/j.ceramint.2015.07.001>.
- [29] C.C. Ban, P.W. Ken, M. Ramli, The hybridizations of coal fly ash and wood ash for the fabrication of low alkalinity geopolymer load bearing block cured at ambient temperature, *Constr. Build. Mater.* 88 (2015) 41–55, <https://doi.org/10.1016/j.conbuildmat.2015.04.020>.
- [30] R.D. Hooton, C. Shi, R.L. Day, Selectivity of alkaline activators for the activation of slags, *Cem. Concr. Aggr.* 18 (1) (1996) 8, <https://doi.org/10.1520/CCA10306>.
- [31] AFNOR XP P18-594, Granulats – Méthodes d'essai de réactivité aux alcalis (aggregates – test methods on reactivity to alkalis).
- [32] N. Granizo, A. Palomo, Effect of temperature and alkaline concentration on metakaolin leaching kinetics, *Ceram. Int.* 40 (2014) 8975–8985, <https://doi.org/10.1016/j.ceramint.2014.02.071>.
- [33] D. Bulteel, E. Garcia-diaz, C. Vernet, H. Zanni, Alkali – silica reaction A method to quantify the reaction degree, *Cem. Concr. Res.* 32 (2002) 1199–1206.
- [34] P. He, M. Wang, D. Jia, S. Yan, J. Yuan, J. Xu, P. Wang, Y. Zhou, Effect of Si/Al ratio on the structure and properties of metakaolin based geopolymer, *J. Ceram. Int.* 42 (2016) 14416–14422, <https://doi.org/10.1016/j.ceramint.2016.06.033>.
- [35] J. Temuujin, A. Van Riessen, R. Williams, Influence of calcium compounds on the mechanical properties of fly ash geopolymer pastes, *J. Hazard. Mater.* 167 (2009) 82–88, <https://doi.org/10.1016/j.jhazmat.2008.12.121>.
- [36] W. Xiao-guang, Z. Xin-hua, J. Chun-ji, L.I. Chun-hong, C. Shan, W.U. Di, Effects of potassium deficiency on photosynthesis and photoprotection mechanisms in soybean (*Glycine max* (L.) Merr.), *J. Integr. Agric.* 14 (5) (2015) 856–863, [https://doi.org/10.1016/S2095-3119\(14\)60848-0](https://doi.org/10.1016/S2095-3119(14)60848-0).
- [37] D.M. Oosterhuis, D.A. Loka, E.M. Kawakami, W.T. Pettigrew, The physiology of potassium in crop production, *Adv. Agron.* 126 (2014) 203–233, <https://doi.org/10.1016/B978-0-12-800132-5.00003-1>.
- [38] A. Hafeez, S. Ali, X. Ma, S. Atta, A. Noor, A. Liu, S. Ahmed, M. Sohaib, G. Yang, Industrial crops & products potassium to nitrogen ratio favors photosynthesis in late-planted cotton at high planting density, *Ind. Crop. Prod.* 124 (2018) 369–381, <https://doi.org/10.1016/j.indcrop.2018.08.006>.
- [39] C.K. Yip, J.L. Provis, G.C. Lukey, J.S.J. van Deventer, Carbonate mineral addition to metakaolin-based geopolymers, *Cem. Concr. Compos.* 30 (2008) 979–985, <https://doi.org/10.1016/j.cemconcomp.2008.07.004>.
- [40] E. Najafi Kani, A. Allahverdi, J.L. Provis, Calorimetric study of geopolymer binders based on natural pozzolan, *J. Therm. Anal. Calorim.* 127 (2017) 2181–2190, <https://doi.org/10.1007/s10973-016-5850-7>.
- [41] P. De Silva, K. Sagoe-Crenstil, V. Sirivivatnanon, Kinetics of geopolymerization: role of  $\text{Al}_2\text{O}_3$  and  $\text{SiO}_2$ , *Cem. Concr. Res.* 37 (2007) 512–518, <https://doi.org/10.1016/j.cemconres.2007.01.003>.
- [42] P. Duxson, A. Fernández-Jiménez, J.L. Provis, G.C. Lukey, A. Palomo, J.S.J. Van Deventer, Geopolymer technology: the current state of the art, *J. Mater. Sci.* 42 (2007) 2917–2933, <https://doi.org/10.1007/s10853-006-0637-z>.
- [43] L.W.E.K. Sagoe-crentsil, Dissolution processes, hydrolysis and condensation reactions during geopolymer synthesis: part I – low Si/Al ratio systems, *J. Mater. Sci.* 42 (2007) 2997–3006, <https://doi.org/10.1007/s10853-006-0820-2>.
- [44] W.K.W. Lee, J.S.J. Van Deventer, The effect of ionic contaminants on the early-age properties of alkali-activated fly ash-based cements, *Cem. Concr. Res.* 32 (2002) 577–584, [https://doi.org/10.1016/S0008-8846\(01\)00724-4](https://doi.org/10.1016/S0008-8846(01)00724-4).
- [45] S.Y. Hong, F.P. Glasser, Alkali sorption by C-S-H and C-A-S-H gels: part II. Role of alumina, *Cem. Concr. Res.* 32 (2002) 1101–1111, [https://doi.org/10.1016/S0008-8846\(02\)00753-6](https://doi.org/10.1016/S0008-8846(02)00753-6).
- [46] B. Lee, G. Kim, R. Kim, B. Cho, S. Lee, C. Chon, Strength development properties of geopolymer paste and mortar with respect to amorphous Si/Al ratio of fly ash, *Constr. Build. Mater.* 151 (2017) 512–519, <https://doi.org/10.1016/j.conbuildmat.2017.06.078>.
- [47] P.N. Lemougna, J.D. Mackenzie, G.N.L. Jameson, H. Rahier, U.F.C. Melo, The role of iron in the formation of inorganic polymers (geopolymers) from volcanic ash: a 57 Fe Mössbauer spectroscopy study, *J. Mater. Sci.* 48 (2013) 5280–5286, <https://doi.org/10.1007/s10853-013-7319-4>.
- [48] E. Najafi, A. Allahverdi, J.L. Provis, Efflorescence control in geopolymer binders based on natural pozzolan, *Cem. Concr. Compos.* 34 (2012) 25–33, <https://doi.org/10.1016/j.cemconcomp.2011.07.007>.